UNIVERSITY OF CALIFORNIA,
IRVINE

G3BP1-positive stress granule pathology in brains of Huntington's disease mice and human patients and a potential role for extracellular vesicle-derived miRNA regulation

DISSERTATION

submitted in partial satisfaction of the requirements
for the degree of

DOCTOR OF PHILOSOPHY

in Biological Sciences

by

Isabella Inez Sanchez

Dissertation Committee:
Dr. Leslie M. Thompson, Chair
Dr. Christie D. Fowler
Dr. Edwin S. Monuki

2020

DEDICATION

This dissertation is dedicated to my family. For their endless encouragement, and the sacrifices they have made for me.

TABLE OF CONTENTS

	Page
LIST OF FIGURES	iv
LIST OF TABLES	vii
LIST OF ABBREVIATIONS	viii
AKNOWLEDGEMENTS	ix
CURRICULUM VITAE	xi
ABSTRACT OF THE DISSERTATION	xvi
INTRODUCTION	1
A) Huntington's disease	1
B) The choroid plexus, cerebrospinal fluid, and exosome secretion	6
C) micro RNAs	11
D) Heterogenous nuclear ribonucleoprotein A2/B1	15
E) Stress granules and neurodegeneration	19
F) Summary of introduction	27
CHAPTER 1: Longitudinal biochemical assay analysis of mutant huntingtin exon 1 protein in R6/2 mice	32
CHAPTER 2: G3BP1-positive stress granule pathology in Huntington's disease	68
CHAPTER 3: Derivation of choroid plexus epithelial cells from Huntington's disease patient-derived induced pluripotent stem cells	135
DISSERTATION CONCLUDING REMARKS	165
REFERENCES	172

LIST OF FIGURES

		Page
Figure 1.1	Progressive motor and transcriptional changes as quality control for R6/2 mice	55
Figure 1.2	Delta CT (dCT) values used to analyze transcriptional alterations detected by qPCR in R6/2 mice	56
Figure 1.3	Progressive mHTT inclusion body formation in cortex and striatum of R6/2 mice	57
Figure 1.4	Detection of mHTTex1p in striatum of R6/2 mice	58
Figure 1.5	Detection of mHTTex1p is highly variable using TRIzol reagent	59
Figure 1.6	Detection of mHTTex1p in cortex of R6/2 mice	60
Figure 1.7	Detection of mHTTex1p in hippocampus and cerebellum of R6/2 mice varies depending on break method	61
Figure 1.8	Detection of mHTTex1p in peripheral tissue varies depending on break method	62
Figure 1.9	Detection of mHTTex1p on AGE gels varies based by break method	63
Figure 2.1	Increase of SG density in the 12-week R6/2 cortex and hippocampus	99
Figure 2.2	SG density analyses in the R6/2 cortex at 8 and 12-week timepoints	100
Figure 2.3	SG density analyses in the R6/2 striatum at 8 and 12-week timepoints	101
Figure 2.4	G3BP1 SGs do not co-localize with EM48-positive nuclear inclusions in the 12-week R6/2 mouse cortex	102
Figure 2.5	Comparison of hnRNPA2/B1 and G3BP1 immunoreactivity in the 12-week R6/2 brain	103
Figure 2.6	G3BP2 SGs are not detected in the 12-week R6/2 mouse brain	104

Figure 2.7	G3BP1 immunoreactivity in the hippocampus of HD patients	105
Figure 2.8	G3BP1 immunoreactivity in the hippocampus of HD patients (higher magnification images)	106
Figure 2.9	G3BP1 immunoreactivity in the superior frontal cortex of HD patients	107
Figure 2.10	G3BP1 immunoreactivity in the parietal cortex of HD patients	108
Figure 2.11	Increased G3BP1 SG density in the superior frontal cortex of HD human brain	109
Figure 2.12	Negative control immunostaining of superior frontal cortex blocks	110
Figure 2.13	G3BP1 immunostaining of superior frontal cortex blocks	111
Figure 2.14	Increased G3BP1 SG density in the superior frontal cortex of HD human brain (control samples)	112
Figure 2.15	Increased G3BP1 SG density in the superior frontal cortex of HD human brain (control samples; continued from Figure 2.14)	113
Figure 2.16	Increased G3BP1 SG density in the superior frontal cortex of HD human brain (HD samples; continued from Figure 2.15)	114
Figure 2.17	Increased G3BP1 SG density in the superior frontal cortex of HD human brain (HD samples; continued from Figure 2.16)	115
Figure 2.18	G3BP1 SGs colocalize with translation initiation factor eIF3H in the superior frontal cortex of HD patients	116
Figure 2.19	Highly immunoreactive G3BP1 positive cells have pyramid-shaped cell bodies and express CaMK2	117
Figure 2.20	Characterization of CSF EV concentration and size using Nanoparticle Tracking Analysis	118
Figure 2.21	Average size distribution curves of individual CSF EV samples	119
Figure 2.22	EV miRNAs in the CSF of HD patients target SG-related mRNAs that are differentially expressed in the prefrontal cortex of HD patients	120

Figure 2.23	Selection of G3BP1-targeting miRNAs for overexpression studies in HEK293T cells	121
Figure 2.24	Downregulation of G3BP1 protein levels by overexpression of synthetic miRNAs in 293T cells	122
Figure 2.25	G3BP1-mediated SG induction is regulated by miRNAs in 293T cells treated with sodium arsenite	123
Figure 2.26	G3BP1-mediated SG induction is regulated by miRNAs in 293T cells treated with sodium arsenite (unstressed condition)	124
Figure 3.1	MG132-dependent proteostatic stress results in mislocalization of hnRNPA2B1 in rat CPECs expressing mHTT	156
Figure 3.2	Inhibiting protein SUMOylation in Z310 rat CPECs results in mislocalization of hnRNPA2B1 into cytoplasmic puncta	157
Figure 3.3	Potential reduction of hnRNPA2B1 protein levels in HD patient-derived postmortem CSF EVs	158
Figure 3.4	Human-derived iPSCs and H1 ESCs throughout BMP4-induced CPEC derivation	159
Figure 3.5	CPEC marker immunoreactivity in iPSC- and H1 ESC-derived CPECs at final day of derivation	160
Figure 3.6	Control 33Q iPSC-derived CPECs express characteristic CPEC markers	161
Figure 3.7	Potential tight junction and cilia formation deficits in HD iPSC-derived CPECs	162
Figure 3.8	General TTR expression in 33Q control iPSC-derived CPECs using the clump-seeding (basic neural induction) approach versus the single-cell seeding (SMADi neural induction) approach	163
Figure 3.9	Discrepancy among CPEC markers in iPSC-derived CPEC cultures using the single-cell seeding, SMADi neural induction approach	164

LIST OF TABLES

		Page
Table 1	Evidence for SGs in various models of HD	31
Table 1.1	Break methods optimized for detection of specific mHTT species	65
Table 1.2	mHTTex1p size fluctuation due to CAG repeat length	66
Table 1.3	Summary heat map of mHTTex1p detected using various break methods and assays at 5, 7, 9, and 11 weeks of age	67
Table 2.1	Patient brain tissue samples	126
Table 2.2	Differentially expressed miRNAs in the prefrontal cortex of HD patients that are predicted to target G3BP1	127
Table 2.3	CSF EV miRNAs from HD vs. control differential expression analysis with P values <0.05, prior to correcting for multiple tests with the Benjamini-Hochberg method	128
Table 2.4	CSF EV miRNAs from HD vs. control differential expression analysis with a log2FoldChange larger than a magnitude of two	129
Table 2.5	Filtered miRNAs from miRNA-mRNA overlap analysis	131
Table 2.6	Top 10 GO terms for biological process, cellular component, and molecular function, using the predicted gene targets of the final 41 filtered CSF EV miRNAs	132
Table 2.7	List of primary antibodies used for tissue staining and western blotting	133
Table 2.8	miRCURY LNA miRNA mimics used in 293T cell transfection studies	134

LIST OF ABBREVIATIONS

AD	Alzheimer's disease
AE2	Anion exchange protein 2
AGE	Agarose Gel Electrophoresis
AGO	Argonaute
ALS	Amyotrophic lateral sclerosis
AQP1	Aquaporin 1
ARL13B	ADP-ribosylation factor-like protein 13B
BMP	Bone morphogenetic protein
CaMK2	Ca^{2+}/calmodulin-dependent protein kinase 2
CCT	Chaperonin containing TCP-1
ChP	Choroid plexus
CPECs	Choroid plexus epithelial cells
CSF	Cerebrospinal fluid
eIF2A	Eukaryotic translation initiation factor 2 subunit 1
eIF3H	Eukaryotic translation initiation factor 3 subunit B
ESCs	Embryonic stem cells
FRα	Folate receptor alpha
G3BP1	Ras GTPase-activating protein-binding protein 1
GO	Gene Ontology
hnRNPA2B1	Heterogenous nuclear ribonucleoprotein A2 B1
HD	Huntington's disease
HMW	High Molecular Weight
HTT	Huntingtin
iPSC	Induced pluripotent stem cell
LPS	Lipopolysaccharide
mHTT	Mutant huntingtin
miRNA	Micro ribonucleic acid
MVs	Microvesicles
MVBs	Multivesicular bodies
MSN	Medium spiny neurons
P Bodies	Processing bodies
PLD	Prion like domain
RBD	RNA binding domain
RBP	RNA binding protein
NT	Non transgenic
polyQ	Polyglutamine tract
SGs	Stress granules
SFEBq	Serum-free floating culture of embryoid body-like aggregates
SUMO	Small ubiquitin-like modifier
SIM	Sumo interaction motif
TIA1	Cytotoxic granule-associated RNA binding protein
TTR	Transthyretin

ACKNOWLEDGEMENTS

I thank the members of my committee for their support and feedback. To Dr. Christie Fowler, thank you for your mentorship during my first graduate school rotation, and for sharing your knowledge of extracellular vesicles with me. To Dr. Edwin Monuki, thank you for sharing your knowledge of the choroid plexus and for your collaboration. I am grateful for having crossed paths with both of you early in my graduate school journey.

Dr. Leslie Thompson, thank you for welcoming me into your laboratory and taking a chance on me. Thank you for believing in me throughout these last six years of personal and scientific growth, and for allowing me to apply my creativity into my scientific work. I will be forever grateful to you for your kindness and support.

To my collaborators, thank you for your support and scientific input. Particularly to Drs. Edward Wild, Robert Spitale, and Whitney England, thank you for helping make my study of miRNAs a possibility. To the New York Brain Bank, the New Zealand Neurological Foundation Human Brain Bank, CHDI and HDClarity, and all of the individuals who make these resources a possibility, thank you for helping make our research applicable to human patients. Most importantly, to all of the patient donors and their families, thank you for joining our quest to find a cure for future generations.

Thank you to the entire Thompson Laboratory for their support towards this work, and for listening to my weird life stories. In particular, I would like to thank Dr. Jack Reidling for his scientific and life advice – I would not have been able to get to this point without your support. To Alice Lau and Iliana Herrera, thank you for your technical assistance and hard

work, I would not have been able to do any of the “mouse work” without your help. To Thai Nguyen, thank you for all of the scientific discussions regarding stress granule biology and the enthusiasm you bring to this work. To Dr. Ryan Lim, thank you for always checking in to see how I was doing and being so willing to help. To Keona Wang, thank you for your friendship, companionship, and midnight gym runs after long days in lab. To Eva Morozko, I am very fortunate for having had the chance to experience this journey with you.

I want to thank my family for their support. I especially want to thank my father for his hard work and determination to succeed, despite the countless obstacles that have crossed his path. Thank you for giving me the gift of starting a new life with endless opportunities. To my friends, especially BPINP and Kirstie Salinas, thank you for all the laughs and dancing – I have made it past the rough patches thanks to you.

This work was supported in parts by NIH TL1 (TL1 TR001415), T32 (1T32NS082174), and NINDS (5P01NS092525). Thank you to the IOS Press and the Journal of Huntington’s disease for permission to include copyrighted figures and text in Chapter 1 of this dissertation.

CURRICULUM VITAE
Isabella Inez Sanchez

EDUCATION

M.D., 2020-Present
University of California, Irvine
Ph.D., Biological Sciences, (2014-2020); GPA 3.98
University of California, Irvine
M.S., Biological Sciences (Ph.D. Track), 2014-2017
University of California, Irvine
B.S., Physiology & Neuroscience, (2009-2014); GPA 3.66
B.S., Cognitive Science w/Spec. in Neuroscience,
University of California, San Diego

AWARDS & FELLOWSHIPS

- **Provost Honors, UCSD** (10 academic quarters, 2010-2014)
- **Provost Honors List, UCSD** (2012-2013)
- **Erion Scholarship, UCSD** (2013-2014)
- **UCI Diversity Recruitment Fellowship,** UCI (2014-2015)
- **Disorders and Stroke (NINDS/NIH) Training Grant Pre-Doctoral Fellowship (Award# NS082174), UCI** (2016-2017)
- **Gordon Research Conference Travel Fellowship** (2017)
- **(NIH/NCATS) Institute of Clinical and Translational Science Training Grant Pre-Doctoral Fellowship (TL1TR001415), UCI** (2018-2020)
- **Renee Harwick Advanced Graduate Student Award** (2019)
- **Granville and Sidney Kirkup Fellowship in Medicine** (2020-2021)

RELEVANT EXPERIENCE & PROFESSIONAL DEVELOPMENT

Volunteer Clinical Research Assistant, March 2018-January 2020
Translational Neurobiology Laboratory, Dr. Michael Yassa, UCI

Advanced Course on Non-Coding RNA, May 26-June 2, 2018
Neuroscience School of Advanced Studies, Italy

Clinical Shadowing with Dr. Neal Hermanowicz, December 2017-November 2019
Health Sciences Clinical Professor, Neurology, UCI School of Medicine

Volunteer Clinical Trial Data Entry Assistant, August 2017-November 2017
UC Irvine Neurology Clinical Trials Unit, UCI School of Medicine

Activate to Captivate Public Speaking Workshop, January 2016-February 2016
Graduate Resource Center, UCI

Trainee, October 2015
CIRM Stem Cell Techniques Course, Stem Cell Research Center, UCI

RESEARCH EXPERIENCE

Graduate Research, March 2015-Present
Thompson Laboratory, Department of Neurobiology & Behavior, UCI

Identified stress granule pathology in the brains of Huntington's disease mouse models and human patients, and proposed the involvement of CSF extracellular vesicle miRNAs in the propagation of brain pathology.

Rotating Graduate Student Researcher, January 2015-March 2015
Blurton-Jones Laboratory, Department of Neurobiology & Behavior, UCI

Performed stereotaxic xenotransplantations of Alzheimer's disease patient-derived iPSC-neurons into immunodeficient mice to investigate specific neuronal cell type vulnerability.

Rotating Graduate Student Researcher, September 2014-December 2015
Fowler Laboratory, Department of Neurobiology & Behavior, UCI

Utilized retrograde tracing techniques to identify hippocampal-habenular neuronal pathways activated by nicotine stimulation in mice.

Undergraduate Research, September 2011-August 2014
Hamilton Laboratory, Department of Cellular & Molecular Medicine, UCSD

Utilized immunofluorescence techniques to investigate the role of Zfp423 in adult neurogenesis at the subventricular zone of the lateral ventricles in mice.

TEACHING/MENTORING EXPERIENCE

Teaching Assistant	Sensation & Perception	UCSD	2011
Teaching Assistant	Neuroanatomy & Physiology	UCSD	2013
Laboratory Tour Day	Histological Techniques	UCI	2015
Teaching Assistant	Neurobiology & Behavior	UCI	2016
Teaching Assistant	Neurobiology & Behavior	UCI	2016
Laboratory Tour Day	Histological Techniques	UCI	2016
Teaching Assistant	Neurobiology Laboratory	UCI	2017
Research Mentor	Biology Undergraduate Student	UCI	2018

PUBLIC SERVICE

Public Outreach Ambassador, October 2017-Present
Center for the Neurobiology of Learning and Memory, UC Irvine

Mentor, October 2018-December 2018
Brain Explorer Academy, UC Irvine

Coordinator, September 2017-June 2018
NeuroBlitz Seminar Series, UC Irvine

Mentor, November-January 2017
Project Together, Mental Health Association of Orange County

Mentor, January 2017-March 2017
Minorities in STEM Mentorship Program, UC Irvine

Science Blog Writer, May 2015-June 2016
http://recreationalscience.tumblr.com/

Recreational Therapist Volunteer Assistant, June 2011-Dec. 2013
UCSD Medical Center, Psychiatry Department, San Diego, CA

Tutor, April 2011- June 2011
Preuss School, UC San Diego, La Jolla, CA

Member, May 2011- October 2011
Revelle Community Outreach Organization, La Jolla, CA

PRESENTATIONS & PUBLICATIONS
Conference Presentations

Sanchez, I.; Nguyen, T.B.; England, W.; Byrne, L.; Spitale, R.; Wild, E.; Monuki, E.; Thompson, L.M. **Potential role of the choroid plexus and CFS secretion in Huntington's disease pathogenesis.** Poster presentation, The Society for Neuroscience 50th Annual Meeting, October 19-23, 2019. Chicago, IL, USA.

Clemson; M. Coburn; M. Farrell; A. Frithsen; M. Gomez; J. Hasselmann; C. Henningfield; V. Lallai, A. McQuade, M. Montchal, L. Nguyen, J. Noche, J. Quintanilla, M. Ren, J. Sanchez, I. Sanchez, B. Siddiqui, A. Smith, M. Yassa. **The brain explorer academy: an 8-week program for children in brain science, scientific communication and critical thinking skills.** Brain Awareness Campaign Event (Action and Potential in Outreach, Education, and Research). The Society for Neuroscience 49th Annual Meeting, Nov. 3-7, 2018. San Diego, CA. USA.

I. Sanchez; T. Nguyen; R. Lim; W. England; L. Byrne; R. Spitale; E. Wild; L.M. Thompson. **Altered miRNA profiles in cerebrospinal fluid exosomes from Huntington's disease patients**. Poster Presentation. Hereditary Disease Foundation Conference. Jun 8-11, 2018. Cambridge, MA. USA.

Overman, J.; Sanchez, I.; Tan, Z.; Lau, A.; Joachimiak, L.A.; Crook, Z.; Ochaba, J.; Tomlinson, A.; Zhao, X.; Reidling, J.C.; Frydman, J.; Wu, C.; Mobley, W.C.; Housman, D.E.; Thompson, L.M. **Delivery of ApiCCT1 as a therapeutic for Huntington's Disease.** Poster Presentation. Gordon Research Conference on CAG Triplet Repeat Disorders. Jun 2-9, 2017. Mt. Snow, VT. USA.

Flores-Garcia, L.; Ray, J.; Cao, K.; Xie, W.; Sanchez, I.; Alcaraz, W.A.; Raponi, E; Hou, A.; Gage, F.H.; and Hamilton, B.A. **Zinc finger protein 423 integrates signaling pathways by the niche and targets hedgehog signaling gene expression during adult neurogenesis.** Nanosymposium presentation, The Society for Neuroscience 43rd Annual Meeting. Nov 9-13, 2013. San Diego, CA. USA.

Sanchez, I.; Flores-Garcia, L.; Cao, K.; Xie, W.; Hamilton, B.A. **Quantification of adult neural stem and progenitor cells in the *Zfp423*^{nur12} ventricular zones of the lateral ventricle.** Poster presentation, Annual Biomedical Research Conference for Minority Students. Nov. 13-16, 2013. Nashville, TN, USA.

Departmental Presentations

Sanchez, I.; Nguyen, T.; Byrne, L.; Monuki, E.; Wild, E.; Thompson, L. **Altered miRNA profiles in cerebrospinal fluid extracellular vesicles from Huntington's disease patients.** Oral presentation (invited speaker), REMIND 10th Annual Emerging Scientists Symposium, UCI MIND. February 11, 2019. Irvine, CA. USA.

Sanchez, I.; Nguyen, T.; Byrne, L.; Monuki, E.; Wild, E.; Thompson, L. **Investigating the CSF extracellular vesicle miRNA signature from Huntington's disease patients.** Oral presentation, Neuroblitz Seminar. October 26, 2018. Irvine, CA. USA.

Sanchez, I.; Lim, R.; Razifar, M.; Byrne, L.; Wild, E.; Thompson, L. **Altered extracellular vesicle miRNA profiles in cerebrospinal fluid from Huntington's disease patients.** Oral presentation, Neuroblitz Seminar. February 28, 2018. Irvine, CA. USA.
Sanchez, I.; Razifar, M.; Thompson, L. **Exosome secretion and Huntington's disease.** Oral presentation, Neuroblitz Seminar. February 22, 2017. Irvine, CA. USA.

Sanchez, I.; Geater, C.; Thompson, L. **Establishing a read-out for dysfunctional proteostasis in neuronally differentiated iPS cells from Huntington disease patients.** Oral presentation, Neuroblitz Seminar. April 27, 2016. Irvine, CA. USA.

Sanchez, I.; Torres, M.; Blurton-Jones, M. **Neuronal differentiation, characterization, and transplantation of human induced pluripotent stem cells.** Oral presentation, Neuroblitz Seminar. April 22, 2015. Irvine, CA. USA.

Publications

Morozko, E.L.; Ochaba, J.; Hernandez, S.J.; Lau, A.; Sanchez, I.; Orellana, I.; Kopan, L.; Crapser, J.; Duong, J.H.; Overman, J.; Yeung, S.; Steffan, J.S.; Reidling, J.; Thompson, L.M. **Longitudinal Biochemical Assay Analysis of Mutant Huntingtin Exon 1 Protein in R6/2 Mice.** J Huntingtons Dis. 2018; 7(4):321- 335. PMID: 30452420.

Work in Progress

Sanchez, I.; Nguyen, T.B.; England, W.; Lim, R.G.; Vu, A.Q.; Miramontes, R.; Byrne, L.; Lau, A.; Orellana, I.; Yeo, G.W.; Fowler, C.; Curtis, M.A.; Faull, R.L.M.; Reidling, J.; Wild, E.; Spitale, R.; Thompson, L. **G3BP1-positive stress granule pathology in Huntington's disease.** *Manuscript under revision.*

PROFESSIONAL MEMBERSHIPS

Society for Neuroscience 2018-Present

Initiative for Maximizing Student Development Program (IMSD) 2011-2014

ABSTRACT OF THE DISSERTATION

G3BP1-positive stress granule pathology in brains of Huntington's disease mice and human patients and a potential role for extracellular vesicle-derived miRNA regulation

By

Isabella Inez Sanchez

Doctor of Philosophy in Biological Sciences

University of California, Irvine, 2020

Professor Leslie M. Thompson, Chair

Stress granules (SGs) are membraneless organelles that form in response to cellular stress. Chronic cellular stress associated with neurodegenerative disease results in the persistence of SG structures. Chronic expression of mutant huntingtin generates various forms of cellular stress, including activation of the unfolded protein response and oxidative stress. However, it has yet to be determined whether SGs are a feature of Huntington's disease (HD) neuropathology. For my dissertation, I investigated localization and levels of the SG nucleating protein G3BP1 and found a significant increase in the density of G3BP1-positive SGs in the cortex and hippocampus of R6/2 transgenic mice, as well as in the superior frontal cortex of HD patient brains. I also examined the miRNA composition of extracellular vesicles (EVs) present in the cerebrospinal fluid (CSF) of HD patients and show that a subset of their target mRNAs is differentially expressed in the prefrontal cortex of HD patients. Of these targets, there is an enrichment of SG components, including G3BP1.

These findings suggest that SG dynamics might play a role in the pathophysiology of HD. Lastly, because the majority of the CSF is produced by choroid plexus epithelial cells, and a significant portion of CSF EVs likely originate from CPECs, I initiated the generation induced pluripotent stem cell (iPSC)-derived CPECs from HD and control lines that will allow for future mechanistic studies of EV secretion. Together, my work provides evidence of a potential role for CSF EV miRNAs in the regulation of SGs, identifies specific miRNAs that modulate the SG component G3BP1, and demonstrates feasibility for the generation of an iPSC-derived CPEC model.

INTRODUCTION

A. Huntington's disease

Huntington's disease (HD) is an autosomal dominant neurodegenerative disease that broadly impacts patients' functional abilities via the manifestation of chronic and progressive involuntary movements, cognitive impairment, and psychiatric disturbances. HD is caused by an expanded CAG repeat in exon 1 of the *HTT* gene (The Huntington's Disease Collaborative Research Group, 1993). CAG repeats of 40 or more are associated with disease expression, repeats of 26 or less are not (Myers, 2004), and CAG repeats in the 36 to 39 range are associated with reduced penetrance (Rubinsztein et al., 1996). CAG repeats in the 27 to 35 range are not associated with disease expression, however these can be meiotically unstable in paternal transmission and result in the inheritance of disease-associated repeats of 40 or more (Trottier et al., 1994). There is an inverse dependency upon repeat length that impacts the age of onset, and CAG repeats of 60 and higher result in juvenile disease onset (Andresen et al., 2007). However, age of disease onset cannot be fully predicted from CAG repeat length (Wexler et al., 2004) and genetic modifiers are being discovered through GWAS and whole genome sequencing patient studies (GeM-HD, 2015, 2019).

The CAG-repeat expansion is a characteristic shared by other neurodegenerative diseases, including six spinocerebellar ataxias, Kennedy's disease (spinal bulbar muscular atrophy) and DRPLA (dentatorubral-pallidoluysian atrophy) (Reddy et al, 1997; Paulson et al, 2009; Klockgether et al., 2019). In HD, disease is primarily driven by a 'gain of function', however it is becoming clear in recent years that disease also involves 'loss of function' of wild type HTT (Schulte et al, 2011; Cisbani et al, 2012; Saudou et al., 2016). Wild-type HTT is mainly

localized in the cytoplasm, but shuttles between the cytosol and nucleus (Truant et al, 2007; Desmond et al, 2013). However, mHTT progressively accumulates in the nucleus (DiFiglia et al, 1997; Sharp et al 1995; Martindale et al, 1998; Hackam et al, 1999), where it forms insoluble intranuclear inclusions (DiFiglia et al, 1997; Davies et al., 1997). mHTT gives rise to a number of aggregated species, and it is yet to be determined which species confer toxicity and which are neuroprotective (Arrasate et al, 2014; Poirier et al, 2002; Legleiter et al, 2010; Zhang et al, 2011). Various reports support the idea that soluble oligomers are a major culprit of cytotoxicity (Takahashi et al., 2008; Lajoie et al., 2010; Leitman et al., 2013), and include an experiment where a mutation in the N17 N-terminal region preceding the disease-associated CAG expansion prevented the formation of large aggregates but not oligomers, leading to an increase in toxicity in a drosophila HD model (Branco-Santos et al., 2017). However, the formation of insoluble intranuclear inclusions has also been found to play a role in cellular dysfunction (Bauerlein et al., 2017; Ramdzan et al., 2017; Hosp et al., 2017).

Neuropathological analysis of post-mortem brains from HD patients reveals profound degeneration of neurons in the striatum (Vonsattel et al., 1985) and various regions of the cortex with a variable pattern of pathology that reflects the variability of symptomatology found in HD patients (Waldvogel et al., 2015). There is also evidence for loss of neurons in other regions of the brain, including the globus pallidus, hypothalamus, and hippocampus (Singh-Bains et al., 2016; Petersen et al., 2005; Spargo et al. 1993), suggesting the potential involvement of propagation of protein pathology between different brain regions as the disease progresses (Park, 2017). In fact, the propagation of mHTT has been detected in three different neural network models: human neurons integrated into HD mouse model

organotypic slices, an *ex vivo* corticostriatal slice model, and the corticostriatal pathway *in vivo* (Pecho-Vrieseling et al., 2014). In another study, exosomes isolated from the conditioned media of HD patient-derived fibroblasts were shown to transmit protein aggregates to healthy host tissue, resulting in motor and cognitive impairments in wild-type mice (Jeon et al., 2016). Finally, a recent study using a parabiosis approach to join the circulatory systems of zQ175 mice with their wild-type littermates revealed that blood serves as a vehicle for the propagation of mHTT, and that healthy blood can rescue some of the pathology seen in HD mice such as blood brain barrier (BBB) leakage and of mHTT aggregate levels (Rieux et al., 2020). The continuation of these exciting investigations will allow us to better understand the mechanisms underlying mHTT propagation and to identify new therapies for disease intervention.

Huntington's disease models and potential therapies

Transgenic mouse models were generated after the discovery of the mutation that causes HD to enable the investigation of molecular pathology and the pre-clinical testing of potential therapies to delay disease onset or slow its progression (Menalled et al., 2002). The R6/2 line, transgenic for the 5' end of the human *HTT* gene carrying 115-150 CAG repeat expansions (Mangiarini et al., 1996), is perhaps the most extensively characterized and used in HD research. These mice exhibit many of the features of HD symptomatology, including impaired movements, involuntary stereotypic movements, tremor, epileptic seizures, and non-movement disorder components (Mangiarini et al., 1996). While these mice exhibit minimal neuronal death, postmortem examination suggests that mHTT accumulates in the nucleus and forms inclusions, reminiscent of those found in the brains of human patients (DiFiglia et al., 1997), as early as 7 weeks of age (Davies et al., 1997).

They also display enlargement of ventricles and brain volume loss. Disease progression in this mouse model is aggressive and rapid, resulting in premature death somewhere between 13-16 weeks of age (Li et al., 2005). Based on this rapid progression and close recapitulation of the later stage human disease, in particular juvenile repeat onset disease, these mice have been used in many studies as a first step to investigate potential treatments (Gil et al., 2008). Despite efforts, there has not yet been a therapy that has successfully translated from animal models to humans, likely due to the difficulty in extrapolating data from animal studies to therapeutic effects in humans and from the fact that to date, there have not been any disease modifying therapies that could inform the most relevant endpoints.

The advent of induced pluripotent stem cell (iPSC) technology (Takahashi et al., 2006) has the potential to provide an understanding of disease pathogenesis in humans at the cellular level. Indeed, iPSC technology has been adopted by the HD field, and has provided invaluable information regarding disease signatures in the affected cell types (e.g. An et al., 2012; Jeon et al., 2012; HD iPSC Consortium 2012 and 2017; Szlachcic et al., 2015; Mattis et al., 2015; Lim et al, 2017). These cells can also be used to assess the therapeutic potential of HD modifiers (Perrier et al., 2012; Engle et al., 2013).

Preventing or reversing the disease is the most pressing unmet need in HD. Many promising clinical trials are underway (Caron et al., 2018), including the IONIS-HTT$_{RX}$ clinical trial for lowering mHTT levels through the degradation of the *HTT* RNA transcript using antisense oligonucleotides (ASOs) (Tabrizi et al., 2019). Because the ASOs do not cross the BBB, they are delivered via intrathecal infusion and will likely require patients to

receive life-long administration. Studies in non-human primates have shown that the ASOs are distributed unevenly throughout the brain, with higher HTT suppression in superficial regions of the cortex and spinal cord compared to deeper cerebral structures such as the striatum. Data from the Phase 1/2a clinical trial led by Ionis Pharmaceuticals demonstrated that the ASO is well tolerated at all doses tested and reduces mHTT levels in the cerebrospinal fluid (CSF) in a dose-dependent manner with mean reductions of ~40% in the CSF of participants treated for 3 months with the two highest doses (Tabrizi et al., 2019). Because this is a non-selective allele targeting approach, both mHTT and wild type HTT levels are reduced, raising potential concerns regarding the functional impact this may have on patients as HTT is a highly conserved and ubiquitous protein with essential roles in multiple cellular processes (Saudou et al., 2016). Other clinical trials are exploring allele-selective approaches to overcome this issue (Tabrizi et al., 2019).

The translation of any therapeutic strategy to the clinic will likely depend on the development of a battery of well characterized biomarkers to test their efficacy. Outcome measures used to assess effect of treatment were once solely based on clinician-derived scores such as the Unified Huntington's Disease Rating Scale (UHDRS) (Huntington Study Group, 1996) or a new composite score that incorporates cognition (Schobel et al., 2017), however studies are underway to identify and implement objective biological biomarkers, such as the detection of mHTT protein levels to assess knockdown in the IONIS-HTT_{RX} clinical trial. Studies to identify potential biomarkers are underway, and include clinical, imaging, electrophysiological, biochemical, and pharmacodynamic measures (Bates et al., 2015). Potential biochemical markers hold great promise, and include the measurement of neurofilament and clusterin in blood plasma and/or CSF (Byrne et al., 2017;

Constantinescu et al., 2009; Dalrymple et al., 2007). A better understanding of CSF dynamics and CSF components will be imperative for therapeutic development.

CSF is in direct contact with the extracellular space and reflects many biological changes occurring in the brain. The stability of extracellular vesicles (EVs) in CSF, including exosomes, allows for their efficient isolation and makes them a good starting point for studies on disease evaluation and biomarker development. Recently, exosomal miRNAs found in CSF and blood have been studied for their potential use as biomarkers for neurodegenerative diseases including Alzheimer's and Parkinson's disease (Lugli et al., 2015; Gui et al., 2015; Cao et al., 2017). Although exosomal miRNAs have not been described to date for HD, Hoss et al. (Hoss et al., 2015) identified miRNA changes in blood plasma that recapitulate some of the miRNA changes observed in the brains of HD patients. The potential use of exosomal miRNA as biomarkers for HD holds great promise, and the benefit from such studies can extend beyond biomarker development by allowing us to understand how transcriptional dysregulation in HD may be mediated via RNA silencing by cell extrinsic mechanisms.

B. The choroid plexus, cerebrospinal fluid, and exosome secretion

The choroid plexus and cerebrospinal fluid

Although HD is characterized by pathology that most prominently impacts neurons of the striatum, human autopsy studies have shown that other brain areas may be affected as disease progresses, and cell-to-cell propagation of some pathologies (Vonsattel and DiFiglia 1998; Bayram-Weston et al., 2012) may be occurring via exosomes (Zhang et al., 2016; Jeon et al., 2016), possibly secreted from tissues such as the ChP. The ChP is a highly specialized

secretory tissue found in the ventricles of the brain. It is composed of an external monolayer of choroid plexus epithelial cells (CPECs) joined by tight junctions, which surround fenestrated capillaries, connective tissue, and specialized leptomeningeal cells (Thouvenot et al., 2006). Following Harvey Cushing's discovery that the ChP secretes CSF (Cushing et al., 1914), early electron microscopy studies began to expand our understanding of CPECs, highly specialized ependymal cells with morphological similarities to that of many epithelial tissues (Maxwell et al., 1956). We now know that, in humans, the ChP secretes about 400-600 mL CSF per day, and CPECs replenish the CSF by maintaining the necessary ionic gradient to drive secretion of water from the blood in ChP capillaries to CSF in the ventricles (Emerich et al., 2005). The CSF serves as a fluid cushion for the brain, regulating neural stem cells, critical periods during development, and overall health of the nervous system via the secretion of various factors, including transport proteins and neurotrophic factors (Lun et al., 2015). CSF flows from the lateral ventricles to the third ventricle, then to the fourth ventricle and into the central canal of the spinal cord or the subarachnoid space, where it is resorbed. Pathology of the ChP has been linked to aging and various central nervous system diseases, including ALS: upregulation of lysyl oxidase in mouse models and patients (Li et al., 2004; Uchino et al., 2004), AD: atrophy, decreased CSF production, diminished polypeptide synthesis and metabolic activity (Serot et al., 2000; Wen et al., 1999) and HD: enhanced immunostaining of 3-nitrotyrosine in a mouse model (Deckel et al., 2001). However, factors secreted by the ChP, possibly via exosomes, may also protect striatal neurons from excitotoxic damage as suggested by the reduction of cell loss and behavioral deficits in a quinolinic acid toxin HD rat model by transplantation of ChP from neonatal pigs (Borlongan et al, 2008).

Extracellular vesicles and exosomes

EVs are membrane bound vesicles that serve as an important mode of cell-to-cell communication, and are generally classified into three categories: exosomes (30-200 nm), microvesicles (MVs) (200-1,000 nm), and apoptotic bodies (0.5-3 um) (Colombo et al., 2014). Although there is a degree of overlap in vesicle size and contents between exosomes and MVs, with apoptotic bodies being larger cell fragments containing various cellular components (Elmore et al., 2007), specific EV subtypes originate from different mechanisms of biogenesis. While MVs and apoptotic bodies are directly released from the plasma membrane from living and dying cells, respectively, exosomes are released after multivesicular bodies (MVBs) fuse with the plasma membrane (Hessvik et al., 2017). The term exosome was first coined in 1981 (Trams et al., 1981), and referred to 40-1,000 nm vesicles secreted by a variety of cultured cells. Three years later, the term was used to define cup-shaped, 40-100 nm vesicles of MVB origin secreted during reticulocyte differentiation (Harding et al., 1984; Pan et al., 1983). However, the field of extracellular vesicles has not reached a consensus as to the universally accepted definition for exosomes (Gould et al., 2013). For this reason, a set of minimal experimental requirements have been established by the International Society for Extracellular Vesicles (ISEV) in order to start to facilitate the establishment of universally accepted definitions for extracellular vesicles and their functions (Lotval et al., 2014). First, EVs must be isolated from extracellular fluids with minimal prior mechanical disruption. Although there is no “gold-standard” method for isolation, the optimal isolation method depends on the scientific questions asked and the downstream applications being used. However, the method(s) used should be described in detail to allow for interpretation and replication by other investigators. Further, although

certain proteins have been shown to be specifically expressed in exosomes, these should not be mistaken as "exosome-specific" proteins, as they are also expressed in other EV subtypes. Thus, it is suggested that publications report both the presence of markers that are expected to be expressed, as well as those that are unique and not previously shown to be enriched in the EV subtype being investigated. For example, proteins such as the tetraspanin CD81, and endosomal proteins TSG101 and Alix are expected to be enriched in exosomes, while the mitochondrial marker Cytochrome C is not. In addition, including the exosome free fraction in quantitation studies, such as western blots, is helpful in order to control for antibody specificity and background functional activity of the extracellular fluid being used. Lastly, it is suggested that the EV fraction be characterized by at least two methods, such as electron microscopy and Nanoparticle Tracking Analysis, in order to identify the heterogeneity of the EV preparation.

Despite the lack of agreement, it is generally accepted that exosomes are released by several cell types, including cells of hematopoietic origin, cytotoxic T cells, mast cells, platelets, intestinal epithelial cells, and neural cells (Simons and Raposo, 2009; Thery et al., 2009). Exosomes have now been isolated from various body fluids, including blood (Caby et al., 2005), urine (Pisitkun et al., 2004), saliva (Ogawa et al., 2011), and CSF (Vella et al., 2007). Furthermore, exosomes from body fluids contain miRNA and mRNA (Hunter et al., 2008; Rabinowitz et al., 2009). Interestingly, comparisons between a cell type's RNA content and its exosomal RNA content demonstrate that specific groups of RNAs are selectively enriched in exosomes (Ratajczak et al., 2006; Nolte-'t Hoen et al., 2012), suggesting that RNA loading of exosomes is regulated by specific mechanisms.

Exosome secretion by the choroid plexus and choroid plexus epithelial cells

A study by Tietje et al., 2016 found that human CSF EVs contain miRNAs bound to the RNA binding protein (RBP) heterogenous nuclear ribonucleoprotein A2/B1 (hnRNPA2B1), which has previously been identified as a key player in the active sorting of miRNAs into exosomes (Villarroya-Beltri et al., 2013). Tietje et al. report that these EVs show an age dependent decline, with individuals <2 years having higher levels by 81% compared to individuals >70 years. Furthermore, they show human CPECs secrete EVs at an average of 559.1 ($x10^9$) EVs per mL, and produce hnRNPA2B1-miRNA containing EVs in vitro (Tietje et al., 2014). Because CPECs have a highly secretory function and are the main producers of CSF (Brown et al., 2004; Redzic et al., 2005; Emrich et al., 2005), and CSF contains EVs (Vella et al., 2007; Harrington et al., 2009; Street et al., 2012) CPECs likely play an important role in cell-to-cell communication mediated by the CSF. Altogether, these findings suggest that CPECs can serve as a promising platform for the investigation of EV miRNA secretion into the CSF in both health and disease conditions.

Additional findings suggest that CPEC EV secretion into the CSF plays an important role in intercellular communication between different brain regions. Firstly, the ChP has been shown to transfer folate via CSF EVs to brain parenchyma (Grapp et al., 2013). The folic acid derivative 5MTHF is distributed to all major organs via the bloodstream, and a decrease in its concentration in the CSF has been associated with functional loss of the folate receptor FRα, which results in childhood neurodegenerative disease caused by mutations in the *FOLR1* gene (Steinfeld et al., 2009; Grapp et al., 2012). The authors show that 5MTHF transport into the CSF is mediated by FRα binding. Intriguingly, they show that FRα is transported from the basolateral to the apical membrane of rat CPECs via

intraluminal vesicles within MVBs, and are secreted with exosomes into the CSF, which enter the brain parenchyma and target both neurons and glia. Although these studies were done using murine models, FRα was also found to be expressed in human CSF exosomes.

Lastly, a recent study suggests that exosome mediated miRNA secretion by the ChP has a functional impact on nearby tissues. In this study, secretion of miR-204 by the ChP was found to regulate adult neurogenesis at the subependymal zone by repressing the translation of neural fate determinants, preventing the activation and subsequent differentiation of quiescent neural stem cells (Lepko et al., 2019). The following section will expand on miRNAs and provide evidence for the potential influence of miRNA dysregulation on aberrant transcriptional signatures observed in HD.

C. micro RNAs

Based on findings such as the ones mentioned above, it is becoming more evident that EV miRNAs play an important role in intercellular communication and are candidates for biomarker development in disease. miRNAs, small interfering (siRNAs), and PIWI-interacting RNAs (piRNAs) are the three major small silencing RNAs in animals (Ghildiyal et al., 2009). miRNAs are small RNA molecules (~22 nucleotides) that regulate post-transcriptional gene expression by acting as guide molecules to promote the degradation or translational repression of their target mRNAs. miRNAs are generated from short RNA hairpins transcribed by RNA polymerase II (Lee et al., 2004), although alternative mechanisms exist (Yang et al., 2011), and their biogenesis is regulated at the following levels: miRNA transcription, processing by RNase III proteins - Drosha in the nucleus and Dicer in the cytoplasm, modification by RNA editing, RNA modification (methylation,

uridylation, and adenylation), Argonaute (AGO) loading, and RNA decay (Ha et al., 2014). The average copy number of an individual miRNA is believed to be ~500 per cell (Pritchard et al., 2012), and the human genome encodes ~1000 miRNAs, compared to ~30000 mRNAs. Thus, it is predicted that one miRNA may be responsible for the regulation of hundreds of mRNAs, which is likely to have significant effects on gene expression networks.

miRNAs are one of the largest gene families and have been identified in animals, plants, protists, and viruses (Griffiths-Jones, 2008). The miRNA database (miRBase) has been created to facilitate the investigation of miRNAs, and serves as the central online repository for miRNA nomenclature, sequence data, annotation, and target prediction. The latest release has catalogued 2,588 mature miRNAs in humans; however, the functional importance of most of these miRNAs is yet to be determined. The nomenclature of miRNAs is somewhat inconsistent as a result of when they were discovered. The first miRNA genes to be discovered in early genetic studies were named after their phenotypes; for example, the first miRNA to be discovered was named *lin-4* because its mutation in *C. elegans* leads to abnormal reiterations in cell lineages (Chalfie et al., 1981; Lee et al., 1993). However, most miRNAs discovered through cloning or sequencing have been given numerical names; for example, the mammalian *lin-4* homologue is called *mir-125*. miRNA "sisters" encoded by paralog genes are identified by letter suffixes, such as *mir-125a* and *mir-125-b*. Numeric suffixes are added to the end of the miRNA loci name if the same miRNA originates from multiple separate loci, such as *mir-125b-1* and *mir-125b-2*. Lastly, each locus produces one miRNA from the 5' strand and one from the 3' strand of the precursor, leading to *mir-125a-5p* and *mir-125a-3p*, for example. From this miRNA duplex, one becomes the 'guide' strand

and is usually more prevalent and biologically active than the other 'passenger' strand, also known as miRNA* (Meijer et al., 2014).

miRNA binding sites are highly conserved in protein-coding genes, and are commonly located in the 3' untranslated region (UTR) of mRNAs (Bartel et al., 2009; Friedman et al., 2009). The 5' end of miRNAs (nt 2-7) has been named the 'miRNA seed'; miRNAs sharing the same seed, which are thought to originate from gene duplication (Hertel et al., 2006; Berezikov et al., 2011), belong to the same 'miRNA family'. The miRNA seed is crucial for target recognition, as it is pre-arranged in an A-form helix conformation that facilitates the survey of target mRNAs for sequence complementarity (Wang et al., 2008; Frank et al., 2010). While the 3' end of miRNAs is less important for target recognition, it has been suggested to be a determinant of AGO protein binding specificity (Moore et al., 2015) and be subject to modification events (Burroughs et al., 2010). miRNAs associate with AGO proteins, which function as effectors and facilitate the recruitment of factors necessary for translational repression, mRNA deadenylation, and mRNA decay (Huntzinger et al., 2011).

miRNAs and transcriptional dysregulation in Huntington's disease

The first study to demonstrate dysregulation of miRNAs in HD proposed that increased levels and activity of nuclear Repressor Element 1 Silencing Transcription Factor (REST) in HD leads to increased repression of miRNAs (Johnson et al., 2008). Increased REST levels is associated with the polyglutamine repeat expansion in mHTT, which inhibits HTT's ability to sequester REST in the cytoplasm of neurons (Zuccato et al., 2003). Since then, the field has begun to investigate the potential role of miRNAs on altered mRNA expression consistently observed in HD. Both human and animal studies have shown that there are

significant differences in mRNA expression between HD and control brain samples (Crocker et al., 2006, Luthi-Carter et al., 2002; Sipione et al., 2002; Seredenina et al., 2012; Valor et al., 2015; Labadorf et al., 2015; Agus et al., 2019), with one microarray study using striatal tissue from HD and unaffected individuals reporting that ~100 mRNAs were significantly upregulated, and slightly fewer significantly downregulated in HD (Hodges et al., 2006). Genome-wide analysis of mRNA expression in human prefrontal cortex, which is largely preserved in HD, suggests that most differentially expressed genes are predominantly upregulated (Labadorf et al., 2015). Although a handful of studies have sought to investigate miRNA dysregulation in HD, results vary from study to study, and the field has not reached a consensus as to whether a specific group of miRNAs can be reproducibly identified as biomarkers for HD.

Work by Johnson and colleagues (Johnson et al., 2008) showed that miRNAs *mir-29a*, *mir-124a*, *mir-132*, and *mir-135b* were significantly downregulated in an HD mouse model. They also examined human HD cortex, and found that miRNAs *mir-29a* and *mir-330* were significantly upregulated, while *mir-132* was significantly downregulated. In 2010, Marti et al (Marti et al., 2010) used Illumina's massive parallel sequencing to analyze miRNA populations in the frontal cortex and striatum of HD and control individuals, and through the analysis of upstream regulators, suggested that REST and p53 might have a role in miRNA downregulation observed in HD. In 2011, Soon-Tae Lee et al. used a miRNA microarray approach to show that miRNAs *mir-22*, *mir-29C*, *mir-128*, *mir-132*, *mir-138*, *mir-218*, *mir-222*, *mir-344*, and *mir-674** are downregulated in the striata of two different HD mouse models (Lee et al., 2011). In 2014, Hoss et al. (Hoss et al., 2014) used next-generation miRNA sequencing in human prefrontal cortex and identified miRNAs *mir-10b*-

5p, *mir-196a-5p*, *mir-196b-5p*, *mir-615-3p*, and *mir-1247-5p* as being upregulated in HD. A year later, they showed that miRNA changes observed in brains of HD patients may be detectable in plasma, and identified *mir-10b-5p* and *mir-486-5p* as being increased in human HD brain and blood plasma (Hoss et al., 2015).

The variability between these studies could be explained by the following factors: the model used (animal/cell model or human); the type of tissue or biofluid studied; the brain area studied, and timeline in regards to disease progression; and the sensitivity of the method used to detect miRNA. One potential confound is that studies in striatal tissue is complicated by the significant degeneration and tissue loss in disease. In conclusion, understanding cell-intrinsic miRNA dysregulation in HD will shed light on potential mechanisms leading to the aberrant gene expression phenotypes observed, and will allow us to gain insights into the molecular pathology of HD. Specific cell-extrinsic mechanisms of miRNA dysregulation have not been addressed, however. For example, although the role of exosomal transfer of miRNA via biofluids has been long studied in cancer as potential biomarkers and therapeutic targets (Thind et al., 2016), and is starting to be investigated in other neurodegenerative diseases (Gui et al., 2015; Lugli et al., 2015), it remains to be investigated in the context of HD. Understanding the effect of exosomal miRNAs on recipient cells' gene expression signatures will unravel a new level of complexity to our understanding of the regulatory mechanisms of transcription.

D. Heterogenous nuclear ribonucleoprotein A2/B1

As previously mentioned, RNA loading of exosomes is regulated by specific mechanisms that are largely orchestrated by RBPs such as hnRNPA2B1. In an influential study, it was

found that miRNAs containing a GGAG motif are bound by SUMOylated heterogenous nuclear ribonucleoprotein A2/B1 (hnRNPA2B1), which tags them for trafficking into multivesicular bodies (MVBs) and secretion via exosomes (Villarroya-Beltri et al., 2013). hnRNPA2B1 is a member of the hnRNP family of RNA binding proteins, which shuttle between the cytoplasm and nucleus, and is involved in a variety of post-transcriptional RNA processing events by associating with transcripts, pre-mRNA, and mRNA (Dreyfuss et al., 2002; Matunis et al., 1994). hnRNPs A/B and C were first identified when the 40S core mRNA-protein complex was isolated by sucrose density gradients (Beyer et al., 1977). Subsequently, immunopurification of hnRNP complexes demonstrated that heterogenous nuclear RNA (hnRNA) associates with a subset of abundant proteins in the nucleus, termed hnRNPs and designated A1 through U (Pinol-Roma et al., 1988; Dreyfuss et al., 1988). These findings suggested that hnRNPs share a common function. Indeed, hnRNPs control the maturation of newly formed pre-mRNAs into mRNAs, stabilize mRNA during cellular transport, and control their translation (Dreyfuss et al., 1993).

Four unique RNA binding domains (RBDs) have been identified in hnRNPs, and include the RNA recognition motif (RRM), the quasi-RRM, a glycine-rich domain (GRD), an RGG box, and a K homology domain. However, the RRM is the most common RBD (Geuen et al., 2016), which is characterized by interconnected β-sheets that contribute to its RNA-binding specificity (Gorlach et al., 1992). Importantly, the specificity in RNA binding is heavily dependent on the 3D structure of the protein, and the structural regions surrounding the RBDs seem to be responsible for fine tuning RNA-protein interactions (Geuens et al., 2016). The sequence of the hnRNPA2B1 protein is highly homologous to that of hnRNPA1, which contains two RRMs at the N-terminus, and a GRD at the C-terminus that

is responsible for interactions with other hnRNPs (Burd et al., 1989; Buvoli et al., 1988; Cartegni et al., 1996). The hnRNPA2B1 gene was split into 12 exons and gives rise to two main isoforms, A2 and B1, with the first being a result of alternative splicing and comprising 2-5% of total hnRNPA2B1 transcripts (Kozu et al., 1995). However, later studies found that the relative amounts of hnRNP A2 and B1 differ among different tissues; in neurons, both A2 and B1 isoforms are abundant compared to glial cells, but their ratio varies based on neuron type (Kamma et al., 1999). Moreover, these can have different nuclear localization patterns depending on RNA integrity and active transcription during the cell cycle (Friend et al., 2008). The B1 isoform contains the insertion of 12 amino acids (exon 2) near the N-terminus (Burd et al., 1989). Notably, this insertion is outside of the RRMs and *in vitro* binding experiments have shown that RNA binding characteristics are indistinguishable between A2 and B1 (Swanson et al., 1988). Two minor splice forms have now been identified in rat neural cells, A2b and B1b, and A2b seems to be predominantly responsible for cytoplasmic RNA trafficking while A2 and B1 mainly carry nuclear roles (Han et al., 2010). Although early studies suggested that the arginine/glycine rich RGG motif located at the C-terminus was important for nucleocytoplasmic shuttling of hnRNPA2b1 and provided additional RNA binding properties (Nichols et al., 2000), later studies established that although arginine methylation of the RGG box does influence arginine-RNA association, it is not involved in the nucleocytoplasmic distribution of hnRNPA2B1 (Friend et al., 2013). Instead, the M9 nuclear localization signal (NLS) located within the GRD seems to be responsible for nucleocytoplasmic shuttling of hnRNPA2B1 (Pollard et al., 1996).

Most of the studies involving hnRNPs have been carried out by the cancer research field, and suggest that the expression level of many hnRNPs are altered in various types of cancer (Han et al., 2013). However, hnRNPs have also been linked to neurodegenerative diseases, including Amyotrophic Lateral Sclerosis (ALS), Spinal Muscular Atrophy (SMA), Alzheimer's disease (AD), and Fronto-Temporal Lobe Dementia (FTLD) (Geuens et al., 2016). Mutations in the prion-like domains (PLDs) within the GRDs of hnRNPA1 and hnRNPA2B1, which under normal conditions have an intrinsic tendency to self-aggregate, are the cause of rare cases of multisystem proteinopathy and ALS/FTLD, and result in the exacerbation of the protein's aggregation propensity (Kim et al., 2013; Le Ber et al., 2014; Paul et al., 2017). Furthermore, iPSC-motor neurons derived from these patients exhibited hnRNPA2B1 and hnRNPA1 positive RNA granules, suggesting hnRNP sequestration as a possible disease mechanism (Mohagheghi et al., 2016), and aberrant splicing (Martinez et al., 2016). In AD, hnRNPA2 and B1 undergo different responses to pathology. Using immunolabeling of hnRNPA2B1 isoform antibodies it was found that while there is an overall decrease of hnRNPA2B1 immunoreactivity in the hippocampus, the A2 isoform is found at increased levels in neurons from hippocampal areas that resist AD pathology (Mizukami et al., 2005). Furthermore, hnRNPA2B1 depletion has been shown to result in the impairment of cortical splicing and cognitive function in mouse models of AD (Berson et al., 2012).

Together, these findings suggest that RBPs and hnRNPs in particular are likely implicated and dysregulated in various neurodegenerative disease pathways. An actively evolving area of neurodegeneration research involving these RBPs is that of RNA granule dynamics in response to cellular stress. Environmental stressors that result in cellular responses

similar to those detected in neurodegeneration have been shown to modify the miRNA composition of EVs (Beninson et al., 2014), suggesting that disease-mediated cellular stress can modify the composition of CSF EVs. The last section of this introduction will expand on RNA granule dynamics and evidence for its dysregulation in neurodegenerative disease.

E. Stress granules and neurodegeneration

RNA granules

RBPs in the cytoplasm regulate transcript activity by forming RNA granules that contain various RBPs, translational machinery, and mRNA transcripts, and this process is mediated via protein-protein interactions. Three main types of RNA granules have been identified: stress granules (SGs), processing bodies (P bodies), and transport RNA granules – all visible by light microscopy. Although SGs are protective in response to acute stress, sustained SG formation in response to chronic stress can interfere with cellular homeostasis by silencing transcripts and sequestering RNPs (Ramaswami et al., 2013). Recent studies suggest that some neurodegenerative diseases are caused, or exacerbated by, toxic accumulation of ribonucleoprotein (RNP) aggregates. This is in part due to the prion-like domains found in RNA binding proteins, which poises them for pathogenicity and the formation of self-propagating beta-amyloids, leading to a disruption of post-transcriptional control. For example, some ALS cases feature aggregates that contain the hnRNPs FUS, EWS and TAF15. Furthermore, point mutations in genes encoding TDP-43, FUS, hnRNPA1, and hnRNPA2B1 cause a dominantly inherited form of ALS or multisystem proteinopathy (Hutten et al., 2016). Thus, it is believed that the involvement of hnRNP

aggregation in some neurodegenerative diseases may originate from an alteration in the assembly or clearance of cytoplasmic SGs.

A defining feature for mammalian SGs is the presence of stalled 48S pre-initiation complexes that form in response to a variety of stresses that inhibit translation initiation (Anderson and Kedersha, 2002). SGs form in response to stressors such as hypoxia, heat-shock, and sodium arsenite, which all inhibit translation initiation (Arimoto et al., 2008). Their elimination, in turn, depends on ATP-driven disaggregases, such as Hsp40 and Hsp70, and granulophagy through the ATP-dependent VCP-autophagy pathway (Kedersha et al., 2005; Buchan et al., 2013). Interestingly, and of importance to HD, proteomic analysis of SGs revealed that the chaperonin-containing T complex (CCT complex), which inhibits mHTT aggregation (Shahmorahdian et al., 2013), localizes to the cores of SGs and inhibits stress granule assembly (Jain et al., 2016). The physical mechanism underlying SG formation is thought to be phase separation within the cytoplasm, resulting from liquid-liquid demixing that creates droplet-like structures (Molliex et al., 2015). This process occurs when low-affinity interactions, like those involving PLDs in hnRNPs (Weber et al., 2012), bring molecules together to form distinct, non-membrane bound complexes in the cytoplasm that remain dynamic enough to actively interact with the cytosol. This process of liquid-liquid phase separation is widely accepted by the field, however super-resolution microscopy and biochemical purification studies now suggest that mature SGs are composed of stable cores surrounded by a phase separated shell of SG mRNPs held together by weak interactions (Jain et al., 2016). This suggests that other mechanisms act in addition to liquid-liquid phase separation to allow for the formation of mature SGs.

A popular hypothesis for the advantage of SGs is that localized protein enrichment within the cytoplasm could regulate the rate of biochemical reactions by accelerating some in areas of high protein concentration, and slowing others due to sequestration of necessary components (Weber et al, 2012). Along these lines, it is hypothesized that SG formation contributes to cellular stress adaptation by orchestrating the selective translation of mRNAs. For example, a transcript partitioning study under sodium arsenite induced stress identified that G3BP1-associated transcripts correlate with reduced expression of encoded mitochondrial proteins, while polysome enriched transcripts encode various survival factors involved in multiple aspects of cell cycle regulation and wound healing (Somasekharan et al., 2020). In addition, the exchange of components between SGs and polysomes or P bodies is thought to prioritize translation or degradation of some transcripts over others, regulating the proteome during stress (Fan and Leung, 2016).

Five eIF2α kinases modulate translation in metazoans, and stress induced phosphorylation of eIF2α inhibits global protein translation via the depletion of the elf2-GTP-tRNA-met ternary complex, which promotes polysome disassembly and mRNA recruitment to SGs (McDonald et al., 2011; Kedersha et al., 1999). During SG formation, interactions between nucleating RBPs, including T-cell intracellular antigen (TIA-1) and Ras-GTPase activating protein SH3-domain-binding protein (G3BP), grow to include other RBPs such as hnRNPA2B1 and hnRNPA1 (Kim et al., 2013), translation initiation proteins, and other regulatory proteins (Kedersha et al., 1999; Tourriere et al., 2003). However, SG composition may vary according to the nature of the stress stimulus (Thomas et al., 2011). In conclusion, SGs sequester hnRNP-bound mRNAs upon stalled translation and function as

a place for the dynamic sorting of these mRNAs for their return back into translation, storage, or degradation (Wolozin et al., 2012).

SGs have been shown to interact with P bodies (Buchan et al., 2009), and transcripts are transferred from SGs to P bodies to facilitate degradation (Kedersha et al., 2005). P bodies are discrete cytoplasmic foci that integrate miRNA machinery (Liu et al., 2005; Sen et al., 2005) and contain many enzymes involved in mRNA turnover, repressed RNAs, and regulatory RNAs. They are thought to be sites of translational suppression and/or mRNA decay; thus, they are present in unstressed cells, but also increase in response to cellular stresses that lead to the inhibition of translation initiation (Decker et al., 2012). Additionally, some mRNAs can exit P bodies and reinitiate translation. P body components include translationally inactive mRNA and 5'-3' decapping factors Dcp1/2 (decapping enzyme), Lsm1-7 complex (decapping activators), Xrn1 (5'-3' exonuclease), and nonsense mediated decay machinery (Adeli, 2011; Eulalio et al., 2007). Interestingly, proteins that function in the 3'-5' mRNA decay pathway, such as the exosome, are not detected in P bodies (Sheth et al., 2003). Of significance to HD, Savas et al. (Savas et al., 2008) discovered that HTT co-purifies with Ago2 and colocalizes with P bodies, and that mHTT expression results in the decrease of P bodies. This suggests that HTT may play a role in RNA-mediated gene silencing and that polyQ expansion interferes with P body formation and or maintenance. Lastly, transport RNA granules play an important role in neurons, where localized activity-dependent mRNA translation is necessary (Martin et al., 2009; Sutton et al., 2006). In mice, HTT has been shown to associate with Ago2, and other components of RNA granules, to transport mRNA to dendrites (Savas et al., 2010). Notably, knockdown of HTT resulted in depletion of granular mRNA and Ago2 staining at dendrites, but

knockdown of Ago2 only affected mRNA staining, suggesting that HTT may function through Ago2 to modulate mRNA localization at dendrites. Because this thesis discusses a role for SGs in HD pathology, the remainder of this section will focus on SGs.

Stress granules in neurodegeneration

Cytoplasmic inclusions with morphologically similar characteristics to SGs are found in the brains of patients suffering from neurodegenerative disease, such as ALS and FTLD (Vanderweyde et al., 2012; Liu-Yesucevitz et al., 2010; Zhang et al., 2018). For this reason, and the fact that these structures are also composed of SG markers, SGs have recently been implicated in the pathophysiology of some neurodegenerative diseases. While proteins such as G3BP1 and TIA-1 are widely used as SG markers (Kedersha and Anderson, 2007), the composition of SGs is diverse and depends on the type of cellular stress that results in their induction, suggesting that different stress pathways are at play. Because aberrant SG dynamics have been linked to neurodegenerative diseases (Wolozin et al., 2019), it will be important to understand the mechanisms underlying different SG subtypes to understand whether specific aspects of these are playing a pivotal role in disease progression. Using ascorbate peroxidase (APEX) proximity labeling (Rhee et al., 2013) with quantitative mass spectrometry and immunofluorescence, Markmiller et al. discovered that approximately 20% of G3BP1-positive SG component diversity is dependent on cell type and the stress stimulus that is used to induce SG formation (Markmiller et al., 2018). The SGs found in neuronal cells were significantly enriched in chaperones and autophagy factors, supporting our hypothesis that a chaperonin protein such as CCT and autophagy dysfunction may play an important role in HD SG dynamics. As for disassembly, spatio-temporal proteomic analysis using APEX revealed that SUMOylation plays a role via the recruitment of SUMO

ligases during disassembly, a process that is dysregulated under ALS-like conditions by C9ORF72-associated dipeptides (Marmor-Kollet et al., 2020). Based on these findings, and our knowledge that SUMOylation is dysregulated in HD (Steffan et al., 2004; O'Rourke et al., 2013), SUMO-mediated SG disassembly may also be altered in the brains of HD patients.

Evidence for stress granules in Huntington's disease

Because the process of SG formation is dependent on physiological protein aggregation, and mutations in the PLDs of SG components result in hyperstable SGs, it is tempting to speculate that they may be involved in nonspecific binding to other protein aggregates, such as mHTT aggregates in HD. A handful of studies have investigated the presence of various SG components in HD (**Table 1**), however only one study has specifically interrogated the co-localization of mHTT in cytoplasmic puncta that are positive for a SG nucleating factor. The work carried out by Ratovitski et al. suggests that mHTT results in altered SG dynamics in an immortalized striatal cell model of HD, by showing that mHTT interacts with SG-associated proteins Caprin-1 and G3BP, and co-localizes to SGs upon induction of ER stress (Ratovitski et al, 2012).

Other studies showed colocalization of HTT and mHTT with TIA-1 upon induction of ER stress in an immortalized striatal cell model of HD (Culver et al., 2012), of HTT inclusions with TIA-1 in the R6/2 hippocampus where it represses its function as a translational silencer (Furukawa et al., 2009), and of perinuclear HTT inclusions with TIA-1 in an 83 CAG repeat HD cell model (Waelter et al., 2001). Other proteins that localize to SGs but are not considered SG effectors have also been associated with HD. For example, TDP-43, a member of the hnRNP family of proteins (Ayala et al., 2008), colocalized with intracellular

inclusions in the cortex of HD patients (Schwab et al., 2008). The RBP FUS, also a member of the hnRNP family (Geuens et al., 2016), localizes to intranuclear inclusions in the R6/2 brain and human cortex of HD patients (Doi et al., 2008), however these are not considered SGs based on their cellular localization. Altogether, these findings suggest that, as is the case in other neurodegenerative diseases, SGs may be involved in the molecular mechanisms underlying HD pathogenesis.

Targeting stress granules in neurodegeneration

The recent advances mentioned above have allowed for a better understanding of SG dynamics and the role these may play in neurodegenerative disease. This information is now being used to investigate multiple interventions to target SG pathology in neurodegenerative diseases, including the targeting of eIF2A phosphorylation, major SG components, factors that mediate SG assembly, and the oxidative stress defense system (Chen et al., 2017).

SG formation induced by oxidative stress is one of the best studied mechanisms in the SG field, and largely depends on the phosphorylation of eIF2A (Kedersha et al., 1999), suggesting that reduction of eIF2A phosphorylation is a viable target to reduce SG formation. If overactive SGs are truly contributing to the pathophysiology of neurodegenerative disease, then one would expect the downregulation of SGs via inhibition of eIF2A phosphorylation to be protective. A study demonstrating this showed that reduction of eIF2A phosphorylation by overexpression of a specific eIF2A phosphatase reduced PrP-induced neurodegeneration in a mouse model of Creutzfeld-Jakob disease and, in contrast, an inhibitor of eIF2A dephosphorylation increased SG formation and

accelerated neurodegeneration (Moreno et al., 2012). Another pathway that has been explored as a potential approach to modulate eiF2A phosphorylation in the context of neurodegeneration is the PKR-like ER-localized eIF2A kinase (PERK) pathway (Hughes et al., 2019). Because PERK is one of the kinases responsible for phosphorylating eIF2A as a result of ER stress, small molecule inhibitors of PERK have been investigated for its potential neuroprotective effect. One study using ALS disease models, which had high phosphorylated eIF2A levels compared to controls, showed that inhibition of the PERK pathway suppressed TDP-43 toxicity in a fly model and mammalian primary cortical neurons (Kim et al., 2014).

While SG pathology and its modulation has not been fully explored in the context of HD, elevated eIF2A phosphorylation levels have been reported in HD models (Leitman et al., 2014). This study found elevated eIF2A phosphorylation levels in a cell line stably expressing mHTT and in the HD mouse cortex and striatum, and this was attributed to high PERK activation resulting from mHTT-dependent ER stress. Inhibition of PERK resulted in reduced mHTT toxicity, suggesting that the dysregulation of eIF2A phosphorylation is a significant contributor to disease pathogenesis in HD and a viable therapeutic target. These results raise questions about the involvement of SGs in HD pathogenesis and whether these could also be exploited as therapeutic targets. However, recent findings by the same group now suggest that PERK activation in response to mHTT expression represents an insufficient cellular attempt to restore homeostasis, showing that treatment with a potent PERK activator resulted in improved motor and executive functions, as well as delayed death, in the R6/2 mouse model (Ganz et al., 2020). These contradicting results raise many questions, and potential explanations involve the timing of the treatment and the life-span

of the mouse models used. It is likely that a mouse model of HD loses the ability to handle cellular stress as disease progresses and the transient induction of eIF2A phosphorylation, which leads to mechanisms that are initially protective (e.g. translational repression and SG formation), is only transiently beneficial. Without the resolution of stress, additional long-term activation of the PERK pathway might in fact be detrimental. For this reason, it will be imperative for these strategies to be eventually tested in long-term HD mouse models, and at different disease stages.

Another factor to consider is that PERK plays an important role in the cellular response to ER stress and has many downstream effectors (Liu et al., 2015), thus its inactivation might result in dangerous off-target effects. In response to this, targeting of specific SG effectors downstream of PERK is actively being explored. For example, a recent study tested and identified several compounds that can prevent the recruitment of disease-associated RBPs to SGs, and while their mechanisms of action have not been elucidated, many of them are believed to act on SGs themselves instead of upstream eIF2A kinases (Fang et al., 2019). Likewise, targeting of the SG nucleator G3BP1 via miRNA repression will be discussed in Chapter 2 of this thesis.

F. Summary of introduction

Huntington's disease is caused by a CAG-repeat expansion in exon 1 of the *HTT* gene, which results in both a loss of function of the HTT protein, and a gain of aberrant functions, including the propensity to aggregate. While medium spiny neurons of the striatum are severely affected as the disease progresses, other regions of the brain, including multiple cortical areas, are also affected over time. While endogenous factors and the transfer of

pathogenic factors among physically contiguous cells may play an important role in disease propagation, it is also likely that the CSF may propagate EV-packaged pathogenic factors between physically distant brain regions. However, the influence of CSF EVs in the propagation of HD pathology between different brain regions has not been addressed.

mHTT mediated toxicity leads to the activation of various cellular stress pathways, including the activation of the UPR pathway in response to ER stress. UPR activation in turn results in activation of the integrated stress response, an evolutionarily conserved signaling pathway that relies on the phosphorylation of the eukaryotic translation initiation factor eIF2A to restore cellular homeostasis. Phosphorylation of eIF2A leads to a decrease in global protein synthesis and the selective translation of specific genes that optimize the cellular stress response. The inhibition of translation results in an accumulation of stalled transcripts in the cytoplasm, which, at high enough concentrations, form distinct membraneless structures termed SGs. While increased phosphorylated-eIF2A levels have been detected in HD mouse models, SG formation has only been investigated in an *in vitro* model, and it is yet to be determined whether SG accumulation is a feature of HD pathology.

Because the low amino acid complexity regions that regulate SG-associated RBPs share a resemblance with expanded mHTT, it is tempting to speculate that SG and mHTT aggregated structures may interact with each other, further enhancing the stability of SGs. In addition to becoming disassembled by disaggregases SGs can let go of their contents by transferring them to P bodies for gene silencing and degradation, or by undergoing degradation via autophagy. However, data suggests P body formation and gene silencing may be disrupted as a result of mHTT expression, and the disruption of autophagy in HD

may affect SG clearance. Taken together, increased SG stability and decreased SG dissolution may result in the pathologic accumulation of SGs in HD.

Data provided in my dissertation describes a potential role for CSF EV miRNAs in the modulation of cellular stress in HD. The questions addressed by this dissertation are: 1) Can SGs be detected in *in vivo* HD models and patient brain tissue? 2) Are CSF EV miRNA contents altered in response to mHTT-mediated cellular stress? 3) Can altered miRNA-mediated mRNA repression modulate SG accumulation? To answer these questions, we relied on a rapidly progressing, transgenic mouse model that allows for the detection of multiple mHTT conformational species (Chapter 1). Using CSF samples acquired from HD patients as a source of EVs, we profiled their miRNA content and investigated the impact these miRNAs may have on gene expression in the superior cortex of HD patients. In addition, we tested the impact of specific CSF EV miRNAs on SG densities upon stress induction (Chapter 2). Lastly, we initiated the derivation of CPECs from HD patient and control iPSCs to investigate the impact of mHTT expression on CPEC function, which may have important implications for CSF and CSF EV secretion (Chapter 3).

INTRODUCTION

TABLES

Table 1. Evidence for SGs in various models of HD.

SG protein involved	HD model used	Stressor	Reference
TIA-1	HDQ83 293 Tet-Off cells	N/A	Waeleter et al., 2001
FUS (nuclear)	R6/2 mice and human cortex	N/A	Doi et al., 2007
TDP-43	Human cortex	N/A	Schwab et al., 2008
TIA-1	R6/2 mice	N/A	Furukawa et al., 2009
Caprin-1, G3BP1	STHdh Q111/Q111 cells	10 μM thapsigargin	Ratovitski et al., 2012
TIA-1	STHdh Q111/Q111 cells	0.5 mM sodium arsenite	Culver et al., 2012

CHAPTER 1

Longitudinal biochemical assay analysis of mutant huntingtin exon 1 protein in R6/2 mice

SUMMARY OF CHAPTER 1

Biochemical analysis of mutant huntingtin (mHTT) aggregation species in HD mice is a common measure to track disease. A longitudinal and systematic study of how tissue processing affects detection of conformers has not yet been reported. Understanding the homeostatic flux of mHTT over time and under different processing conditions would aid in interpretation of pre-clinical assessments of disease interventions. The objective of this study was to provide a systematic evaluation of tissue lysis methods and molecular and biochemical assays in parallel with behavioral readouts in R6/2 mice to establish a baseline for HTT exon1 protein accumulation. Established biochemical methods were used to process tissue from R6/2 mice of specific ages following behavior tasks. Aggregation states and accumulation of mHTT exon 1 protein were evaluated using multiple break and assay methods to determine potential conformational flux assay specificity in detection of mHTT species, and tissue specificity of conformers. I contributed to this study by comparing how biochemical processing affected detection of oligomeric mHTT species resolved by Agarose Gel Electrophoresis (AGE). Detection of mHTT exon 1 protein species varied based on biochemical processing and analysis providing a baseline for subsequent studies in R6/2 mice. Insoluble, high molecular weight species of mHTT exon 1 protein increased and tracked with onset of behavioral impairments in R6/2 mice using multiple assay methods. We found that conformational flux from soluble monomer to high molecular weight,

insoluble species of mHTT exon 1 protein was generally consistent for multiple assay methods throughout R6/2 disease progression; however, the results support the use of multiple biochemical techniques to detect mHTT exon 1 protein species for preclinical assessments in HD mouse models expressing mHTT exon 1 protein.

Chapter reprinted with permission from IOS Press from publication:

Morozko E.L., Ochaba J., Hernandez S., Lau A., **Sanchez I.,** Orellana I., Kopan L., Overman J., Yeung S., Steffan J.S., Reidling J., and Thompson L.M. 'Longitudinal Biochemical Assay Analysis of Mutant Huntingtin Exon 1 Protein in R6/2 Mice.' J. Huntingtins Dis., November 2018, 7(4):321-335. The publication is available at IOS Press through http://dx.doi.org/10.3233/JHD-180329

INTRODUCTION

Huntington's disease (HD), an autosomal-dominant neurodegenerative disorder, is caused by a trinucleotide CAG repeat expansion within exon 1 of the *Huntingtin* (*HTT*) gene (The Huntington's Disease Collaborative Research Group, 1993). Neuropathological hallmarks are degeneration of medium spiny neurons of the striatum and atrophy of the cortex (Rub et al., 2016). The CAG-coding polyglutamine repeat (polyQ) expansion results in aberrant misfolding, incomplete splicing, proteolysis, and accumulation of the mutant huntingtin protein (mHTT), which may contribute to disease pathogenesis (Koyuncu et al., 2017; Sathasivam et al., 2013).

Investigations into the biological mechanisms underlying HD and identification of pathways that impact disease have implicated progressive mHTT accumulation as an indicator of pathogenesis. Accrued evidence from multiple studies supports the following. Mutant HTT undergoes conformational flux, modification, and processing resulting in increased protein fragmentation and accumulation of insoluble aggregate species as the disease progresses (Hoffner et al., 2015; Hoffner et al., 2014; Ross et al., 2017). Intranuclear inclusions of aggregated, amino-terminal fragments and ubiquitin are one of the hallmarks of HD pathogenesis (Davies et al., 1997; DiFiglia et al. 1997) with the degree of aggregation corresponding with the stage of disease, likely as a surrogate marker of disease progression and aberrant protein homeostasis. Juvenile onset cases of HD, which are caused by longer repeat lengths above ~60 polyQs, have an even higher aggregate load (DiFiglia et al. 1997). Aggregates accumulate in medium spiny neurons (MSNs) of the striatum and cortex, which are significantly impacted by disease, but are notably absent

from the cerebellum (DiFiglia et al. 1997). However, mHTT undergoes changes in conformation prior to entering the visible inclusion phase (Hoffner et al., 2014).

Many HD-associated studies have focused on mHTT exon 1 protein (mHTTex1p) due to its robust effects on mHTT accumulation and aggregation, and on behavioral and biochemical deficits associated with HD in mice and flies (Mangiarini et al., 1996; Steffan et al., 2001). For *in vivo* studies, the first HD mouse model generated was an amino-terminal human exon 1 transgenic mouse (Mangiarini et al., 1996). Recently, the Bates and Housman groups showed that incomplete splicing can produce an endogenous, pathogenic mHTTex1p in full-length knock-in mouse models and human patient fibroblasts, equivalent to the transgene expressed in R6/2 mice (Mangiarini et al., 1996), that may contribute to disease progression in HD (Sathasivam et al., 2013; Neueder et al., 2017). The process of aggregation is representative of the progressive nature of the disease, beginning from soluble monomers, assembly into soluble species such as oligomers and β-sheet fibrils and ultimately forming insoluble aggregates and inclusions (Hoffner et al., 2014; Arndt et al., 2015). Soluble oligomers can go on to form spherical prefibrillar or protofibrilar soluble oligomers (Poirier et al., 2002) before maturing into amyloid-like aggregates (Scherzinger et al., 1997) and fibrils (Wanker et al., 1999). However, aggregation of mHTT and other amyloidgenic disease-associated proteins appears to progress in a non-linear path (Arndt et al., 2015; Eisele et al., 2015).

While the precise contribution of aberrant accumulation and aggregation of protein to disease pathogenesis is complex, altered proteostasis may serve as a useful surrogate in evaluating preclinical efficacy of genetic and pharmacologic interventions on pathologies.

Therefore, systematic detection of mHTT protein and the overlap with disease phenotypes is important for evaluating *in vivo* perturbations and their impact on disease onset and progression. Conformational species of mHTT have been tracked over time previously in HdhQ150 mice using uniform processing (Marcellin et al., 2012). However, due to biochemical heterogeneity of mHTT conformers, we suggest that sample processing may impact detection of different mHTT species. As a first step in systematically evaluating conformational transitions throughout disease progression, we performed a longitudinal analysis of tissues from transgenic R6/2 mice expressing human mHTTex1p using a battery of biochemical cell lysis methods (**Table 1.1**) and several specific assays developed over the years to detect and resolve mHTT protein species to investigate how they impact detection of mHTTex1p. Conformational transitions we measured include soluble oligomeric species (Weiss et al., 2008; Legleiter et al., 2010; Sontag et al., 2012), insoluble accumulated species (Kim et al., 2011; Ochaba et al., 2016; Ochaba et al., 2018; O'Rourke et al., 2013), and insoluble fibrillary species (Wanker et al., 1999). We tracked these species in parallel with behavioral phenotypes to provide a baseline to guide studies, and also show that the ability to detect specific species and their abundance is influenced by the tissue processing techniques employed.

RESULTS

R6/2 mice exhibit classical behavioral deficits

A longitudinal assessment of mHTTex1p species and tissue processing methods was performed in R6/2 transgenic mice based on their rapid progression of HD modeled phenotypes, the formation of detergent-insoluble aggregated species of mHTT and the

extensive use of this model for preclinical studies (Li et al., 2005). These mice express the first exon of human HTT (CAG repeat of ~125) encoding mHTTex1p and show reproducible and rapidly progressing motor and metabolic symptoms at 6 weeks of age and eventually develop tremors, lack of coordination, excessive weight loss, and early death (~12 weeks). Animals were assessed in behavior tasks and tissue collected for biochemical assays at time points of 5, 7, 9 and 11 weeks of age. Behavioral deficits were consistent with reported data (Mangiarini et al., 1996; Hickey et al., 2005), allowing direct comparison to molecular readouts. R6/2 mice had a significantly decreased latency to fall in the Rotarod task compared to non-transgenic controls (NT) at 7, 9, and 11 weeks of age (**Figure 1.1, A**; $p<0.0001$). This latency to fall was progressive over time in R6/2 mice ($F_{2,49}=5.62$, $p<0.01$). Motor deficits were further characterized by a significantly increased time to descend on the pole test task between NT and R6/2 mice at 8 ($p<0.001$) and 10 ($p<0.01$) weeks of age, which represented maximal dysfunction that did not progress further in the later time points (**Figure 1.1, B**; $F_{2,51}=2.86$, $p>0.05$). At 6, 8, and 10 weeks of age, R6/2 mice show significantly impaired forelimb strength as measured by the grip strength test compared to NT mice (**Figure 1.1, C**; $p<0.0001$), progressively worsening over time in R6/2 mice ($F_{2,51}=10.99$, $p<0.0001$). Additionally, clasping phenotype increased over the course of the disease indicating progressive dyskinesia and beginning at week 7, R6/2 mice show plateaued weight gain as compared to their NT littermates (**Figure 1.1, D and E**; Genotype: $F_{1, 272} =70.69$, $p<0.0001$).

For quality control and to assess a molecular readout of disease progression supporting the validity of protein fluctuations in our longitudinal cohort of R6/2 animals, qPCR analysis was conducted on *Ppp1r1b (Darpp-32),* known to be dysregulated in R6/2 mice (Luthi-

Carter et al., 2000; Bibb et al., 2000), endogenous murine *huntingtin* (*Htt*), and the R6/2 transgene. *Darpp-32* was significantly decreased at all ages in R6/2 mice compared to NT littermates in both the striatum (Genotype: $F_{1,16}$=58.54, p<0.0001) and the cortex (Genotype: $F_{1,16}$=160.1, p<0.0001, **Figures 1.1, F and G, and 1.2, A and B**) as reported (Luthi-Carter et al., 2000; Bibb et al., 2000). In the striatum, endogenous *Htt* increased in R6/2 mice at week 11 compared to week 11 NT littermates showing a significant genotype effect ($F_{1,16}$=5.22, p<0.05). A significant increase in R6/2 transgene by week 11 compared to week 7 was detected in R6/2 mice ($F_{3,8}$=4.41, p<0.05, **Figures 1.1, F and 1.2, A**). In the cortex there was no detectable difference in *Htt* in R6/2 compared to NT littermates at each age tested (Age: $F_{3,16}$=2.69, p>0.05, Genotype: $F_{1,16}$=0.02, p>0.05, **Figures 1.1, G, and 1.2, B**). While there was a significant increase in R6/2 transgene between weeks 7 and 11 of age in the striatum, there was no significant change in R6/2 transgene in the cortex ($F_{3,8}$=0.62, p>0.05). No genotype-related transcriptional changes were detected for *Rplp0*, which was used as a normalization factor. Further, reverse-transcriptase-negative controls showed no significant signal in any sample (data not shown).

Mutant HTT undergoes conformational flux over time in R6/2 mice

A standard outcome measure used to measure mHTT flux is the detection of intranuclear inclusion bodies by immunohistochemistry using aggregation specific antibodies (e.g. EM48, (Gutekunst et al., 1999)), therefore, we evaluated inclusions in the R6/2 mouse striatum and cortex over time. R6/2 mice showed a progressive increase in mHTT inclusion body formation in both the striatum ($F_{3,8}$=13.28, p<0.01) and the cortex ($F_{3,8}$=25.42, p<0.001) compared from 5 weeks of age to later time points (**Figure 1.3**). This

is consistent with a conformational flux towards insoluble, aggregate species of mHTT beginning at the time of overt disease onset. Although striatum shows the most overt degeneration at late stages, cortical regions have significantly more inclusion bodies by 9 and 11 weeks of age compared to the striatum (Region: $F_{1, 16}$=34.69, p<0.0001, Age: $F_{3, 16}$=37.89, p<0.0001), consistent with what has previously been reported (**Figure 1.3**) (Davies et al., 1997).

We have previously described a Soluble/Insoluble Fractionation protocol and Western blot analysis to distinguish soluble monomeric and accumulated insoluble mHTT species in late stage R6/2 mice (Ochaba et al., 2016; Ochaba et al., 2018). This technique was used for this longitudinal analysis of R6/2 mouse tissue and compared to other tissue lysis methods of striatum, cortex, hippocampus, cerebellum, and peripheral tissues (liver and skeletal muscle) using a HTT antibody that selectively detects human mHTTex1p.

Striatum: Following fractionation, the soluble protein fragment of human HTT encoded by the transgene in R6/2 mice, mHTTex1p, was detectable as a monomeric protein species in the Soluble Fraction, with highest levels at the first time point tested at 5 weeks of age in the striatum (**Figure 1.4, A**). Over the disease course the detectable amount of soluble mHTTex1p monomer decreased significantly ($F_{3,8}$=15.51, p<0.01) and appeared to be accompanied by a corresponding increase in the insoluble, HMW species of mHTTex1p, potentially reflecting the dynamic shift in mHTTex1p conformation from soluble monomer into an insoluble, accumulated species. However, significance was only supported by 1-way ANOVA and was not detected following post-hoc analysis ($F_{3,8}$=4.274, p<0.05, **Figure 1.4, A**). The observed fluctuation in size of the detectable monomer is not likely due to a

somatic expansion in the striatum as the number of repeats present in the transgene was similar in the striatum compared to tail genomic DNA (**Table 1.2**, CAG repeat sizes in tails and striatum). Accompanying the apparent increase in insoluble HMW mHTTex1p resolved by PAGE and western blotting was an observed increase in insoluble fibrils of mHTTex1p from the Insoluble Fraction as detected by a filter retardation assay (**Figure 1.4, A**). To examine methods used to process samples then assess levels of mHTTex1p, a series of commonly used tissue lysis buffers specific for given assays were tested to compare outcomes (**Table 1.1**). An inverse fluctuation from monomeric mHTTex1p towards progressive detection of HMW mHTTex1p retained in the top of the gels were detected in striatal samples lysed in either T-PER (Monomer: $F_{3,8}$=5.85, $p<0.05$, HMW: $F_{3,8}$=12.12, $p<0.01$) or RIPA (Monomer: $F_{3,8}$=25.44, $p<0.001$, HMW: $F_{3,8}$=4.06, $p>0.05$) buffers as with the Soluble/Insoluble Fractionation (**Figure 1.4, B and C**) and summarized in **Table 1.3**. TRIzol reagent was also tested since it has the advantage of collection of both RNA and protein from processed tissue. However, TRIzol reagent showed extensive variability in detection of both soluble monomer and HMW species of mHTTex1p compared to other methods, precluding its use as an assay for shifts in solubility (**Figure 1.5, A**).

Cortex: Cortical tissue samples were processed using the same methods in parallel and samples showed a similar dynamic shift from soluble, monomeric mHTTex1p to HWM mHTTex1p as observed in the striatum (**Table 1.3 and Figure 1.6**). Insoluble, HWM mHTTex1p significantly increased ($F_{3,8}$=9.88, $p<0.01$), while soluble, monomeric mHTTex1p significantly decreased ($F_{3,8}$=8.78, $p<0.01$, **Figure 1.6, A**). This shift was also accompanied by an observed increase in insoluble fibrils from the Insoluble Fraction similar to striatal samples (**Figure 1.6, A**). T-PER-processed samples showed significant

reduction in monomeric mHTTex1p and increase in HMW mHTTex1p (Monomer: $F_{3,8}$=10.91, p<0.01, HMW: $F_{3,8}$=8.42, p<0.01, **Figure 1.6, B**), similarly seen in RIPA-processed samples (Monomer: $F_{3,8}$=7.21, p<0.05, HMW: $F_{3,8}$=10.85, p<0.01, **Figure 1.6, C**). Extensive variability in TRIzol-processed samples was again observed (**Figure 1.5, C**).

Hippocampus and Cerebellum: The dynamic shift between soluble monomer and insoluble HMW mHTTex1p was observed in the hippocampus following Soluble/Insoluble Fractionation, showing significant conformational flux (Monomer: $F_{3,8}$=142.2, p<0.0001, HMW: $F_{3,8}$=21.05, p<0.001; **Table 1.3 and Figure 1.7, A**). R6/2 mice have been previously reported to have deficits in spatial learning (Lione et al., 1999), a hippocampal-dependent process, as well as decreased hippocampal volume (Rattray et al., 2013) and spine density (Bulley et al., 2012), suggesting that this insoluble, HMW mHTTex1p protein could correlate with observed deficits in these animals. This shift, however, was not detected in tissue samples processed in T-PER reagent, showing no decrease in monomeric mHTTex1p (Monomer: $F_{3,8}$=0.13, p>0.05) but an increase in the unresolved, HMW accumulated mHTTex1p species ($F_{3,8}$=5.41, p<0.05, **Figure 1.7, B**). Insoluble, HMW mHTTex1p in the cerebellum significantly increased ($F_{3,8}$=29.11, p<0.0001), but the Soluble Fraction did not show significant soluble monomer flux throughout disease progression ($F_{3,8}$= 2.51, p>0.05), indicating that mHTTex1p may be sequestered into a different form or aggregate species in the cerebellum and may provide insight into tissue specificity and vulnerability in HD (**Table 1.3 and Figure 1.7, C**). Cerebellar tissue samples broken in T-PER reagent, however, showed a significant increase in accumulated mHTTex1p ($F_{3,8}$=6.32, p<0.05) and a corresponding decrease in soluble monomer ($F_{3,8}$=4.25, p<0.05, **Figure 1.7, D**). These results suggest that while accumulated HMW mHTTex1p tracks with disease pathogenesis

and may serve as a robust measure of disease progression, additional methods to detect additional species of mHTT or levels of full-length endogenous HTT may be necessary to investigate tissue specific vulnerabilities or normal HTT levels (Franich et al., 2018).

Liver and Skeletal Muscle: We also evaluated liver and skeletal muscle samples for accumulation of HMW mHTTex1p in comparison to the brain tissue results. Liver samples show significant accumulation of insoluble, HMW mHTTex1p ($F_{3,8}$=83.34, p<0.0001). The soluble monomer, however, was not detectable using Soluble/Insoluble Fractionation (Sup. **Figure 1.8, A**, data not shown). Significant accumulation of HMW mHTTex1p was detected in samples broken in T-PER reagent ($F_{3,8}$=12.79, p<0.01) and interestingly, soluble monomeric mHTTex1p was also detectable in liver samples broken in T-PER reagent but no change in protein abundance during disease progression was detected with this break method ($F_{3,8}$=2.95, p>0.05, **Figure 1.8, B**). Like liver, significant accumulation of insoluble, HMW mHTTex1p was detectable in skeletal muscle only using Soluble/Insoluble Fractionation ($F_{3,8}$=7.53, p<0.05). No soluble monomer of mHTTex1p was detectable in skeletal muscle broken with either Soluble/Insoluble Fractionation or T-PER reagent. HMW mHTTex1p was not detected in T-PER (**Figure 1.8, C**, data not shown).

Oligomeric mHTT detection varies based on tissue processing

Agarose Gel Electrophoresis (AGE) has been used to resolve soluble, oligomeric species of mHTT in RIPA buffer as described (Weiss et al., 2008; Sontag et al., 2012). Tissue samples from striatum and cortex that were lysed using methods as above (**Table 1.1**) were also analyzed using AGE to compare how biochemical processing affected detection of mHTT species resolved by AGE. Detection of oligomeric mHTTex1p species on AGE gels

throughout the course of the disease in R6/2 mice varied greatly depending on break method as summarized in **Table 1.3** (**Figure 1.9**). Striatal tissue samples from R6/2 mice broken in RIPA buffer showed an increase in oligomeric mHTTex1p through week 9 followed by a significant decrease by week 11 ($F_{3,8}$=27.21, p<0.001). However, R6/2 striatal samples showed increased oligomeric mHTTex1p through week 11 in both Insoluble ($F_{3,8}$=27.31, p<0.001) and Soluble ($F_{3,8}$=7.30, p<0.05) Fractions, and samples broken in T-PER ($F_{3,8}$=24.70, p<0.001, **Figure 1.9, A**), and TRIzol ($F_{3,8}$=16.02, p<0.001, **Figure 1.5, B**). Cortical tissue samples broken using identical methods more consistently showed a significant increase in oligomer formation (RIPA: $F_{3,8}$=19.56, p<0.001, Insoluble: $F_{3,8}$=29.95, p<0.001, T-PER: $F_{3,8}$=109.3, p<0.0001, **Figure 1.9, B**) with the exception of the Soluble Fraction ($F_{3,8}$=2.291, p>0.05) and of TRIzol samples ($F_{3,8}$=0.95, p>0.05, **Figure 1.5, D**) which showed no significant accumulation of mHTTex1p oligomers. Therefore, the variability in detectable oligomeric mHTTex1p among tissue processing methods is an important consideration when analyzing data in preclinical studies.

DISCUSSION

Proteostasis in HD is perturbed by the expression of mHTT, shifting homeostatic balance and associated downstream cascades. Molecular and biochemical readouts such as aberrant mHTT accumulation and transcriptional alterations can be correlated to behavioral phenotypes in an effort to track disease modification. Our longitudinal cohort of R6/2 mice exhibited behavioral phenotypes as previously reported (**Figure 1.1**, (Mangiarini et al., 1996; Hickey et al., 2005; Luthi-Carter et al., 2000; Bibb et al., 2000)),

allowing for a systematic comparison of changes in mHTTex1p conformations using selected cell lysis and biochemical assays in an HD model over time.

At the level of transcription, expression of *Darpp-32* (Luthi-Carter et al., 2000; Bibb et al., 2000) was decreased in R6/2 mice as expected, thus providing a reliable molecular quality control marker (**Figures 1.1 and 1.2**). While previously reported that transgene expression was within range of the endogenous murine gene in R6/2 mice (Mangiarini et al., 1996), there was a moderate increase in the levels of endogenous *Htt* transcript in R6/2 mice in this study by 11 weeks of age in the striatum compared to age-matched NT controls, perhaps indicating an upregulation to compensate for transgene genotoxic stress or for the declining wild-type endogenous HTT protein levels observed in HD knock-in mice during aging (Franich et al., 2018). Intriguingly, this increase also extended to expression of the R6/2 transgene in striatum, potentially reflecting compensatory upregulation of *Htt* given that the transgene is expressed from the human *Htt* promoter (Mangiarini et al., 1996). The upregulation of the transgene and of endogenous *Htt* was not observed in cortex, potentially reflecting some aspect of tissue specificity. Thus, when making assessments of protein levels, differential transcription may be considered in addition to changes in protein clearance mechanisms, such that the observed increase in R6/2 transgene expression in the striatum could also contribute to the detected increase in accumulated species of mHTTex1p.

Given that mHTT conformations have different biochemical properties, it is important to evaluate how tissue processing and analytical technique impact detection of conformers, and we assessed this *in vivo* assaying mHTTex1p from transgenic R6/2 HD mice. We first

sought to resolve soluble and insoluble species of mHTTex1p in different brain regions and peripheral tissues. Accumulation of insoluble, HMW mHTTex1p resolved from the Insoluble Fraction was consistently detected in every tissue tested (**Table 1.3 and Figures 1.7, 1.8**), and the appearance of the insoluble mHTTex1p accumulation tracked with onset of disease phenotypes. In striatum, cortex, and hippocampus, this increase was accompanied with a progressive decrease in the soluble mHTTex1p monomer associated with the transgene. The decrease in soluble mHTTex1p and corresponding increase in insoluble HMW species of mHTTex1p, tracking with disease progression, suggests that preventing this flux through therapeutic modulation may be therapeutically beneficial. Supporting this, our previous data showed that modulation of the insoluble, HMW species by reduction of the E3 SUMO ligase, Protein Inhibitor of Activated Stat 1 (PIAS1) in the striatum of R6/2 mice corresponded with beneficial behavioral and molecular alterations (Ochaba et al., 2016) and treatment with a compound that corresponds with worsened behavioral phenotypes, JQ1, increased levels of this insoluble, HMW specifies (unpublished results, Thompson). However, while this insoluble, HMW species tracked with disease progression and observed behavioral deficits, it did not provide insight into tissue specificity involved in disease pathogenesis. Therefore, this species may serve as a reliable readout for molecular progression of disease but not of tissue-specific vulnerabilities. An alternative methodology to further define levels of HTT species recently reported that levels of full-length mHTT protein do not decline robustly in cerebellum with aging, unlike in cortex and striatum, in two homozygous knock-in models, highlighting the importance of tracking multiple full-length and protein fragment species of both HTT and mHTT (Franich et al., 2018).

While accumulation of insoluble, HMW mHTTex1p was detectable in peripheral tissue (skeletal muscle and liver), Soluble/Insoluble Fractionation was unable to resolve the soluble, monomeric transgene protein product (**Figure 1.8**). This could indicate an accelerated or differential aggregation pathway or preferential clearance of the monomer in peripheral tissue. Being able to accurately detect mHTT conformers would aid in establishing tissue intrinsic differences.

Whole-cell lysis techniques, such as RIPA and T-PER reported here, were able to resolve soluble monomeric mHTTex1p albeit with variability compared to other techniques used (**Table 1.3**). Interestingly, a HMW mHTTex1p species from whole-cell tissue processing methods was retained at the top of the gel when analyzed by PAGE and Western blot. It is possible that this HMW species contains both soluble and insoluble proteins and multiple mHTTex1p conformers and therefore cannot be directly compared to the insoluble, HMW mHTTex1p detected in the Insoluble Fraction that resolves in low-percentage PAGE gels. However, the whole-cell lysis HMW species reliably increased in some brain regions broken in both RIPA and T-PER buffers and therefore may also serve as a readout for molecular progression of disease.

Soluble oligomeric mHTT was previously shown to be detectable at an early age in HdhQ150 mice. Levels of this soluble species, detected by size exclusion chromatography, diminished over time and corresponded with an increase in intranuclear inclusion formation (Marcellin et al., 2012). Though our findings present a similar trend, detection of an earlier oligomeric species of mHTTex1p is dependent on tissue processing (**Table 1.3 and Figures 1.5, B, D, and 1.9**). Alternatively, due to the heterogeneity of oligomeric

mHTT (Hoffner et al., 2014), certain biochemical processing methods may favor one soluble species over the other. Conformation-specific antibodies facilitate studies of various mHTT species and their association with pathogenesis (e.g. 3B5H10 (Miller et al., 2011), 1C2 (Trottier et al., 1995), MW8 (Ko et al., 2001), EM48 (Gutekunst et al., 1999)). Therefore, future in depth analysis using conformer specific antibodies may provide further insight (Legleiter et al., 2009).

Taken together, the data presented here is consistent with the dynamic shift of the soluble mHTT transgene protein product in R6/2 mice to an insoluble, HMW accumulated mHTTex1p species accompanied by a change in oligomeric mHTTex1p over the time course of the disease. Significantly, protein processing methods influence the detection and temporal effects. Protein processed in TRIzol reagent yielded the greatest amount of variation between assays for detecting different species of mHTTex1p (**Figure 1.5**), precluding its use in these studies. However, TRIzol may be useful in detection of non-aggregating proteins to enable parallel protein and RNA processing.

The shift to insoluble, HMW and aggregated mHTTex1p from soluble monomer is associated with increasing behavioral dysfunction compared to NT mice and represents a robust protein assay to track disease progression in R6/2 mice. Understanding the outcomes of standard protein homeostasis assays to assess mHTTex1p flux in R6/2 mice provides a baseline for cross comparisons of preclinical interventions. It will be beneficial to conduct similar assessments of mHTTex1p flux in brain expressing full-length mutant HTT, given that mHTTex1p is expressed in knock-in HD mouse models and in patient brain (Sathasivam et al., 2013; Neueder et al., 2017), and may be relevant to the onset of HD

pathogenesis. A recent report showed a decrease in soluble mHTTex1p monomer in the zQ175 HD knock-in mouse model over time (Neueder et al., 2017), suggesting that detecting this species as well as the insoluble, mHTTex1p species may be powerful cross-model molecular correlates. Indeed, in the assays here, decreasing monomeric mHTTex1p from fractionation of striatal tissue or breaking in RIPA appeared qualitatively to track most closely with the progression of phenotypes in the R6/2 mice. We have previously published a decrease in full-length HTT with age in striatum and cortex of two HD homozygous knock-in models and in wild-type controls, which may reflect a loss of full-length HTT protein function over time (Franich et al., 2018). Due to the dynamic shift between mHTTex1p conformations throughout the course of the disease we propose using multiple, optimized biochemical analyses, potentially in combination with high context histological approaches as described for knock-in zQ175 mice (Carty et al., 2015) to determine the impact of potential therapeutics on the protein flux of both mHTTex1p and full-length HTT protein.

EXPERIMENTAL PROCEDURES

Animals

R6/2 mice were obtained from Jackson Laboratories at 5 weeks of age and allowed to age to 7, 9, or 11 weeks. CAG repeat sizing of genomic DNA harvested from tails was performed by Laragen. Experiments were carried out in strict accordance with the Guide for the Care and Use of Laboratory Animals of the NIH and an approved animal research protocol by the Institutional Animal Care and Use Committee (IACUC) at the University of California, Irvine. Animals were humanely euthanized by an injection of Euthasol at age 5, 7, 9 or 11 weeks

followed by cardiac perfusion with PBS then decapitation. Brain and peripheral tissues used for biochemical assessment were flash-frozen on dry ice and stored at -80°C until further use. Brain tissue used for immunofluorescence was drop fixed in 4% paraformaldehyde for 48 hours then protected in 30% sucrose with 0.02% sodium azide.

Behavioral Paradigms

Motor deficits were assessed in pole test, rotarod, and grip strength assays as previously described (Ochaba et al., 2016). For pole test, mice were tested at 6, 8, and 10 weeks of age for their ability to descend a vertical pole (1 cm in diameter, 60 cm high) by recording and averaging time to descend over four trials for analysis. Rotarod was carried out using an accelerating apparatus (Dual Species Economex Rota-Rod; 0207-003M; Columbus Instruments) at 7, 9, and 11 weeks of age. Animals were trained on Rotarod for 5 minutes on day 1 and tested the following day by an accelerating assay recording and averaging time to fall for three, 5-minute trials test day.

Grip strength was assessed 6, 8, and 10 weeks of age to measure forelimb strength using a meshed force gauge which retained the peak force applied (IITC Life Science instrument, Woodland Hills, CA) and averaging the top 4 strongest pulls of 5 trials in grams of force applied to the meter. Dyskinesia was assessed by recording percent of animals clasping from weeks 5-11 as described previously (Mangiarini et al., 1996) and body weights were recorded at the same time daily from weeks 5-11.

Immunohistochemistry and Quantitation

Post-fixed brains were processed as 40 μm sections, used for immunohistochemistry and imaged by confocal microscopy. The following primary antibodies were used: anti-HTT

mEM48 (Millipore MAB5374) and anti-DARPP-32 (Santa Cruz SC-11365). Following antibody incubation, nuclei of slices were stained with TO-PRO™-3 iodide nuclear stain (Thermo Fisher T3605) and mounted onto microscope slides using Fluoromount-G (SouthernBiotech 0100-01). A LeicaDM2500 confocal microscope was used to acquire images. Six representative sections were used per animal. Two comparable z-stack images per section were acquired at 40x and used for quantification. EM48-positive puncta were automatically counted using Imaris Bitplane 5.0 spots setting with a diameter threshold of 0.5 μm and consistent threshold between samples.

Tissue Lysis

Flash frozen brain and peripheral mouse tissue were lysed by douncing 30 times in a glass 2 mL vial. Soluble and Insoluble Fractionation was performed on tissue samples in lysis buffer containing 10 mM Tris (pH 7.4), 1% Triton X-100, 150 mM NaCl, 10% glycerol, and 0.2 mM PMSF, and supplemented with protease inhibitors and NEM as previously described (Ochaba et al., 2016; Ochaba et al., 2018; O'Rourke et al., 2013). Samples were lysed for 60 minutes on ice followed by a 20-minute centrifugation at 15,000 xg at 4°C. Supernatant served as Soluble Fraction and pellet was washed twice with lysis buffer before being re-suspended in lysis buffer supplemented to 4% SDS and served as the Insoluble Fraction. Insoluble samples were sonicated for 30 seconds at 40% amplitude and boiled for 30 minutes. Protein fractions were quantified using Lowry protein assay (Bio-Rad). Whole cell tissue lysis was performed in T-PER or RIPA buffers supplemented with protease inhibitors protease inhibitors (Complete Mini, Roche Applied Science), 0.1 mM PMSF, 25 mM NEM, 1.5 mM aprotinin, and 23.4 mM leupeptin by douncing as above then sonicated for 10 seconds, 3 times at 40% amplitude on ice. T-PER samples were quantified

using Bradford protein assay and RIPA samples were analyzed using Lowry protein assay. Protein fraction from tissue samples processed using TRIzol™(Thermo Fisher A33251) reagent was prepared according to manufacturer's protocol to solubilize organic protein phase and analyzed by Bradford protein assay.

Western Blot analysis

Soluble Fractions, T-PER, and RIPA lysates were resolved by reducing and running 30µg of protein on 4-12% Bis-Tris Poly-Acrylamide gels (PAGE) at 150V and transferred onto 0.45µM nitrocellulose membrane. 30µg of reduced, insoluble protein from Insoluble Fractions were resolved on 3-8% Tris-Acetate Poly-Acrylamide gels run at 150V and transferred onto 0.45µM nitrocellulose membrane. Membranes were blocked in Starting block (Invitrogen) for 20 minutes at room temperature and probed in primary antibody overnight at 4°C. The following primary antibodies were used: anti-HTT (Millipore MAB5492) to detect HTTex1p, anti-actin (Sigma A5060), and anti-GAPDH (Novus Biologicals NB100-56875). Western blot data was quantified by determining the mean pixel intensity using Scion Image processing software. Soluble Fractions, T-PER, and RIPA lysates were normalized to house-keeping protein loading control (GAPDH or Actin) prior to statistical analysis. Insoluble protein was quantified as relative protein abundance as previous (Ochaba et al., 2016; Ochaba et al., 2018).

Agarose Gel Electrophoresis analysis

Oligomeric species of mHTTex1p were detected using Agarose Gel Electrophoresis (AGE) as previously described (Sontag et al., 2012) using a 1%, 375mM Tris-HCl, pH 8.8, 1% SDS agarose gel. 30µg of protein was suspended in a non-reducing loading buffer (4x, 300 mM

Tris-HCl pH 6.8, 66% glycerol, 2.4%SDS with BPB) and loaded onto an agarose gel without boiling. Samples were run in a 192 mM glycine, 24.8 mM Tris base, 0.1% SDS running buffer and transferred using an Invitrogen Novex Semi-Dry blotter onto 0.45 um PVDF membrane at 10V for 1 hour. Membranes were blocked in starting block (Invitrogen) for 1 hour at room temp and probed with primary antibody overnight at 4°C. mHTTex1p was detected using anti-HTT (Millipore MAB5492) antibody. AGE data was quantified by determining the mean pixel intensity using Scion Image processing software as a relative protein abundance.

Filter Retardation assay

Insoluble fibrils of mHTTex1p were detected using a filter retardation assay (Wanker et al., 1999) with modifications. 30µg of insoluble samples obtained from Soluble/Insoluble Fractionation were suspended in 200 ul of 0.1% SDS, boiled for 5 minutes, loaded on to a dot blot apparatus (BioRad), and blotted onto 0.2 µm Cellulose Acetate membrane. Membrane was blocked for 1 hour at room temperature in 5% milk in TBST. Fibrils were detected with anti-HTT antibody (Enzo PW0595).

RNA Isolation and Real-Time qPCR

Flash frozen brain regions harvested from R6/2 longitudinal animals were homogenized in TRIzol™ (Thermo Fisher A33251) and RNA was collected using manufacturer's procedures then purified using RNEasy Mini kit (QIAGEN). Residual DNA was removed by DNase treatment incorporated into RNEasy protocol as per manufacturer's suggestion. Following RNA isolation, reverse transcription was performed using SuperScript 3 First-strand synthesis system according to manufacturer's protocol (Invitrogen). Both oligo (dT) and

random hexamer primers were used in a 1:1 ratio with a total of 1 µg RNA per sample. Final synthesized cDNA was diluted 1:10 in DEPC treated water and stored at -20°C until use. The following primers were used to amplify and detect cDNA from transcripts: full-length *Htt* (F: GCAGGG-AAAGAGCTTGAGACAC, R: CCTCATTCTCCTTGTGGCACTG), R6/2 transgene (F: CCGCTCAGGTTCTGCTTTTA, R: TGGAGGGACTTGAGGGACTC), *Darpp-32/Ppp1r1b* (F: TCTCAGAGCACTCCTCACCAGA, R: CACTCAAGTTGCTAATGGTCTGC), *Rplp0* (F: GCTTCGTGTTCACCAAGGAGGA, R: GTCCTAGACCAGTGTTCTGAGC).

Statistical analysis

All data represented as mean ± SEM with a p value of $p<0.05$ considered statistically significant. Analyses were completed in GraphPad Prism software. Student's two-tailed t-tests, assuming equal variance were performed for behavioral comparisons at designated time points between non-transgenic (NT) and R6/2 mice. Behavioral comparisons between R6/2 animals over time were completed by performing a 1-way ANOVA. Densitrometry and aggregate count from EM48 positive immunolabeling studies were analyzed by performing a 1-way ANOVA to assess changes overtime or 2-way ANOVA to compare between brain regions. Pixel intensity values were obtained from western blots and subjected to 1-way ANOVA to assess changes in protein quantify overtime in R6/2 mice. Statistical analysis was completed on the delta CT (dCT) values obtained from qPCR reactions normalized to *Rplp0*. When comparing relative to NT week 5, a 2-way ANOVA was used to assess changes in genotype and time. When comparing between R6/2 mice only, a 1-way ANOVA was used to assess changes over time in transcription. All 1-way ANOVAs were followed by Tukey's multiple comparisons test. All 2-way ANOVAs were followed by Sidak's multiple comparisons test.

CHAPTER 1

FIGURES

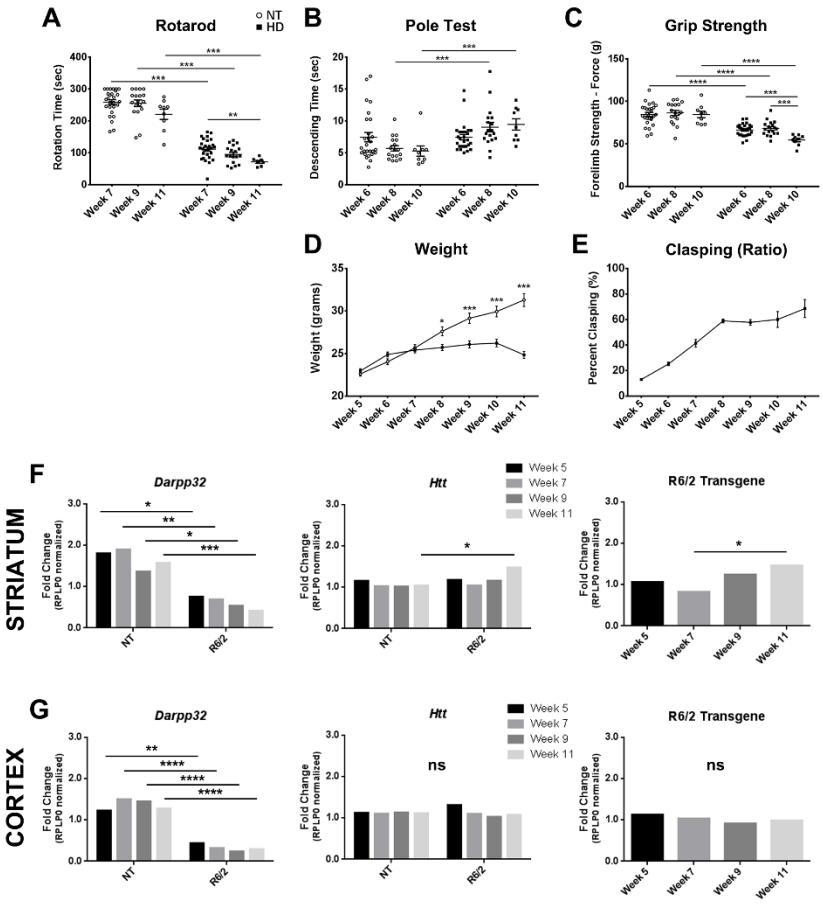

Figure 1.1. Progressive motor and transcriptional changes as quality control for R6/2 mice. A) R6/2 mice have significantly decreased latency to fall compared to non-transgenic controls (NT) that progressed over time. **B)** R6/2 mice display progressive and significantly increased time to descend on the pole test task through disease progression. **C)** R6/2 mice show significantly impaired forelimb strength as measured by the grip strength test compared to NT and progressively worsened over time. **D)** R6/2 mice show plateaued weight gain beginning at week 7 (Genotype: $F_{1,\ 272}$ =70.69, p<0.0001). **E)** Clasping deficits increase over the course of the disease. **F)** Striatal RNA shows significant fold change in *Darpp-32* (Genotype: $F_{1,16}$=58.54, p<0.0001) and full length murine *Htt* (Genotype: $F_{1,16}$=5.22, p<0.05) relative to NT week 5. An increase in the R6/2 Transgene ($F_{3,8}$=4.41, p<0.05) fold change relative to R6/2 week 5 is observed. **G)** Cortical RNA shows significant changes in *Darpp-32* (Genotype: $F_{1,16}$=160.1, p<0.0001) but not *Htt* (Age: $F_{1,16}$=2.69, p>0.05, Genotype: $F_{1,16}$=0.02, p>0.05) relative to NT week 5 or R6/2 transgene relative to week 5 R6/2 animals ($F_{3,8}$=0.62, p>0.05). Behavior: n= 36 (week 5); 27 (week 7); 18 (week 9); 9 (week 11). *P<0.05, **P<0.01, ***P<0.001, values represent means ± SEM. Statistical significance of genotypic differences was determined by unpaired, 2-tailed t-test for all behavioral analysis. 2-way ANOVA followed by Bonferroni post-hoc test for weight comparison. qPCR: n=3 for each gene and timepoint. Statistical analysis was completed using 2-way ANOVAs for comparing to NT animals followed by Sidak's multiple comparison's test and 1-way ANOVAs comparing R6/2 mice at different ages followed by Tukey's multiple

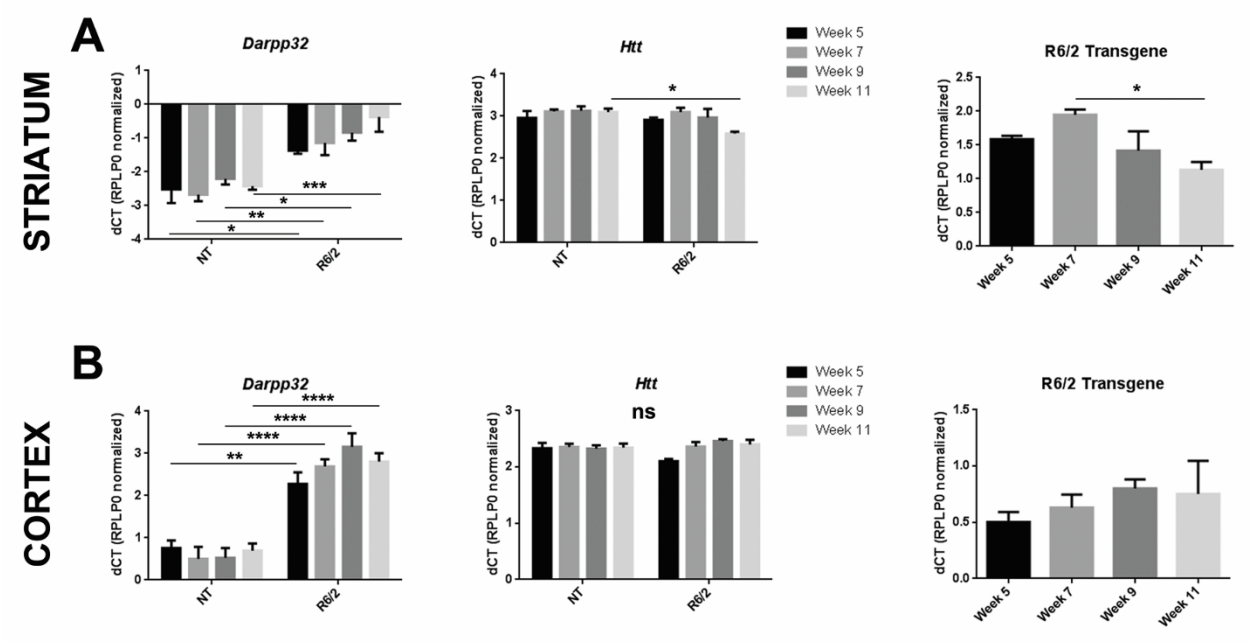

Figure 1.2. Delta CT (dCT) values used to analyze transcriptional alterations detected by qPCR in R6/2 mice. A) Striatal gene dCT values relative to NT week 5 shows a significant progressive increase in full length murine *Htt* (Genotype: $F_{1,16}$=5.22, p<0.05) and decrease in *Darpp-32* (Genotype: $F_{1,16}$=58.54, p<0.0001). Striatal gene dCT values relative to R6/2 week 5 shows a progressive increase of R6/2 Transgene expression ($F_{3,8}$=4.41, p<0.05). **B)** Cortical gene dCT values relative to NT week 5 shows significant changes in *Darpp-32* (Genotype: $F_{1,16}$=160.1, p<0.0001) but not *Htt* (Age: $F_{1,16}$=2.69, p>0.05, Genotype: $F_{1,16}$=0.02, p>0.05) or R6/2 transgene relative to week 5 R6/2 animals ($F_{3,8}$=0.62, p>0.05). *P<0.05, **P<0.01, ***P<0.001, ****P<0.0001, values represent mean fold change. n=3 for each gene and timepoint. Statistical analysis was completed using 2-way ANOVAs for comparing to NT animals followed by Sidak's multiple comparison's test and 1-way ANOVAs comparing R6/2 mice at different ages followed by Tukey's multiple comparison test.

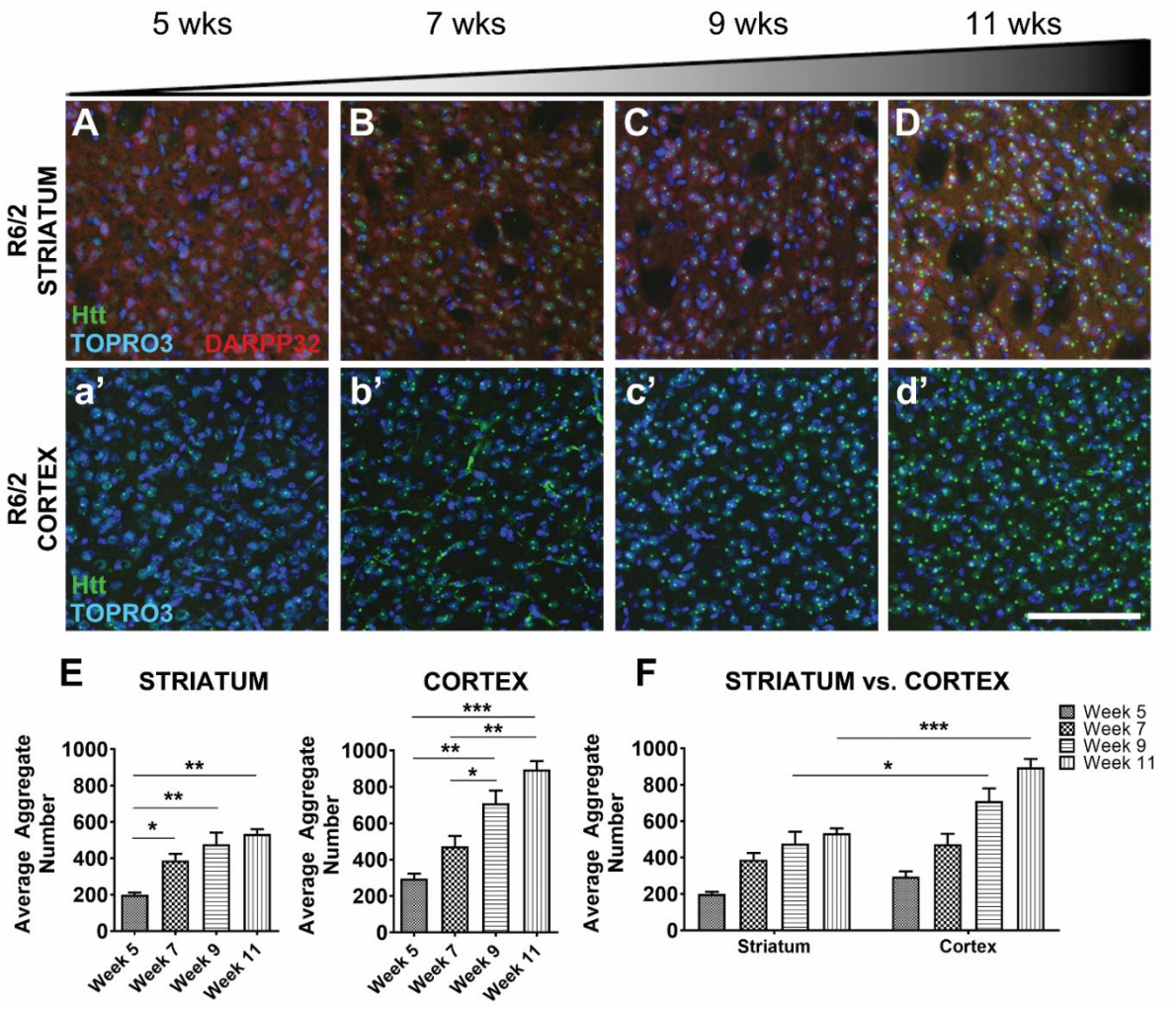

Figure 1.3. Progressive mHTT inclusion body formation in cortex and striatum of R6/2 mice. A-D) 5-11 week-old R6/2 mice show progressive inclusion body formation in striatum. **a'-d')** Corresponding cortical area at 5-11 weeks indicates this site shows early and progressive inclusion formation (Striatum: $F_{3,8}$=13.28, p<0.01, Cortex: $F_{3,8}$=25.42, p<0.001) with more inclusions in the cortex than striatum (Region: $F_{1,\ 16}$=34.69, p<0.0001, Age: $F_{3,\ 16}$=37.89, p<0.0001). mHTT inclusion bodies stained with EM48 (green). Striatal tissue marked with DARPP-32 (red) and nuclei of all cells stained with TOPRO3 (blue). All images taken from coronal slices at 10x magnification, striatal and cortical images were taken from the same slice, quantified by IMARIS software, and analyzed by 1-way ANOVA followed by Tukey's multiple comparison test or 2-way ANOVA followed by Sidak's multiple comparison test. Representative images shown. Scale bar 100 µm. *P<0.05, **P<0.01, ***P<0.001, values represent means ± SEM. n=3 for all time points.

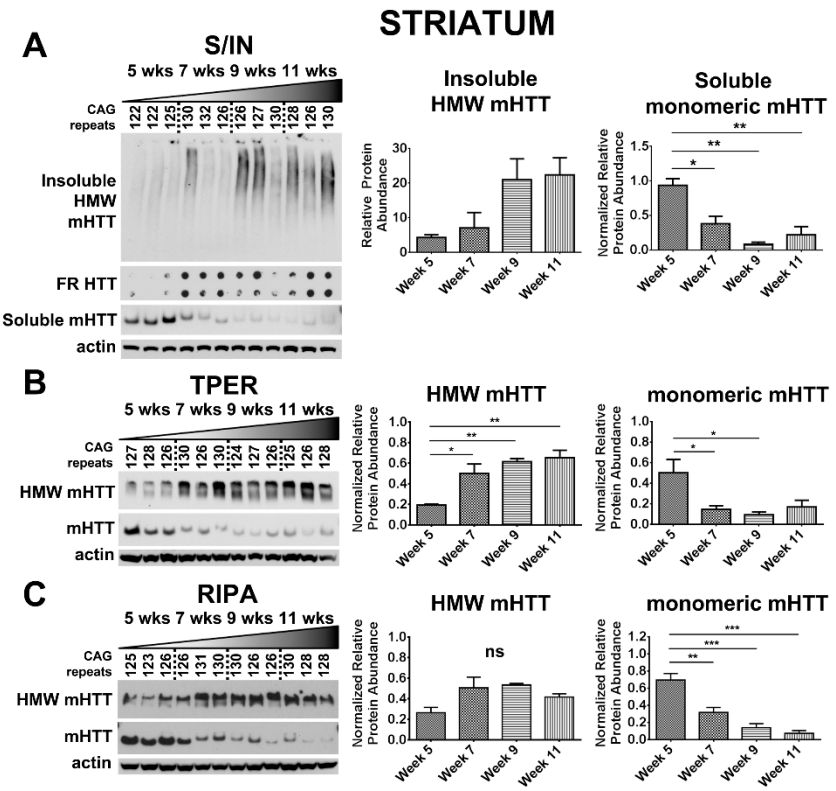

Figure 1.4. Detection of mHTTex1p in striatum of R6/2 mice. A) Striatal time-course samples were fractionated into Soluble and Insoluble proteins. Insoluble fraction reveals an increase in a HMW species of mHTTex1p throughout disease progression ($F_{3,8}$=4.274, p<0.05). Soluble fraction shows an inverse, significantly decreased monomeric form of mHTTex1p throughout disease progression ($F_{3,8}$=15.51, p<0.01). Insoluble aggregates detected by filter retardation assay may show a slight increase throughout disease progression‡. Striatal tissue samples broken in **B)** T-PER (Monomer: $F_{3,8}$=5.85, p<0.05, HMW: $F_{3,8}$=12.12, p<0.01) and **C)** RIPA (Monomer: $F_{3,8}$=25.44, p<0.001, HMW: $F_{3,8}$=4.06, p>0.05) reagents show a significant reduction of monomeric mHTex1pT throughout disease progression. Fluctuations in soluble, monomeric mHTTex1p correspond to varying CAG repeats in R6/2 mice. Western blots quantified by mean pixel value. Soluble fraction normalized to actin and analyzed by 1-way ANOVA followed by Tukey's multiple comparison test. *P<0.05, **P<0.01, values represent means ± SEM. n=3 for all time points. HTT antibody MAB5492 used to detect mHTTex1p. Panel (A) has been modified with permission [Grima et al. 2017]. ‡Reprinted from Grima et al., 2017 with permission from Elsevier.

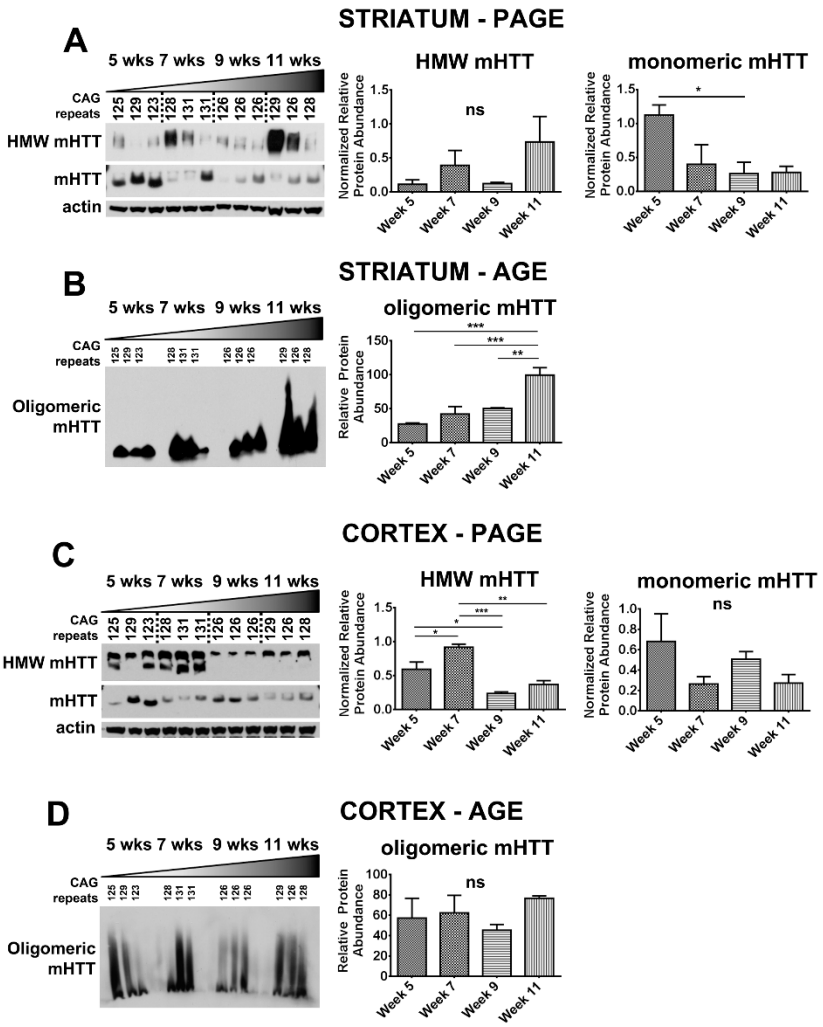

Figure 1.5. Detection of mHTTex1p is highly variable using TRIzol reagent. A) Striatal and **C)** Cortical protein samples recovered from TRIzol preparations show highly variable detection of both soluble monomeric and soluble HMW mHTTex1p as analyzed by PAGE and western blot. AGE analysis of **B)** Striatal and samples show a significant change in oligomer levels ($F_{3,8}$=16.02, p<0.001) while **D)** Cortical samples do not ($F_{3,8}$=0.95, p>0.05). Western blots quantified by mean pixel value and normalized to actin. AGE blots were quantified by mean pixel value. Data analyzed by 1-way ANOVA followed by Tukey's multiple comparison test. *P<0.05, **P<0.01, values represent means ± SEM. n=3 for all time points. HTT antibody MAB5492 used to detect mHTTex1p.

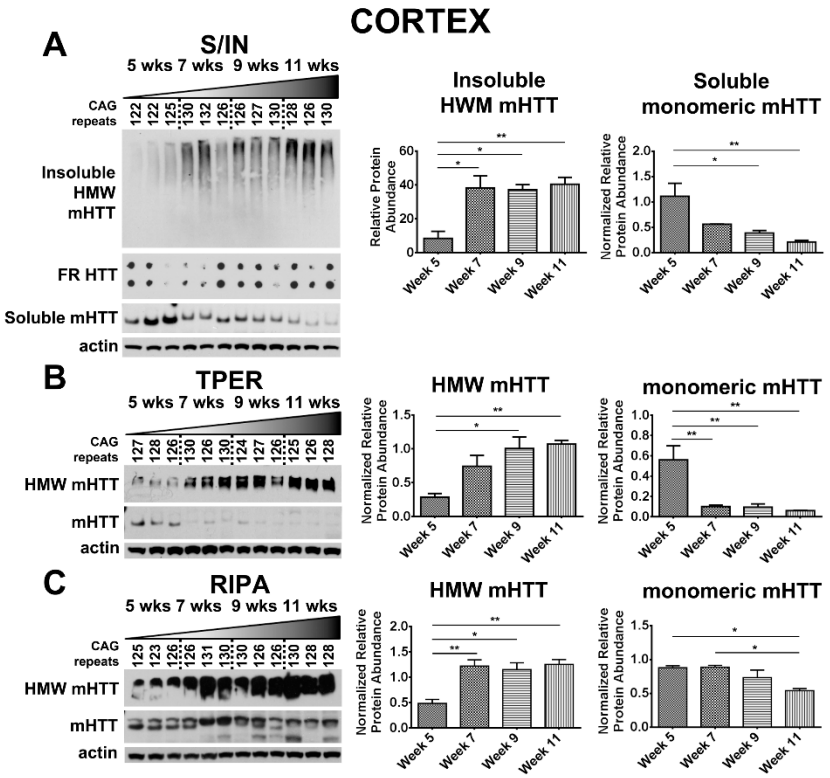

Figure 1.6. Detection of mHTTex1p in cortex of R6/2 mice. A) Cortical time-course samples were fractionated into Soluble and Insoluble proteins. Insoluble fraction reveals a significant increase in a HMW species of mHTT throughout disease progression ($F_{3,8}$=9.88, p<0.01). Soluble fraction shows an inverse, significantly decreased monomeric form of mHTTex1p throughout disease progression ($F_{3,8}$=8.78, p<0.01). Insoluble aggregates detected by filter retardation assay show no apparent change. Cortical tissue samples broken in **B)** T-PER (Monomer: $F_{3,8}$=10.91, p<0.01, HMW: $F_{3,8}$=8.42, p<0.01) and **C)** RIPA (Monomer: $F_{3,8}$=7.21, p<0.05, HMW: $F_{3,8}$=10.85, p<0.01) reagents show a significant reduction of monomeric mHTTex1p throughout disease progression accompanied by a significant increase in HMW mHTTex1p detected in the soluble fraction. Fluctuations in soluble, monomeric mHTTex1p correspond to varying CAG repeats in R6/2 mice. Western blots quantified by mean pixel value. Soluble fraction normalized to actin and analyzed by 1-way ANOVA followed by Tukey's multiple comparison test. *P<0.05, **P<0.01, values represent means ± SEM. n=3 for all time points. HTT antibody MAB5492 used to detect mHTTex1p.

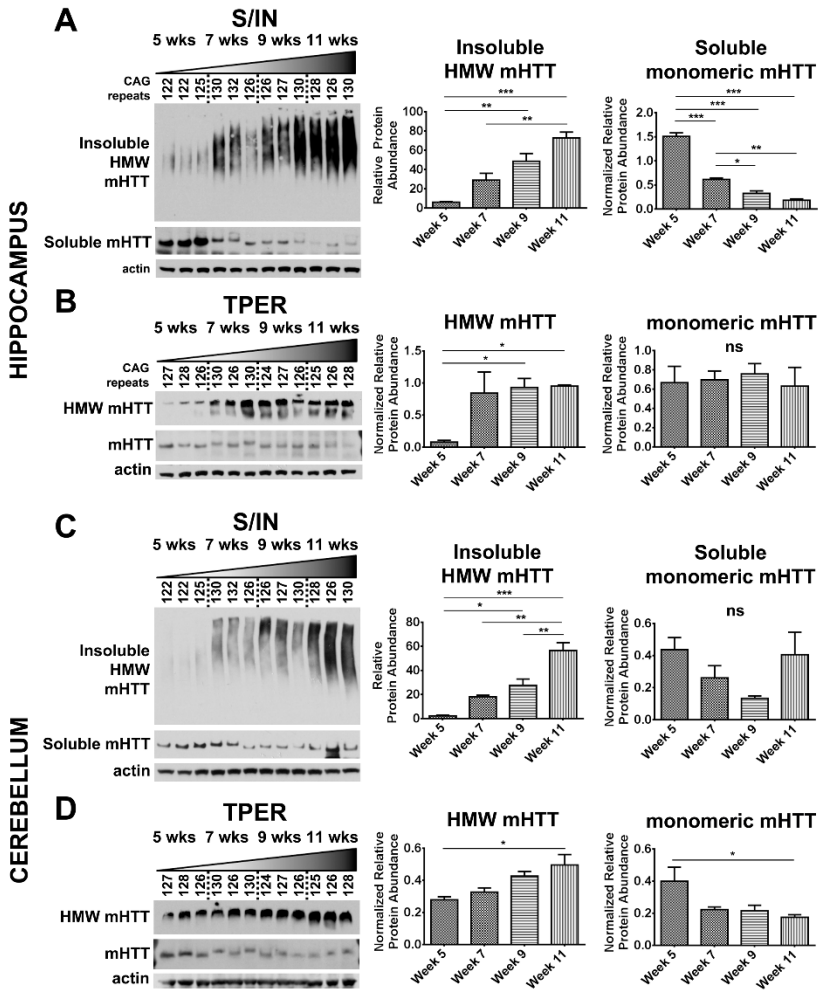

Figure 1.7. Detection of mHTTex1p in hippocampus and cerebellum of R6/2 mice varies depending on break method. Insoluble fraction in **A)** hippocampus reveals a significant increase in a HMW species of mHTTex1p throughout disease progression ($F_{3,8}$=21.05, p<0.001). Soluble fraction shows an inverse, significantly decreased monomeric form of mHTTex1p throughout disease progression ($F_{3,8}$=142.2, p<0.0001). **B)** T-PER processed hippocampal tissue samples did not show decrease in soluble monomeric mHTTex1p ($F_{3,8}$=0.13, p>0.05) or HMW accumulated mHTTex1p ($F_{3,8}$=5.41, p<0.05). Insoluble fraction in **C)** cerebellum reveals a significant increase in HMW species of mHTTex1p throughout disease progression ($F_{3,8}$=29.11, p<0.0001). Soluble fraction did not detect a significant decreased monomeric form of mHTTex1p ($F_{3,8}$= 2.51, p>0.05). However, soluble monomeric mHTTex1p decrease was detected in **D)** T-PER processed cerebellar tissue samples (HMW: $F_{3,8}$=6.32, p<0.05, Monomer: $F_{3,8}$=4.25, p<0.05). Fluctuations in soluble, monomeric mHTTex1p correspond to varying CAG repeats in R6/2 mice. Western blots quantified by mean pixel value. Soluble fraction normalized to actin and analyzed by 1-way ANOVA followed by Tukey's multiple comparison test. *P<0.05, **P<0.01, values represent means ± SEM. n=3 for all time points. HTT antibody MAB5492 used to detect mHTTex1p.

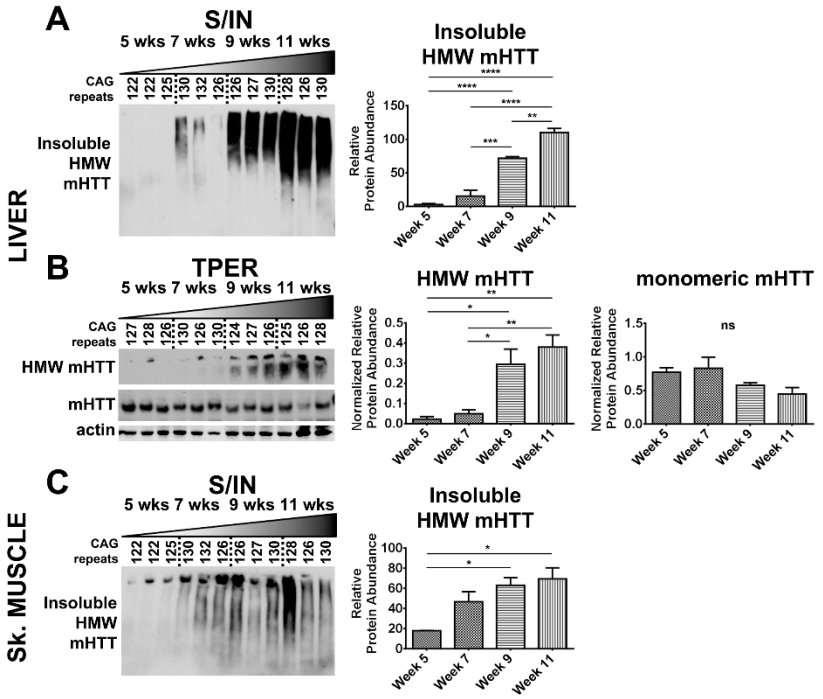

Figure 1.8. Detection of mHTTex1p in peripheral tissue varies depending on break method. A) Insoluble HMW mHTTex1p increases significantly throughout disease progression in Liver ($F_{3,8}$=83.34, p<0.0001) but Soluble, monomeric mHTTex1p is not detectable. **B)** Liver tissue broken in T-PER resolves soluble monomer revealing no change in detectable protein abundance ($F_{3,8}$=2.95, p>0.05) while HMW mHTTex1p showed a significant increase ($F_{3,8}$=12.79, p<0.01). **C)** Skeletal muscle also reveals a significant increase in insoluble HMW mHTTex1p ($F_{3,8}$=7.53, p<0.05). Soluble monomer is not detected in either Soluble/Insoluble fractionated samples. Western blots quantified by mean pixel value. Soluble fraction normalized to actin (liver) or GAPDH (Skeletal Muscle) and analyzed by 1-way ANOVA followed by Tukey's multiple comparison test. *P<0.05, **P<0.01, values represent means ± SEM. n=3 for all time points. HTT antibody MAB5492 used to detect mHTTex1p.

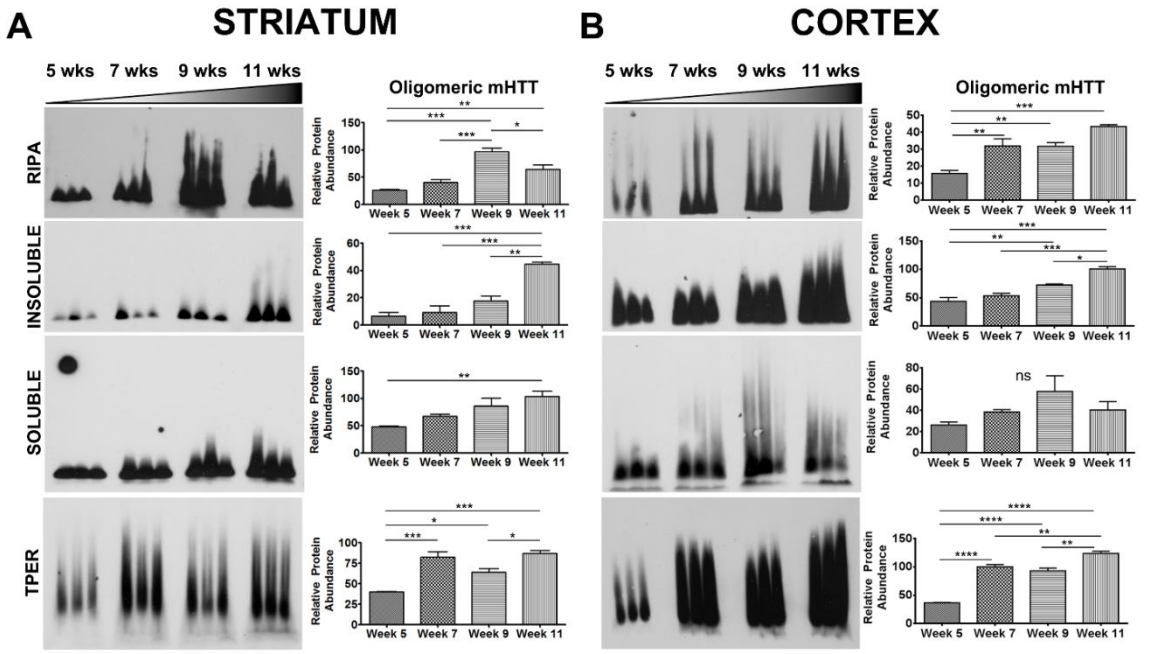

Figure 1.9. Detection of mHTTex1p on AGE gels varies based by break method. **A)** Striatal tissue samples broken in indicated buffers and analyzed by Agarose Gel Electrophoresis (AGE). R6/2 mice show an increase in oligomeric mHTTex1p through week 9 followed by a significant decrease by week 11 in RIPA broken samples ($F_{3,8}$=27.21, p<0.001). Increased, disease-endpoint mHTTex1p detected in Insoluble ($F_{3,8}$=27.31, p<0.001), Soluble ($F_{3,8}$=7.30, p<0.05), and T-PER ($F_{3,8}$=24.70, p<0.001) broken samples showed a significant increase by week 7, followed by a decrease in week 9 before increased again by week 11. **B)** Cortical samples broken in RIPA buffer ($F_{3,8}$=19.56, p<0.001), Insoluble ($F_{3,8}$=29.95, p<0.001) and Soluble fractionation ($F_{3,8}$=2.291, p>0.05), and T-PER buffer ($F_{3,8}$=109.3, p<0.0001) show either no change or significant increase in formation of oligomers by week 11. AGE blots were quantified by mean pixel value and analyzed by 1-way ANOVA followed by Tukey's multiple comparison test. *P<0.05, **P<0.01, ***P<0.001, ****P<0.0001 values represent means ± SEM. n=3 for all time points. HTT antibody MAB5492 used to detect mHTTex1p.

CHAPTER 1

TABLES

Table 1.1 Break methods optimized for detection of specific mHTT species.

Break Method	Optimized detection/rationale	Optimized Assay	Reference
Soluble/Insoluble fractionation	Soluble monomeric mHTT Insoluble HMW, accumulated mHTT	SDS-PAGE Filter retardation	[22, 23, 25, 40]
RIPA whole cell break	Soluble, Oligomeric mHTT	AGE	[19-21]
T-PER whole cell break	Aggregated protein species, commercially available and common reagent	SDS-PAGE	[41]
TRIZOL	Allows for analysis of RNA, DNA, and protein	SDS-PAGE	n/a

Table 1.2. CAG repeats from genomic tail DNA comparable to counts obtained from striatal cDNA from the same animal showing lack of somatic expansion in these animals. cDNA generated from RNA harvested from striatum. CAG repeat sizing of cDNA was performed by Laragen.

Animal	Age (weeks)	$(CAG)_n$ Genomic DNA (Tail)	$(CAG)_n$ cDNA (Striatum)
1	5	125	125
2	5	129	129
3	5	123	123
4	7	128	128
5	7	131	131
6	7	131	130
7	9	126	126
8	9	126	126
9	9	126	126
10	11	129	129
11	11	126	127
12	11	128	127

Table 1.3. Summary heat map of mHTTex1p detected using various break methods and assays at 5, 7, 9, and 11 weeks of age. Representative gradient for each assay based on ease of detection for general comparison. Cannot quantify between assay methods for relative protein abundance.

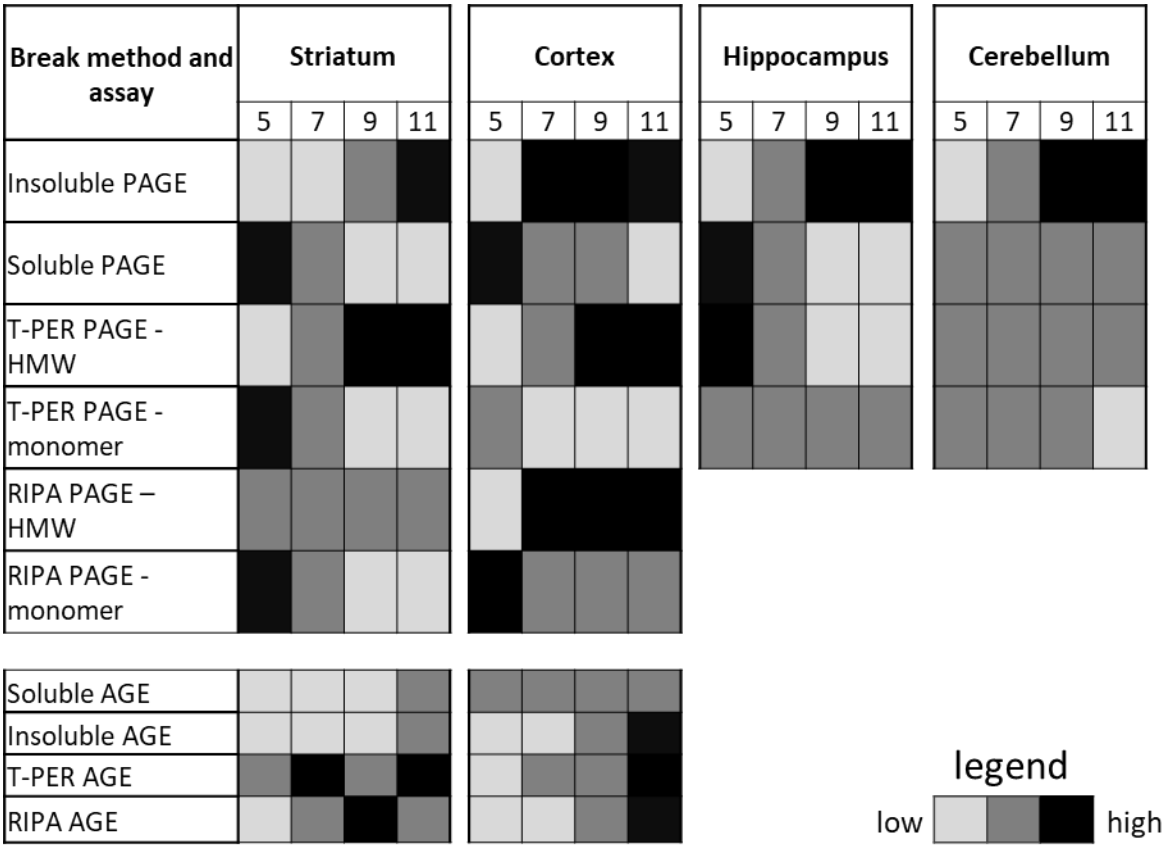

CHAPTER 2

G3BP1-positive stress granule pathology in Huntington's disease

SUMMARY OF CHAPTER 2

Stress granules (SGs) are membraneless organelles that form in response to cellular stress. Chronic cellular stress associated with neurodegenerative disease results in the persistence of SG structures. Chronic expression of mutant huntingtin generates various forms of cellular stress, including activation of the unfolded protein response and oxidative stress. However, it has yet to be determined whether SGs are a feature of Huntington's disease (HD) neuropathology. We investigated localization and levels of the SG nucleating protein G3BP1 and found a significant increase in the density of G3BP1-positive SGs in the cortex and hippocampus of R6/2 transgenic mice, as well as in the superior frontal cortex of HD patient brains. We also examined the miRNA composition of extracellular vesicles (EVs) present in the cerebrospinal fluid (CSF) of HD patients and show that a subset of their target mRNAs is differentially expressed in the prefrontal cortex of HD patients. Of these targets, there is an enrichment of SG components, including G3BP1. These findings suggest that SG dynamics might play a role in the pathophysiology of HD. We propose a potential role for CSF EV miRNAs in the regulation of SGs and identify specific miRNAs that can be employed to modulate G3BP1-positive SGs.

INTRODUCTION

Huntington's disease (HD) is a progressive, inherited neurodegenerative disease caused by an expanded CAG repeat in exon 1 of the huntingtin (*HTT*) gene (The Huntington's Disease Collaborative Research Group), encoding an expanded polyglutamine repeat tract within the HTT protein. The gene is ubiquitously expressed throughout the body and brain (Li et al., 1993; Strong et al., 1993). Although HD is characterized by pathology that most prominently affects neurons of the striatum, human autopsy studies show that other brain areas are also impacted, raising the question of whether intercellular and intertissue communication could in part contribute to the spread of pathogenesis.

The expression of mutant HTT gives rise to a number of cellular stress responses, including oxidative and endoplasmic reticulum (ER) stress, potentially as a neuroprotective strategy against cellular toxicity (Fulda et al., 2010; Duennwald et al., 2015; Browne et al., 1999; Shacham et al., 2019). Multiple cellular stress responses converge on key translation factors and interfere with general protein synthesis to optimize cell survival and stress recovery (Liu et al., 2014). One of these translation factors, eIF2A, is inactivated in HD due to ER stress and this alteration is proposed to play an important role in striatal cell death (Leitman et al., 2014). Overall, these studies hint at a direct connection between the regulated expression of translation factors, but any evidence of how these are regulated is far from understood.

A myriad of stress signals are known to induce stress granule (SGs) formation. SGs are assemblies of protein and RNAs that form in the cytoplasm in response to stressors such as hypoxia, heat-shock, and sodium arsenite, which all inhibit translation initiation (Arimoto

et al., 2008). Their elimination, in turn, depends on ATP-driven disaggregases, such as Hsp40 and Hsp70, and granulophagy through the ATP-dependent VCP-autophagy pathway (Kedersha et al., 2005; Buchan et al., 2013). Pathologic SG accumulation has been implicated in several neurodegenerative diseases (Li et al., 2013; Wolozin and Ivanov, 2019; Baradaran-Heravi et al., 2020; Chew et al., 2019). However, although *in vitro* experiments using fragments of the HTT protein suggest that expanded HTT interacts with SG-associated proteins and is redistributed to SGs under ER-stress conditions (Ratovitski et al., 2012), it has not been demonstrated for HD *in vivo*. Interestingly, the SG component TIA1 Cytotoxic Granule Associated RNA Binding Protein (TIA1) can be sequestered by HTT aggregates *in vitro* and in the R6/2 mouse model of HD (Furukawa et al., 2009). In addition, bioinformatic studies determined that the expression of 395 out of 464 putative SG related components are altered in HD (Nunes et al., 2019); of these 395 components, 195 are induced and 200 are repressed in HD patient brain. These findings support the need for further investigations into potentially pathologic SG dynamics in HD.

HD is characterized by a progressive spreading of neuropathology (Rub et al., 2016), and recent findings suggest that the 'spreading effect' that is characteristic of many neurodegenerative disorders might be mediated by extracellular vesicles (EVs) (Scott et al., 2017; Raposo et al., 2013). EVs that contain RNA, protein and lipids are one potential mediator given that multiple studies demonstrate that EVs can transfer their contents to other cells and mediate intra- and inter-cellular signaling (Bang et al., 2012; Mathieu et al., 2019). EVs containing pathogenic cargo could facilitate the spread of pathology between brain regions (Scott et al., 2017); modulators of SG dynamics would be among the possible candidates for facilitating such spread. One type of EV are exosomes, 40-150 nm vesicles of

multivesicular body (MVB) origin secreted by several cell types, including neural cells (Harding et al., 2013; Pan et al., 1985; Simons et al., 2009; Thery et al., 2009), that can be isolated from various biofluids including the cerebrospinal fluid (CSF) (Soares Martins et al., 2018). Due to the lack of consensus on specific exosome markers and the recommendations put forth by the International Society of Extracellular Vesicles (Thery et al., 2018), we will use the generic term "EV" in place of all cell-secreted nanovesicles mentioned in this study.

The composition of EVs is highly regulated. Comparisons between *in cellulo* RNA content and EV RNAs demonstrate selective enrichment of specific EV RNA (Ratajczak et al., 2006; Nolte-'t Hoen et al., 2012), suggesting regulation of RNA loading into EVs (Janas et al., 2015; Shurtleff et al., 2016; Villarroya-Beltri et al., 2013). One class of RNA enriched in EVs are microRNAs, small RNA molecules (~22 nucleotides) that regulate post-transcriptional gene expression by acting as guide molecules to promote the degradation or translational repression of their target mRNAs. The human genome encodes ~2000 miRNAs and it is predicted that they collectively regulate one third of the genes in the genome (Hammond et al., 2015). Thus, miRNA dysregulation is likely to have a significant effect on gene expression networks. Furthermore, *in vitro* and *in vivo* studies have revealed that environmental stressors, including heat shock and hypoxia, can modify the miRNA composition of EVs (Beninson et al., 2014). Similarly, it is plausible that disease-mediated cellular stress, such as that caused in neurodegenerative disease, can modify the miRNA composition of CSF EVs.

Cell-to-cell shuttling of miRNAs via EVs is a critical mediator of transcriptional regulation in recipient cells (Scott et al., 2017; Zhang et al., 2015). There is evidence that selected groups of miRNAs are altered in HD cells and tissues (Hoss et al., 2014; Hoss et al., 2015; Johnson et al., 2008; Lee et al., 2011; Kocerha et al., 2014), which suggests that miRNA dysregulation might be involved in gene expression changes detected in the HD brain, and in turn affect cellular function. A recent study identified an EV miRNA secreted from the choroid plexus, a tissue located in the ventricles which produces the majority of the CSF, that regulates adult neurogenesis at the subependymal zone by repressing translation of neural fate determinants (Lepko et al., 2019). Thus, it is possible that EV miRNAs secreted into the CSF of HD patients could be taken up by brain tissues situated near the ventricular zone and regulate the translation of selected proteins, thereby playing a role in the propagation of pathology in the brains of HD patients. However, characterizing the interplay between the molecular features of HD pathology and their regulation is still a major challenge in the field.

To initiate investigations into the relationship between mutant HTT-mediated cellular stress and the miRNA composition of CSF EVs, we first evaluated R6/2 mouse and human HD postmortem brain tissue for altered SG dynamics and found that there is a significant SG density increase in the superior frontal cortex of both R6/2 and human brain. This increase was particularly noted in pyramidal neurons of the superior frontal cortex, and a similar pattern of immunoreactivity was detected in the human parietal cortex and hippocampus. To examine whether miRNAs secreted into the CSF may have a connection to the observed pathology, we isolated EVs from HD and control CSF to assess changes in packaged miRNAs. 81 miRNAs were dysregulated and were evaluated for functional

enrichment through mRNA targets. Among these are SG components, including the Ras GTPase-activating protein-binding protein 1 (G3BP1), a critical effector of SG assembly (Tourriere et al., 2003) and central node of the core SG network (Yang et al., 2020) in eIF2A-mediated mechanisms of SG formation. We then tested the hypothesis that miRNAs could modulate the protein expression and SG nucleating function of G3BP1 in cells treated with sodium arsenite, a SG inducer, and find that a set of miRNAs do indeed modulate G3BP1-positive SG density. These data suggest that increased SG density is a component of the brain's response to chronic mutant HTT expression and that miRNAs secreted within EVs from human CSF have the capacity to modulate G3BP1-mediated SG nucleation.

RESULTS

Increased G3BP1 SG density and immunoreactivity in the R6/2 mouse cortex and hippocampus

Based on the notion that HD induces a form of chronic stress and that SGs have been detected in other neurodegenerative diseases using established SG markers (Wolozin and Ivanov, 2019; Vanderweyde et al., 2012; Zhang et al., 2018), we investigated whether SGs are present as a consequence of chronic mutant HTT expression using the critical SG marker G3BP1 — the molecular switch that triggers SG formation (Yang et al., 2020). We evaluated whether SG formation could be detected in the R6/2 mouse brain, which express a transgene encoding human amino terminal exon1 and have a rapidly progressing phenotype (Mangiarini et al., 1996). Localization and intensity of the G3BP1 protein and SG density were evaluated by immunofluorescence and confocal microscopy. A statistically significant increase in G3BP1 immunoreactivity and SG density was detected in the cortex

(p=0.021 and 0.001, respectively; Student's t-test), and of SG density in region CA1 of the hippocampus (p=0.028) (**Figures 2.1 and 2.2**). We did not detect any significant differences in G3BP1 staining or SG density in the striatum at the 12 or 8-week time points (**Figure 2.3**).

Because HTT aggregation has been implicated in the fibrillation of the SG marker TIA1 in R6/2 hippocampus (Furukawa et al., 2009; Gilks et al., 2004), we assessed the potential colocalization of G3BP1-positive SGs with HTT at 12 weeks. We first tested the EM48 antibody, which recognizes HTT inclusions (Gutekunst et al., 1999), but did not detect G3BP1 colocalization with EM48-positive nuclear inclusions (**Figure 2.4, A**). However, we detected modest degrees of fluorophore colocalization between G3BP1 and HTT with 3B5H10 (which recognizes monomeric and small oligomeric polyQ species of mutant HTT (Miller et al., 2011)), 5490 (which recognizes wild type and mutant HTT (Lunkes et al., 2002)), and the polyQ antibody 1C2 (which preferentially binds expanded polyQs (Trottier et al., 1995; Klein et al., 2013) (**Figure 2.4, A-C**). To confirm that the observed increase in G3BP1 immunoreactivity in R6/2 cortex and hippocampus is not due to a nonspecific increase in antibody binding due to the tissue preparation and fixation methods, we investigated the immunoreactivity of the RNA binding protein hnRNPA2/B1 (Geuens et al., 2016) based on our observations that its immunoreactivity is decreased in the R6/2 hippocampus (**Figure 2.5**). Unlike G3BP1 immunoreactivity, hnRNPA2/B1 immunoreactivity is not higher in the R6/2 brain, suggesting that the observed increase in G3BP1 immunoreactivity is not due to nonspecific antibody binding. Lastly, because it has been suggested that G3BP2, a G3BP1 homolog expressed in mouse brain, to also contribute to the formation of SGs (Cirillo et al., 2020; Matsuki et al., 2013), we evaluated whether

G3BP2 is involved in SG pathology in the R6/2 brain. Using the same analyses, we did not detect G3BP2-positive granular structures in R6/2 or non-transgenic brains (**Figure 2.6**), suggesting that G3BP1 and G3BP2 might not be functionally redundant in *in vivo* SG formation. Overall, these results point toward stress induced G3BP1-SG formation in R6/2 HD mouse cortex and hippocampus and a potential association with HTT.

Increased G3BP1 SG density in the superior frontal cortex of Huntington's disease patients

We next set out to determine whether we could also observe this cortical G3BP1 SG phenotype in human HD patient brain tissue. While HD neurodegeneration has been described primarily in the striatum, neuronal loss has also been detected in other areas, including pyramidal projection neurons of the cortex (Cudkowicz et al., 1990). Topologically selective cortical changes are thought to explain some of the clinical heterogeneity among patients (Rosas et al., 2008; Nana et al., 2014; Mehrabi et al., 2016), with the superior frontal and parietal cortices exhibiting the highest overall cortical loss (Nana et al., 2014), suggesting that these regions might be especially vulnerable to mutant HTT-mediated cellular stress. Based on this, we investigated SG pathology in the superior frontal and parietal cortices, as well as hippocampus, based on pyramidal neurons being one of the principal cell types of this region and that memory dysfunction is a clinical feature of HD (Montoya et al., 2006).

First, we examined the superior frontal and parietal cortices, and the hippocampus of 2 HD (pathological grade 2, which designates initial gross striatal atrophy (Vonsattel et al., 1985)) and 2 control postmortem brains (**Table 2.1**). We observed high G3BP1

immunoreactivity in the HD patient brains (**Figures 2.7-2.10**), particularly in the superior frontal cortex, where overall neuronal loss is also highest (Nana et al., 2014). To quantitatively assess whether HD tissues have increased SG density, we repeated the G3BP1 SG analysis performed in the R6/2 mice in 6 HD (pathological grade 3) and 6 control superior frontal cortex postmortem samples (**Table 2.1**). We found a statistically significant G3BP1 SG density increase in the superior frontal cortex of HD brains compared to controls (p=0.008, Student's t-test), suggesting that this brain region is particularly reactive to cellular stress in HD (**Figure 2.11, A, B and 2.12-2.17**). Because SGs are compositionally diverse and their components depend on the type of stress the cell is exposed to (Panas et al., 2016), we investigated the colocalization of G3BP1-positive SGs with another SG marker. We found that some G3BP1 SGs colocalize with the translation initiation factor and SG marker eIF3H (**Figure 2.11, C and 2.18**), which colocalizes with poly(GR) dipeptide repeat protein in the brains of c9FTD/ALS patients (Zhang et al., 2018). This colocalization is not present in all cases, potentially suggesting that each of these markers represents a different SG subtype under mutant HTT-mediated cellular stress, and that *in vivo* SGs may assemble via more than just one mechanism.

As mentioned above, pyramidal cell loss is detected in various cortical regions in human HD, including the superior frontal cortex (Nana et al., 2014), the region where we observe a significant increase in G3BP1 SG density. It has been proposed that pyramidal neurons residing in the deep layers of the cortex, which project directly to the striatum, are selectively vulnerable to mutant HTT-mediated toxicity (Sieradzan et al., 2001). While G3BP1 appears to be widely expressed throughout the HD brain, a subgroup of cells demonstrates higher G3BP1 immunoreactivity. These cells have pyramid-shaped cell

bodies, are immunoreactive for the pyramidal neuron marker Ca2+/calmodulin-dependent protein kinase 2 (CaMK2) and are primarily located in the cortical ribbon of the cortex and areas CA1/CA2/CA3 of the hippocampus (**Figure 2.19**). These findings suggest that pyramidal neurons might be especially vulnerable to cellular stress in HD.

Characterization of HD and control CSF extracellular vesicles

In vitro and *in vivo* experiments have demonstrated that various forms of cellular stress can modify the miRNA composition of EVs (Beninson et al., 2014). Because EV-packaged miRNAs distributed via the CSF can have important implications by altering gene expression (Scott et al., 2017) and have potential to serve as biomarkers (Kanninen et al., 2016), we next investigated the CSF EV miRNA profile of HD patients and their potential connection to SG pathology. miRNA dysregulation has been described in the prefrontal cortex of HD patients (Hoss et al., 2015), and out of 75 differentially expressed miRNAs, 35 are predicted to target G3BP1 (**Table 2.2**). From those 35 miRNAs predicted to target G3BP1, 22 are upregulated in HD, suggesting a potential compensatory mechanism in response to pathologic SG formation. While miRNAs are synthesized within the cell, they can also originate from EV-mediated intercellular communication via biofluids such as the CSF (Lepko et al., 2019). Once released from the donor cell, EV miRNAs can manipulate gene expression in recipient cells of neighboring tissues via post-transcriptional repression (Lepko et al., 2019; Thomou et al., 2017). Due to the high stability of EVs in biofluids (Sanz-Rubio et al., 2018; Ge et al., 2014), and the fact that CSF is in direct contact with the extracellular space and reflects the biological changes occurring in the brain, CSF EV miRNAs are being investigated in the context of various neurodegenerative diseases (Gui et

al., 2015; Wang et al., 2020; Riancho et al., 2017). Based on this rationale, we investigated whether differential miRNA packaging into CSF EVs occurs and whether these patterns might be consistent with transcriptional dysregulation that is observed in the human HD prefrontal cortex (Labadorf et al., 2015).

To investigate differential packaging of miRNAs into EVs in the CSF of HD patients compared to unaffected individuals, EVs were isolated by membrane affinity column centrifugation from 10 HD patient and 10 control CSF samples and RNA contents extracted for miRNA sequencing. CSF samples were acquired by lumbar puncture as described in the Methods section, and patient demographic characteristics are summarized in **Figure 2.20, A**. Given that the profile of CSF miRNAs varies between vesicular and non-vesicular fractions, and that the distribution of their mode of transport can differ between normal and pathological conditions (Kopkova et al., 2018; Yagi et al., 2017), we employed a membrane affinity-based approach to isolate miRNAs from CSF EVs which ensures that non-vesicular CSF miRNAs are washed out prior to final elution. To characterize the size distribution of the EV fractions collected, we performed Fluorescent Nanoparticle Tracking Analysis (F-NTA) on a subset of 5 HD and control CSF samples. This NTA method prevents the inclusion of protein aggregates, membrane fragments, and background particles present in heterogenous biofluid samples. Each sample was measured in triplicate, and videos of data collection were analyzed to give the mean, mode, and estimated concentration for each particle size (**Figure 2.21).** Because EV subtypes are generally characterized by size, and the CSF is likely to contain a heterogeneous mixture of EVs, we analyzed EV particle concentration by EV size increments of 25 nm. We did not detect a significant difference in concentration of any EV size subtype between the HD and control

CSF samples (**Figure 2.20, B**). Similarly, we did not detect a significant difference in mode diameter size, or overall particle concentration (**Figure 2.20, C, D**).

Cerebrospinal fluid extracellular vesicles from Huntington's disease patients contain miRNAs that target SG-associated genes

During the miRNA Library Kit construction process, each individual miRNA molecule was tagged with a Unique Molecular Index (UMI). Following sequencing and trimming, reads were analyzed for the presence of UMIs and an average of ~10 million reads were generated per mapped sample. Differential expression analysis of the HD versus control samples was carried out using DESeq2. We did not detect any statistically significant differences after correcting for multiple comparisons using the Benjamini-Hochberg method. A subsequent sample size analysis (Hart et al., 2013) was carried out using a coefficient of variation estimated from this DESeq2 differential expression analysis which suggested that 143 samples per group would be needed to observe significant differences of about a 2-fold change in expression. This calculation suggested a limitation in the ability to identify statistically significant expression changes; however, we sought to investigate the potential functional relevance of the CSF EV miRNAs detected in our studies by overlapping the predicted gene targets of the miRNAs detected in CSF EVs with a publicly available dataset of genes that are differentially expressed (DEGs) in the prefrontal cortex of HD patients (Labadorf et al., 2015), a brain region proximal to the CSF and thus has the potential to serve as the recipient of CSF EV cargo. Our reasoning here is that miRNAs in the CSF may be coming from many different cell types and thus some miRNAs could be very

highly expressed in locally released EVs, to impart biology in close-proximity target cells, all the while being undetectable from bulk CSF isolation.

Previous studies have integrated miRNA and mRNA expression profiles to better understand miRNA-mRNA interactions in specific biological contexts (van Iterson et al., 2013; Nuzziello et al., 2019). Similarly, using the results from the DESeq2 differential expression analysis of CSF EV miRNAs, we generated a list of 22 differential miRNAs (**Table 2.3**) with a p-value <0.05 before correcting for multiple comparisons, and another list of 59 miRNAs (**Table 2.4**) with log2FC values larger than a magnitude of 2 (81 miRNAs total) (**Figure 2.22, A**). We next performed a target analysis on the 81 miRNAs and generated a list of predicted mRNA targets. The list of mRNA targets was then overlapped with a dataset of DEGs from the prefrontal cortex of HD patients (Labadorf et al., 2015), and the number of targets ranged from 72-2,509 DEGs for each miRNA. Since the expression level of a miRNA is negatively correlated to the expression level of its target gene, we filtered out miRNAs whose fold changes were not the inverse of their target genes 50% or more of the time. This resulted in a list of 41 miRNAs that target DEGs in the HD prefrontal cortex, and whose differential expression in HD CSF EVs is negatively correlated to at least 50% of their prefrontal cortex DEG targets **(Table 2.5,** GO enrichment analysis of predicted gene targets in **Table 2.6**).

Using this filtering approach, we evaluated whether SG-related genes were targets of these miRNAs detected in CSF EVs. In the context of SG component regulation, miRNAs may either directly repress the translation of SG mRNAs, or indirectly induce the translation of SG mRNAs by silencing upstream negative regulators of SG components. We asked whether

SG genes are significantly enriched in the list of gene targets belonging to these 41 miRNAs, and found that 120 of 4,689 CSF EV miRNA gene targets belong to the list of 464 mammalian SG genes (Nunes et al., 2019), which is significantly higher than what is expected by chance ($P<0.05$ using the Fisher's exact, hypergeometric test) (**Figure 2.22, B**). G3BP1 was one of the SG genes that fit these criteria and is upregulated in the HD prefrontal cortex, together with other SG genes include TIAL1, FUS, and various hnRNP RNA binding proteins (**Figure 2.22, C**). Of note, one of the 41 miRNAs was miR-1322, which has been previously identified as a potential prodromal biomarker for HD in CSF samples containing both vesicular and extravesicular miRNAs (Reed et al., 2018). Of relevance to HD, the majority of miR-1322 binding sites are located in their targets' coding domain sequences (CDS), many of which code for polyglutamine repeats, and include HTT (Niyazova et al., 2015). Overall, these results suggest that miRNAs packaged in vesicles may serve as regulators of stress response genes and given the G3BP1 SG phenotype detected in the HD brain, we investigated whether miRNA overexpression is sufficient for the inhibition of G3BP1-positive SGs *in vitro*.

G3BP1 protein levels and G3BP1-positiveSG density are reduced in 293T cells with the overexpression of miRNAs miR-6129, miR-4725-3p, miR-4700-5p, and miR-449

G3BP1 is a key SG nucleator, acting a as the molecular switch that triggers phase separation during SG formation (Yang et al., 2020). We therefore tested whether G3BP1 expression is modulated by miRNAs. We carried out these initial miRNA validation studies using human immortalized 293T cells, which have high transfection efficiency and are commonly employed to investigate SG dynamics *in vitro*. We hypothesized that the overexpression of

specific miRNAs detected in CSF EVs of HD patients might modulate G3BP1 protein levels and therefore could be regulators of SG assembly. To select the miRNAs to be used in the overexpression studies, the filtered list of CSF EV miRNAs obtained from patient CSF were ranked based on predicted strength of miRNA repression on G3BP1, or "G3BP1 seed strength," using TargetScan and miRmap (Vejnar et al., 2012; Agarwal et al., 2015). We created a composite list of ranked miRNAs with highest seed strength toward G3BP1 (**Figure 2.23**) and selected the following miRNAs to carry out transfection studies *in vitro*: miR-6129, miR-4725-3p, miR-4700-5p, miR-449a, miR-605-3p, miR-4476, and miR-1322. Three of these miRNAs were downregulated (miR-605-3p, miR-4476, and miR-1322), and four of them upregulated (miR-6129, miR-4725-3p, miR-4700-5p, miR-449a), in HD CSF EVs.

There is evidence that combinatorial miRNA overexpression can achieve greater specificity and minimize off-target effects (Cursons et al., 2018; Bracken et al., 2016), therefore to test the effect of these miRNAs on G3BP1 protein expression, we overexpressed locked nucleic acid (LNA) miRNA mimics in 293T cells using a combinatorial approach. The three downregulated miRNAs (miR-605-3p, miR-4476, and miR-1322) were labeled "Set 1," and the four upregulated miRNAs (miR-6129, miR-4725-3p, miR-4700-5p, miR-449a) were labeled "Set 2." Protein expression of G3BP1 was significantly reduced in cells treated with the "Set 2" 4-miRNA cocktail (One-way ANOVA, Dunnett's multiple comparison test, $p=0.0190$), but not the "Set 1" 3-miRNA cocktail (One-way ANOVA, Dunnett's multiple comparison test, $p=0.0550$), when compared to cells transfected with a negative control miRNA (**Figure 2.24, A-C**). It is possible that the "Set 1" miRNA cocktail treatment did not result in a significant reduction of G3BP1 protein expression due to its 3 miRNAs having a

lower combined G3BP1 seed strength compared to the "Set 2" miRNA cocktail consisting of 4 miRNAs (**Figure 2.23, B**). Another possibility worth considering is that the miRNAs in "Set 2" have a lower amount of total targets, resulting in a higher miRNA:G3BP1 ratio and thus higher repression of G3BP1. However, "Set 2" had 10,081 predicted targets and "Set 1" had 9,371. As an additional control, we measured hnRNPA2/B1 protein expression, which was not predicted to be a co-target of the miRNA cocktails based on seed strength scores. Indeed, hnRNPA2/B1 protein expression did not change with miRNA treatment (**Figure 2.24, B, D-F**). Next, we investigated the functional relevance of the miRNA cocktails by testing their effect on SG formation *in vitro*.

We hypothesized that treatment with the "Set 2" miRNA cocktail would result in lower SG seed formation (Panas et al., 2016) and thus decrease SG density upon cellular stress induction. SGs can be induced in mammalian cells as a result of sodium arsenite treatment, a form of oxidative stress (Kedersha et al., 1999; Jain et al., 2016). To test whether the miRNA cocktail treatments have an effect on SG formation *in vitro*, we repeated the transfection experiments in 293T cells, and subsequently subjected them to sodium arsenite treatment to induce SGs. Stressed cells that were treated with the "Set 2" 4-miRNA cocktail had a lower SG density compared to cells transfected with a negative control miRNA (**Figure 2.25 and 2.26**, One-way ANOVA, Dunnett's multiple comparison test, p=0.0362). Transfection of the "Set 1" 3-miRNA cocktail did not result in reduced SG density (One-way ANOVA, Dunnett's multiple comparison test, p=0.1248). These findings suggest that miRNAs can modulate SG biology via the post-transcriptional regulation of SG components and suggests their potential use as an investigative and therapeutic tool to target SG pathology in neurodegenerative disease.

DISCUSSION

Perturbations of SG dynamics have been implicated in neurodegenerative diseases such as amyotrophic lateral sclerosis, frontotemporal dementia, and Alzheimer's disease (Wolozin and Ivanov, 2019; Chew et al., 2019, Vanderweyde et al., 2012; Mackenzie et al., 2017; Chen et al., 2017; Gopal et al., 2017), although the consequence of these changes is not yet clear. Our study provides, for the first time, evidence for the presence of a G3BP1 SG phenotype in the brains of the R6/2 mouse model and human HD, and the identification of miRNAs that can modulate G3BP1 SG density. Our findings also show that EV miRNAs altered in the CSF of HD patients are predicted to target mRNAs that are differentially expressed in the HD prefrontal cortex, with SG genes being significantly overrepresented. The data suggest that the dysregulation of CSF EV miRNAs likely acts as a compensatory mechanism to modulate the recipient cell's response to intrinsic cellular stress resulting from mutant HTT expression by repressing G3BP1, as opposed to miRNA dysregulation in HD as a cause of G3BP1 SG pathology.

The majority of our knowledge of SG biology is currently based on *in vitro* experiments using a stress time course that is likely shorter than what an organism experiences in the context of chronic diseases such as neurodegeneration. Under acute stress conditions, SGs appear to provide a pro-survival benefit and are highly dynamic (Arimoto et al., 2008; Arimoto-Matsuzaki et al., 2016). Current hypotheses regarding mechanism include the regulation of translation of a specific subgroup of mRNAs or activation of pro-survival signaling pathways (Reineke et al., 2019). Efforts have been made to better understand SG biology in the context of chronic stress *in vitro* by using prolonged nutrient starvation as a stressor, suggesting that chronic stress SGs differ significantly from acute stress SGs by way

of their contents, decreased exchange with cytoplasmic mRNP pools, and promotion of cell death (Reineke et al., 2018). Interestingly, SG depletion in the context of chronic starvation resulted in increased cell survival, corroborating other findings in fly and mouse models of neurodegeneration (Kim et al., 2014; Radford et al., 2015; Zhang et al., 2018), and providing a rationale for further investigating therapies to target SG pathology in neurodegenerative disease.

SG assembly is promoted by RNA binding proteins that oligomerize in response to cellular stress. One of these key proteins is G3BP1 (Kedersha et al., 2007), which is dephosphorylated and oligomerizes as a response to cellular stress, resulting in the nucleation of SGs (Tourriere et al., 2003). Recently, G3BP1 has been identified as a central node of the protein-RNA interaction network that triggers RNA-dependent liquid-liquid phase separation during SG formation under eIF2A-mediated cellular stress (Yang et al., 2020). Previous reports demonstrate that mutant HTT-mediated ER stress results in PERK activation, leading to the phosphorylation of eIF2A, and inhibition of general protein synthesis (Leitman et al., 2014), all of which are involved in SG formation *in vitro* (Panas et al., 2016). This study found both total and phosphorylated eIF2A levels to be higher in the HD mouse cortex compared to striatum, perhaps explaining why we detected a significant increase of G3BP1 SG density in the cortex but not striatum. That is, if the available eIF2A concentration is not large enough, the threshold for SG liquid-liquid phase separation might not be reached. A limitation of this study is that we exclusively investigated G3BP1-mediated SG pathology, and the question remains whether the density of other SG subtypes is affected when G3BP1-positive SGs are repressed with miRNAs. Lastly, the miRNA cocktails used to target G3BP1 were designed based on whether the miRNAs were

upregulated or downregulated in HD CSF EVs, however the strength of target repression could potentially be further optimized by grouping miRNAs in such a way that increases the combined G3BP1 seed-strength. Employing this type of *in vitro* system will narrow down miRNAs that are highly effective at modulating SG densities and will be used to inform future patient-derived iPSC model and *in vivo* studies that focus on the impact of SGs on disease progression.

One potential mechanism through which SGs might be detrimental in diseases where proteostasis is impaired is if SG components, of which a majority are RNA binding proteins, have the potential to cross-seed with protein aggregates via their low complexity domains (Furukawa et al., 2009, Dobra et al., 2018), exacerbating proteotoxicity. Conversely, some studies suggest that SGs might serve a more protective role in disease. For instance, more G3BP SGs are present in neurons that do not accumulate tau aggregates (Vanderweyde et al., 2012), suggesting that this SG subtype might provide a neuroprotective role in cases where protein aggregates are cytotoxic. Another study found SG induction to be protective in mouse cochlear sensory hair cells during aminoglycoside ototoxicity (Goncalves et al., 2019), however one could argue that the stress time course utilized in these studies, 24 hours after systemic kanamycin/bumetanide treatment in C57BL/6 mice, is considered to be acute compared to the time course of cellular stress resulting from neurodegeneration. Testing of small molecule compounds that modulate SG accumulation (Fang et al., 2019), miRNAs such as described here, and other approaches to target SG formation will be informative in future studies to evaluate the consequence of altered SG dynamics in HD.

Our finding that pyramidal neurons demonstrate high G3BP1 SG immunoreactivity, and previous findings of pyramidal neuron loss in the cortex of HD patients (Nana et al., 2014), poses the question of whether pyramidal neurons are especially vulnerable to mutant HTT-mediated cellular stress. If SGs are serving a protective role at any point during HD progression, this finding of high SG formation might also explain why neuron loss in the cortex is not as profound as that which is detected in the striatum. Memory dysfunction is an important feature in the early clinical presentation of HD (Josiassen et al., 1983). A meta-analysis of multiple studies identified episodic memory impairments in HD (Montoya et al., 2006), a type of memory that relies heavily on the hippocampus and prefrontal cortex (Eichenbaum et al., 2017). Interestingly, the hippocampus and cortex are areas of the brain with highest G3BP1 expression (Martin et al., 2013). In the hippocampus, high G3BP1 expression is detected in the cell bodies of the dentate granule cell layer and CA pyramidal regions of hippocampal formation. Furthermore, G3bp1-knockout (KO) mice demonstrate behavioral defects linked to the CNS as well as altered Ca2+ homeostasis in hippocampal neurons, and behavioral studies suggest that G3BP1 plays a role in synaptic transmission and plasticity in the hippocampus (Martin et al., 2013). It is tempting to speculate that SG pathology in pyramidal neurons of the cortex and hippocampus could be associated with the memory impairments presented by HD patients.

Our SG timepoint study observations in 8 and 12-week R6/2 mice suggest that G3BP1 SG immunoreactivity progressively increases, becoming statistically significant sometime between the 8 and 12-week timepoints. This has important implications for postmortem brain studies, as many of the available control samples often originate from older individuals. Therefore, both postmortem interval and age matching are important

parameters to consider when selecting postmortem cases to study SG pathology in disease. Based on our findings and the potential for HTT aggregates to participate in cross-seeding with SG components, we speculate that the SG pathology in HD may result from an accumulation of SGs that perhaps initially served a protective function, but develop into hyper-stable structures due to chronic mutant HTT-mediated stress and compromised autophagy (Buchan et al., 2013, Cortes et al., 2014). Specifically, HTT is essential for normal selective autophagy in mice, and loss of wildtype HTT function may play a role in the dysregulation of SG clearance by granulophagy — a type of selective autophagy (Ochaba et al., 2014). Over time, chronic sequestration of SG components in pathogenic aggregate structures may exacerbate protein toxicity in the cell, and cause cells to lose their ability to form SGs in response to additional stress. Therefore, the therapeutic modulation of SGs in models of neurodegenerations at various timepoints of disease progression will inform

It is also worth noting the reciprocal reactivity detected between G3BP1 and hnRNPA2/B1, an RNA binding protein implicated in the sorting of specific miRNAs into EVs (Villarroya-Beltri et al., 2013) and found in human CSF EVs (Tietje et al., 2014). While we did not detect hnRNPA2/B1 localization with SGs or HTT in the context of HD (*in vivo* or *in vitro*), others have reported that hnRNPA2/B1 transitions into an insoluble state with disease progression in the R6/2 mouse model, potentially resulting in a loss-of-function (Hosp et al., 2017). Thus, hnRNPA2/B1 mislocalization might be one of the mechanisms via which miRNAs are differentially packaged in HD CSF EVs.

Lastly, because the EV miRNAs with strongest seed-strength for G3BP1 are upregulated in the CSF of HD patients, we speculate that G3BP1 upregulation in the prefrontal cortex

would be even greater in the absence of these miRNAs. This is corroborated by the fact that of the 75 miRNAs differentially expressed in the HD prefrontal cortex (Hoss et al., 2015), 35 are predicted to target G3BP1, and 22 of those are upregulated in HD. In contrast, there is no overlap between the prefrontal cortex and CSF EV differentially expressed miRNAs, suggesting that both intrinsic and extrinsic miRNA-mediated repression of G3BP1 is at play. Another potential mechanism to consider is based on findings that additional induced stress on a transgenic mouse model of tauopathy resulted in deficient SG assembly (Shelkovnikova et al., 2017), suggesting that chronically stressed cells lose their ability form SGs and cope with additional stress. Therefore, future studies can investigate both the therapeutic potential of targeting SG pathology and to determine whether increased SG density in HD affects the ability of cells to deal with additional environmentally induced stress, as this may elucidate mechanisms though which SG pathology contributes to neurodegeneration.

EXPERIMENTAL PROCEDURES

R6/2 mice and tissue processing

Male R6/2 mice and NT littermates (Transgene non-carrier C57B16/CBA) were obtained from Jackson Laboratories at 5 weeks and aged to 8 or 12 weeks for SG immunofluorescence experiments. All mice were group housed on a 12/12-hr light/dark schedule with as libitum access to food and water. Mice were euthanized by Euthasol injection at 8 or 12 weeks, followed by transcardial perfusion with 1X PBS and 4% PFA, and decapitation. The whole brain was dissected for immunofluorescence experiments and

drop fixed in 4% PFA for one hour, then cryoprotected in 30% sucrose, frozen, and serially sectioned into 40 um slices using a vibratome.

Postmortem human brain tissue

Brain tissue samples from human superior frontal cortex, parietal cortex, and hippocampal formation were obtained from the New York Brain Bank at Columbia University (Vonsattel et al., 2008). Additional superior frontal cortex samples used for SG density statistical analysis were obtained from the Neurological Foundation of New Zealand Human Brain Bank. Paraffin-embedded samples from healthy controls (N=8) and Huntington's disease (pathological grade 2 and 3) patients (N=8) were used for immunofluorescence experiments. Patient demographic and clinical information is described in **Table 2.1**.

Free-floating immunofluorescence staining

Floating brain sections were washed in 3x5 minutes in 1X PBS and blocked for 1 hour at room temperature with 5% Normal Donkey Serum in 0.3% Triton X-100. Sections were incubated in primary antibody overnight at 40C in 5% Normal Donkey Serum (cat. #017-000-121, Jackson Immuno Research Laboratories) in 0.3% Triton X-100. The following primary antibodies were used (details in **Table 2.7**): G3BP1, G3BP2, hnRNPA2/B1, EM48 (reacts with the first 256 amino acids from human huntingtin), 1C2 (reacts with homopolymeric glutamine stretches), 3B5H10 (reacts with human huntingtin N-terminal fragment of 171 amino acids), 5490 (reacts with huntingtin protein amino acids 115-129). Sections were then washed 3x5 minutes in 1X PBS, and incubated in secondary antibodies for 1 hour at room temperature in 1X PBS. Secondary antibodies were used as follows: Alexa Fluor 488 (1:400, cat. #A-21202, ThermoFisher), Alexa Fluor 555 (1:400, cat. #A-

31570, ThermoFisher). Sections were washed 3x5 minutes in 1X PBS and incubated in DAPI for 10 minutes at room temperature. Sections were then washed 3x5 minutes in 1X PBS. Mounting was performed using Fluoromount-G (cat. #00-4958-02).

Paraffin-embedded immunofluorescence staining

Tissue sections were deparaffinized, rehydrated, and treated with 10mM sodium citrate for 30 minutes at 95^{o}C. Sections were washed 2x5 minutes in 1X PBS and blocked for 1 hour at room temperature with 5% Normal Donkey Serum in 0.1% Triton X-100. Sections were incubated in primary antibody overnight at 4^{0}C in 1% Normal Donkey Serum (cat. #017-000-121, Jackson Immuno Research Laboratories) in 0.1% Triton X-100. The following primary antibodies were used (details in **Table 2.7**): G3BP1, CaMK2, eIF3H. Sections were then washed 3x5 minutes in 1X PBS and incubated in secondary antibodies for 1 hour at room temperature in 1X PBS. Secondary antibodies were used as follows: Alexa Fluor 488 (1:400, cat. #A-21202, ThermoFisher), Alexa Fluor 555 (1:400, cat. #A-31570, ThermoFisher). Sections were washed 3x5 minutes in 1X PBS, treated with TrueBlack® Lipofuscin Autofluorescence Quencher (cat. #23007, Biotium), washed 3x5 minutes in 1X PBS, and incubated in DAPI for 10 minutes at room temperature. Sections were then washed 3x5 minutes in 1X PBS, and cover slips were mounted using Fluoromount-G (cat. #00-4958-02).

Microscopy

Confocal images were acquired with an Olympus FLUOVIEW FV 3000 microscope and images were taken with 10X, 20X, 40X and 60X oil objectives. All brain scan images were done using a ZEISS Axio Scan.Z1 imaging system.

SG analysis

SGs were quantified using the Imaris Surface tool (Imaris Single Full software, BITPLANE). G3BP1 and hnRNPA2/B1 immunoreactivity was quantified using an in-house script (CellProfiler Cell Image Analysis software). Nuclei (DAPI stained) were counted using the Imaris Spots tool and used for normalization of SG and G3BP1 immunoreactivity quantitation. A previously described SG quantitation approach (Markmiller et al., 2018) was also used for validation.

Study participants and CSF sample collection

CSF samples were obtained from HDClarity (ClinicalTrials.gov identifier: NCT02855476), a multi-site cerebrospinal collection initiative to facilitate therapeutic development for Huntington's disease. CSF was collected in the morning after an overnight fast by lumbar puncture, using a Whitacre 20G spinal needle. CSF was processed on ice within 15 minutes of collection and cleared by centrifugation before storage in polypropylene cryotubes at -80^{0}C.

EV RNA isolation, library preparation, and next generation sequencing

All experiments were conducted by QIAGEN Genomic Services. RNA was isolated from 4mL CSF using the exoRNeasy Serum/Plasma Maxi Kit (cat. #77064, QIAGEN) according to the manufacturer's instructions. The library preparation was performed using the QIAseq miRNA Library Kit (cat. #331505, QIAGEN). A total of 5ul total RNA was converted into miRNA NGS libraries. Adapters containing UMIs were ligated to the RNA and RNA converted to cDNA. The cDNA was amplified using PCR (22 cycles) and during the PCR indices were added. After PCR the samples were purified, and library preparation QC was

performed using either Bioanalyzer 2100 (Agilent). Based on quality of the inserts and the concentration measurements, the libraries were pooled in equimolar ratios, quantified using qPCR and sequenced on a NextSeq500 sequencing instrument. Raw data was de-multiplexed and FASTQ files for each sample generated using the bcl2fastq software (Illumina inc.). FASTQ data were checked using the FastQC tool.

EV characterization by fluorescent nanoparticle tracking analysis

EVs were isolated from 600uL CSF using the exoEasy Maxi Kit (cat. #76064, Qiagen) according to the manufacturer's instructions. EVs were visualized and quantified using ExoGlow-NTA fluorescent labeling kit on an LM10 NanoSight instrument (cat. #EXONTA200A-1, SBI Systems Biosciences, Palo Alto, CA). Each sample was measured in triplicate, and videos of data collection were analyzed to give the mean, mode, and estimated concentration for each particle size.

Analysis of miRNA sequencing data

Reads containing ambiguous bases or with a mean quality score < 30 were removed from analysis using Prinseq (Schmieder et al., 2011), and UMIs were identified and extracted from the remaining reads using UMI-Tools (Smith et al., 2017). Reads were aligned to all human mature miRNAs or pre-miRNAs from miRBase v22 (Kozomara et al., 2019) using bowtie2 (Langmead et al., 2012) with "very sensitive" parameters and a seed length of 8bp with no mismatches allowed in the seed (Tam et al., 2015). Primary mappings >= 16bp in length were retained for further analysis. Mapped reads were deduplicated with UMI-Tools (Smith et al., 2017) using the unique grouping method, considering each unique UMI an

individual miRNA. Read counts for each miRNA were determined using samtools (Li et al., 2009). High-throughput sequencing data will be deposited in GEO.

Enrichment analysis

The PANTHER Classification System (Mi et al., 2009) was used to generate GO terms that are significantly overrepresented in the miRNA targets list versus the background of all genes for all three GO aspects (biological process, molecular function, cellular components). For the enrichment analysis of SG genes in the miRNA targets list versus the 464 SG genes (Nunes et al., 2019), a Fisher's exact test was used to determine whether the number of overlapping genes is significantly higher than what is expected by chance based on a human genome larger than 21,000 genes.

miRNA target prediction and dataset overlap

An initial list of miRNAs was generated by pooling together miRNAs that were detected in the miRNAs sequencing studies with P values <0.05 before correcting for multiple comparisons, and miRNAs with log2FoldChanges >= 2 or <= -2, which were filtered based on interquartile range of the counts. IQR was calculated from the counts in the HD and control groups, and miRNAs were excluded if any count value was greater than Quantile3 + 3*IQR for either group. A list of predicted gene targets for the miRNAs that passed the filtering process was generated using TargetScan (Agarwal et al., 2015). The list of predicted gene targets for each miRNA was checked for overlap with a list of DEGs detected in the prefrontal cortex of HD patients (Labadorf et al., 2015), and the number of overlapping targets that had an opposite fold change sign to the miRNA fold change were counted.

Seed strength ranking and LNA miRNA mimics

Seed strength values for all filtered miRNAs were acquired with TargetScan and miRmap, two different open-source software that combine multiple predictor features to predict the strength of miRNA repression on targeted mRNAs, in this case G3BP1 mRNA (Vejnar et al., 2012; Agarwal et al., 2015). miRNAs were ranked from strongest to weakest seed strength values using each predictive model, a composite list was made, and 7 miRNAs with the strongest seed strength values were selected for overexpression experiments. miRCURY LNA miRNA Mimics (QIAGEN) were used as listed in **Table 2.8**.

293T cell transfection and SG induction experiments

293T cells were plated onto six-well plates at a density of $1.0x10^6$ cells/well for LNA miRNA mimic transfections. Transfection with HiPerFect (Qiagen cat. #301705) and respective microRNA cocktails was done 6 hours after plating (10ul/well HiPerFect, 5nM LNA cocktail working concentration). Complete media change was performed 24 hours after transfection and passaging of cells 48 hours after transfection. Each condition (negative control, set 1, set 2) was done in triplicates and plated onto 1X PDL coated (1hr) Millicell EZ 4-well glass chamber slides (cat. #PEZGS0416) at a density of $3.0x10^5$ cells per well. For SG induction, cells were stressed with 250μM sodium arsenite (Sigma-Aldrich cat. #1062771000) for 30 minutes at 37°C, followed by fixation with 4%PFA for 10 minutes. For immunofluorescence staining, cells were permeabilized for 10 minutes with 0.5% triton-X in 1X PBS, blocked with 5% normal donkey serum (cat. #017-000-121, Jackson Immuno Research Laboratories), incubated overnight with a G3BP1 primary antibody (**Table 2.7**), 2 hours secondary (1:400, cat. #A-21202, ThermoFisher), and coverslips were mounted using Fluoromount-G (cat. #00-4958-02). For biochemistry experiments, cell

pellets were sonicated with a buffer containing 10mM Tris (pH 7.4), 158 mM NaCl, 1mM ethylenediaminetetraacetic acid (EDTA) (pH 8), 0.1% sodium dodecyl sulfate (SDS), 1% Triton X-100, protease inhibitors (Pierce Protease Inhibitor Tablets, cat. #A32963, ThermoFisher), and phosphatase inhibitors (Phosphatase Inhibitor Cocktail 2, cat. #P5726; Phosphatase Inhibitor Cocktail 3, cat. #P0044). Protein concentration was determined using the Lowry protein assay. Invitrogen 4%–12% bis-tris mini gels were used for SDS-PAGE, proteins were transferred to a PVDF membrane and nonspecific proteins were blocked with 5% milk in TBS (Tris-buffered saline). The following primary antibodies were used (details in **Table 2.7**): G3BP1, hnRNPA2/B1, alpha-tubulin. Blot was imaged with the LI-COR Odyssey System.

Statistics

All mouse and human tissue immunofluorescence and SG quantitation data were analyzed in GraphPad Prism software using a Student's two-tailed t-test, assuming equal variance. NTA data were analyzed in GraphPad Prism software using a Two-way ANOVA with Boferroni's multiple comparison test or a Student's two-tailed t-test, assuming equal variance. The overlap of CSF EV miRNA targets with mammalian SG genes was analyzed using a Fisher's exact test, based on a genome larger than 21,000 genes. Differential expression for HD versus control miRNA sequencing samples was analyzed using the DESeq2 package (Love et al., 2014) in R (R Development Core Team, 2010) with a significance cutoff of $p < 0.05$. Sample size calculation for miRNA sequencing experiments was done using an established statistical model to calculate sample size estimates for RNA sequencing data (Hart et al., 2013), where given any 4 of Type I error, Type II error/power, sequencing depth, coefficient of variation, and samples per group, the fifth

can be calculated. All 293T cell immunofluorescence, western blot, and SG quantitation data were analyzed in GraphPad Prism software using a One-way Anova with Dunnett's multiple comparison test, or Two-way ANOVA with Sidak's multiple comparison test for SG density comparisons among stressed and unstressed conditions. All data are represented as mean ±SEM with a p value of $p<0.05$ considered statistically significant.

Study approval

Mouse studies were carried out following the Guide for the Care and Use of Laboratory Animals of the NIH and an approved animal research protocol by the Institutional Animal Care and Use Committee (IACUC) at the University of California, Irvine.

CHAPTER 2

FIGURES

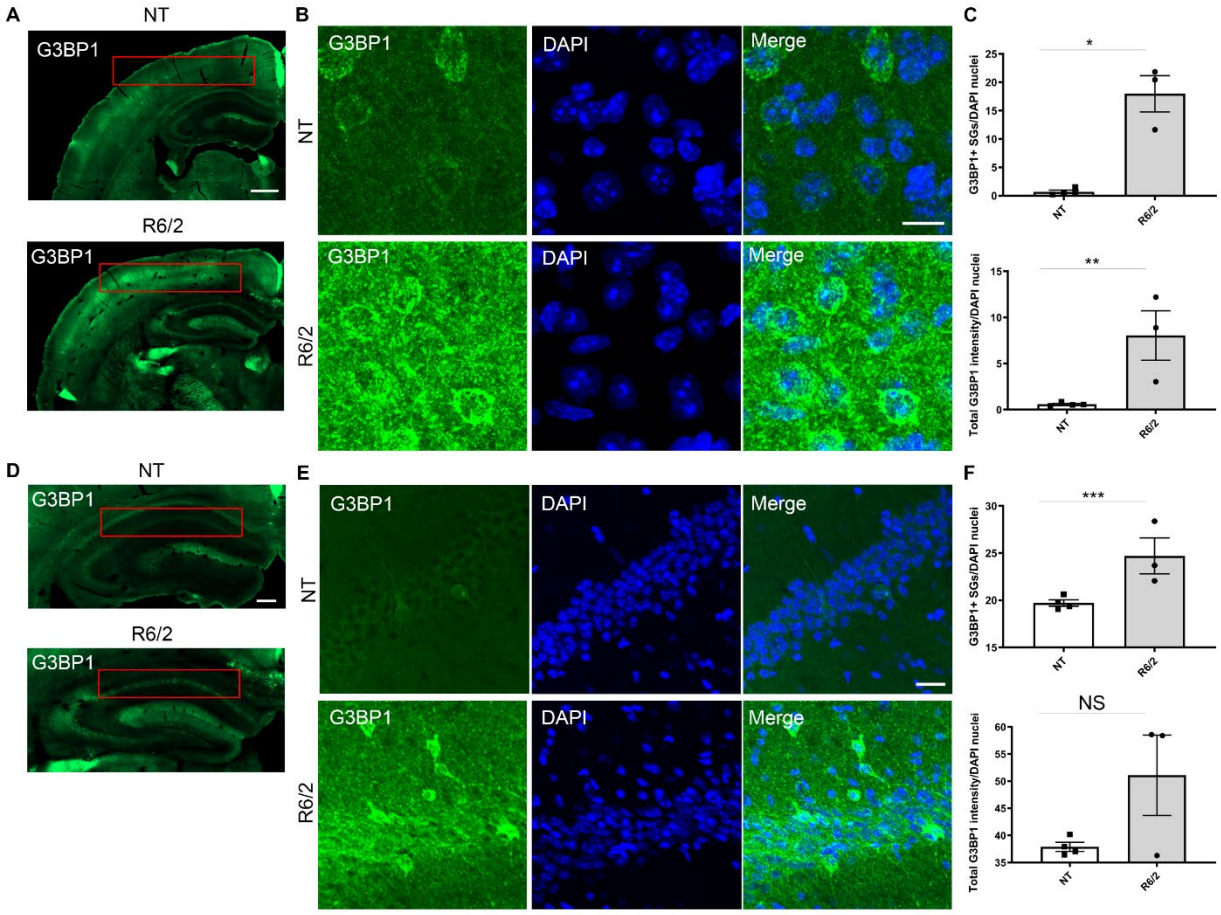

Figure 2.1. Increase of SG density in the 12-week R6/2 cortex and hippocampus. A and **D)** lmmunoreactivity of G3BP1 (green) is higher in the R6/2 cortex and hippocampus CA **1** region when compared to the non-transgenic controls (regions of interest boxed in red). Band **E)** high magnification images of cortical and hippocampal CA1 regions suggest that G3BP1 immunoreactivity varies between neural cell subtypes. **C)** SG density and G3BP1 immunoreactivity are significantly higher in the R6/2 cortex (Student's t-test, unpaired, two-tailed, *=0.0014;**=0.0210); these were calculated using lmaris image analysis software surface tool and CellProfiler, respectively, and normalized to the number of nuclei per frame (DAPI in blue). **F)** The same analysis was used to analyze the CA1 region of the hippocampus (boxed in red in **D),** which led to the detection of significantly higher SG density in the R6/2 (Student's t-test, unpaired, two-tailed, ***=0.0285), but not G3BP1 immunoreactivity. Analyses were done using four frames per mouse brain (N= 3 R6/2; 4 NT). Scale bars: A=500um; B=10um; C=200um; D=10um.

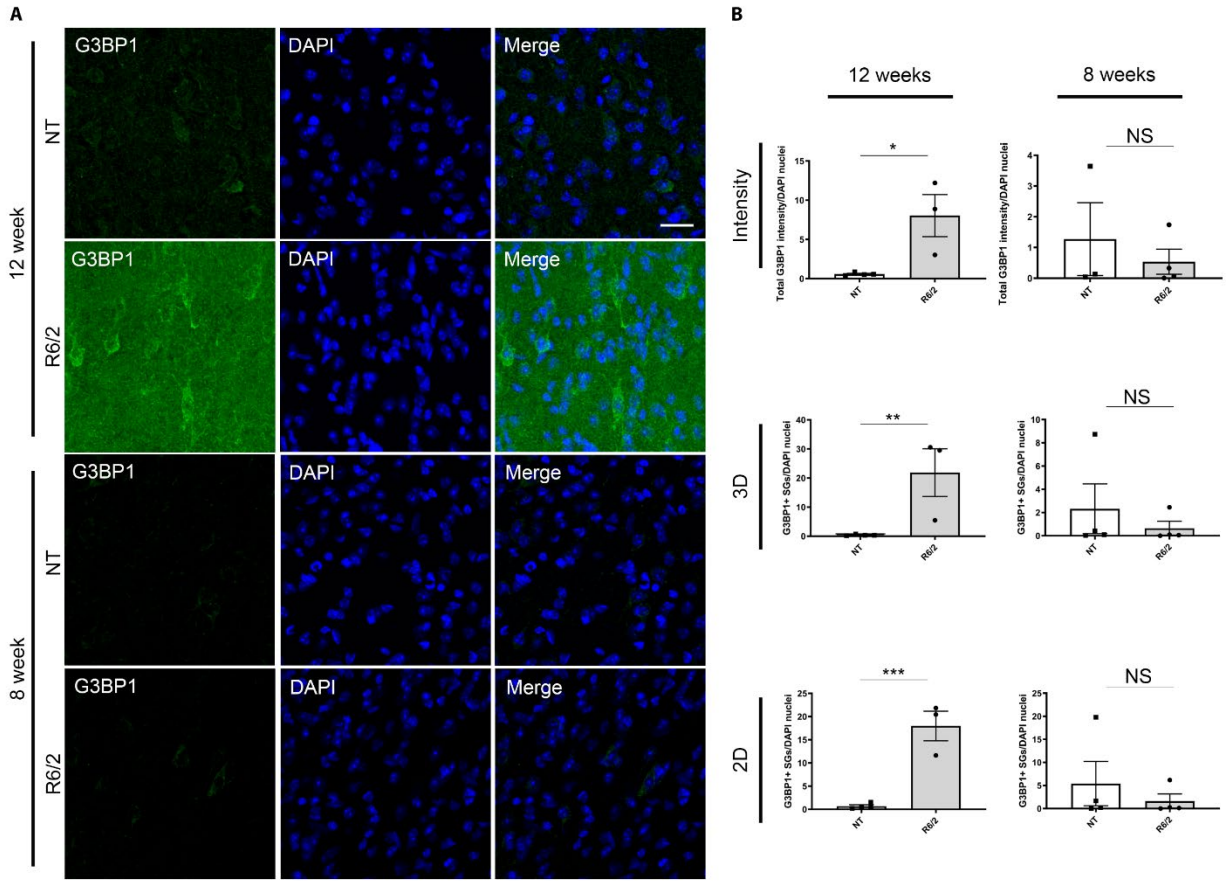

Figure 2.2. SG density analyses in the R6/2 cortex at 8 and 12-week timepoints. A) Representative images of the R6/2 cortex at 12 weeks demonstrate an increase in G3BP1 immunoreactivity compared to the NT cortex. Scale bar=20um. **B)** SG pathology was measured by G3BP1 immunoreactivity intensity with CellProfiler, as well as G3BP1 granule density using the Imaris surface tool (3-dimensional granule surface detection), and a previously described CellProfiler protocol (2-dimensional granule detection; Markmiller et al, 2018). G3BP1 immunoreactivity and SG density were significantly higher by all measures in the R6/2 cortex at 12 weeks (Student's t-test, unpaired, two-tailed, *=0.0210;**=0.0014; ***=0.0259), but not at 8 weeks. Analyses were done using four frames per mouse brain (N= 12 weeks: 3 R6/2, 4 NT; 8 weeks: 4 R6/2, 4 NT). G3BP1 intensity and SG counts were normalized to the number of nuclei per frame (DAPI). For the creation of this figure, the gamma setting for the green channel was equally adjusted to 0.5 for all images. All analyses were carried out with the original, unedited images.

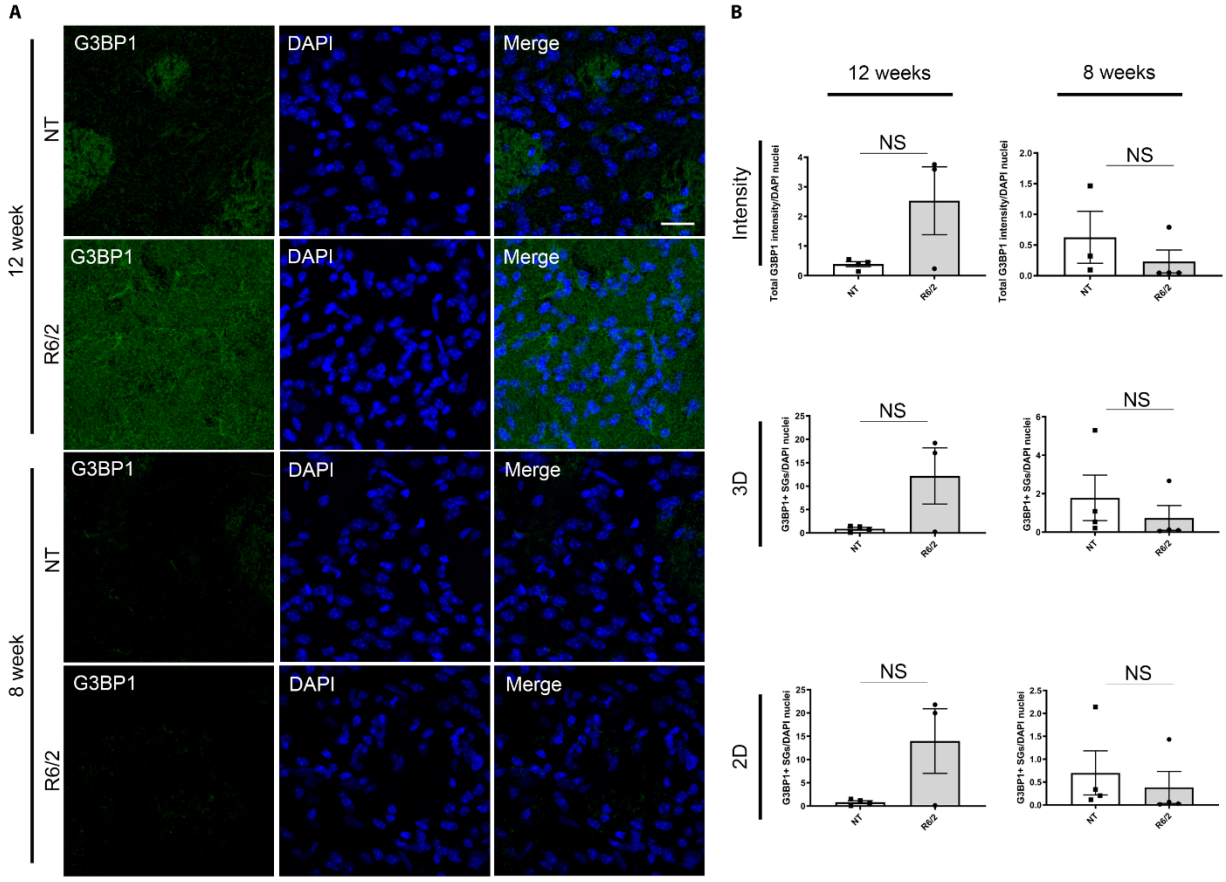

Figure 2.3. SG density analyses in the R6/2 striatum at 8 and 12-week timepoints. A) Representative images of the R6/2 and NT striatum. Scale bar=20um. **B)** SG pathology was assessed by measuring G3BP1 immunoreactivity intensity with CellProfiler, as well as G3BP1 granule density using the Imaris surface tool (3-dimensional granule surface detection) and a previously described CellProfiler protocol (2-dimensional granule detection; Markmiller et al, 2018). No statistically significant differences were detected between R6/2 and NT mice in regards to G3BP1 immunoreactivity or SG density in the striatum, at either the 8- or 12-week timepoint. Analyses were done using four frames per mouse brain (N= 12 weeks: 3 R6/2, 4 NT; 8 weeks: 4 R6/2, 4 NT). G3BP1 intensity and SG counts were normalized to the number of nuclei per frame (DAPI). For the creation of this figure, the gamma setting for the green channel was equally adjusted to 0.5 for all images. All analyses were carried out with the original, unedited images.

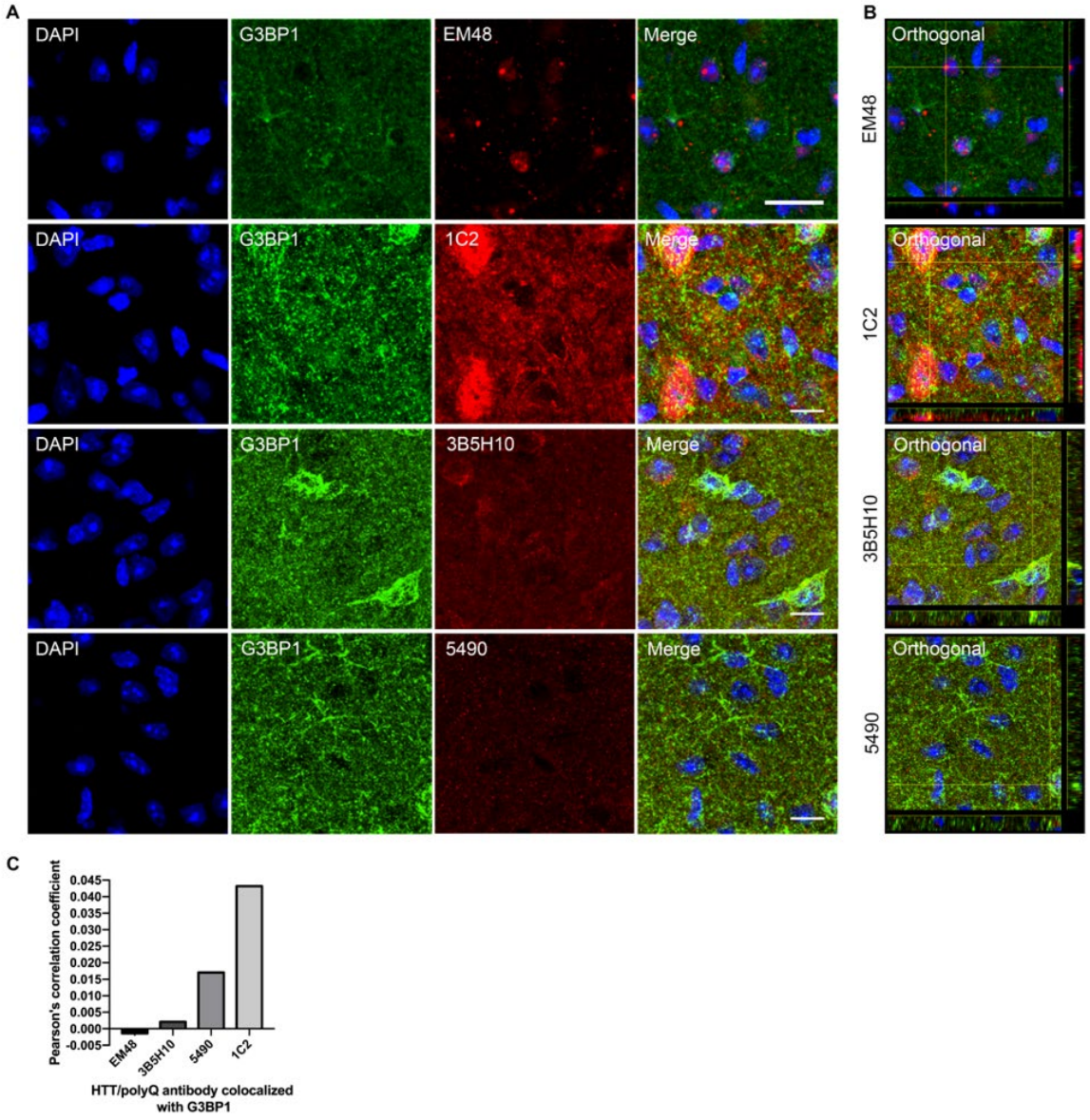

Figure 2.4. G3BP1 SGs do not co-localize with EM48-positive nuclear inclusions in the 12-week R6/2 mouse cortex. A) Colocalization of G3BP1 (in green) and HTT/polyQ (in red) was assessed using the antibodies EM48, 1C2, 3B5H10, and 5490. All images shown are maximum intensity projections of 10 slice Z-stacks taken at a thickness of 0.5 um per slice. **B)** Orthogonal views of the maximum intensity projections show modest colocalization of G3BP1 and Htt/polyQ antibodies 1C2, 3B5H10, and 5490, but not EM48. **C)** Pearson's correlation coefficient was calculated for each Z-stack using the Imaris colocalization tool (N=1), with 1C2 having the highest degree of fluorophore colocalization with G3BP1. Scale bars= 10um.

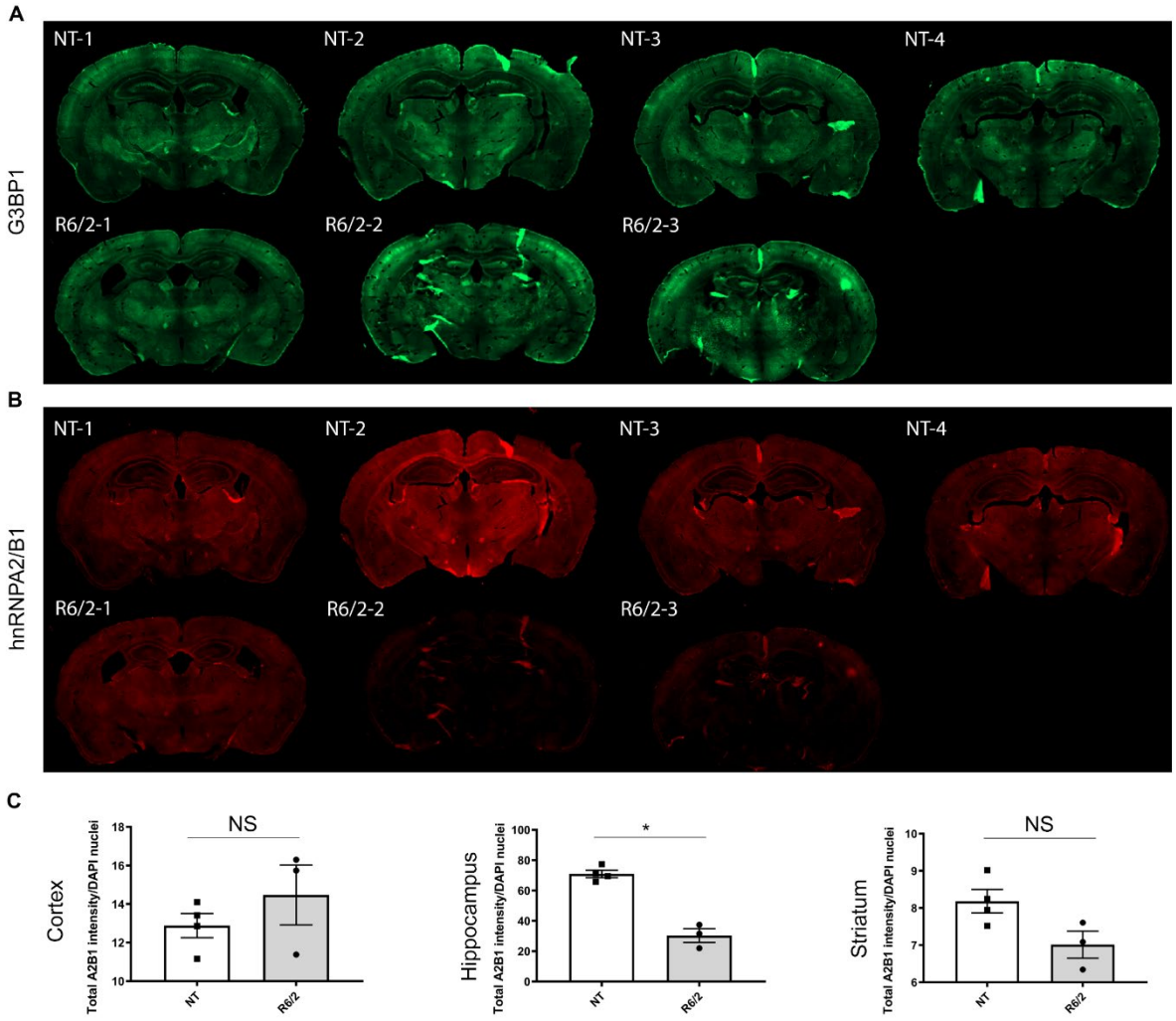

Figure 2.5. Comparison of hnRNPA2/B1 and G3BP1 immunoreactivity in the 12-week R6/2 brain. Coronal brain section images of **A)** G3BP1 demonstrate higher G3BP1 immunoreactivity in cortical areas, particularly in R6/2 mice #2 and #3. Conversely, **B)** hnRNPA2/B1 immunoreactivity appears to be lower in the mouse brain sections with highest G3BP1 immunoreactivity. **C)** hnRNPA2B1 immunoreactivity is significantly lower in the hippocampus (Student's t-test, unpaired, two-tailed, *=0.0003)**,** but not the cortex or striatum. Immunoreactivity intensity was assessed using CellProfiler and normalized to number of nuclei per frame. Analyses were done using four frames per mouse brain (N= 3 R6/2; 4 NT).

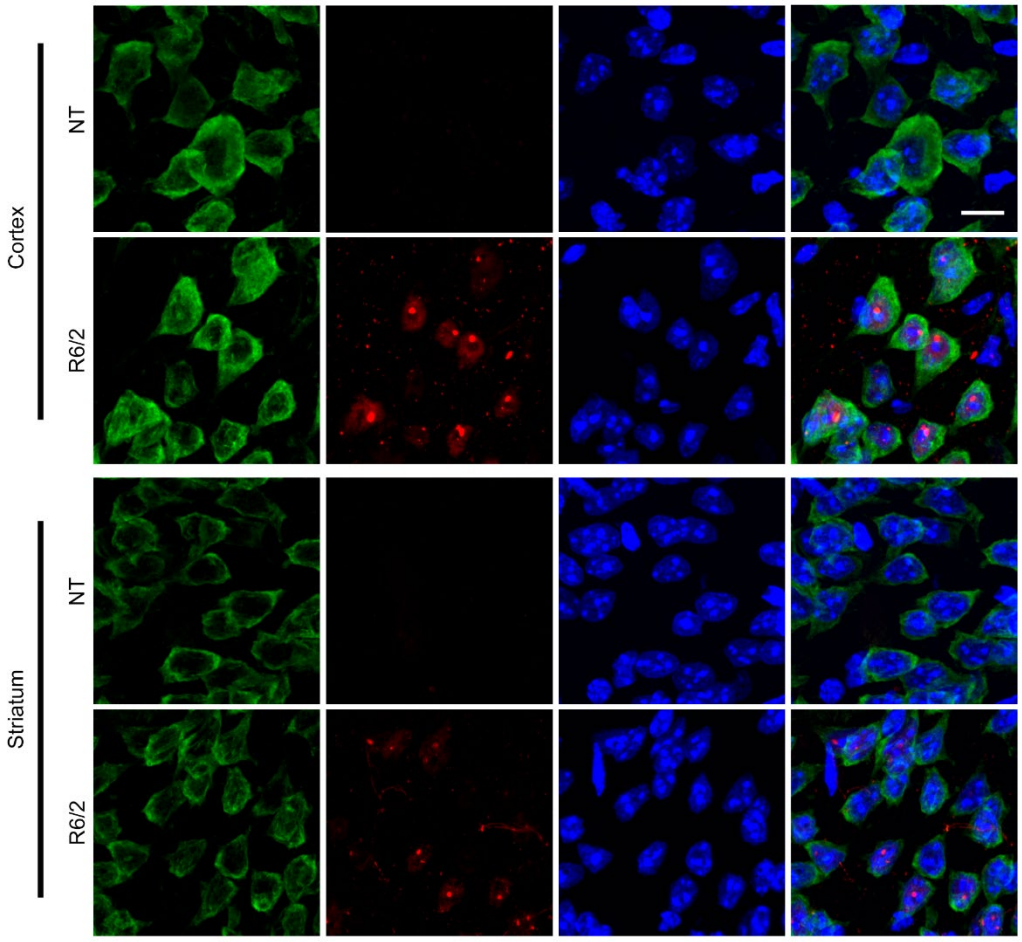

Figure 2.6. G3BP2 SGs are not detected in the 12-week R6/2 mouse brain. Immunofluorescence was used to investigate whether the G3BP1 homolog, G3BP2, contributes to SG pathology in the R6/2 brain. The pattern of G3BP2 immunoreactivity (in green) suggests that, although the majority is localized to the cytoplasm, G3BP2 does not localize to granule-like cytoplasmic structures in the cortex or striatum of either the R6/2 or NT mouse brain. Co-staining with the HTT antibody EM48 suggests that G3BP2 does not localize to HTT nuclear inclusions. Scale bar: 10um.

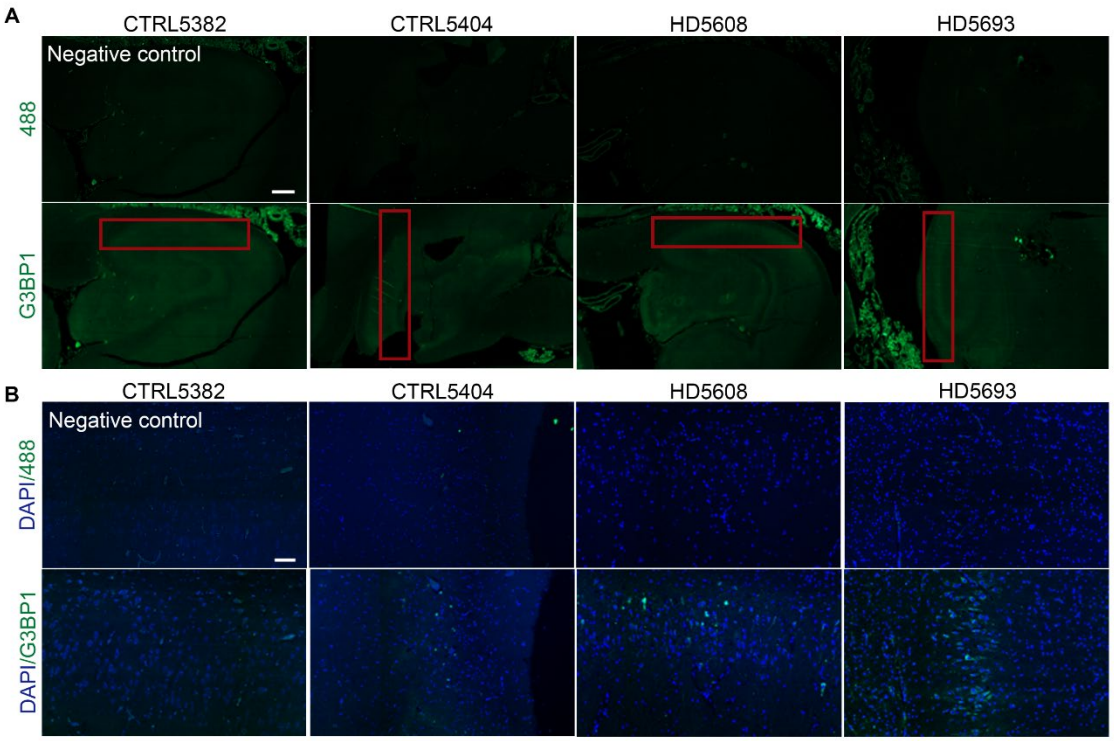

Figure 2.7. G3BP1 immunoreactivity in the hippocampus of HD patients. G3BP1 immunofluorescence of the hippocampal formation in HD (grade 2) and control brains. **A)** Scans of the full hippocampal formation with a negative control and G3BP1 stain (both in green). Red boxes enclose the CA1/CA2 region shown in zoomed in images. **B)** Zoomed in scan image of area CA1/CA2 of the hippocampus (with DAPI co-stain in blue). Scale bars: A=1000um; B=100um; C=20um.

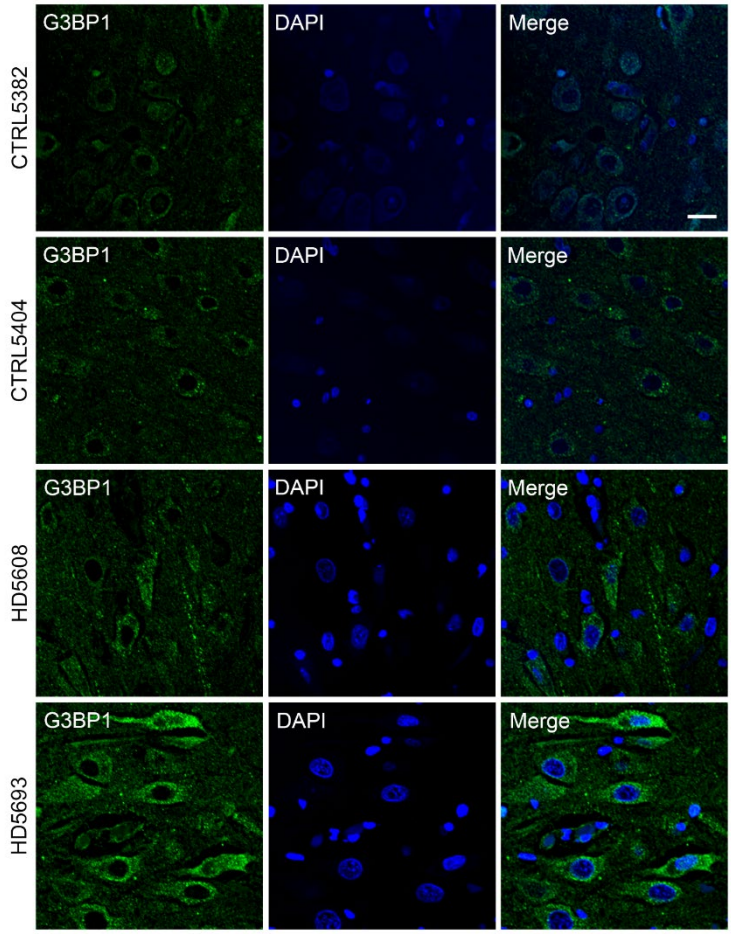

Figure 2.8. G3BP1 immunoreactivity in the hippocampus of HD patients (higher magnification images). G3BP1 immunofluorescence of the hippocampal formation of HD (grade 2) and control brains. Confocal images of hippocampal area CA1 depicting G3BP1-positive cells (in green). Scale

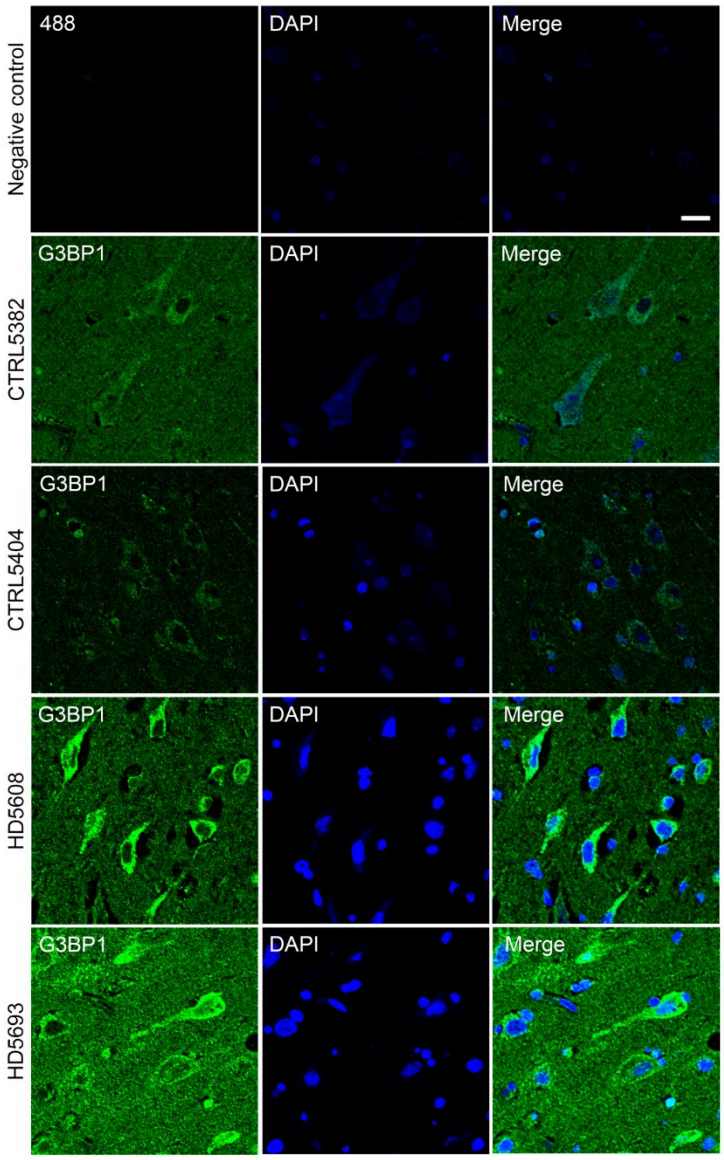

Figure 2.9. G3BP1 immunoreactivity in the superior frontal cortex of HD patients. G3BP1 immunofluorescence (in green) of the superior frontal cortex of HD (grade 2) and control human brains. Lower DAPI intensity was noted in control samples. Scale bar= 20um.

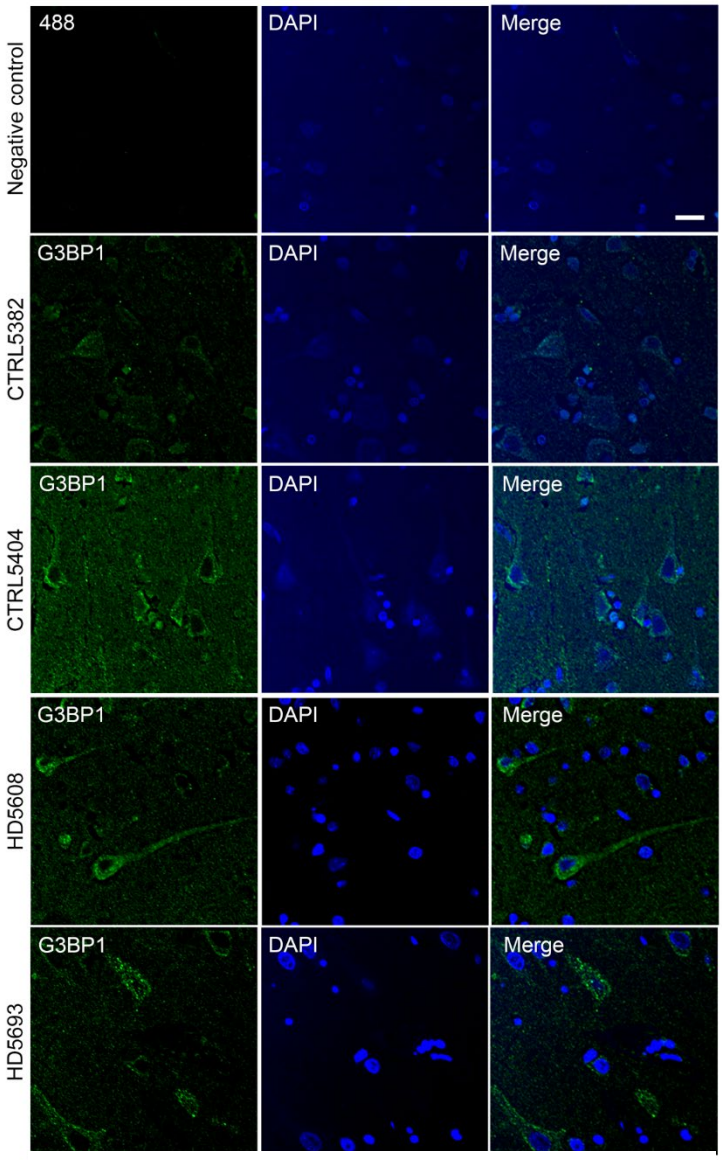

Figure 2.10. G3BP1 immunoreactivity in the parietal cortex of HD patients. G3BP1 immunofluorescence (in green) of the parietal cortex of HD (grade 2) and control human brains. Lower DAPI intensity was noted in control samples. Scale bar= 20um.

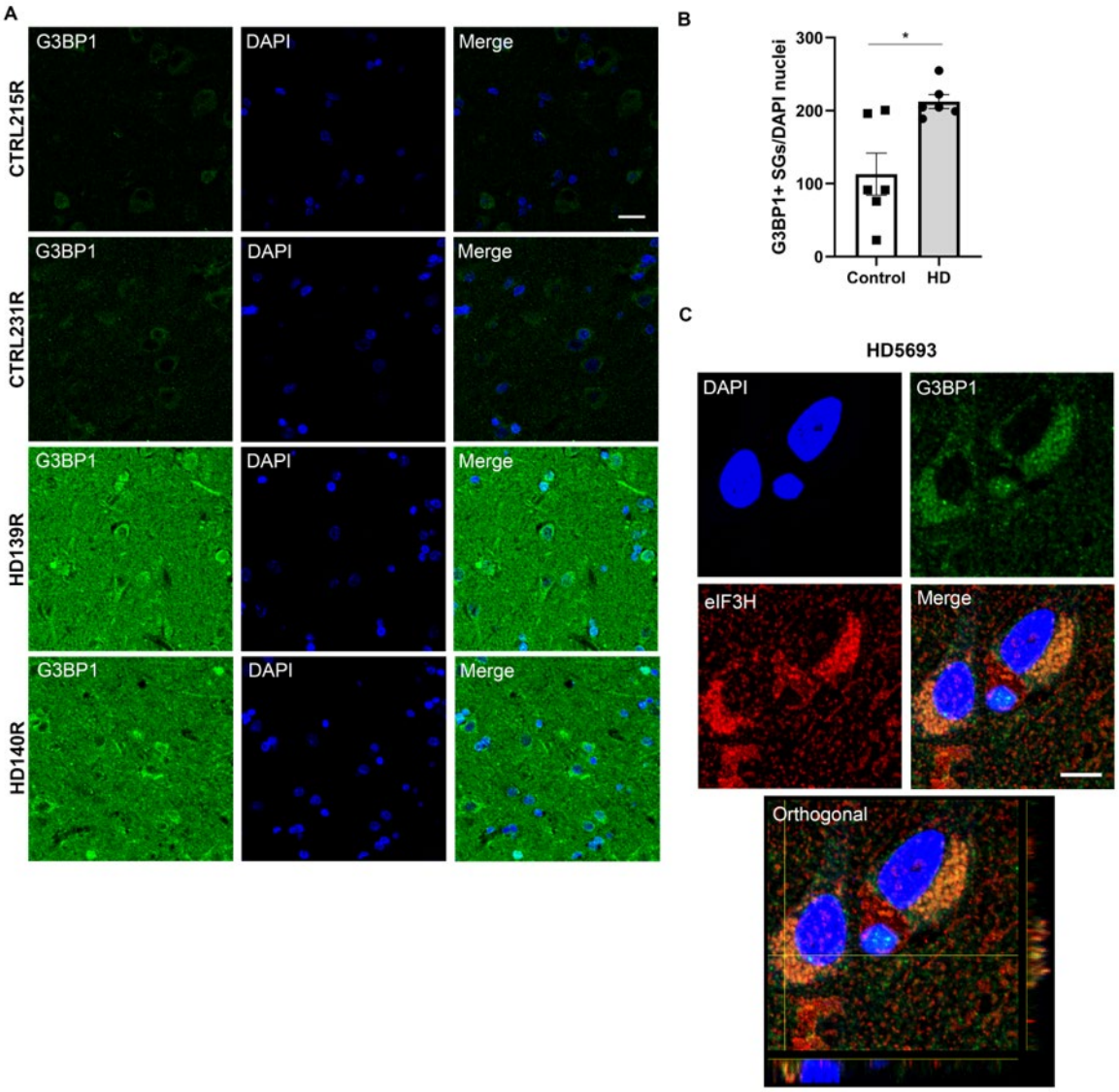

Figure 2.11. Increased G3BP1 SG density in the superior frontal cortex of HD human brain. G3BP1 (in green) SGs were immunostained and their density was calculated using lmaris image analysis software surface tool and normalized to the number of nuclei per frame (DAPI in blue). **A, B)** G3BP1 SG density is significantly higher in the superior frontal cortex of HD brains (grade 3) compared to controls (Student's t-test, unpaired, two-tailed, *=0.0085). Analysis was done using three frames per case (N= 6 HD; 6 Control). **C)** Co-staining of stress granule markers G3BP1 and elF3H (in red) in the superior frontal cortex demonstrates colocalization in some HD cases. Scale bars: A=20um; C=10um.

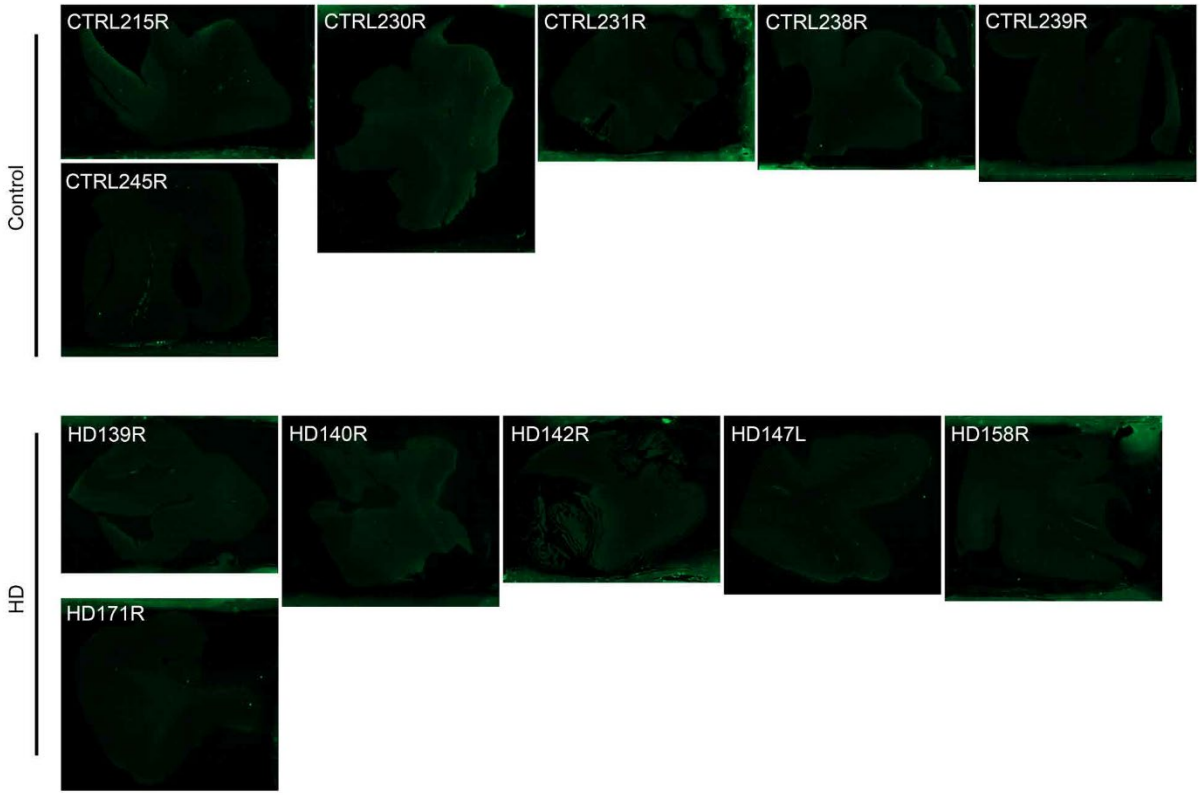

Figure 2.12. Negative control immunostaining of superior frontal cortex blocks. Slide scanner images of postmortem superior frontal cortex blocks with negative control immunostaining (secondary antibody only, in green). Images represent the background fluorescence present on blocks, and suggest relatively small background differences among samples.

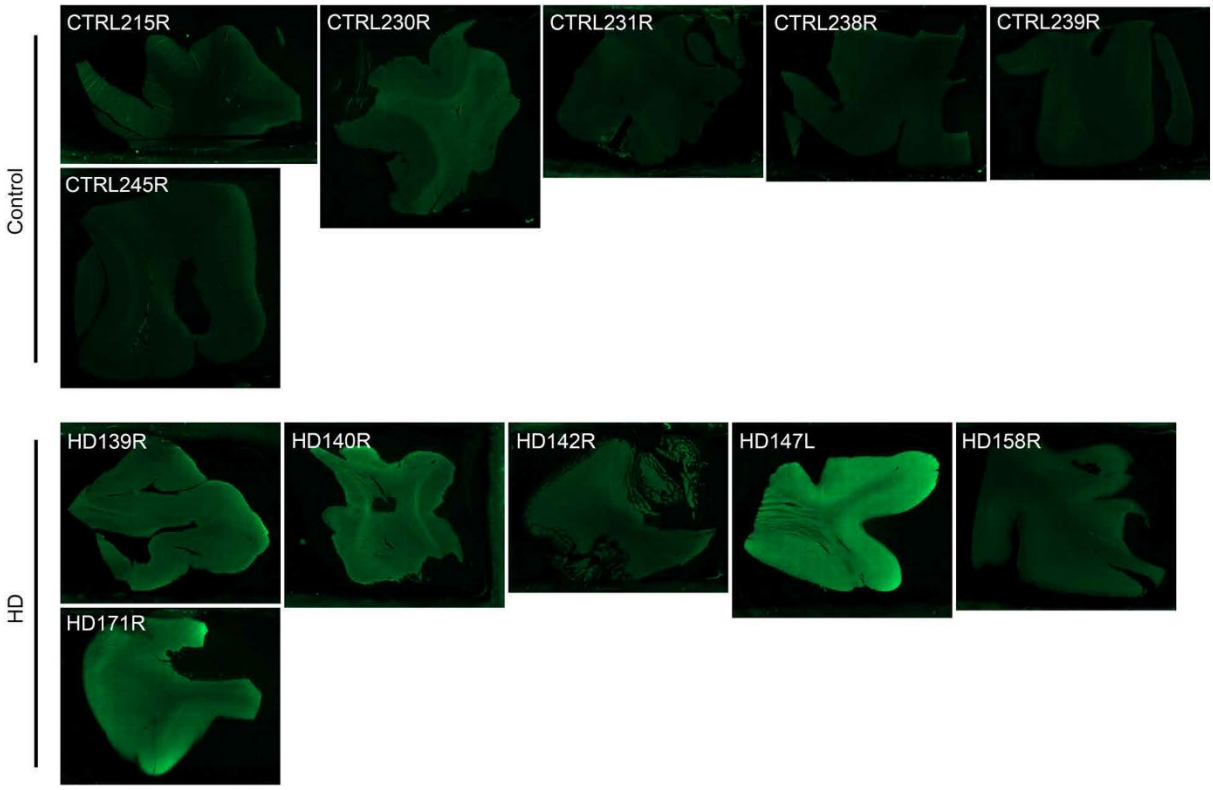

Figure 2.13. G3BP1 immunostaining of superior frontal cortex blocks. Slide scanner images of postmortem superior frontal cortex blocks immunostained with G3BP1 (in green) and used to quantitate G3BP1 SG densities for statistical analysis.

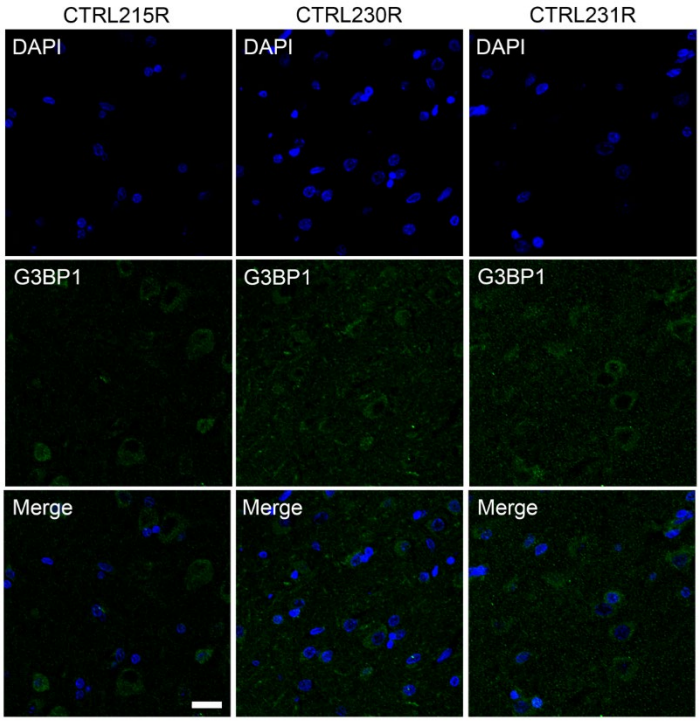

Figure 2.14. Increased G3BP1 SG density in the superior frontal cortex of HD human brain (control samples). Complementary representative images to Figure 2.11. Images were used to make quantitative G3BP1 SG density comparisons between HD and control samples. N= 6 HD; 6 Control. Scale bars: A=20um

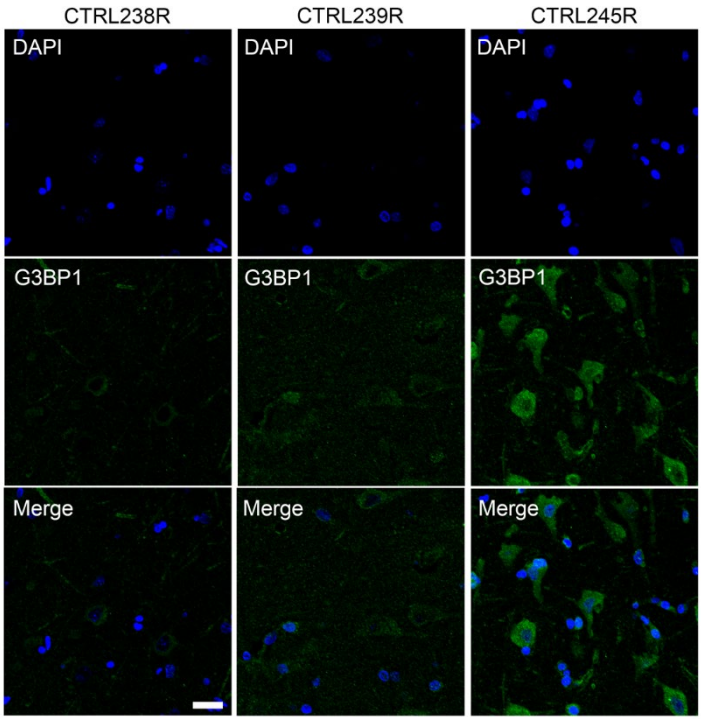

Figure 2.15. Increased G3BP1 SG density in the superior frontal cortex of HD human brain (control samples; continued from Figure 2.14). Complementary representative images to Figure 2.11. Images were used to make quantitative G3BP1 SG density comparisons between HD and control samples. N= 6 HD; 6 Control. Scale bars: A=20um

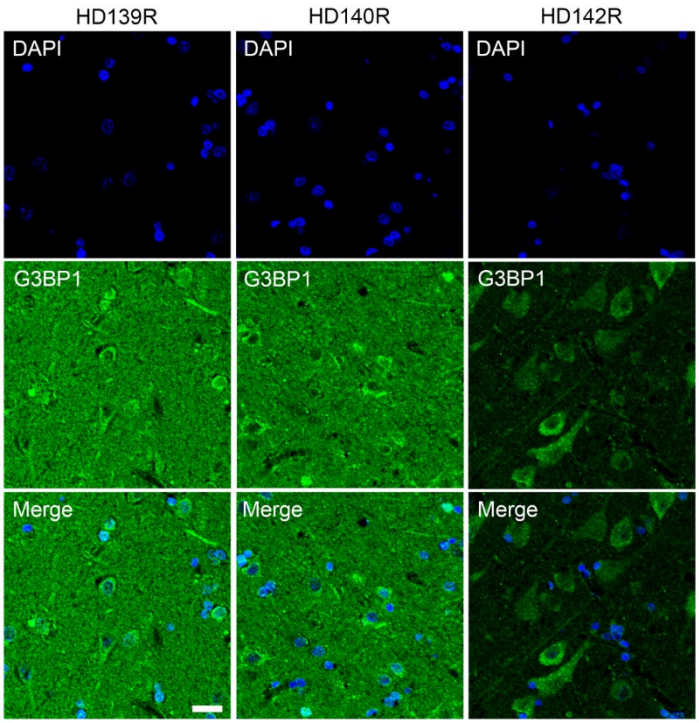

Figure 2.16. Increased G3BP1 SG density in the superior frontal cortex of HD human brain (HD samples; continued from Figure 2.15). Complementary representative images to Figure 2.11. Images were used to make quantitative G3BP1 SG density comparisons between HD and control samples. N= 6 HD; 6 Control. Scale bars: A=20um

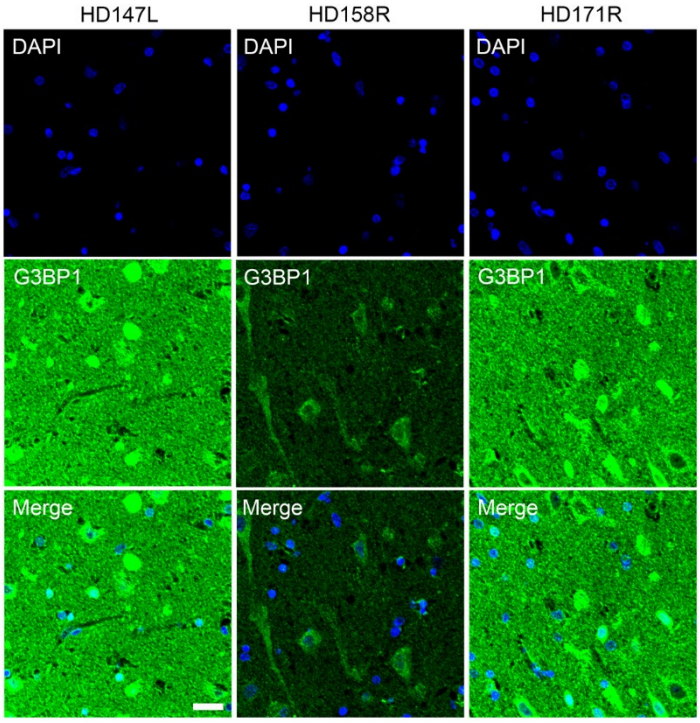

Figure 2.17. Increased G3BP1 SG density in the superior frontal cortex of HD human brain (HD samples; continued from Figure 2.16). Complementary representative images to Figure 2.11. Images were used to make quantitative G3BP1 SG density comparisons between HD and control samples. N= 6 HD; 6 Control. Scale bars: A=20um

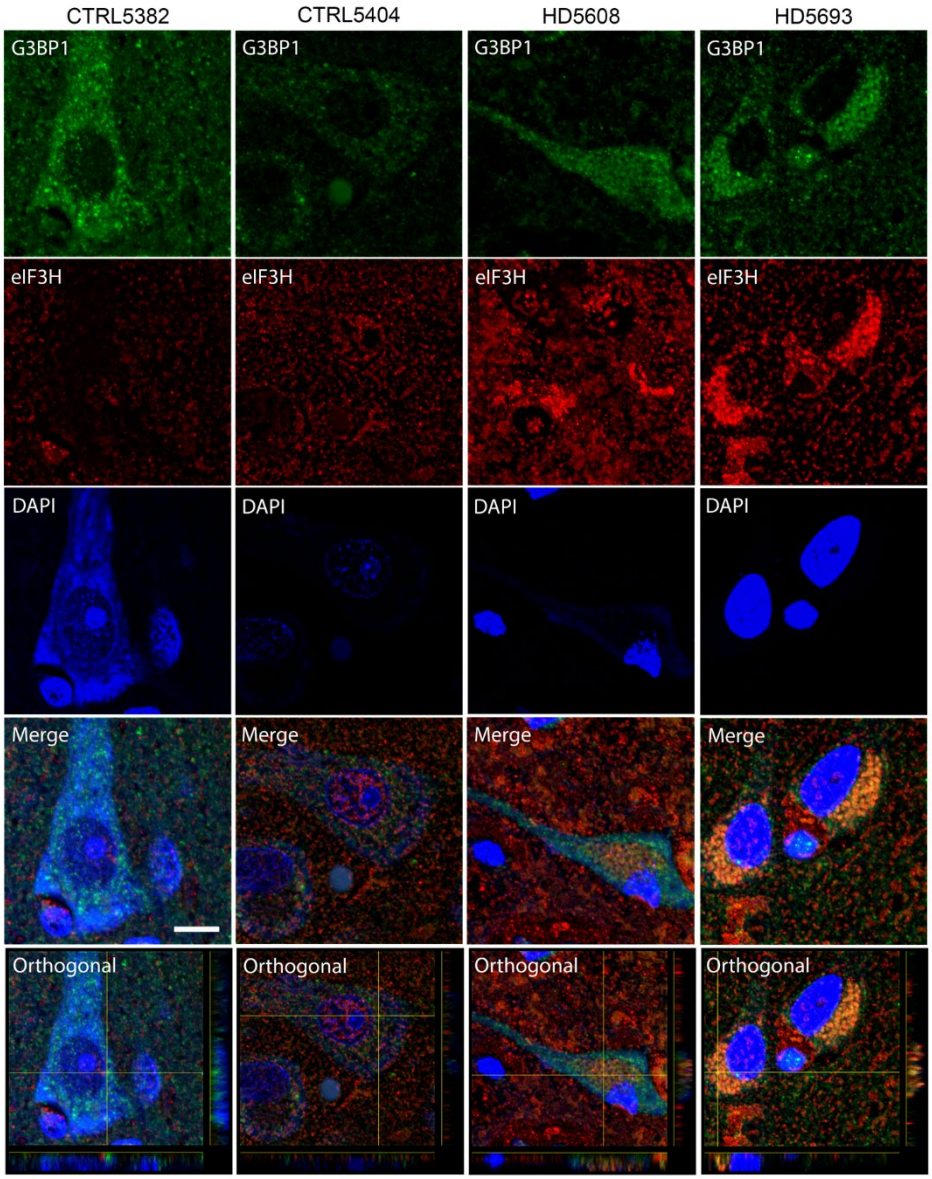

Figure 2.18. G3BP1 SGs colocalize with translation initiation factor eIF3H in the superior frontal cortex of HD patients. Co-staining of stress granule markers G3BP1 (in green) and eIF3H (in red) demonstrates colocalization in some, but not all HD cases. Images were taken 2 HD (grade 2) and 2 control cases. Orthogonal images show colocalization. Scale bar=10um.

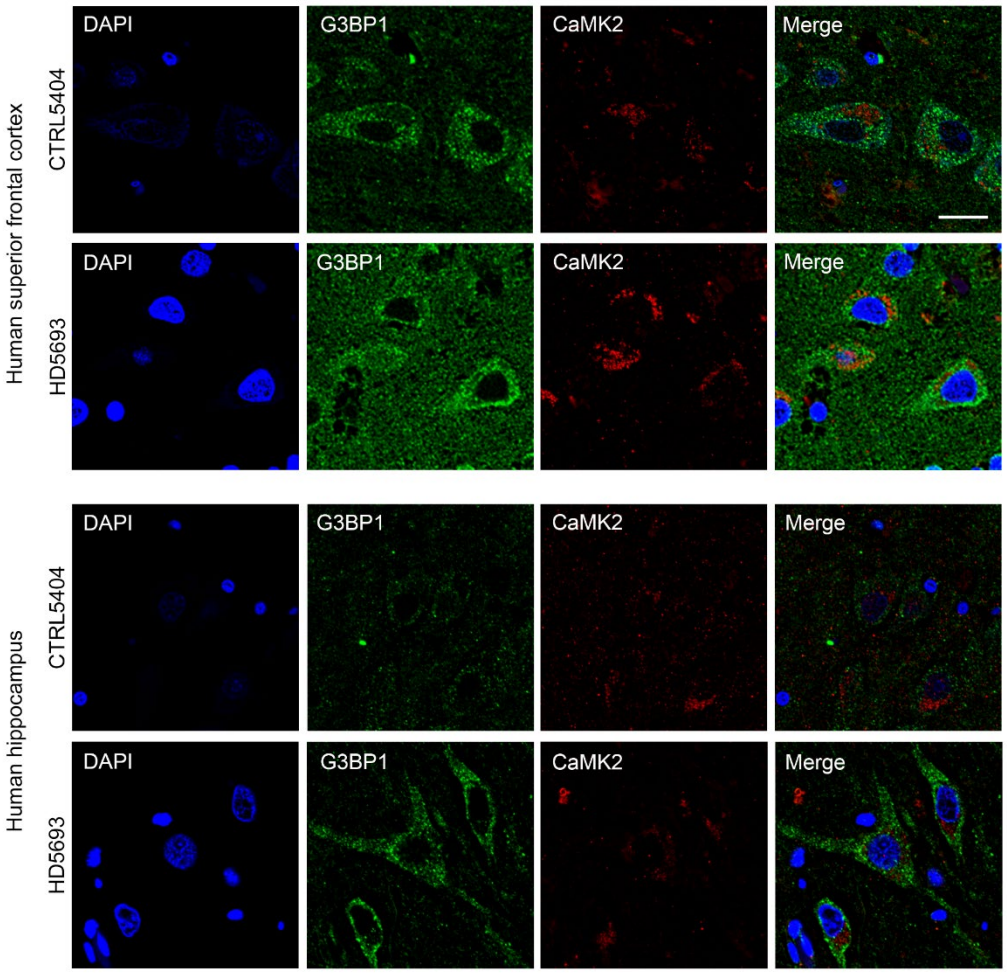

Figure 2.19. Highly immunoreactive G3BP1 positive cells have pyramid-shaped cell bodies and express CaMK2. Co-staining of G3BP1 (in green) and the pyramidal neuron marker CaMK2 (in red), as well as cell morphology, suggest that cells with high-density G3BP1+ SGs are likely to be pyramidal neurons. This pattern of reactivity was observed for both HD and control cases. Representative images of the human parietal cortex and hippocampus. Nuclei were stained with DAPI (in blue). Scale bar= 20um.

A

Clinical features	Huntington's disease	Healthy controls
Number of subjects	10	10
Mean age	51.1	50.4
Gender	5F/5M	5F/5M
CAG length	40-45	N/A
Disease stage*	Early HD	N/A

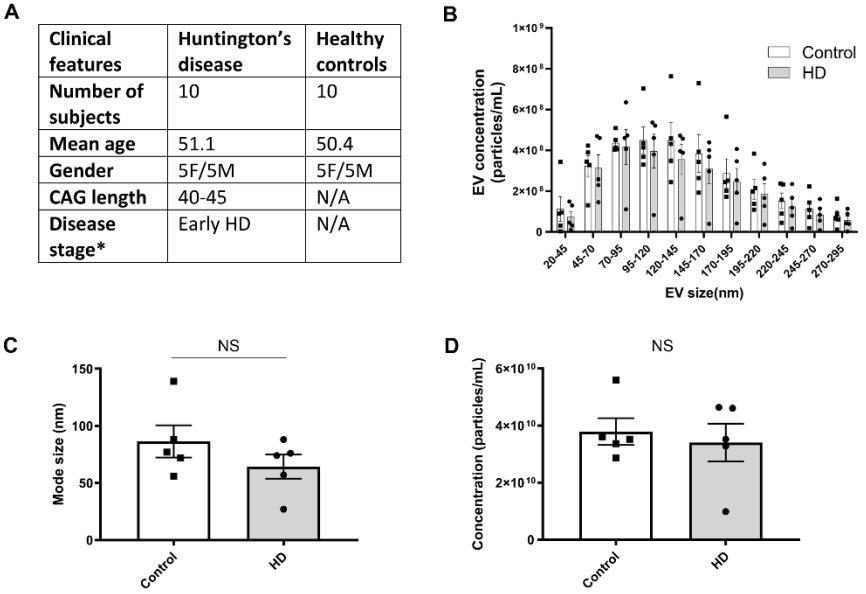

Figure 2.20. Characterization of CSF EV concentration and size using Nanoparticle Tracking Analysis. A) Clinical features of patient CSF samples used for EV miRNA extraction and next generation sequencing studies. A subset of CSF samples (N= 5 HD, 5 control) was used to determine the size distribution of Evs using fluorescent nanoparticle tracking analysis. *Standard disease stage according to total functional capacity (Shoulson, 1981). **B)** CSF EV particle concentration was characterized by EV size subgroups in increments of 25nm (Two-way ANOVA, Boferroni's multiple comparisons test, P>0.05), as well as by **C)** mode size (Student's t-test, unpaired, two-tailed, P>0.05), and D) concentration (Student's t-test, unpaired, two-tailed, P>0.05). Error bars depict mean ± SEM.

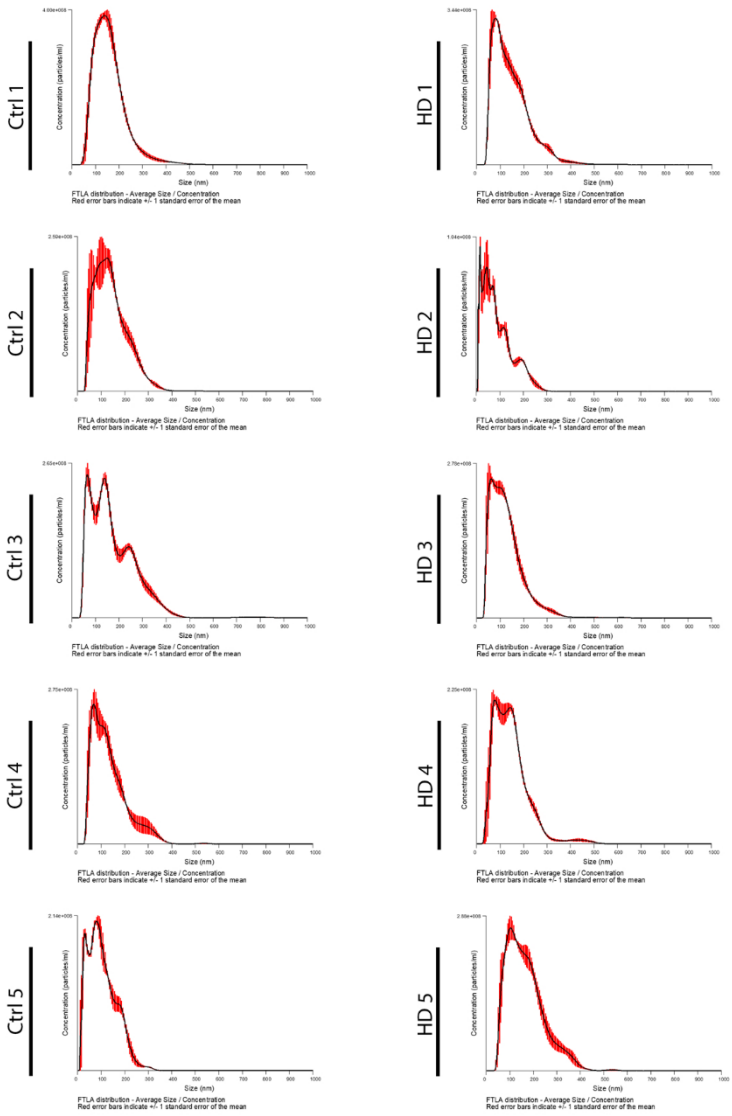

Figure 2.21. Average size distribution curves of individual CSF EV samples. EVs were isolated from CSF collected from HD and control patients by membrane affinity column centrifugation and resuspended in PBS (N= 5 HD, 5 control). Isolated EVs were analyzed in triplicate by fluorescent nanoparticle tracking analysis. Red error bars indicate ±1 SEM.

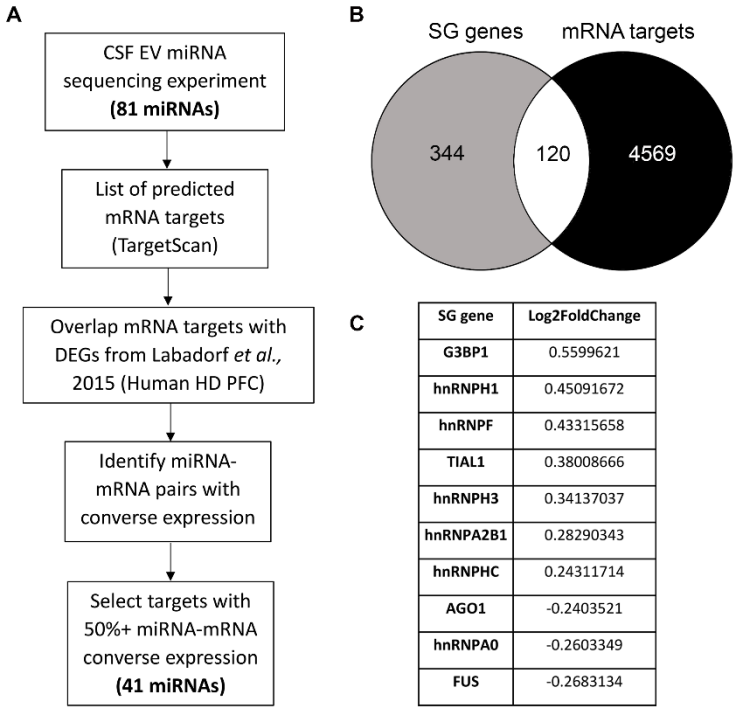

SG gene	Log2FoldChange
G3BP1	0.5599621
hnRNPH1	0.45091672
hnRNPF	0.43315658
TIAL1	0.38008666
hnRNPH3	0.34137037
hnRNPA2B1	0.28290343
hnRNPHC	0.24311714
AGO1	-0.2403521
hnRNPA0	-0.2603349
FUS	-0.2683134

Figure 2.22. EV miRNAs in the CSF of HD patients target SG-related mRNAs that are differentially expressed in the prefrontal cortex of HD patients. A) Workflow used to identify CSF EV miRNAs with likelihood of functional relevance based on overlap with RNA sequencing data from the prefrontal cortex of HD patients (Labadorf et al., 2015). **B)** Overlap of 4,689 CSF EV mRNAtargets and 464 mammalian SG genes (Nunes et al., 2019) is significantly higher than what is expected based on a genome larger than 21 ,000 genes ($P<0.05$ using the Fisher's exact, hypergeometric test). **C)** Table of selected SG genes that are differentially expressed in the prefrontal cortex of HD patients, with their respective log2FoldChange (Labadorf et al., 2015).

A

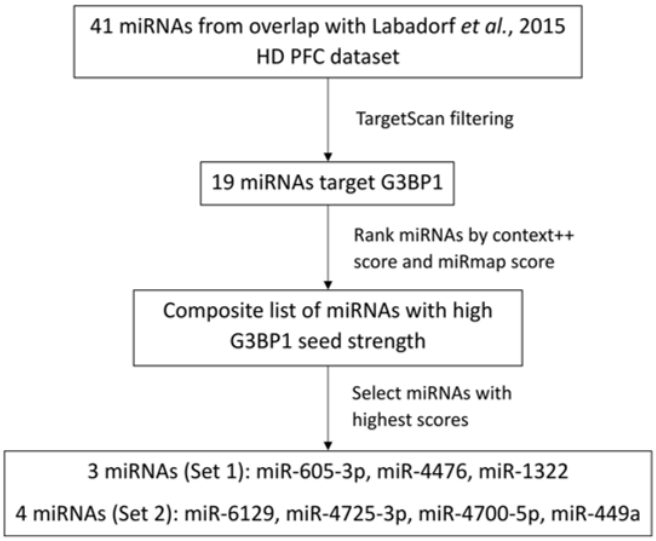

B

	miRNA	Context++ score	miRmap score
Set 2	miR-6129	-0.44	99.35
	miR-4725-3p	-0.23	98.88
	miR-4700-5p	-0.11	98.21
	miR-449a	-0.03	96.04
Set 1	miR-605-3p	-0.15	-
	miR-4476	0	95.4
	miR-1322*	-0.01	49.05

Figure 2.23. Selection of G3BP1-targeting miRNAs for overexpression studies in HEK293T cells. A) Workflow of miRNA ranking, and selection, based on predicted strength of miRNA repression on G3BP1 , or "G3BP1 seed strength". **B)** Ranked list of selected miRNAs with context++ and miRmap scores (*miRNA selected based on overlap with previously published HD CSF miRNA sequencing results (Reed et al., 2018)). PFC= prefrontal cortex.

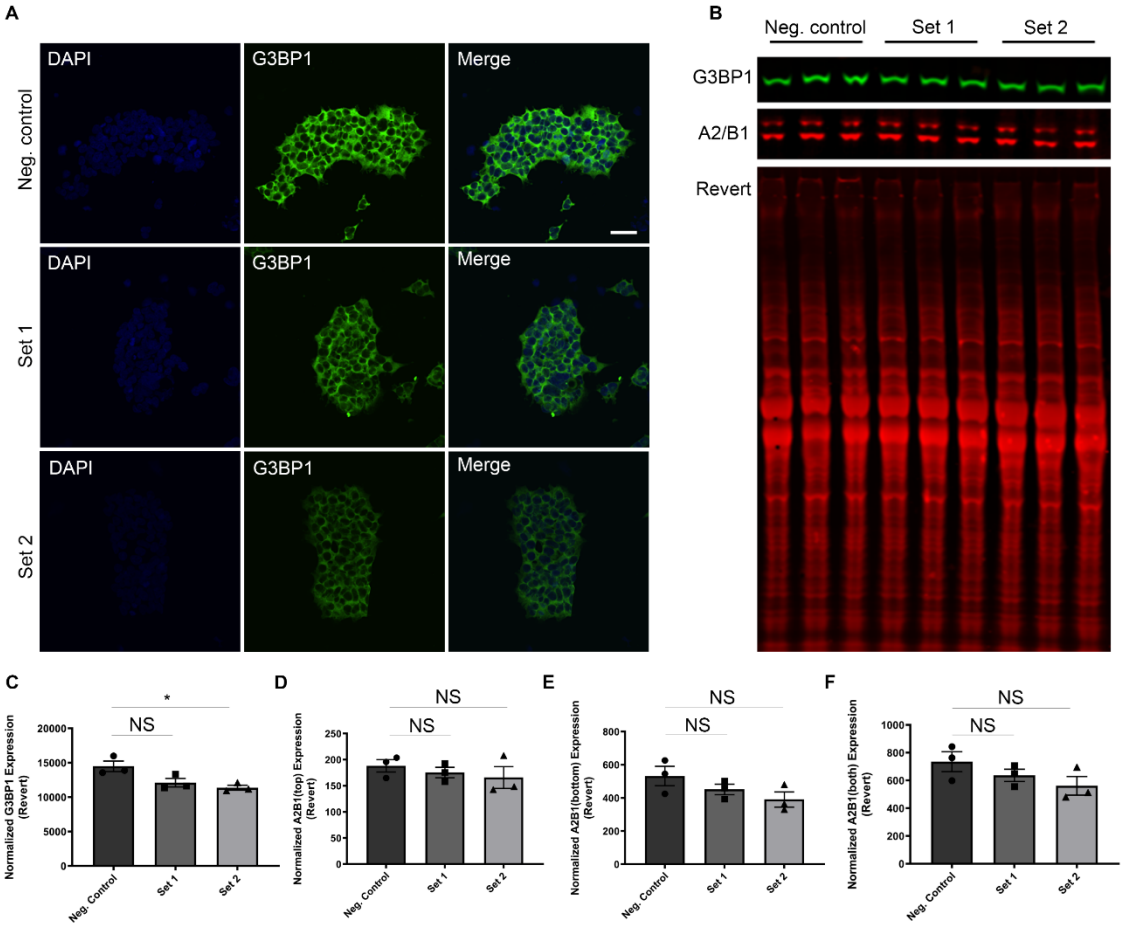

Figure 2.24. Downregulation of G3BP1 protein levels by overexpression of synthetic miRNAs in 293T cells. A) Representative images of G3BP1 immunofluorescence (in green) in 293T cells transfected with a negative control (Neg. control) miRNA, a cocktail of three miRNAs downregulated in the CSF EV mi RNA dataset (Set 1), and of four miRNAs upregulated in the CSF EV mi RNA dataset (Set 2) (n=3 per condition). Scale bar= 40um. **B)** Western blot of G3BP1, hnRNPA2/B1 (A2/B1), and total protein (Revert). **C)** G3BP1 protein expression normalized to total protein is significantly lower in Set 2 miRNA cocktail treated cells compared to the negative control (One-way ANOVA, Dunnett's multiple comparison test, *=0.019), but not Set 1 miRNA cocktail treated cells. **D-F)** hnRNPA2/B1 expression of individual isoforms ('top' vs. 'bottom') and both isoforms together normalized to total protein is also not significantly different among treatment groups.

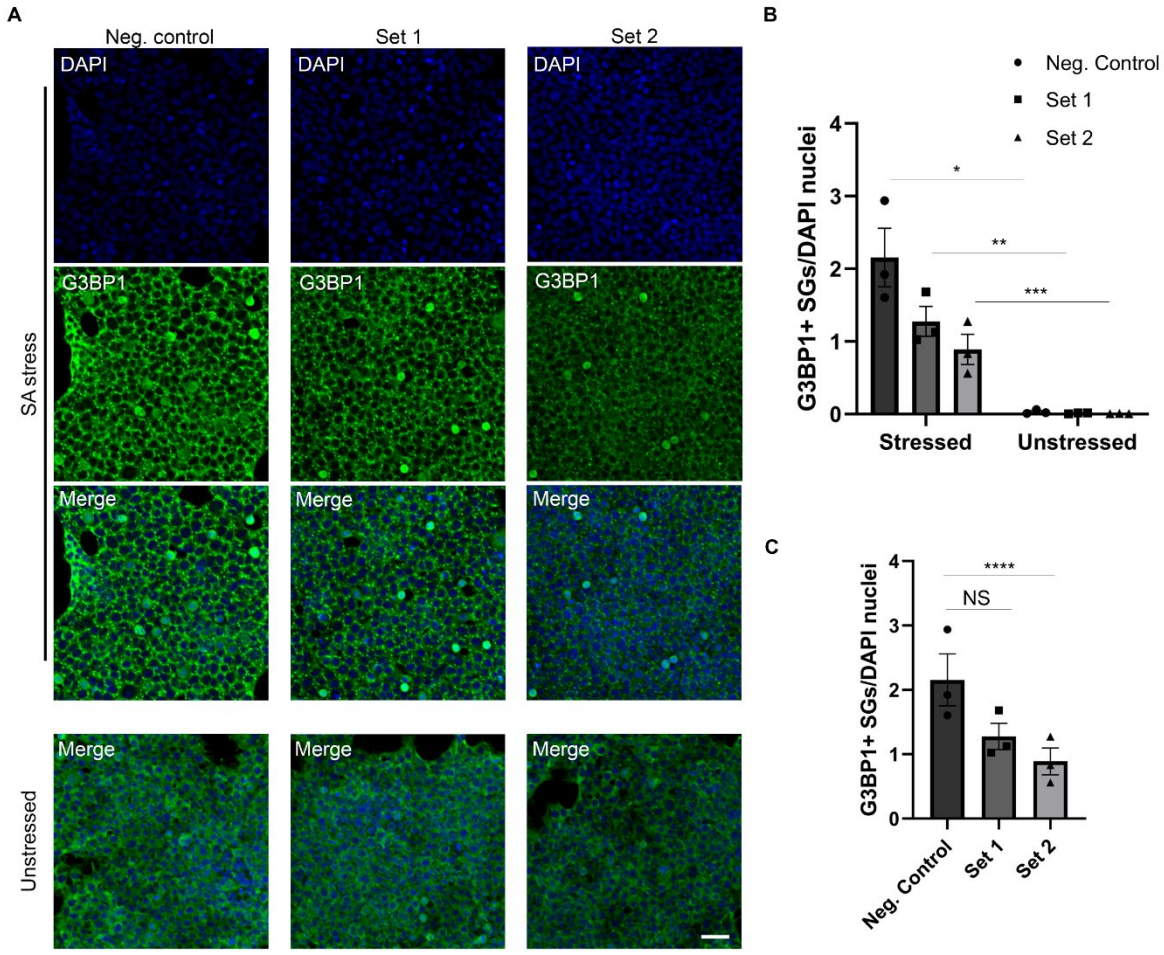

Figure 2.25. G3BP1-mediated SG induction is regulated by miRNAs in 293T cells treated with sodium arsenite. A) G3BP1 immunofluorescence (in green) of unstressed cells and cells stressed with sodium arsenite (SA). Cells were transfected with either a negative control mi RNA (Neg . Control), a 3-miRNA cocktail (Set 1), or a 4-miRNA cocktail (Set 2) (N=3 per condition). Scale bar= 40um. **B)** Quantitation of SG density (normalized to DAPI stained nuclei) in both stressed and unstressed conditions suggests that treatment with sodium arsenite resulted in a significant SG density increase within each condition (Two-way ANOVA with Sidak's multiple comparison test, *<0.0001; **=0.0025; ***=0.0283). **C)** SG density is significantly decreased in "Set 2" treated cells compared to cells treated with the negative control miRNA (One-way ANOVA with Dunnett's multiple comparison test, ****=0.0362), but not in "Set 1" treated cells. Analysis was done using three frames per condition, per replicate (N=3, n=3).

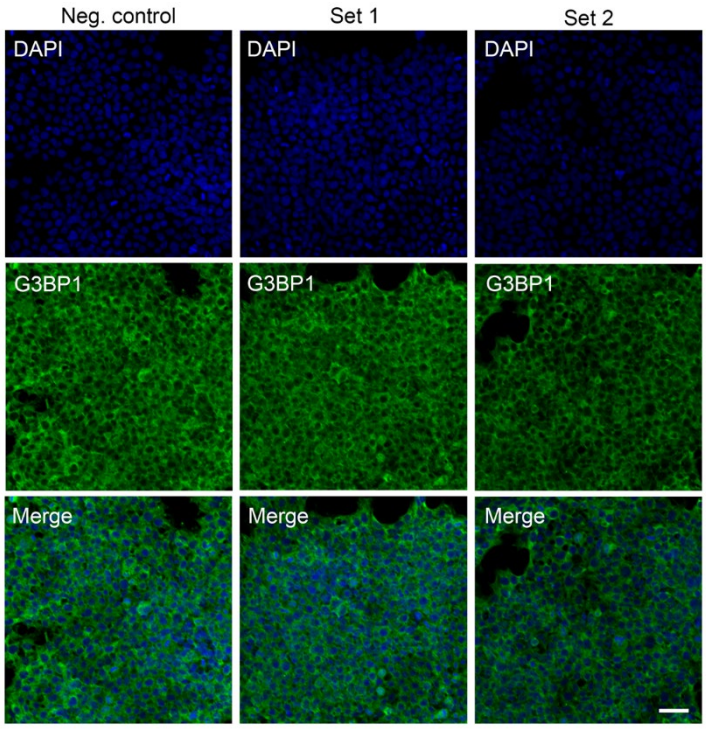

Figure 2.26. G3BP1-mediated SG induction is regulated by miRNAs in 293T cells treated with sodium arsenite (unstressed condition). Complementary representative images to Figure 2.25 (unstressed condition). Scale bar= 40um.

CHAPTER 2

TABLES

Table 2.1. Patient brain tissue samples. PMI=postmortem interval, PC=parietal cortex, SFC=superior frontal cortex, HF=hippocampal formation.

Case ID	Diagnosis	Age	Gender	PMI	Brain area
HC140-R	HD-3	62	M	22	SFC
HC147-L	HD-3	64	M	18	SFC
HC171-R	HD-3	51	M	24	SFC
HC139-R	HD-3	67	F	5	SFC
HC142-R	HD-3	55	F	25	SFC
HC158-R	HD-3	52	F	19	SFC
T-5608	HD-2	58	M	31	SFC, PFC, HIF
T-5693	HD-2	80	F	7	SFC, PFC, HIF
H239-R	control	64	M	15.5	SFC
H245-R	control	63	M	20	SFC
H231-R	control	65	M	8	SFC
H215-R	control	67	F	23.5	SFC
H238-R	control	63	F	16	SFC
H230-R	control	57	F	32	SFC
T-5382	control	62	M	5.5	SFC, PFC, HIF
T-5404	control	54	F	16.5	SFC, PFC, HIF

Table 2.2. Differentially expressed miRNAs in the prefrontal cortex of HD patients that are predicted to target G3BP1. Adapted from Hoss et al., 2015 list of 75 miRNAs differentially expressed in HD brain, combined study

miRNA	logFC	p-value	FDR q-value
miR-10b-3p	1.45	2.13E-12	4.98E-10
miR-1298-3p	−0.78	5.52E-09	1.03E-06
miR-302a-3p	0.81	3.72E-06	4.98E-04
miR-223-3p	0.75	1.94E-05	1.82E-03
miR-3200-3p	−0.32	4.85E-05	4.14E-03
miR-302a-5p	0.7	5.70E-05	4.46E-03
miR-1264	−0.53	9.49E-05	6.36E-03
miR-6734-5p	−0.79	8.86E-05	6.36E-03
miR-144-5p	0.94	1.04E-04	6.53E-03
miR-138-2-3p	−0.38	1.43E-04	8.38E-03
miR-490-5p	−0.62	2.62E-04	1.04E-02
miR-5695	0.47	2.73E-04	1.04E-02
miR-885-5p	−0.35	2.77E-04	1.04E-02
miR-1298-5p	−0.81	3.84E-04	1.20E-02
miR-16-2-3p	0.71	3.98E-04	1.21E-02
miR-106a-5p	0.44	5.64E-04	1.43E-02
miR-142-5p	0.6	5.77E-04	1.43E-02
miR-549a	0.95	5.67E-04	1.43E-02
miR-5680	−0.35	9.93E-04	2.27E-02
miR-3065-5p	0.42	1.04E-03	2.33E-02
miR-4787-3p	−0.33	1.23E-03	2.62E-02
miR-101-5p	0.28	1.47E-03	2.88E-02
miR-483-5p	1.16	1.52E-03	2.91E-02
miR-1185-1-3p	−0.41	1.70E-03	3.12E-02
miR-129-5p	−0.35	1.95E-03	3.22E-02
miR-888-5p	0.56	1.91E-03	3.22E-02
miR-126-5p	0.29	2.46E-03	3.88E-02
miR-34c-5p	−0.64	2.48E-03	3.88E-02
miR-218-1-3p	0.35	2.53E-03	3.89E-02
miR-548n	0.52	3.14E-03	4.46E-02
miR-148a-5p	0.52	3.31E-03	4.57E-02
miR-29a-3p	0.23	3.46E-03	4.70E-02
miR-153-5p	0.37	3.78E-03	4.79E-02
miR-28-5p	0.27	3.75E-03	4.79E-02
miR-7-2-3p	0.27	3.78E-03	4.79E-02

Table 2.3. CSF EV miRNAs from HD vs. control differential expression analysis with P values <0.05, prior to correcting for multiple tests with the Benjamini-Hochberg method. N= 10 HD, 10 control. Sequencing studies were performed in two batches, "1st batch and 2nd batch", following the same EV RNA isolation protocol.

	miRNA	baseMean	log2FoldChange	lfcSE	stat	p-value	padj
Batch 1	hsa-miR-30e-5p	54.0066	-1.3356	0.429	-3.1134	0.00185	0.96335
	hsa-miR-1307-5p	6.06509	-6.1314	2.0375	-3.0093	0.00262	0.96335
	hsa-miR-449a	3.93847	4.8305	2.06734	2.33658	0.01946	0.96335
	hsa-let-7f-2-3p	3.49976	-5.3405	2.38671	-2.2376	0.02525	0.96335
	hsa-miR-584-5p	10.7835	-1.8939	0.87022	-2.1764	0.02953	0.96335
	hsa-miR-4634	7.04013	-5.1387	2.44135	-2.1048	0.03531	0.96335
	hsa-miR-381-3p	4.04843	4.09951	1.99834	2.05145	0.04022	0.96335
	hsa-miR-3907	6.15003	-6.12	3.03296	-2.0178	0.04361	0.96335
	hsa-miR-127-3p	5.29822	-3.2987	1.65742	-1.9903	0.04656	0.96335
	hsa-miR-29b-3p	28.6266	1.32361	0.66731	1.9835	0.04731	0.96335
Batch 2	hsa-miR-12136	3.57178	-2.2974	0.81625	-2.8146	0.00488	0.99845
	hsa-miR-6852-5p	1.05441	-3.4144	1.40459	-2.4309	0.01506	0.99845
	hsa-miR-4476	2.84722	-3.6436	1.51218	-2.4095	0.01597	0.99845
	hsa-miR-4750-3p	3.87093	-2.6797	1.14557	-2.3392	0.01933	0.99845
	hsa-miR-762	7.43113	1.07142	0.47626	2.24965	0.02447	0.99845
	hsa-miR-12126	3.54035	-2.962	1.43171	-2.0689	0.03856	0.99845
	hsa-miR-3675-3p	18.3645	0.92447	0.4521	2.04486	0.04087	0.99845
	hsa-miR-4725-3p	2.14193	1.95724	0.98018	1.99681	0.04585	0.99845
	hsa-miR-8069	16.2964	0.87203	0.43997	1.982	0.04748	0.99845
	hsa-miR-181c-3p	12.2489	-2.1381	1.08024	-1.9793	0.04778	0.99845
	hsa-miR-6785-5p	29.6265	0.90042	0.45688	1.97082	0.04874	0.99845
	hsa-miR-4687-3p	0.9087	2.64169	1.34676	1.96152	0.04982	0.99845

Table 2.4. CSF EV miRNAs from HD vs. control differential expression analysis with a log2FoldChange larger than a magnitude of two.

miRNAs	baseMean	log2 FoldChange	lfcSE	stat	pvalue	padj
hsa-miR-3944-5p	0.759	3.113	3.073	1.013	0.311	0.998
hsa-miR-3189-3p	0.741	3.079	2.264	1.36	0.174	0.998
hsa-miR-4767	0.672	2.914	1.802	1.617	0.106	0.998
hsa-miR-3917	0.586	2.729	3.087	0.884	0.377	0.998
hsa-miR-3190-3p	0.568	2.687	3.089	0.87	0.384	0.998
hsa-miR-135a-2-3p	0.565	2.671	2.383	1.121	0.262	0.998
hsa-miR-4687-3p	0.909	2.642	1.347	1.962	0.05	0.998
hsa-miR-5692a	0.536	2.607	2.375	1.098	0.272	0.998
hsa-miR-4763-3p	0.532	2.599	2.432	1.069	0.285	0.998
hsa-miR-3136-5p	0.52	2.571	3.094	0.831	0.406	0.998
hsa-miR-616-5p	0.501	2.525	2.425	1.041	0.298	0.998
hsa-miR-4689	0.499	2.514	3.097	0.812	0.417	0.998
hsa-miR-4429	1.301	2.444	1.297	1.884	0.06	0.998
hsa-miR-6846-3p	1.717	2.414	1.272	1.897	0.058	0.998
hsa-miR-557	0.444	2.363	3.105	0.761	0.447	0.998
hsa-miR-5589-5p	0.434	2.303	3.108	0.741	0.459	0.998
hsa-miR-4442	0.427	2.282	3.109	0.734	0.463	0.998
hsa-miR-8086	0.427	2.282	3.109	0.734	0.463	0.998
hsa-miR-6782-5p	0.425	2.277	3.11	0.732	0.464	0.998
hsa-miR-6840-3p	0.425	2.277	3.11	0.732	0.464	0.998
hsa-miR-6529-5p	0.421	2.255	1.904	1.185	0.236	0.998
hsa-miR-6842-5p	0.416	2.245	2.457	0.914	0.361	0.998
hsa-miR-3127-5p	0.411	2.233	3.112	0.718	0.473	0.998
hsa-miR-4700-5p	1.122	2.201	1.651	1.333	0.183	0.998
hsa-miR-4457	0.392	2.179	2.454	0.888	0.375	0.998
hsa-miR-6129	1.027	2.162	1.373	1.574	0.115	0.998
hsa-miR-1305	0.383	2.148	2.452	0.876	0.381	0.998
hsa-miR-4257	1.081	2.069	1.386	1.493	0.135	0.998
hsa-miR-7150	1.04	2.029	1.37	1.481	0.139	0.998

Table 2.4 (continued). CSF EV miRNAs from HD vs. control differential expression analysis with a log2FoldChange larger than a magnitude of two.

miRNAs	baseMean	log2 FoldChange	lfcSE	stat	pvalue	padj
hsa-miR-10523-5p	1.869	2.016	1.371	1.47	0.142	0.998
hsa-miR-605-3p	0.388	-2.027	3.112	-0.651	0.515	0.998
hsa-miR-6789-5p	2.066	-2.057	1.201	-1.713	0.087	0.998
hsa-miR-9985	0.419	-2.098	2.503	-0.838	0.402	0.998
hsa-miR-181c-3p	12.249	-2.138	1.08	-1.979	0.048	0.998
hsa-miR-1322	0.446	-2.191	2.512	-0.872	0.383	0.998
hsa-miR-3679-3p	0.433	-2.196	3.103	-0.708	0.479	0.998
hsa-miR-8076	0.433	-2.196	3.103	-0.708	0.479	0.998
hsa-miR-3610	1.207	-2.215	1.345	-1.646	0.1	0.998
hsa-miR-3940-5p	0.442	-2.229	2.462	-0.905	0.365	0.998
hsa-miR-7106-3p	1.217	-2.254	1.73	-1.303	0.193	0.998
hsa-miR-12136	3.572	-2.297	0.816	-2.815	0.005	0.998
hsa-miR-6827-3p	0.472	-2.304	2.408	-0.957	0.339	0.998
hsa-miR-10392-5p	1.376	-2.407	1.326	-1.815	0.069	0.998
hsa-miR-4535	0.516	-2.408	2.417	-0.996	0.319	0.998
hsa-miR-6880-3p	0.516	-2.422	2.422	-1	0.317	0.998
hsa-miR-3621	2.702	-2.425	1.26	-1.924	0.054	0.998
hsa-miR-2116-3p	1.417	-2.449	1.261	-1.942	0.052	0.998
hsa-miR-4750-3p	3.871	-2.68	1.146	-2.339	0.019	0.998
hsa-miR-4638-5p	0.637	-2.709	3.08	-0.879	0.379	0.998
hsa-miR-3124-5p	0.64	-2.713	3.08	-0.881	0.378	0.998
hsa-miR-1915-5p	0.655	-2.738	1.852	-1.479	0.139	0.998
hsa-miR-130b-5p	0.66	-2.755	3.079	-0.895	0.371	0.998
hsa-miR-1243	0.673	-2.822	3.076	-0.917	0.359	0.998
hsa-miR-12126	3.54	-2.962	1.432	-2.069	0.039	0.998
hsa-miR-5698	2.864	-2.967	1.611	-1.842	0.065	0.998
hsa-miR-6852-5p	1.054	-3.414	1.405	-2.431	0.015	0.998
hsa-miR-624-5p	1.03	-3.439	1.813	-1.897	0.058	0.998
hsa-miR-4476	2.847	-3.644	1.512	-2.41	0.016	0.998
hsa-miR-6800-3p	1.217	-3.665	2.326	-1.576	0.115	0.998

Table 2.5. Filtered miRNAs from miRNA-mRNA overlap analysis. List of 41 miRNAs that target differentially expressed genes (DEGs) in the prefrontal cortex (PFC) of HD patients. Because the expression level of a miRNA is negatively correlated to the expression level of its target gene, miRNAs whose expression levels were not the inverse of their target genes 50% or more of the time (% overlap) were filtered out.

miRNA	Total targets	Targets in HD PFC DEGs	Inverse direction	% overlap
hsa-miR-8076	2950	855	564	65.96
hsa-miR-3610	438	131	86	65.65
hsa-miR-624-5p	2078	646	421	65.17
hsa-miR-1243	3200	964	608	63.07
hsa-miR-146a-5p	283	74	46	62.16
hsa-miR-130b-5p	5727	1779	1100	61.83
hsa-miR-1322	2962	906	560	61.81
hsa-miR-181c-3p	1675	541	331	61.18
hsa-miR-4767	1203	391	238	60.87
hsa-miR-4442	644	188	109	57.98
hsa-miR-339-3p	729	283	164	57.95
hsa-miR-3125	5385	1666	965	57.92
hsa-miR-3917	710	214	123	57.48
hsa-miR-29b-3p	1265	426	244	57.28
hsa-miR-6846-3p	2673	880	500	56.82
hsa-miR-762	5621	1845	1046	56.69
hsa-miR-3679-3p	4906	1570	887	56.5
hsa-miR-6827-3p	2298	707	397	56.15
hsa-miR-4763-3p	6300	2050	1151	56.15
hsa-miR-6842-5p	4250	1412	786	55.67
hsa-miR-605-3p	4722	1486	823	55.38
hsa-miR-6782-5p	3452	1129	622	55.09
hsa-miR-3940-5p	3284	1033	561	54.31
hsa-miR-4700-5p	5553	1812	983	54.25
hsa-miR-6129	5364	1728	933	53.99
hsa-miR-6800-3p	3197	1014	540	53.25
hsa-miR-449a	754	256	136	53.13
hsa-miR-4535	2092	665	348	52.33
hsa-miR-3189-3p	4423	1397	730	52.25
hsa-miR-4634	638	196	102	52.04
hsa-miR-3127-5p	4249	1351	703	52.04
hsa-miR-4476	5956	1873	974	52
hsa-miR-6785-5p	7852	2509	1294	51.57
hsa-miR-7150	5077	1626	838	51.54
hsa-miR-2116-3p	4929	1572	810	51.53
hsa-miR-378b	223	72	37	51.39
hsa-miR-6840-3p	6772	2194	1126	51.32
hsa-miR-5589-5p	6349	2042	1043	51.08
hsa-miR-3158-3p	3263	1058	535	50.57
hsa-miR-4725-3p	5776	1816	918	50.55
hsa-miR-3944-5p	3815	1267	639	50.43

Table 2.6. Top 10 GO terms for biological process, cellular component, and molecular function, using the predicted gene targets of the final 41 filtered CSF EV miRNAs.

	GO term	Fold enrichment	Raw p-value	FDR
Biological process	glutamate secretion (GO:0014047)	2.69	2.03E-03	4.86E-02
	embryonic forelimb morphogenesis (GO:0035115)	2.58	1.73E-03	4.30E-02
	forelimb morphogenesis (GO:0035136)	2.52	8.85E-04	2.47E-02
	positive regulation of sodium ion transport (GO:0010765)	2.51	2.08E-03	4.92E-02
	macrophage activation (GO:0042116)	2.46	3.37E-04	1.07E-02
	cellular extravasation (GO:0045123)	2.46	1.01E-03	2.76E-02
	regulation of sodium ion transmembrane transporter activity (GO:2000649)	2.41	2.82E-04	9.19E-03
	regulation of sodium ion transmembrane transport (GO:1902305)	2.31	1.82E-04	6.22E-03
	synaptic vesicle exocytosis (GO:0016079)	2.24	4.13E-04	1.27E-02
	regulation of myeloid leukocyte mediated immunity (GO:0002886)	2.24	1.24E-03	3.25E-02
Cellular component	presynaptic active zone membrane (GO:0048787)	2.6	2.32E-03	4.35E-02
	presynaptic active zone (GO:0048786)	2.15	3.89E-04	9.52E-03
	specific granule membrane (GO:0035579)	2.12	1.10E-04	3.30E-03
	tertiary granule (GO:0070820)	1.97	3.99E-06	1.57E-04
	tertiary granule membrane (GO:0070821)	1.97	2.17E-03	4.11E-02
	plasma membrane raft (GO:0044853)	1.92	3.69E-04	9.14E-03
	specific granule (GO:0042581)	1.87	4.35E-05	1.41E-03
	secretory granule membrane (GO:0030667)	1.82	7.67E-08	3.95E-06
	sarcolemma (GO:0042383)	1.79	4.39E-04	1.06E-02
	clathrin-coated vesicle membrane (GO:0030665)	1.79	1.77E-03	3.48E-02
Molecular function	DNA-binding transcription repressor activity, RNA polymerase II-specific (GO:0001227)	1.8	1.52E-06	2.30E-04
	DNA-binding transcription repressor activity (GO:0001217)	1.8	1.52E-06	2.23E-04
	DNA-binding transcription activator activity, RNA polymerase II-specific (GO:0001228)	1.6	7.94E-07	1.33E-04
	DNA-binding transcription activator activity (GO:0001216)	1.6	1.05E-06	1.69E-04
	RNA polymerase II regulatory region DNA binding (GO:0001012)	1.52	2.65E-09	1.13E-06
	RNA polymerase II proximal promoter sequence-specific DNA binding (GO:0000978)	1.51	1.73E-06	2.26E-04
	RNA polymerase II regulatory region sequence-specific DNA binding (GO:0000977)	1.51	5.73E-09	1.92E-06
	amide binding (GO:0033218)	1.5	1.70E-04	1.42E-02
	proximal promoter sequence-specific DNA binding (GO:0000987)	1.5	2.86E-06	3.44E-04
	transcription regulatory region sequence-specific DNA binding (GO:0000976)	1.49	7.38E-09	2.31E-06

Table 2.7. List of primary antibodies used for tissue staining and western blotting. FF= free floating, PE= paraffin embedded, IF= immunofluorescence, WB= western blotting.

Antigen	Type	Dilution	Manufacturer
Anti-G3BP1	Rabbit Polyclonal	1:300 (FF- and PE-IF) 1:1000 (cell culture IF) 1:1000 (WB)	cat. #RN048PW, MBL
Anti-G3BP2	Rabbit Polyclonal	1:200 (FF-IF)	cat. #ab86135, Abcam
Anti-hnRNPA2/B1	Mouse Monoclonal	1:250 (FF-IF) 1:100 (PE-IF) 1:1000 (WB)	cat. #sc-53531, Santa Cruz Biotech.
Anti-eIF3H	Mouse Monoclonal	1:200 (PE-IF)	cat. #sc-137214, Santa Cruz Biotech.
Anti-Huntingtin (EM48)	Mouse Monoclonal	1:200 (FF-IF)	cat. #MAB5374, Millipore
Anti-Polyglutamine (1C2)	Mouse Monoclonal	1:500 (FF-IF)	cat. #MAB1574, Millipore
Anti-Huntingtin (3B5H10)	Mouse Monoclonal	1:500 (FF-IF)	cat. #MABN821, Millipore
Anti-Huntingtin (5490)	Mouse Monoclonal	1:500 (FF-IF)	cat. #MAB5490, Millipore
Anti-CaMK2	Mouse Monoclonal	1:300 (PE-IF)	cat. #ab22609, Abcam
Anti-alpha-tubulin	Mouse Monoclonal	1:5000 (WB)	cat. #05-829, Sigma-Aldrich

Table 2.8. miRCURY LNA miRNA mimics used in 293T cell transfection studies.

miRCURY LNA miRNA mimic	QIAGEN Catalog #
Negative Control	#YM00479902-ADB
hsa-miR-6129	#YM00473318-ADB
hsa-miR-4725-3p	#YM00472882-ADB
hsa-miR-605-3p	#YM00470339-ADB
hsa-miR-4700-5p	#YM00472802-ADB
hsa-miR-449a	#YM00473262-ADB
hsa-miR-4476	#YM00472685-ADB
hsa-miR-1322	#YM00470309-ADB

CHAPTER 3

Derivation of choroid plexus epithelial cells from Huntington's disease patient-derived induced pluripotent stem cells

SUMMARY OF CHAPTER 3

The previous chapter of this dissertation focused on the SG component G3BP1 and the accumulation of G3BP1-positive SGs in HD. Additionally, it was proposed that EV miRNAs in the CSF of HD patients that are differentially packaged have the potential to regulate SG dynamics via the post-transcriptional repression of SG components such as G3BP1. Recent studies provide evidence for pathological differences in the CSF composition from Alzheimer's disease and ALS patients. CSF production and maintenance are largely regulated by the choroid plexus (ChP), a highly specialized secretory tissue within the third, fourth, and lateral ventricles. The outer layer of the ChP is composed of cuboidal choroid plexus epithelial cells (CPECs). Sealed by tight junctions, CPECs form the interface between vascular tissue and CSF, produce CSF, and secrete miRNA-containing EVs. Thus, the generation of an *in vitro* CPEC system would allow for mechanistic studies to investigate CSF EV miRNA secretion in health and disease. In this chapter, we provide a preliminary proof of concept for the derivation of CPECs from patient-derived induced pluripotent stem cells (iPSCs), and initial evidence for altered tight junction and cilia formation in HD iPSC-CEPCs.

INTRODUCTION

Because CPECs are the interface of the blood-CSF barrier and are responsible for the maintenance of the CSF, there is potential for their involvement in the seeding and spread of neurodegenerative disease pathology (Smith et al., 2015). In ALS, the blood-CSF barrier structure is compromised due to the disruption of tight junction components of the CPEC layer, which lines the ChP, and disruption of vascular integrity of the ChP (Saul et al., 2020). Additionally, the CSF from ALS patients contains altered levels of proteins including increased inflammatory and extracellular matrix proteins, as well as increased CSF to serum ratios of albumin, IgG, and complement C3 (Leonardi et al., 1984; Annunziata et al., 1985; Apostolski et al., 1991; Ryberg et al., 2011; Blasco et al., 2013; Collins et al., 2015), corroborating the disruption of blood-CSF barrier in ALS. In Alzheimer's disease, CSF production and turnover are decreased (Serot et al., 2000), CPEC height is decreased (Serot et al., 2003), there is increased accumulation of Lipofuscin vacuoles and Biondi bodies (Wen et al., 1999), and increased Aβ deposition, resulting in the breakdown of barrier integrity (Vargas et al, 2010). Altogether, these findings warrant further investigation of the ChP to better understand its involvement in neurodegenerative disease.

The investigation of CPECs has been limited to postmortem tissue samples, which do not allow for the study of early cellular and molecular mechanisms underlying disease phenotypes. Very few studies have investigated CPECs *in vitro*, potentially due to the difficulty to expand or generate them in culture. However, exploiting the fact that CPECs arise from pre-neurogenic epithelial cells and require bone morphogenic protein (BMP) signaling for differentiation, Watanabe et al. showed that BMP4 is sufficient to induce CPEC fate from neural progenitors of neuroepithelial lineage derived from mouse and human

embryonic stem cells (ESCs) (Watanabe et al, 2012). To do this, they used a serum-free culture of embryoid body-like aggregation (SFEBq) based method to derive cells of neuroepithelial lineage from mESCs and hESCs, followed by treatment with BMP4. Importantly, the SFEBq method recapitulates spatial and temporal aspects of early corticogenesis, and gives rise to neuroepithelial cells with apical-basal polarity (Eiraku et al, 2008). BMP4 sufficiency was demonstrated by qRT-PCR, ICC, and ISH data showing increased expression of CPEC markers, and electron microscopy analysis provided ultrastructural data demonstrating that these cells contained microvilli and juxtalumenal tight junctions. However, derivation efficiency was low and the authors stated that protocol optimization will be necessary. Recently, the development of human ChP organoids was achieved, which contain CPECs that recapitulate *in vivo* characteristics, and display CSF secretion and barrier formation properties (Pellegrini et al., 2020). These *in vitro* systems will play an instrumental role in the identification of the specific CSF components that originate from CPECs, and coupled with iPSC technology, will make possible mechanistic studies of CPECs in disease.

The few studies that have investigated EV secretion by CPECs, however, mainly use the immortalized rat CPEC line Z310 (Zheng et al, 2002), or commercially available CPECs isolated from human ChP (ScienCell). Mouse models have also been used to study the ChP and its secretory functions. For example, a study by Balusu et al. identified EV release by the choroid plexus and presents it as a mechanism for blood-brain communication during systemic inflammation, in which pro-inflammatory miRNAs become overrepresented in CSF EVs (Balusu et al., 2016). In this study, they show that ChP derived EVs enter the brain parenchyma when injected intraventricularly into the mouse brain, are taken up by

astrocytes and microglia, and induce miRNA target repression and inflammatory gene up-regulation. They claim that EVs that cross the ependymal cell lining of the ventricles contain specific proteins that target astrocytes and microglia, but not neurons. However, the manner in which EVs were isolated has to be taken into consideration before making and/or adopting these general claims. The EVs used for this procedure were isolated from pooled CSF, obtained from mice that had been treated with the endotoxin lipopolysaccharide (LPS), which induces an inflammatory response. LPS also induced an upregulation of EV secretion; thus, it's possible that this treatment had a selective effect on the specific subtype of EVs generated, and more importantly, the type of membrane protein receptors present. For example, LPS treatment, which induces microglia and astrocyte activation (Chen et al, 2012; Tarassishin et al, 2014), could have resulted in increased EV secretion specifically from glial cells, which are probably rich in membrane proteins that selectively induce uptake by glial cells.

Nonetheless, their studies provide strong support that the ChP is a major contributor of EVs found in the CSF. Transthyretin (TTR) is a common ChP marker, as it is exclusively produced and secreted by the ChP (Herbert et al, 1986; Aldred et al, 1995). Balusu et al. found that EV samples isolated from CSF contained TTR, suggesting that the ChP is an important source of CSF EVs. Furthermore, when exosome production was inhibited *in vivo* with GW4869, Nanoparticle Tracking Analysis demonstrated a reduced amount of EVs in the CSF, and an accumulation of miRNAs in the ChP. This is corroborated by findings from Grapp et al., where 36% of all human CSF exosomes were found to contain folate receptor-α (Grapp et al., 2013). Since brain FRα is almost exclusively expressed in the ChP, this also suggests that the ChP may be a major source of CSF exosomes.

Reports suggest that human CPECs secrete EVs at an average of 559.1 ($x10^9$) EVs per mL, and that these EVs contain hnRNPA2B1-miRNA complexes (Tietje et al., 2016). Specifically, the post-translational modification of hnRNPA2B1 by SUMO has been proposed to act as a molecular switch for the packaging of miRNAs into exosomes (Villarroya-Beltri et al, 2013), and previous work from our laboratory shows that SUMOylation is altered in HD (Steffan et al., 2004; O'Rourke et al., 2013). Post-translational protein modifications facilitate cell signaling by allowing cells to spatially and temporally regulate the functional diversity of their proteome. SUMOylation is a post-transcriptional modification in which a member of the small (~11 kDa) ubiquitin-like modifier (SUMO) family of proteins reversibly binds to lysine residues in target proteins (Geiss-Friedlander et al, 2007). Processing to yield mature protein is carried out by a family of SUMO-specific proteases (SENPs), SUMO proteins are activated by ATP-dependent heterodimer of SUMO1 activating enzyme subunit 1 (SAE1), and are then passed on to the conjugating enzyme 9 (UBC9). UBC9 then works in conjunction with an E3 ligating enzyme to catalyze SUMO conjugation to the substrate (Cappadocia et al., 2017; Dye et al., 2007). Four SUMO isoforms are found in mammalian cells, designated SUMO1 to SUMO4, although SUMO4 is only present in kidney and its function is not well characterized. SUMOylation functions are diverse and best characterized for nuclear functions (Nuro-Gyina et al, 2016); however, cytosolic roles have also been identified and include regulation of G-protein signaling, kinase and phosphatase signaling, mitochondrial fission and apoptosis, regulation of RNA metabolism and trafficking, and protein homeostasis (Geiss-Friedlander et al, 2007; Liebelt et al, 2016). Synaptic proteins are also SUMO modified (Matsuzaki et al., 2016). The effects of SUMOylation vary depending on the target, and include revealing or blocking sites for other

post-translational modifications, and promoting novel protein interactions by the non-covalent binding of proteins with SUMO interacting motifs (SIMs) (Yang et al., 2017; Zhao, 2018).

A proteomic analysis of HeLa cells treated with the proteasome inhibitor MG132 found that all SUMO paralogues could be identified in the resulting insoluble protein inclusions, suggesting that aberrant SUMOylation may occur in response to the presence of misfolded or oligomerized proteins, including HTT (Tatham et al., 2011). Mutant HTT fragments have been shown to co-localize with SUMO1 in co-transfection studies performed on mouse immortalized striatal cells, suggesting that HTT is either SUMOylated, or that it interacts with SUMOylated proteins (Sipione et al., 2002). The direct SUMO modification of a neurodegenerative disease protein was first described by Steffan et al. (Steffan et al, 2004), showing that the HTT protein could be SUMO modified. The involvement of SUMO in HD pathogenesis was further studied in cells and in drosophila. Additionally, a study conducted on post-mortem striatal tissue from HD patients showed an accumulation of SUMO2 and, to a lesser extent, SUMO1 modified proteins in the insoluble protein fraction, suggesting *in vivo* relevance for the potential involvement of SUMO modification on aberrant mHTT accumulation (O'Rourke et al., 2013). Lastly, reduction of the SUMO E3 ligase PIAS1 rescues disease-associated phenotypes in the R6/2 HD mouse model (Ochaba et al., 2016), although to date direct *in vivo* SUMO modification of HTT has not yet been feasible, given that endogenous SUMO modification is highly transient.

Several members of the hnRNP RBP family are post-translationally modified by SUMO (hnRNPs A1, A3, F, H1, K, and U) (Li et al, 2004), suggesting that SUMOylation may be a key

player in the regulation of mRNA metabolism. Interestingly, the putative SUMOylation sites of most hnRNPs, including hnRNPA2B1, are located in the RRM, suggesting that SUMOylation might regulate the protein's RNA binding activity. Villarroya-Beltri et al. identified a role for hnRNPA2B1 in the sorting of miRNAs into exosomes (Villaroya-Beltri et al, 2013), which appears to be dependent on SUMO modification of hnRNPA2B1 and recognition of the GGAG motif in the 3' end of miRNAs. These results were subsequently corroborated by a separate study that identified hnRNPA2B1-miRNA complexes in CSF exosomes (Tietje et al, 2014). While hnRNPA1 and hnRNPC are also able to bind miRNAs, a binding motif has not been identified (Villarroya-Beltri et al, 2013).

In conclusion, we propose that CPECs are an ideal model to study the packaging and secretion of EV miRNAs, which in turn will help elucidate the cellular and molecular mechanisms underlying the propagation of pathology via the CSF. Because CPECs express hnRNPA2B1, and miRNA-hnRNPA2B1 complexes are found within CPEC EVs, these cells will allow for the investigation of hnRNPA2B1-mediated miRNA packaging. In this chapter, we provide evidence of a potential role for SUMOylated hnRNPA2B1 in HD, and demonstrate feasibility for the derivation of CPECs from patient-derived iPSCs to investigate disease mechanisms.

RESULTS

hnRNPA2B1 mislocalization as a result of proteostatic stress in rat CPECs

SGs, which assemble when RNA binding proteins such as hnRNPA2B1 aggregate through their glycine rich domains, might contribute to neurodegeneration via toxic gain or loss-of-function mechanisms (Kim et al., 2013; Martinez et al., 2016; Wolozin et al., 2019). If hnRNPA2B1 is

sequestered in SGs, other functions such as the packaging of miRNAs into EVs might become impacted. To begin to investigate mechanisms underlying hnRNPA2B1 mislocalization, we used an immortalized CPEC cell system as a first step. Z310 rat CPECs (Zheng et al., 2002) were transfected with increasing concentrations of 97Q-expanded Exon 1-GFP of HTT and treated with MG132 to inhibit the proteasome and lysosome. This proteostatic stress resulted in mislocalization of hnRNPA2B1 from a detergent insoluble (roughly nuclear) to a soluble (roughly cytoplasmic) fraction (**Figure 3.1, A**), and of SUMO-1 (**Figure 3.1, D**) and SUMO-2/3 (**Figure 3.1, E**) from the insoluble fraction to a larger, insoluble fibrillar aggregated species (**Figure 3.1, G**). MG132 treatment also resulted in increased fragmentation and accumulation of FL-HTT (**Fig 3.1, B**). These results suggest that hnRNPA2B1, which is normally most abundant in the nucleus, may be mislocalized to the cytoplasm under conditions of proteostatic stress.

hnRNPA2B1 is translocated to cytoplasmic puncta as a result of inhibited SUMOylation, and CSF EVs from HD patients contain altered hnRNPA2B1 protein levels

While hnRNPA2B1 is largely a nuclear protein, it carries out specific functions that require cytoplasmic localization (Han et al., 2010), such as the trafficking of mRNAs to dendrites (Shan et al., 2003). In addition to this, it has been reported that the SUMOylation of hnRNPA2B1 regulates the packaging of specific miRNAs into exosomes for secretion (Villarroya-Beltri et al., 2013). This has been supported by the detection of hnRNPA2B1-miRNA complexes within EVs secreted by CPECs, which are also detected in human CSF (Tietje et al., 2016).

To begin to explore the impact of SUMO modification on hnRNPA2B1 localization within CPECs, we treated Z310 rat CPECs with the SUMOylation inhibitor anacardic acid (Fukuda et al., 2009). Z310 cells were treated with either DMSO or anacardic acid as previously described (Fukuda et al., 2009), and co-stained with SUMO-1 and hnRNPA2B1. Cells treated with anacardic acid showed mislocalization of hnRNPA2B1 into the cytoplasm compared to DMSO treated cells (**Figure 3.2, A**). The percentage of hnRNPA2B1 puncta in the cytoplasm of anacardic acid treated cells was 60%, compared to 8% in DMSO treated cells ($p=3.73x10^{-7}$, Student's t-test) (**Figure 3.2, B**). These results suggest the inhibition of SUMOylation has an effect on hnRNPA2B1 localization within the cell.

Based on findings that SUMOylation is dysregulated in HD (Steffan et al., 2004; O'Rourke et al., 2013), it has been hypothesized that SUMO may be sequestered by mHTT aggregated species that are not cleared appropriately, resulting in depleted functional SUMO stores. If this is true, and if the hnRNPA2B1 puncta that result from inhibition of SUMOylation are non-functional due to hindered solubility, then miRNA packaging into EVs by SUMOylated hnRNPA2B1 will be hindered in mHTT-expressing cells. As a first step to test this hypothesis, we isolated EVs from the CSF of postmortem HD and control patients to analyze hnRNPA2B1 protein levels by western blotting. The EV fraction was run side-by-side with the CSF background fraction (supernatant from EV fraction precipitation), and a Z310 whole cell lysate control (**Figure 3.3, A and B**). The exosome markers Alix and TSG101 were only detected in the EV fraction, and the mitochondrial protein cytochrome C was only detected in the Z310 whole cell lysate control. hnRNPA2B1 was detected at around 54 kDa in the CSF EV samples, compared to 37 kDa in the whole cell lysate samples. This is consistent with the expected 12 kDa increase resulting from SUMOylation by SUMO-1

(Bayer et al., 1998), and with previous findings by Villarroya-Beltri et al. in which SUMOylated hnRNPA2B1-miRNA complexes were detected in exosomes. Compared to control CSF EV samples, HD CSF EVs appear to contain lower levels of hnRNPA2B1; however, the identification of a reliable EV loading control will be needed in order to make definite conclusions.

BMP4-instructed derivation of CPECs from iPSCs

To investigate CPEC CSF EV secretion in an HD patient context, we initiated the generation of CPECs derived from patient iPSCs. CPECs arise from pre-neurogenic epithelial cells and require bone morphogenic protein (BMP) signaling for differentiation. Based on previous findings by Watanabe et al. which showed that BMP4 is sufficient to induce CPEC fate from neural progenitors of neuroepithelial lineage derived from mouse and human embryonic stem cells (ESCs) (Watanabe et al., 2012), and in collaboration with the Monuki laboratory that generated this protocol, we tested the ability of BMP4 to instruct CPEC derivation from iPSCs.

The 35-day CPEC derivation protocol begun with the seeding of iPSCs in small clumps, which expanded over 2 days in iPSC maintenance media (**Figure 3.4, A**). On day 5, neural induction was instructed and BMP4 was added to the media starting one day after neural induction, when cells are at a pre-neurogenic neuroepithelial cell stage. On the last day of neural induction, the media was completely switched to CPEC differentiating media until day 35. The derivation was carried out side-by-side with H1 ESCs due to the derivation protocol being initially developed with this specific cell type (unpublished results). Additionally, while the original derivation protocol was developed with the E8 iPSC/ESC

maintenance media, we also tested mTeSR iPSC/ESC maintenance media due to the fact that our iPSC lines have been historically maintained and expanded with mTeSR. Brightfield microscopy images suggest that, over time, CPECs form multi-layered folds that persist until the last day of the derivation (**Figure 3.4, B**). These folds were more prominent in the ESCs, and iPSCs cultured with the mTeSR maintenance media. Of note, the iPSCs cultured with mTeSR media also formed prominent, vesicle-like, fluid-filled structures that persisted until the last day of the derivation.

We characterized derived CPECs by immunofluorescence and qPCR. CPEC marker immunoreactivity, namely the co-expression of key CPEC markers aquaporin 1 (AQP1), anion exchange protein 2 (AE2), claudin 1 (CLDN1), transthyretin (TTR), and ADP-ribosylation factor-like protein 13B (ARL13B), was assessed. Out of the two iPSC conditions tested, iPSC-CPECs grown in mTeSR had a higher amount of CPEC marker co-localization, encompassing larger areas (**Figure 3.5, A and B**). Compared to iPSCs, ESC-CPECs had larger areas of TTR-positive cells, and the highest amount of CPEC marker co-localization (**Figure 3.5, C**). Because our goal was to investigate CPECs in an HD patient context, we decided to move forward with the iPSC mTeSR condition for CPEC derivation. Further analysis showed that these iPSC-CPECs form structures that are characteristic of CPECs *in vivo,* such as apical-basolateral polarization (**Figure 3.6, A and D**), CLDN1 tight junctions (**Figure 3.6, B**), and cilia (**Figure 3.6, C**). Furthermore, CPEC gene expression analysis by qPCR shows an increase of CPEC marker expression along the following CPEC derivation stages: neural induction, CPEC day 15, and CPEC day 35 (**Figure 3.6, E**). These data provide evidence for the specification of CPEC identity in iPSC-derived cells using the BMP4-instructed derivation approach.

Potential dysregulation of tight junction and cilia formation in HD iPSC-CPECs

Tight junctions between CPECs form the blood-CSF barrier (Liddelow, 2015) andhave been shown to be disrupted in postmortem tissue from ALS patients (Saul et al., 2020), and resemble the blood-brain-barrier tight junctions that are disrupted in HD iPSC-derived brain microvascular endothelial cells (Lim et al., 2017). As a first step to examine potential tight junction formation deficits in HD, we compared CLDN1 tight junction immunoreactivity between 33Q control and 109Q HD iPSC-derived CPECs (**Figure 3.7, A**). Our results show the 109Q HD line formed less defined, punctate, tight junction structures compared to the 33Q control iPSC-CPECs.

An additional CPEC structure investigated were cilia, which are ubiquitously expressed in most cells, and function as a sensory platform to help regulate CSF production by mature CPECs (Narita et al., 2015). While this CPEC property has not been investigated in the context of HD, previous studies have shown that pericentriolar material 1 protein (PCM1) accumulates and alters ciliogenesis in HD mouse model ependymal cells that line the lateral ventricle (Keryer et al., 2011), which share a resemblance with CPECs. To investigate a potential disruption in ciliogenesis, we stained cilia with an antibody against ARL13B in both 33Q control and 109Q HD iPSC-CPECs. The 109Q HD line formed visibly larger cilia compared to the 33Q control iPSC-CPECs. Together, these results warrant further investigation of tight junction and cilia properties in HD iPSCs, which, if disrupted, may have important implications for CSF production and maintenance.

Neural induction with dual SMAD inhibition does not result in efficient iPSC-CPEC derivation

While BMP4-instructed derivation of CPECs allowed for the differentiation of iPSCs into cells that express CPEC markers and form CPEC structures, the derivation efficiency did not reach levels that would allow for accurate comparisons between multiple patient lines. Therefore, we attempted to increase CPEC derivation efficiency by employing a SMAD inhibition (STEMCELL technologies kit), neural induction approach, which has been shown to increase neural induction efficiency in iPS and ES cells (Chambers et al., 2009).

The basic neural induction approach gave rise to iPSC-CPEC cultures that formed large vesicle-like structures, and smaller multilayered structures that coincide in size and location with TTR-positive cells (**Figure 3.8, A and B**). In contrast, the SMAD inhibition neural induction approach gave rise to mono-layered TTR-positive cultures that span the entire surface (**Figure 3.8, B**). CPEC marker co-expression was not detected in these cultures (**Figure 3.9, A-C**). In particular, AQ1-positive cells did not correspond to cells with high TTR immunoreactivity (**Figure 3.9, A**), and neither did CLDN1-positive cells (**Figure 3.9, C**), suggesting these cells do not resemble true iPSC-CPECs, and a high degree of culture heterogeneity. Based on these results, the investigation of other approaches will be necessary to improve CPEC derivation from iPSCs.

DISCUSSION

CPECs produce most of the CSF in the central nervous system (Damkier et al., 2013), and the CSF EV contribution by the ChP appears significant, based on evidence that proteins exclusively expressed in CPECs are enriched in CSF EVs (Balusu et al., 2016). Based on this,

it follows that CPECs are an ideal model to investigate CSF EV secretion. In this chapter, we showed that hnRNPA2B1 protein localization is affected by proteostatic stress and SUMOylation. Furthermore, we provide preliminary evidence suggesting a reduction of hnRNPA2B1 levels in CSF EV postmortem samples from HD patients. We also show, through preliminary proof-of-concept studies, that CPECs can be derived from HD patient iPSCs, although future optimization of the protocol will be necessary to improve derivation efficiency and decrease line-to-line variation.

The inhibition of SUMOylation with anacardic acid resulted in the appearance of cytoplasmic hnRNPA2B1 puncta in rat Z310 CPECs, suggesting that SUMO modification affects hnRNPA2B1's cellular localization. In fact, SUMOylation is known to stabilize proteins and affect their cellular localization (Wilkinson et al., 2010). It was recently discovered that SUMOylation also plays a role in the disassembly of SGs (Marmor-Kollet et al., 2020), structures that hnRNPA2B1 and other hnRNP members are recruited to in the presence of ALS-associated mutations (Martinez et al., 2016). Taken together, these data support the hypothesis that SUMOylation of hnRNPA2B1 inhibits hnRNPA2B1-hnRNPA2B1 interactions, similar to its function in SG disassembly. When SUMOylation of hnRNPA2B1 is inhibited, increased hnRNPA2B1-hnRNPA2B1 interactions in the cytoplasm may result in the sequestration of free-floating hnRNPA2B1 into granular structures. If this is the case, and SUMOylation of hnRNPA2B1 is altered in HD, this could in turn affect miRNA packaging into CSF exosomes.

The CPEC derivation studies support previous findings that BMP4 is sufficient to instruct CPEC fate (Watanabe et al., 2012). Preliminary comparisons between 33Q control and

109Q HD iPSC-derived CPECs suggest tight junctions and cilia structures may be affected in HD. Relevant to these findings, previous studies suggest tight junction formation is disrupted in iPSC-derived HD brain microvascular endothelial cells (Lim et al., 2017), and that ciliogenesis is disrupted in response to mHTT expression (Keryer et al., 2011). If these structures are truly disrupted in HD CPECs, CSF contents may be affected as a result of blood-CSF barrier leakage and altered CSF production orchestrated by primary cilia. In addition to optimizing the CPEC derivation protocol to allow for large scale differentiations to compare among multiple patient-derived cell lines, future studies might benefit from investigating the CSF proteome and metabolome, which has been shown to be affected in ALS and Alzheimer's disease due to disruption of the blood-CSF barrier (Saul et al., 2020; Serot et al., 2003). Additionally, postmortem tissue studies can be used to validate CPEC tight junction disruption and altered cilia formation in the brains of HD patients.

In conclusion, we demonstrate feasibility for the generation of CPECs from patient-derived iPSCs to investigate HD-dependent phenotypes. Future optimization approaches will be needed to increase derivation efficiency and culture homogeneity. Our findings suggest that inhibiting the SMAD pathway does not result in enhanced CPEC derivation. Other avenues should be investigated, such as increasing culture comparability across multiple lines at the time of BMP4 or CPEC media introduction, introducing additional signaling molecules to further instruct CPEC fate, or testing alternative extracellular matrix components. These improvements will allow for mechanistic studies to address the influence that intercellular CSF EV communication has on health and disease. Specifically, this *in vitro* model could be employed to help answer specific questions that arise from the findings presented in Chapter 2 of this dissertation.

EXPERIMENTAL PROCEDURES

Z310 cell transfection and MG132 treatment

Z310 rat CPECs were cultured as previously described (Zheng et al., 2002). Briefly, cells were grown in Dulbecco's Modified Eagle's Medium (cat. #D6429, Millipore Sigma) supplemented with 10% FBS (cat. #F6178, Millipore Sigma), and 10 ng/mL EGF (cat. #236-EG, R&D Systems) in a humidified incubator at 37°C. Cells were passaged (1:7) 3 times a week and plated onto 6-well plates for transfections with Lipofectamine 2000 (cat. #11668027, Thermo Fisher; construct 97QP- VL*-eGFP cDNA at 0.5 ug, 1 ug, and 2 ug) and MG132 treatment (cat. # M8699, Millipore Sigma, 2.5 uM for 18 hours).

Soluble/insoluble fractionation

Soluble/insoluble fractionation protocol was done as previously described (Ochaba et al., 2018).

Filter retardation assay

30 ug of detergent-insoluble protein in 200 uL of 2% SDS was boiled for 5 min and run through a dot blot apparatus under a vacuum onto a cellulose acetate membrane. The membrane was then washed 3 times with 1% SDS and blocked in 5% milk and processed for western blot analysis. Filter retardation protocol was previously described (Sontag et al., 2012; Wanker et al. 1999).

Western blot analysis

4-12% Bis-Tris and 3-8% Tris-Acetate gels (Invitrogen) were used for SDS-PAGE, proteins were transferred to nitrocellulose or polyvinylidene difluoride membranes, and non-specific proteins were blocked with either StartingBlock (Thermo Scientific), or 5% milk for EV proteins. Chemiluminescence was used to detect proteins. Primary antibodies were used as follows: hnRNPA2B1 (1:500, cat. #sc-374053, Santa Cruz Biotechnologies); Alix (1:1000, cat. #ab186429, abcam); TSG101 (1:1000, cat. #ab83, abcam); Cytochrome C

(1:500, cat. #ab13575, abcam); alpha-tubulin (1:1000, cat. # T5168, Millipore Sigma), D7F7 (1:500, cat. # 5656, Cell Signaling), GFP (1:1000, cat. #632592, Clontech), SUMO1 (1:500, cat. #BML-PW9460-0025, Enzo Life Sciences), SUMO2/3 (1:500, cat. #51-9100, Zymed). Primary antibodies were conjugated to an HRP secondary (cat. # G-21040 and G-21234, Thermo Fisher), and detected using Pico (cat. # 34579, Thermo Fisher) or Dura (cat. # 34076, Thermo Fisher) on Kodak film.

Anacardic acid treatment of Z310 rat CPECs

Z310 cells were grown on 24-well plates with Poly-D-Lysine/Laminin coated coverslips (Corning BioCoat 12mm glass coverslips, cat. # 08-774-385, Fisher Scientific) and maintained in Dulbecco's Modified Eagle's Medium (cat. #D6429, Millipore Sigma) supplemented with 10% FBS (cat. #F6178, Millipore Sigma) and 10 ng/mL EGF (cat. #236-EG, R&D Systems). Upon reaching 60-70% confluency, cells were treated with DMSO or the small molecule SUMOylation inhibitor anacardic acid (125 uM, cat. #A7236-5MG, Millipore Sigma) as previously described in Fukada et al., 2009.

ExoQuick EV isolation and protein extraction

ExoQuick (cat. #EXOTC10A-1, System Biosciences) was utilized for EV protein extraction from post-mortem CSF samples. CSF was precleared by centrifugation at 3000xg for 15 min at 40C, and incubated with ExoQuick precipitation solution (650 uL CSF:164 uL ExoQuick) overnight at 40C. The ExoQuick/CSF mixture was then centrifuged at 1500 xg for 30 min at 40C. The supernatant was recovered as 'background' and the pellet as 'EV fraction.'

Whole cell and EV lysis

Cells and EV pellets were lysed using RIPA lysis buffer (1M Tris (pH7.4), 5M NaCl, 0.5M EDTA (pH8.0), 20% NP40, 20% SDS, and protease inhibitors). Cell pellets were sonicated 2 times (10 pulses), and EV pellets were sonicated 3 times (5 min each) with 1 min vortexing in between. Protein concentration was quantified using the Lowry protein assay.

CPEC differentiation from human iPSCs and ESCs

iPSCs or ESCs were plated on Matrigel (1mg/6mL Matrigel Growth Factor Reduced, cat. #354230, Corning) coated 4-well chamber slides (cat. #PEZGS0416, Millipore Sigma) at about 20-30 clumps of 50-150 um in diameter per chamber. For single cell seeding protocol, cells were seeded at 500,000 cells per chamber. Cells were seeded with mTeSR 1 media (cat. #85850, STEMCELL Technologies) or E8 media (cat. #05940) supplemented with 10 uM ROCK inhibitor (cat. #Y-025, R&D Systems), and maintained in mTeSR/E8 without ROCK inhibitor for 2 days. On the first day of neural induction (day 0), mTeSR/E8 media was removed and cells were fed either PSC Neural Induction Media (cat. #A1647801, Thermo Fisher) or STEMdiff SMADi Neural Induction Media (cat. # 08581, STEMCELL Technologies). Cells were full-fed daily except on days 2 and 4, and supplementation with BMP4 (cat. #314-BP-010, R&D Systems) was started on day 1. Neural induction was halted on day 5, and media was completely switched to CPEC differentiating media: Gibco Advanced DMEM/F12 (cat. # 12-634-010, Fisher Scientific), N2 (100X, cat. #17502048, Thermo Fisher), NEAA (100X, cat. #11140050, Thermo Fisher), Heparin 0.2% (cat. #07980, STEMCELL technologies), BMP4 (cat. #314-BP-010, R&D Systems). Cells were half-fed every day until day 35, with BMP4 removed on day 16.

RNA extraction and qPCR of CPEC markers

iPSC-CPEC cultures were harvested and flash-frozen at three timepoints (final day of neural induction, CPEC day 15, and CPEC day 35). Pellets were homogenized in TRIzol (cat. #A33251, Thermo Fisher) and RNA was collected following the manufacturer's procedures, and purified using RNEasy Mini kit (cat. # 74104, QIAGEN). Residual RNA was removed by DNase treatment following the RNEasy protocol following manufacturer's suggestion. Following RNA isolation, the SuperScript 3 first-strand synthesis system (cat. #11904018, Thermo Fisher) was used to perform reverse transcription following the manufacturer's protocol. Oligo (dT) and random hexamer primers were used in a 1:1 ratio with a total of 1ug RNA per sample. Synthesized cDNA was diluted 1:10 in DEPC treated water and stored at -20°C until further use. The following human primers were used to determine CPEC identity of iPSC-derived cells across three multiple derivation timepoints: *CLDN1* (F: CCTCCTGGGAGTGATAGCAAT, R: GGCAACTAAAATAGCCAGACCT), *KL* (F: CCCTAAGCTCTCACTGGATCA, R: GGCAAACCAACCTAGTACAAAGT), *AQP1* (F: AGCCCTGGCTGTACTCATCT, R: ACCCTGGAGTTGATGTCGTC), *TTR* (F: ATCCAAGTGTCCTCTGATGGT, R: GCCAAGTGCCTTCCAGTAAGA).

Immunofluorescence staining

Cells were fixed with 4% PFA for 10 minutes and washed 3x5 minutes in 1X PBS, blocked with 5% normal donkey serum (cat. #017-000-121, Jackson Immuno Research Laboratories) in 0.3% Triton X-100 for 20 minutes, and incubated in primary antibody overnight at 4^0C in 1% Normal Donkey Serum (cat. #017-000-121, Jackson Immuno Research Laboratories) in 0.3% Triton X-100. The following primary antibodies were used: TTR (1:3000, cat. #ab9015, abcam), CLDN1 (1:500, cat. #71-7800, Thermo Fisher), AQP1

(1:1000, cat. #AB2219, Millipore), AE2 (1:250, cat. #sc-376632, Santa Cruz Biotechnologies), ARL13B (1:1000, cat. #17711-1-AP, Proteintech), PCM1 (1:500, cat. #sc-398365, Santa Cruz Biotechnology), CAV1 (1:500, cat. #ab17052, abcam), ZO1 (1:500, cat. #339100, Thermo Fisher), SUMO1 (1:500, cat. #BML-PW9460-0025, Enzo Life Sciences), hnRNPA2B1 (1:250, cat. #sc-374053, Santa Cruz Biotechnologies). The next day, cells were washed 3x5 minutes in 1X PBS and incubated in secondary antibodies diluted in 1% Normal Donkey Serum in 0.3% Triton X-100. The following secondary antibodies were used: Alexa Fluor donkey anti-rabbit 488 (1:400, cat. #A-21206, Thermo Fisher), Alexa Fluor donkey anti-sheep 555 (1:400, cat. #A-21436, Thermo Fisher), Alexa Fluor donkey anti-mouse 555 (1:400, cat. #A-31571, Thermo Fisher). Cells were washed 3x5 minutes in 1X PBS, incubated in DAPI for 10 minutes at room temperature, washed 3x5 minutes in 1X PBS, and coverslips were mounted using Fluoromount-G (cat. #00-4958-02).

Cell culture imaging

Brightfield images were taken with an EVOS Digital Inverted Brightfield and Phase Contrast Microscope (Invitrogen™ AME3300). Confocal images were acquired with an Olympus FLUOVIEW FV 3000 microscope.

CHAPTER 3

FIGURES

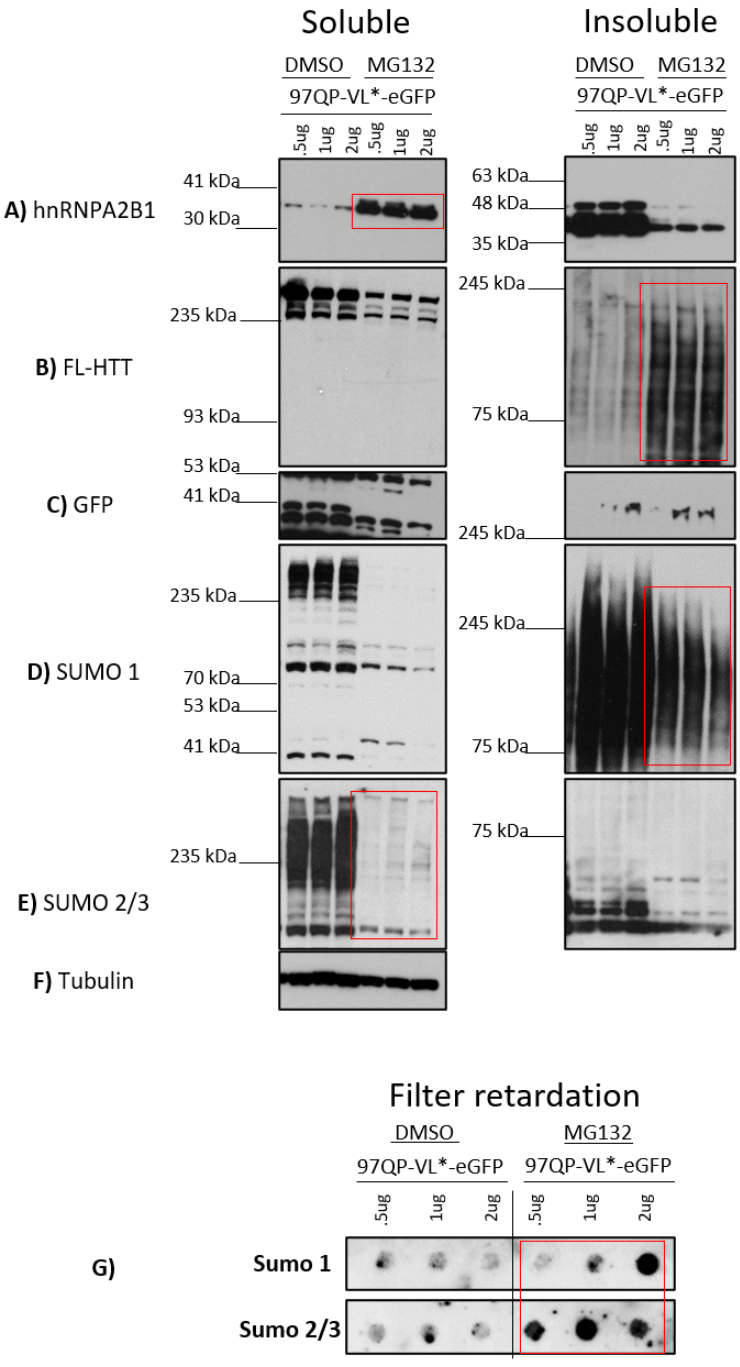

Figure 3.1. MG132-dependent proteostatic stress results in mislocalization of hnRNPA2B1 in rat CPECs expressing mHTT. Z310 rat CPECs overexpressing mHTT(Exon 1)-97Q were treated with the proteasome inhibitor MG132, which resulted in the mislocalization of hnRNPA2B1 and SUMO**.** Western blot of detergent soluble and insoluble protein fractions shows that MG132 treatment results in **A)** hnRNPA2B1 shift to soluble fraction, **B)** increased fragmentation and accumulation of full length HTT, and **D)** decrease of SUMO 1 and **E)** SUMO 2/3. **G)** Filter retardation assay of the insoluble fraction shows mislocalization of SUMO 1 and SUMO 2/3 in insoluble fibrillar aggregated species. **C)** and **F)** are controls for transfection and loading, respectively. FL-HTT= full length HTT.

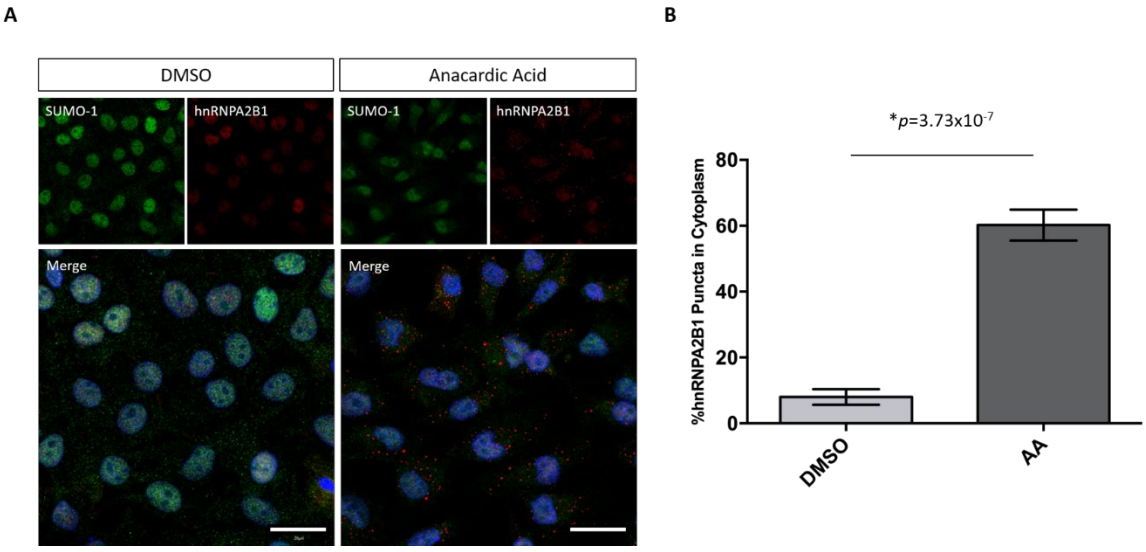

Figure 3.2. Inhibiting protein SUMOylation in Z310 rat CPECs results in mislocalization of hnRNPA2B1 into cytoplasmic puncta. A) Immunofluorescence staining of hnRNPA2B1 (In red) and SUMO-1 (in green) in Z310 rat CPECs treated with the small molecule SUMOylation inhibitor anacardic acid (AA). **B)** Cells treated with AA (as described in Fukuda et al., 2009), show mislocalization of hnRNPA2B1 into the cytoplasm compared to DMSO treated cells. Percentage of hnRNPA2B1 puncta in cytoplasm: DMSO= 8%; AA=60%; $p=3.73x10^{-7}$, N=7. Scale bar = 20 um.

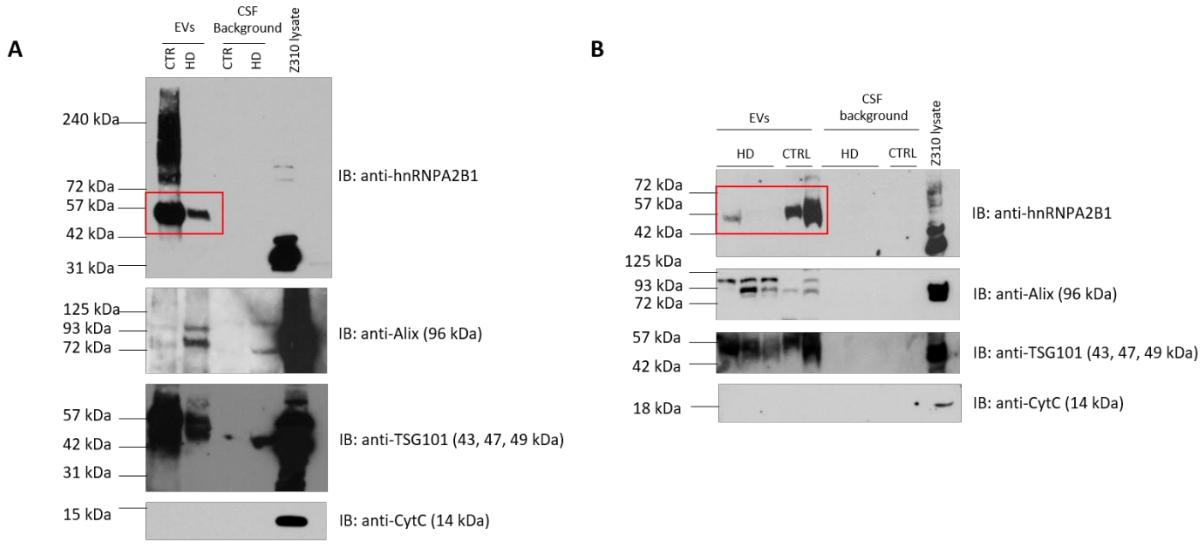

Figure 3.3. Potential reduction of hnRNPA2B1 protein levels in HD patient-derived postmortem CSF EVs. EVs were isolated from postmortem HD and control patient CSF samples, EVs were lysed, and protein contents were analyzed by western blot. The 'EV' fraction contains proteins packaged in EVs, while the 'CSF background' fraction contains proteins free-floating in CSF. For western blot **A)** N= 1 HD, 1 control, and western blot **B)** N= 3 HD, and 2 control, hnRNPA2B1 levels (boxed in red) are decreased in the HD samples compared to controls. The established exosome markers Alix and TSG101 were detected in the EV fraction only, suggesting this fraction is enriched with exosomes and that there was no significant leakage into the CSF background fraction for any of the samples. Cytochrome C is a mitochondrial marker and should only be detected in whole cell samples. Z310 lysate= whole cell sample control.

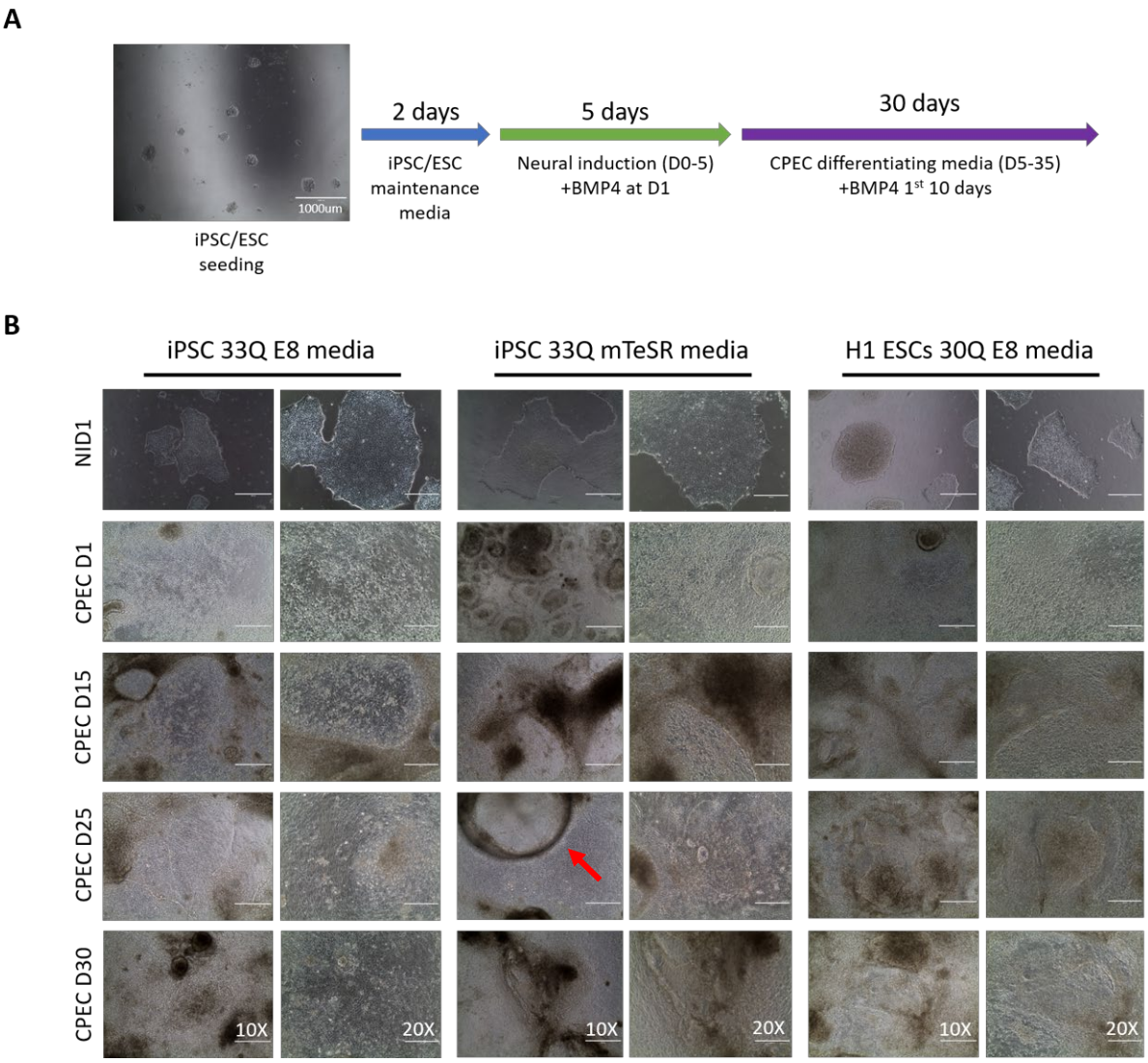

Figure 3.4. Human-derived iPSCs and H1 ESCs throughout BMP4-induced CPEC derivation. A) The 35-day CPEC derivation protocol starts with seeding of either iPSCs or ESCs in small clumps, which are allowed to expand in iPSC/ESC maintenance media for 2 days. On day 5, neural induction is started with BMP4 addition starting at day 1. On the last day of neural induction, CPEC D5, the neural induction media is switched to CPEC differentiating media until day 35. **B)** Brightfield microscopy images of iPSCs under two maintenance media conditions (E8 vs mTeSR media), and H1 ESCs (E8 media), taken throughout the BMP4-induced CPEC derivation protocol. During neural induction day 1 (NID1), cell colonies remain isolated. By the start of CPEC derivation on CPEC D1, cell colonies have merged and multi-layered cell areas with folds begin to appear. These continue to grow into thicker layers with more folds throughout the derivation until the final day, CPEC D30. iPSCs grown with mTeSR maintained media formed prominent vesicle-like, fluid-filled, structures by CPEC D25 (red arrow). Images were taken at 10X and 20X magnification.

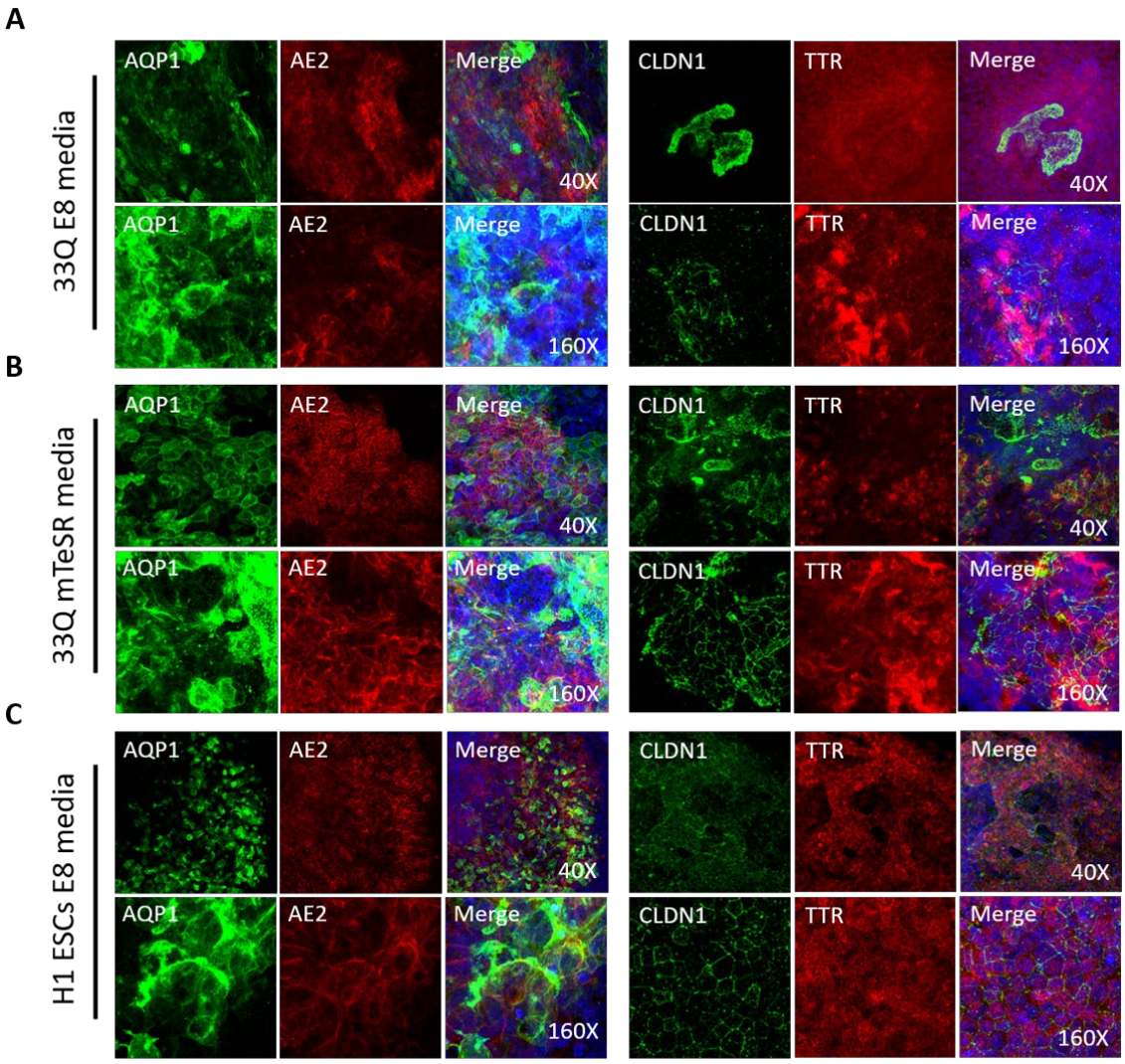

Figure 3.5. CPEC marker immunoreactivity in iPSC- and H1 ESC-derived CPECs at final day of derivation. Derived CPECs were fixed at final day of derivation and CPEC markers were examined by immunofluorescence. CPEC markers examined included AQP1 (in green), AE2 (in red), CLDN1 (in green), and TTR (in red). Control iPSC-CPECs grown in **A)** E8 iPSC maintenance media did not form as many CLDN1 tight junctions co-localized with TTR as control iPSCs grown in **B)** mTeSR media. Overall, iPSCs grown in mTeSR media resulted in a higher amount of CPEC marker co-localization, encompassing larger areas, than those grown with E8 media. **C)** ESCs had larger areas of TTR-positive cells, and highest amount of CPEC marker co-localization, than iPSCs from any condition. Images were taken at 40X and 160X magnification.

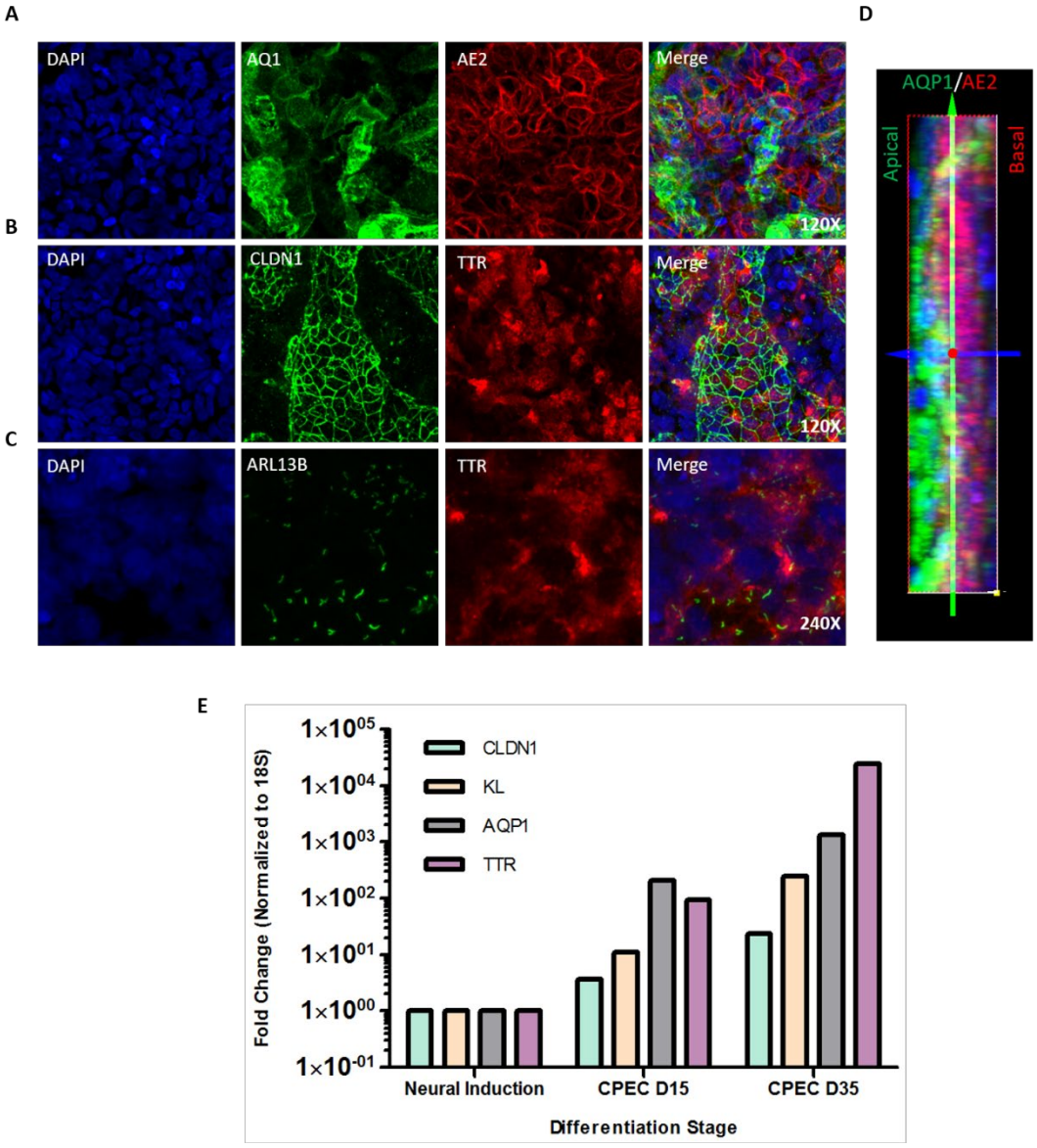

Figure 3.6. Control 33Q iPSC-derived CPECs express characteristic CPEC markers. Immunofluorescence of CPEC markers at the final day of derivation suggests that iPSC-CPECs form cellular structures that are characteristic of CPECs. Cells express **A)** the aquaporin channel AQ1 (in green) and the ion transporter AE2 (in red), **B)** the tight junction protein CLDN1 (in green) and transport protein TTR (in red), and **C)** cilia protein ARL13B (in green). **D)** Of note, iPSC-CPECs appear to be following the expected apical-basolateral polarization based on localization of AQ1 and AE2 across a cell layer. Images were taken at 120X and 240X magnification. **E)** Expression level of CPEC gene markers at neural induction, CPEC day 15, and CPEC day 35. The fold changes were plotted on a logarithmic scale due to the remarkably large fold change increase of CPEC markers on the final day of differentiation compared to neural induction. N=1 per differentiation stage.

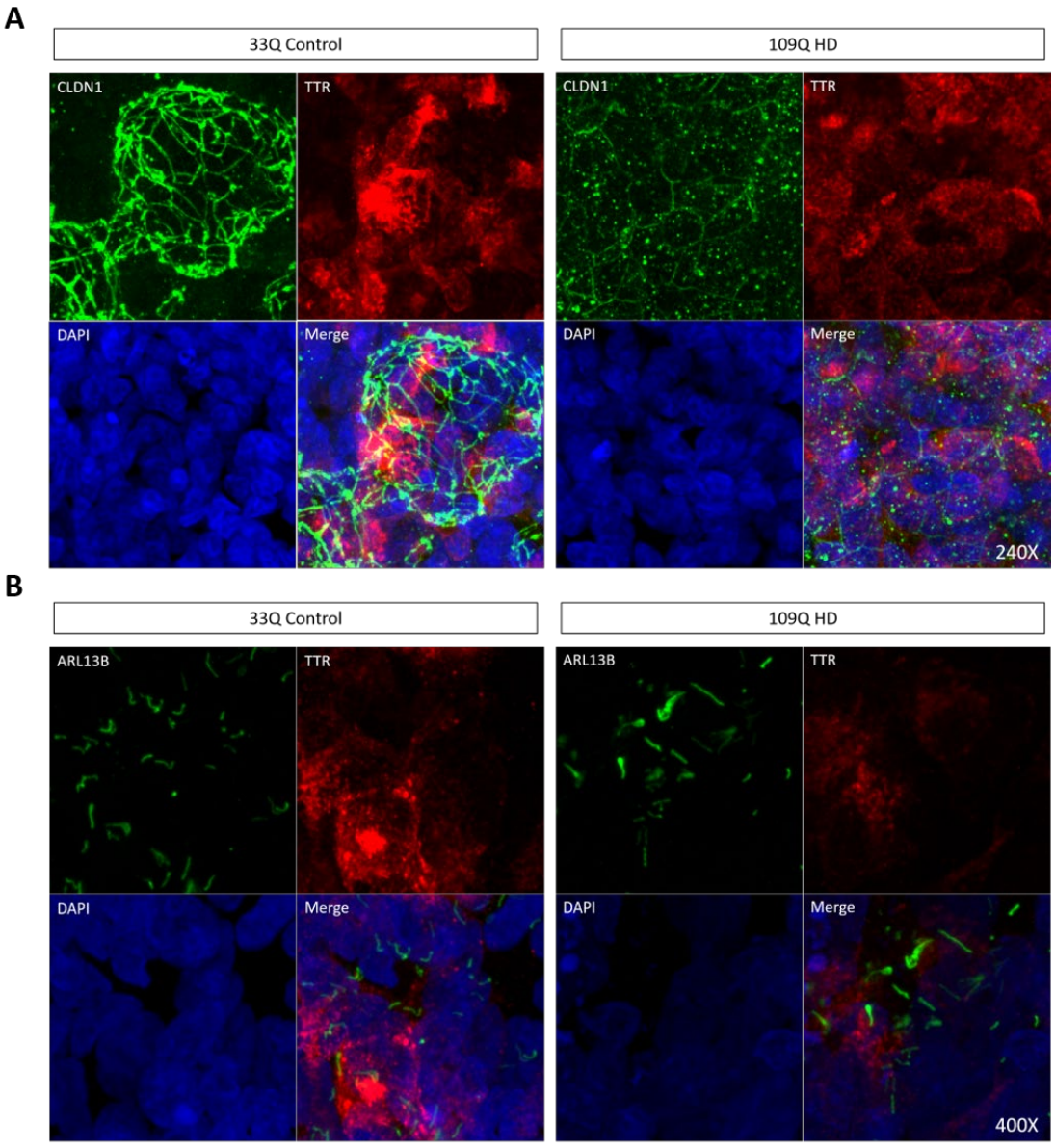

Figure 3.7. Potential tight junction and cilia formation deficits in HD iPSC-derived CPECs. iPSC-derived CPECs were fixed on the final derivation day (CPEC D35) and immunofluorescence was used to examine tight junctions and cilia. **A)** Tight junctions were stained with the tight junction marker CLDN1 (in green), and co-stained with TTR (in red). The 109Q HD line formed less defined, punctate, tight junction structures compared to the 33Q control. **B)** Cilia were stained with the cilia marker ARL13B (in green), and co-stained with TTR (in red). The 109Q HD line formed visibly larger cilia compared to the 33Q control. Tight junction images were taken at 240X magnification, and cilia images at 400X magnification.

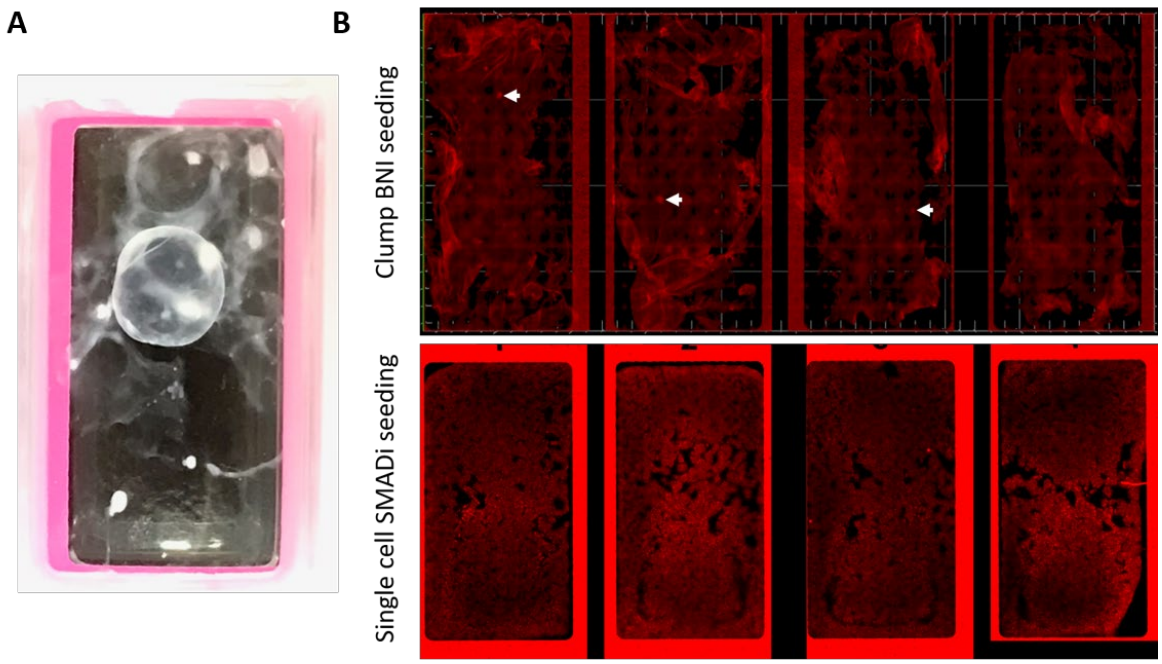

Figure 3.8. General TTR expression in 33Q control iPSC-derived CPECs using the clump-seeding (basic neural induction) approach versus the single-cell seeding (SMADi neural induction) approach. Immunofluorescence staining for CPEC marker TTR was used to qualitatively assess the number of TTR-positive cells at the final day of differentiation. **A)** iPSC-CPEC slide chamber at the final day of differentiation using the clump seeding approach depicts large vesicle-like, fluid-filled, structures and small multi-layered structures that coincide in size and location with TTR-positive cells. **B)** Scanner images of TTR immunofluorescence suggest that the clump-seeding approach gives rise to very few TTR-positive cells that localize to discrete areas, and the single-cell SMADi approach gives rise to more TTR-positive cells that are highly dispersed across the chamber. BNI = basic neural induction.

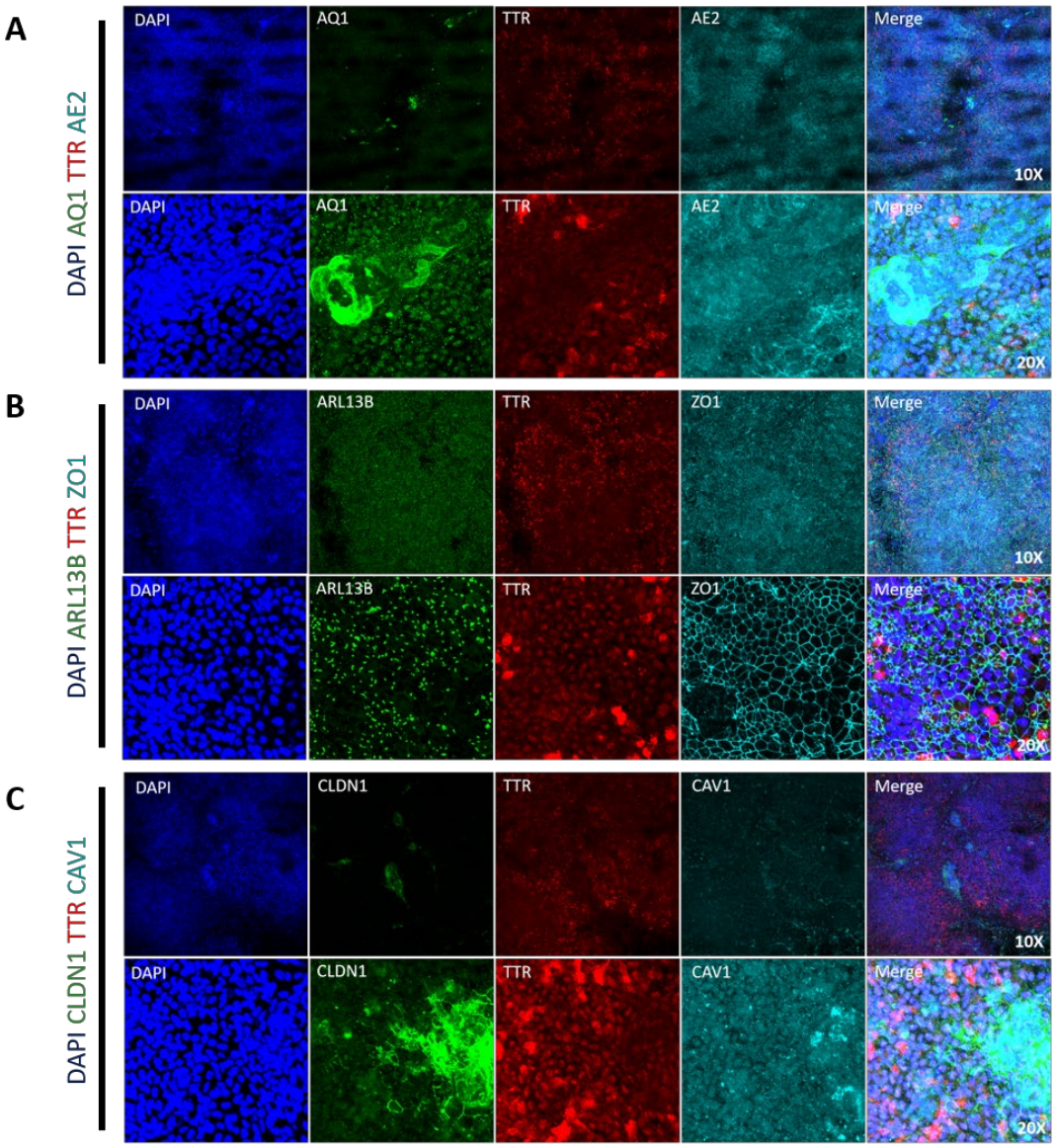

Figure 3.9. Discrepancy among CPEC markers in iPSC-derived CPEC cultures using the single-cell seeding, SMADi neural induction approach. Immunofluorescence staining for CPEC markers do not show colocalization of key markers that are used to suggest CPEC identity, suggesting cultures are not reaching the expected level of maturity. **A)** Cells that are positive for AQ1 are not TTR positive, and AE2 immunoreactivity follows a diffuse pattern that is not indicative of CPECs. **B)** ARL13B and ZO1 are readily detected, however they do not colocalize to TTR-positive cells. **C)** CLDN1 and CAV1 are detected, however they do not localize to TTR-positive cells. Images were taken at 10X and 20X magnification.

DISSERTATION CONCLUDING REMARKS

Data provided in this dissertation show, for the first time, evidence of SG neuropathology in HD mouse and human patient brain. SG formation results from the activation of cellular stress pathways and function to restore cellular homeostasis by temporarily sequestering stalled mRNA transcripts. However, in the case of neurodegeneration and aging, SGs persist and can function as a focal point for the aggregation of disease-associated proteins (Wolozin et al., 2019). Similarly, the cellular stress resulting from chronic mHTT expression likely results in the accumulation of SGs. My findings suggest that SG persistence, much like it has been identified in ALS and frontotemporal dementia, is also a neuropathologic feature of HD.

The first chapter of this dissertation provided evidence for the homeostatic flux of mHTT over a longitudinal period of disease progression. Multiple tissue lysis methods and biochemical assays were investigated in conjunction with behavioral readouts to establish a baseline for the detection of accumulated mHTT exon 1 protein species. In turn, this better understanding of mHTT accumulation dynamics over disease progression in R6/2 mice aided the experimental design of the SG pathology study introduced in Chapter 2.

In the second chapter of this dissertation, we show that G3BP1-positive SGs are detected in in vivo HD models and patient brain tissue, and that G3BP1-positve SG accumulation is a neuropathologic characteristic of HD. We also show that miRNAs that are different packaged in the CSF EVs of HD patients potentially target G3BP1 and other SG components that are differentially expressed in the prefrontal cortex of HD patients. In addition to this, we identified specific miRNAs that target the accumulation of G3BP1-positive SGs in vitro,

an approach that may have therapeutic implications for multiple neurodegenerative diseases in which SG accumulation is a feature.

Because neurodegeneration results in the chronic activation of cellular stress pathways, SG formation in mouse model and human brains is likely to have different properties than those which orchestrate SG formation *in vitro* under acute stress conditions. Despite these differences, the majority of the work that currently defines SG properties has been done *in vitro* using acute stress conditions. The few studies that have investigated chronic SG formation in vitro, which is defined as a stress condition lasting six hours or longer, suggest that some of the components in chronic SGs differ from those of acute stress SGs (Reineke et al., 2019). For example, while SGs resulting from chronic nutrient starvation contain translation initiation factors, RBPs, and mRNAs, they lack 18s rRNA and the 40S-associated proteins RPS6 and RACK1. In addition, these chronic SGs do not actively exchange their contents with the cytoplasm as in the case of acutely formed SGs. Under these conditions, SG depletion results in improved cell survival, a finding that contradicts the pro-survival function of SGs that result from acute stress. Furthermore, the presence of SGs in cells that express disease-associated proteins with intrinsically disordered domains, such as in the case of HD, might lead to the exacerbation of protein toxicity via cross-seeding interactions.

In chapter 3, we explored the effect of cellular stress and SUMOylation on hnRNPA2B1 cellular localization, and show that EV hnRNPA2B1 protein levels might be depleted in the CSF of HD patients. These CSF EV studies were limited by the lack of reliable loading controls for EV proteins. Due to the fact that different EV and exosome subpopulations exist, and the contents for these vary across cell types (Willms et al., 2016), there is a lack

of consensus as to which loading markers to use for CSF EVs. The EV markers used in our studies, Alix and TSG-101, which have been adopted by the International Society for Extracellular Vesicles, were detected in the EV fraction only. This suggests the EV isolation procedure was successful and EV contents did not leak during processing. Interestingly, Alix protein levels appear to be higher in the HD samples compared to controls, suggesting a potential HD-dependent phenomenon that could be further investigated. Future studies will explore the use of a total protein stain as a normalization approach. In an attempt to generate an *in vitro* model system in which to investigate the cellular and molecular mechanisms underlying CSF EV miRNA secretion, we explored the possibility to generate CPECs from HD patient and control iPSCs. While our preliminary data suggest the generation of this *in vitro* system is likely feasible, future optimization will be necessary in order to allow for large scale comparisons among multiple patient-derived cell lines.

Altogether, the data presented in this dissertation supports the notion that SG pathology is a shared pathologic feature in various neurodegenerative diseases. The accumulation of G3BP1-positive SGs in the HD brain likely results from chronic stress mediated by mHTT expression. This stress response, in turn, may be regulated by intercellular communication via the distribution of EV miRNAs in the CSF. Given that the CSF is in contact with multiple regions of the central nervous system, and that non-contiguous brain regions are progressively affected in HD patient brain, the cells that produce CSF and maintain its homeostasis are a potential player in HD progression. My preliminary data provide initial evidence for the feasibility of generating CPECs from HD-patient derived iPSCs, and encourage future investigations to interrogate altered CPEC phenotypes in HD. In

conclusion, these data emphasize the importance of defining the impact of CSF-mediated intercellular communication in the progression of HD pathology.

Future directions

A pivotal and outstanding question is whether SGs found in the brains of neurodegenerative disease patients is protective or deleterious. One way to address this question is to carry out preclinical studies on mouse models of neurodegeneration that focus on investigating the effect of SG modulators on disease progression. As described earlier, different approaches have been utilized to modulate SGs *in vitro* and *in vivo* (Kim et al, 2014; Radford et al, 2015; Zhang et al, 2018). In addition to continuing our studies with G3BP1-targetting miRNA mimics *in vitro* with the goal of one day testing them in mice, we are also investigating the use of a SG disaggregase to inhibit SG formation *in vivo.* The TRiC/CCT chaperonin protein has been detected in SG cores and identified as an inhibitor of SG formation (Jain et al., 2016). TRiC/CCT has been and is actively being investigated by our laboratory and collaborators for its potential to inhibit the aggregation of mHTT (Behrends et al., 2006; Kitamura et al., 2006; Tam et al., 2006). Overexpression of a single subunit, CCT1, is sufficient to alter aggregation and reduce HTT-induced toxicity in neuronal cells (Tam et al. 2006). Excitingly, ApiCCT1's apical domain crosses the cell membrane, and reduces oligomeric and insoluble mHTT in an *in vitro* HD model (Sontag et al., 2013).

Based on previous findings that TRiC/CCT inhibits stress granule assembly potentially by inhibiting interactions between polyQ domains on SG components (Jain et al., 2016), we will overexpress the apical domain of the TRiC/CCT subunit CCT1 (ApiCCT1) in the brains

of R6/2 mice. ApiCCT1 will be delivered with an AAV-PHP.eB-ApiCCT1 vector using retro-orbital intravenous administration, which results in transduction of 69% cortical and 55% striatal neurons (Chan et al., 2017; unpublished results). ApiCCT1 is engineered to be secreted from transduced cells by fusion to an IL2 signal sequence leader peptide, which is predicted to allow for increased biodistribution since ApiCCT1 is permeable to the cell membrane (Sontag et al., 2013). R6/2 mice, in which we show the G3BP1-positive SG phenotype can be detected at 12 weeks, will be treated at 5 weeks and sacrificed at 12 weeks for SG detection using immunofluorescence. Brain regions investigated will include the cortex, striatum, and hippocampus. The degree of mHTT aggregates and total CCT immunoreactivity will also be assessed. Based on our previous observations, G3BP1-positive SG accumulation starts sometime between 8 weeks and 12 weeks of age. Because successful transduction efficiency has been characterized at 3 weeks after administration (Chan et al., 2017), treatment at 5 weeks should allow enough time for neurons to be transduced before the onset of G3BP1-positive SG accumulation. Tissue will be processed and analyzed with the methods used in Chapter 2.

In addition to investigating ApiCCT1 as a modulator of SG accumulation, these studies will allow us to determine whether the use of a virus as delivery approach will interfere with SG dynamics in response to activation of the immune response. In the case that viral delivery proves to be problematic for SG modulation studies, EVs can be explored as a delivery mechanism. As in the case of viruses, EVs cross the BBB, are stable in both physiologic and diseases environments, and deliver their contents directly to cells (Li et al., 2019). In addition to this, EVs have been shown to have low toxicity and immunogenicity (Zhu et al., 2017), a characteristic that potentially arises due to their very small surface area.

Because EVs carry and deliver their contents to recipient cells under physiological conditions, they are being actively explored as a natural drug carrier system. Excitingly, at least eleven clinical trials are underway to determine the safety and efficacy of EV-based therapeutics (Elsharkasy et al., 2020). Various EV loading techniques can be employed to package the drug of interest either during EV biogenesis, or at the EV isolation stage. In terms of routes of administration, EVs are commonly administered by a direct injection to a region of interest, or systemically via intranasal or intravenous administration (Lakhal et al., 2011; Yi et al., 2020). Interestingly, a study done with a mouse model of striatal ischemia showed that intranasally delivered EVs selectively accumulate at the lesion site (Betzer at al., 2017), suggesting that this non-invasive route of administration might be of use in the treatment of neurodegenerative diseases. Another study which investigated intranasal EV biodistribution in status epilepticus-induced rats as well as naïve rats found that EVs are incorporated into neurons and microglia in most regions of the forebrain, including the cerebral cortex, hippocampus, and striatum (Kodali et al., 2020).

Many of the SG modulating approaches that have been investigated rely on the inhibition of upstream SG regulators, such as PERK, which are involved in mechanisms that extend beyond the SG induction pathway. Based on this, recent efforts have focused on finding reagents that disrupt the nonspecific weak interactions that hold SGs together. The targeting of G3BP1 by miRNAs and overexpression of ApiCCT1 are hypothesized to bypass inhibition of upstream stress response regulators that often result in toxic off-target effects. Thus, they might serve as additional viable approaches to therapeutically target SGs and warrant further investigation in pre-clinical mouse studies.

Based on our findings and the potential for HTT aggregates to participate in cross-seeding with SG components, we speculate that the SG pathology in HD may result from an accumulation of SGs that perhaps initially served a protective function, but develop into hyper-stable structures due to chronic mutant HTT-mediated stress and compromised autophagy (Buchan et al., 2013, Cortes et al., 2014). Specifically, HTT is essential for normal selective autophagy in mice, and loss of wildtype HTT function may play a role in the dysregulation of SG clearance by granulophagy — a type of selective autophagy (Ochaba et al., 2014). Over time, chronic sequestration of SG components in pathogenic aggregate structures may exacerbate protein toxicity in the cell, and cause cells to lose their ability to form SGs in response to additional stress. The therapeutic modulation of SGs in models of neurodegeneration will elucidate the impact of SGs at various timepoints of disease progression, and allow for the identification of a time window in which SG modulation is protective and optimal.

In this dissertation, we provide evidence that SG accumulation is a feature of HD pathology, and propose that it may be modulated by intercellular communication via CSF EV miRNAs. Because SG accumulation in neurodegenerative disease likely results from chronic cellular stress, and because there is evidence that chronic SGs are deleterious unlike acute stress SGs, we recommend that future studies examine SG accumulation in *in vivo* models of neurodegeneration. We also suggest that future studies investigate the role of other SG components in the HD brain, keeping in mind that these could potentially interact with mHTT aggregated species and exacerbate toxicity. Lastly, we recommend that the targeting of SGs be considered a new avenue for HD therapeutics.

REFERENCES

Adeli, K. "Translational Control Mechanisms in Metabolic Regulation: Critical Role of Rna Binding Proteins, Micrornas, and Cytoplasmic Rna Granules." [In eng]. *Am J Physiol Endocrinol Metab* 301, no. 6 (Dec 2011): E1051-64.

Agarwal, V., G. W. Bell, J. W. Nam, and D. P. Bartel. "Predicting Effective Microrna Target Sites in Mammalian Mrnas." [In eng]. *Elife* 4 (Aug 12 2015).

Agus, F., D. Crespo, R. H. Myers, and A. Labadorf. "The Caudate Nucleus Undergoes Dramatic and Unique Transcriptional Changes in Human Prodromal Huntington's Disease Brain." [In eng]. *BMC Med Genomics* 12, no. 1 (Oct 16 2019): 137.

Aldred, A. R., C. M. Brack, and G. Schreiber. "The Cerebral Expression of Plasma Protein Genes in Different Species." [In eng]. *Comp Biochem Physiol B Biochem Mol Biol* 111, no. 1 (May 1995): 1-15.

An, M. C., N. Zhang, G. Scott, D. Montoro, T. Wittkop, S. Mooney, S. Melov, and L. M. Ellerby. "Genetic Correction of Huntington's Disease Phenotypes in Induced Pluripotent Stem Cells." [In eng]. *Cell Stem Cell* 11, no. 2 (Aug 3 2012): 253-63.

Anderson, P., and N. Kedersha. "Visibly Stressed: The Role of Eif2, Tia-1, and Stress Granules in Protein Translation." [In eng]. *Cell Stress Chaperones* 7, no. 2 (Apr 2002): 213-21.

Andresen, J. M., J. Gayan, L. Djousse, S. Roberts, D. Brocklebank, S. S. Cherny, U. S-Venezuela Collaborative Research Group*, et al.* "The Relationship between Cag Repeat Length and Age of Onset Differs for Huntington's Disease Patients with Juvenile Onset or Adult Onset." [In eng]. *Ann Hum Genet* 71, no. Pt 3 (May 2007): 295-301.

Annunziata, P., and N. Volpi. "High Levels of C3c in the Cerebrospinal Fluid from Amyotrophic Lateral Sclerosis Patients." [In eng]. *Acta Neurol Scand* 72, no. 1 (Jul 1985): 61-4.

Apostolski, S., J. Nikolic, C. Bugarski-Prokopljevic, V. Miletic, S. Pavlovic, and S. Filipovic. "Serum and Csf Immunological Findings in Als." [In eng]. *Acta Neurol Scand* 83, no. 2 (Feb 1991): 96-8.

Arimoto-Matsuzaki, K., H. Saito, and M. Takekawa. "Tia1 Oxidation Inhibits Stress Granule Assembly and Sensitizes Cells to Stress-Induced Apoptosis." [In eng]. *Nat Commun* 7 (Jan 7 2016): 10252.

Arimoto, K., H. Fukuda, S. Imajoh-Ohmi, H. Saito, and M. Takekawa. "Formation of Stress Granules Inhibits Apoptosis by Suppressing Stress-Responsive Mapk Pathways." [In eng]. *Nat Cell Biol* 10, no. 11 (Nov 2008): 1324-32.

Arndt, J. R., M. Chaibva, and J. Legleiter. "The Emerging Role of the First 17 Amino Acids of Huntingtin in Huntington's Disease." [In eng]. *Biomol Concepts* 6, no. 1 (Mar 2015): 33-46.

Arrasate, M., S. Mitra, E. S. Schweitzer, M. R. Segal, and S. Finkbeiner. "Inclusion Body Formation Reduces Levels of Mutant Huntingtin and the Risk of Neuronal Death." [In eng]. *Nature* 431, no. 7010 (Oct 14 2004): 805-10.

Ayala, Y. M., P. Zago, A. D'Ambrogio, Y. F. Xu, L. Petrucelli, E. Buratti, and F. E. Baralle. "Structural Determinants of the Cellular Localization and Shuttling of Tdp-43." [In eng]. *J Cell Sci* 121, no. Pt 22 (Nov 15 2008): 3778-85.

Balusu, S., E. Van Wonterghem, R. De Rycke, K. Raemdonck, S. Stremersch, K. Gevaert, M. Brkic*, et al.* "Identification of a Novel Mechanism of Blood-Brain Communication During Peripheral Inflammation Via Choroid Plexus-Derived Extracellular Vesicles." [In eng]. *EMBO Mol Med* 8, no. 10 (Oct 2016): 1162-83.

Bang, C., and T. Thum. "Exosomes: New Players in Cell-Cell Communication." [In eng]. *Int J Biochem Cell Biol* 44, no. 11 (Nov 2012): 2060-4.

Baradaran-Heravi, Y., C. Van Broeckhoven, and J. van der Zee. "Stress Granule Mediated Protein Aggregation and Underlying Gene Defects in the Ftd-Als Spectrum." [In eng]. *Neurobiol Dis* 134 (Feb 2020): 104639.

Bartel, D. P. "Micrornas: Target Recognition and Regulatory Functions." [In eng]. *Cell* 136, no. 2 (Jan 23 2009): 215-33.

Bates, G. P., R. Dorsey, J. F. Gusella, M. R. Hayden, C. Kay, B. R. Leavitt, M. Nance*, et al.* "Huntington Disease." [In eng]. *Nat Rev Dis Primers* 1 (Apr 23 2015): 15005.

Bauerlein, F. J. B., I. Saha, A. Mishra, M. Kalemanov, A. Martinez-Sanchez, R. Klein, I. Dudanova*, et al.* "In Situ Architecture and Cellular Interactions of Polyq Inclusions." [In eng]. *Cell* 171, no. 1 (Sep 21 2017): 179-87 e10.

Bayer, P., A. Arndt, S. Metzger, R. Mahajan, F. Melchior, R. Jaenicke, and J. Becker. "Structure Determination of the Small Ubiquitin-Related Modifier Sumo-1." [In eng]. *J Mol Biol* 280, no. 2 (Jul 10 1998): 275-86.

Bayram-Weston, Z., L. Jones, S. B. Dunnett, and S. P. Brooks. "Light and Electron Microscopic Characterization of the Evolution of Cellular Pathology in Hdhq92 Huntington's Disease Knock-in Mice." [In eng]. *Brain Res Bull* 88, no. 2-3 (Jun 1 2012): 171-81.

Behrends, C., C. A. Langer, R. Boteva, U. M. Bottcher, M. J. Stemp, G. Schaffar, B. V. Rao*, et al.* "Chaperonin Tric Promotes the Assembly of Polyq Expansion Proteins into Nontoxic Oligomers." [In eng]. *Mol Cell* 23, no. 6 (Sep 15 2006): 887-97.

Beninson, L. A., and M. Fleshner. "Exosomes: An Emerging Factor in Stress-Induced Immunomodulation." [In eng]. *Semin Immunol* 26, no. 5 (Oct 2014): 394-401.

Berezikov, E. "Evolution of Microrna Diversity and Regulation in Animals." [In eng]. *Nat Rev Genet* 12, no. 12 (Nov 18 2011): 846-60.

Berson, A., S. Barbash, G. Shaltiel, Y. Goll, G. Hanin, D. S. Greenberg, M. Ketzef*, et al.* "Cholinergic-Associated Loss of Hnrnp-a/B in Alzheimer's Disease Impairs Cortical Splicing and Cognitive Function in Mice." [In eng]. *EMBO Mol Med* 4, no. 8 (Aug 2012): 730-42.

Betzer, O., N. Perets, A. Angel, M. Motiei, T. Sadan, G. Yadid, D. Offen, and R. Popovtzer. "In Vivo Neuroimaging of Exosomes Using Gold Nanoparticles." [In eng]. *ACS Nano* 11, no. 11 (Nov 28 2017): 10883-93.

Beyer, A. L., M. E. Christensen, B. W. Walker, and W. M. LeStourgeon. "Identification and Characterization of the Packaging Proteins of Core 40s Hnrnp Particles." [In eng]. *Cell* 11, no. 1 (May 1977): 127-38.

Bibb, J. A., Z. Yan, P. Svenningsson, G. L. Snyder, V. A. Pieribone, A. Horiuchi, A. C. Nairn, A. Messer, and P. Greengard. "Severe Deficiencies in Dopamine Signaling in Presymptomatic Huntington's Disease Mice." [In eng]. *Proc Natl Acad Sci U S A* 97, no. 12 (Jun 6 2000): 6809-14.

Blasco, H., P. Corcia, P. F. Pradat, C. Bocca, P. H. Gordon, C. Veyrat-Durebex, S. Mavel*, et al.* "Metabolomics in Cerebrospinal Fluid of Patients with Amyotrophic Lateral

Sclerosis: An Untargeted Approach Via High-Resolution Mass Spectrometry." [In eng]. *J Proteome Res* 12, no. 8 (Aug 2 2013): 3746-54.

Borlongan, C. V., C. G. Thanos, S. J. Skinner, M. Geaney, and D. F. Emerich. "Transplants of Encapsulated Rat Choroid Plexus Cells Exert Neuroprotection in a Rodent Model of Huntington's Disease." [In eng]. *Cell Transplant* 16, no. 10 (2008): 987-92.

Bracken, C. P., H. S. Scott, and G. J. Goodall. "A Network-Biology Perspective of Microrna Function and Dysfunction in Cancer." [In eng]. *Nat Rev Genet* 17, no. 12 (Dec 2016): 719-32.

Branco-Santos, J., F. Herrera, G. M. Pocas, Y. Pires-Afonso, F. Giorgini, P. M. Domingos, and T. F. Outeiro. "Protein Phosphatase 1 Regulates Huntingtin Exon 1 Aggregation and Toxicity." [In eng]. *Hum Mol Genet* 26, no. 19 (Oct 1 2017): 3763-75.

Brown, P. D., S. L. Davies, T. Speake, and I. D. Millar. "Molecular Mechanisms of Cerebrospinal Fluid Production." [In eng]. *Neuroscience* 129, no. 4 (2004): 957-70.

Browne, S. E., R. J. Ferrante, and M. F. Beal. "Oxidative Stress in Huntington's Disease." [In eng]. *Brain Pathol* 9, no. 1 (Jan 1999): 147-63.

Buchan, J. R., R. M. Kolaitis, J. P. Taylor, and R. Parker. "Eukaryotic Stress Granules Are Cleared by Autophagy and Cdc48/Vcp Function." [In eng]. *Cell* 153, no. 7 (Jun 20 2013): 1461-74.

Buchan, J. R., and R. Parker. "Eukaryotic Stress Granules: The Ins and Outs of Translation." [In eng]. *Mol Cell* 36, no. 6 (Dec 25 2009): 932-41.

Bulley, S. J., C. J. Drew, and A. J. Morton. "Direct Visualisation of Abnormal Dendritic Spine Morphology in the Hippocampus of the R6/2 Transgenic Mouse Model of Huntington's Disease." [In eng]. *J Huntingtons Dis* 1, no. 2 (2012): 267-73.

Burd, C. G., M. S. Swanson, M. Gorlach, and G. Dreyfuss. "Primary Structures of the Heterogeneous Nuclear Ribonucleoprotein A2, B1, and C2 Proteins: A Diversity of Rna Binding Proteins Is Generated by Small Peptide Inserts." [In eng]. *Proc Natl Acad Sci U S A* 86, no. 24 (Dec 1989): 9788-92.

Burroughs, A. M., Y. Ando, M. J. de Hoon, Y. Tomaru, T. Nishibu, R. Ukekawa, T. Funakoshi*, et al.* "A Comprehensive Survey of 3' Animal Mirna Modification Events and a Possible Role for 3' Adenylation in Modulating Mirna Targeting Effectiveness." [In eng]. *Genome Res* 20, no. 10 (Oct 2010): 1398-410.

Buvoli, M., G. Biamonti, P. Tsoulfas, M. T. Bassi, A. Ghetti, S. Riva, and C. Morandi. "Cdna Cloning of Human Hnrnp Protein A1 Reveals the Existence of Multiple Mrna Isoforms." [In eng]. *Nucleic Acids Res* 16, no. 9 (May 11 1988): 3751-70.

Byrne, L. M., F. B. Rodrigues, K. Blennow, A. Durr, B. R. Leavitt, R. A. C. Roos, R. I. Scahill*, et al.* "Neurofilament Light Protein in Blood as a Potential Biomarker of Neurodegeneration in Huntington's Disease: A Retrospective Cohort Analysis." [In eng]. *Lancet Neurol* 16, no. 8 (Aug 2017): 601-09.

Caby, M. P., D. Lankar, C. Vincendeau-Scherrer, G. Raposo, and C. Bonnerot. "Exosomal-Like Vesicles Are Present in Human Blood Plasma." [In eng]. *Int Immunol* 17, no. 7 (Jul 2005): 879-87.

Cao, X. Y., J. M. Lu, Z. Q. Zhao, M. C. Li, T. Lu, X. S. An, and L. J. Xue. "Microrna Biomarkers of Parkinson's Disease in Serum Exosome-Like Microvesicles." [In eng]. *Neurosci Lett* 644 (Mar 22 2017): 94-99.

Cappadocia, L., and C. D. Lima. "Ubiquitin-Like Protein Conjugation: Structures, Chemistry, and Mechanism." [In eng]. *Chem Rev* 118, no. 3 (Feb 14 2018): 889-918.

Cartegni, L., M. Maconi, E. Morandi, F. Cobianchi, S. Riva, and G. Biamonti. "Hnrnp A1 Selectively Interacts through Its Gly-Rich Domain with Different Rna-Binding Proteins." [In eng]. *J Mol Biol* 259, no. 3 (Jun 14 1996): 337-48.

Carty, N., N. Berson, K. Tillack, C. Thiede, D. Scholz, K. Kottig, Y. Sedaghat*, et al.* "Characterization of Htt Inclusion Size, Location, and Timing in the Zq175 Mouse Model of Huntington's Disease: An in Vivo High-Content Imaging Study." [In eng]. *PLoS One* 10, no. 4 (2015): e0123527.

Chalfie, M., H. R. Horvitz, and J. E. Sulston. "Mutations That Lead to Reiterations in the Cell Lineages of C. Elegans." [In eng]. *Cell* 24, no. 1 (Apr 1981): 59-69.

Chambers, S. M., C. A. Fasano, E. P. Papapetrou, M. Tomishima, M. Sadelain, and L. Studer. "Highly Efficient Neural Conversion of Human Es and Ips Cells by Dual Inhibition of Smad Signaling." [In eng]. *Nat Biotechnol* 27, no. 3 (Mar 2009): 275-80.

Chan, K. Y., M. J. Jang, B. B. Yoo, A. Greenbaum, N. Ravi, W. L. Wu, L. Sanchez-Guardado*, et al.* "Engineered Aavs for Efficient Noninvasive Gene Delivery to the Central and Peripheral Nervous Systems." [In eng]. *Nat Neurosci* 20, no. 8 (Aug 2017): 1172-79.

Chen, L., and B. Liu. "Relationships between Stress Granules, Oxidative Stress, and Neurodegenerative Diseases." [In eng]. *Oxid Med Cell Longev* 2017 (2017): 1809592.

Chen, Z., W. Jalabi, K. B. Shpargel, K. T. Farabaugh, R. Dutta, X. Yin, G. J. Kidd*, et al.* "Lipopolysaccharide-Induced Microglial Activation and Neuroprotection against Experimental Brain Injury Is Independent of Hematogenous Tlr4." [In eng]. *J Neurosci* 32, no. 34 (Aug 22 2012): 11706-15.

Chew, J., C. Cook, T. F. Gendron, K. Jansen-West, G. Del Rosso, L. M. Daughrity, M. Castanedes-Casey*, et al.* "Aberrant Deposition of Stress Granule-Resident Proteins Linked to C9orf72-Associated Tdp-43 Proteinopathy." [In eng]. *Mol Neurodegener* 14, no. 1 (Feb 15 2019): 9.

Cisbani, G., and F. Cicchetti. "An in Vitro Perspective on the Molecular Mechanisms Underlying Mutant Huntingtin Protein Toxicity." [In eng]. *Cell Death Dis* 3 (Aug 30 2012): e382.

Collins, M. A., J. An, B. L. Hood, T. P. Conrads, and R. P. Bowser. "Label-Free Lc-Ms/Ms Proteomic Analysis of Cerebrospinal Fluid Identifies Protein/Pathway Alterations and Candidate Biomarkers for Amyotrophic Lateral Sclerosis." [In eng]. *J Proteome Res* 14, no. 11 (Nov 6 2015): 4486-501.

Colombo, M., G. Raposo, and C. Thery. "Biogenesis, Secretion, and Intercellular Interactions of Exosomes and Other Extracellular Vesicles." [In eng]. *Annu Rev Cell Dev Biol* 30 (2014): 255-89.

Constantinescu, R., M. Romer, D. Oakes, L. Rosengren, and K. Kieburtz. "Levels of the Light Subunit of Neurofilament Triplet Protein in Cerebrospinal Fluid in Huntington's Disease." [In eng]. *Parkinsonism Relat Disord* 15, no. 3 (Mar 2009): 245-8.

Cortes, C. J., and A. R. La Spada. "The Many Faces of Autophagy Dysfunction in Huntington's Disease: From Mechanism to Therapy." [In eng]. *Drug Discov Today* 19, no. 7 (Jul 2014): 963-71.

Crocker, S. F., W. J. Costain, and H. A. Robertson. "DNA Microarray Analysis of Striatal Gene Expression in Symptomatic Transgenic Huntington's Mice (R6/2) Reveals Neuroinflammation and Insulin Associations." [In eng]. *Brain Res* 1088, no. 1 (May 9 2006): 176-86.

Cudkowicz, M., and N. W. Kowall. "Degeneration of Pyramidal Projection Neurons in Huntington's Disease Cortex." [In eng]. *Ann Neurol* 27, no. 2 (Feb 1990): 200-4.

Culver, B. P., J. N. Savas, S. K. Park, J. H. Choi, S. Zheng, S. O. Zeitlin, J. R. Yates, 3rd, and N. Tanese. "Proteomic Analysis of Wild-Type and Mutant Huntingtin-Associated Proteins in Mouse Brains Identifies Unique Interactions and Involvement in Protein Synthesis." [In eng]. *J Biol Chem* 287, no. 26 (Jun 22 2012): 21599-614.

Cursons, J., K. A. Pillman, K. G. Scheer, P. A. Gregory, M. Foroutan, S. Hediyeh-Zadeh, J. Toubia*, et al.* "Combinatorial Targeting by Micrornas Co-Ordinates Post-Transcriptional Control of Emt." [In eng]. *Cell Syst* 7, no. 1 (Jul 25 2018): 77-91 e7.

Cushing, H. "Studies on the Cerebro-Spinal Fluid : I. Introduction." [In eng]. *J Med Res* 31, no. 1 (Sep 1914): 1-19.

Dalrymple, A., E. J. Wild, R. Joubert, K. Sathasivam, M. Bjorkqvist, A. Petersen, G. S. Jackson*, et al.* "Proteomic Profiling of Plasma in Huntington's Disease Reveals Neuroinflammatory Activation and Biomarker Candidates." [In eng]. *J Proteome Res* 6, no. 7 (Jul 2007): 2833-40.

Damkier, H. H., P. D. Brown, and J. Praetorius. "Cerebrospinal Fluid Secretion by the Choroid Plexus." [In eng]. *Physiol Rev* 93, no. 4 (Oct 2013): 1847-92.

Davies, S. W., M. Turmaine, B. A. Cozens, M. DiFiglia, A. H. Sharp, C. A. Ross, E. Scherzinger*, et al.* "Formation of Neuronal Intranuclear Inclusions Underlies the Neurological Dysfunction in Mice Transgenic for the Hd Mutation." [In eng]. *Cell* 90, no. 3 (Aug 8 1997): 537-48.

Deckel, A. W., A. Gordinier, D. Nuttal, V. Tang, C. Kuwada, R. Freitas, and K. A. Gary. "Reduced Activity and Protein Expression of Nos in R6/2 Hd Transgenic Mice: Effects of L-Name on Symptom Progression." [In eng]. *Brain Res* 919, no. 1 (Nov 16 2001): 70-81.

Decker, C. J., and R. Parker. "P-Bodies and Stress Granules: Possible Roles in the Control of Translation and Mrna Degradation." [In eng]. *Cold Spring Harb Perspect Biol* 4, no. 9 (Sep 1 2012): a012286.

Desmond, C. R., T. Maiuri, and R. Truant. "A Multifunctional, Multi-Pathway Intracellular Localization Signal in Huntingtin." [In eng]. *Commun Integr Biol* 6, no. 2 (Mar 1 2013): e23318.

"Developmental Alterations in Huntington's Disease Neural Cells and Pharmacological Rescue in Cells and Mice." [In eng]. *Nat Neurosci* 20, no. 5 (May 2017): 648-60.

DiFiglia, M., E. Sapp, K. O. Chase, S. W. Davies, G. P. Bates, J. P. Vonsattel, and N. Aronin. "Aggregation of Huntingtin in Neuronal Intranuclear Inclusions and Dystrophic Neurites in Brain." [In eng]. *Science* 277, no. 5334 (Sep 26 1997): 1990-3.

Dobra, I., S. Pankivskyi, A. Samsonova, D. Pastre, and L. Hamon. "Relation between Stress Granules and Cytoplasmic Protein Aggregates Linked to Neurodegenerative Diseases." [In eng]. *Curr Neurol Neurosci Rep* 18, no. 12 (Nov 8 2018): 107.

Doi, H., K. Okamura, P. O. Bauer, Y. Furukawa, H. Shimizu, M. Kurosawa, Y. Machida*, et al.* "Rna-Binding Protein Tls Is a Major Nuclear Aggregate-Interacting Protein in Huntingtin Exon 1 with Expanded Polyglutamine-Expressing Cells." [In eng]. *J Biol Chem* 283, no. 10 (Mar 7 2008): 6489-500.

Dreyfuss, G., V. N. Kim, and N. Kataoka. "Messenger-Rna-Binding Proteins and the Messages They Carry." [In eng]. *Nat Rev Mol Cell Biol* 3, no. 3 (Mar 2002): 195-205.

Dreyfuss, G., M. J. Matunis, S. Pinol-Roma, and C. G. Burd. "Hnrnp Proteins and the Biogenesis of Mrna." [In eng]. *Annu Rev Biochem* 62 (1993): 289-321.

Dreyfuss, G., M. S. Swanson, and S. Pinol-Roma. "Heterogeneous Nuclear Ribonucleoprotein Particles and the Pathway of Mrna Formation." [In eng]. *Trends Biochem Sci* 13, no. 3 (Mar 1988): 86-91.

Duennwald, M. L. "Cellular Stress Responses in Protein Misfolding Diseases." [In eng]. *Future Sci OA* 1, no. 2 (Sep 2015): FSO42.

Dye, B. T., and B. A. Schulman. "Structural Mechanisms Underlying Posttranslational Modification by Ubiquitin-Like Proteins." [In eng]. *Annu Rev Biophys Biomol Struct* 36 (2007): 131-50.

Eichenbaum, H. "Prefrontal-Hippocampal Interactions in Episodic Memory." [In eng]. *Nat Rev Neurosci* 18, no. 9 (Sep 2017): 547-58.

Eiraku, M., K. Watanabe, M. Matsuo-Takasaki, M. Kawada, S. Yonemura, M. Matsumura, T. Wataya*, et al.* "Self-Organized Formation of Polarized Cortical Tissues from Escs and Its Active Manipulation by Extrinsic Signals." [In eng]. *Cell Stem Cell* 3, no. 5 (Nov 6 2008): 519-32.

Eisele, Y. S., C. Monteiro, C. Fearns, S. E. Encalada, R. L. Wiseman, E. T. Powers, and J. W. Kelly. "Targeting Protein Aggregation for the Treatment of Degenerative Diseases." [In eng]. *Nat Rev Drug Discov* 14, no. 11 (Nov 2015): 759-80.

Elmore, S. "Apoptosis: A Review of Programmed Cell Death." [In eng]. *Toxicol Pathol* 35, no. 4 (Jun 2007): 495-516.

Elsharkasy, O. M., J. Z. Nordin, D. W. Hagey, O. G. de Jong, R. M. Schiffelers, S. E. Andaloussi, and P. Vader. "Extracellular Vesicles as Drug Delivery Systems: Why and How?" [In eng]. *Adv Drug Deliv Rev* (Apr 16 2020).

Emerich, D. F., S. J. Skinner, C. V. Borlongan, A. V. Vasconcellos, and C. G. Thanos. "The Choroid Plexus in the Rise, Fall and Repair of the Brain." [In eng]. *Bioessays* 27, no. 3 (Mar 2005): 262-74.

Engle, S. J., and D. Puppala. "Integrating Human Pluripotent Stem Cells into Drug Development." [In eng]. *Cell Stem Cell* 12, no. 6 (Jun 6 2013): 669-77.

Eulalio, A., I. Behm-Ansmant, and E. Izaurralde. "P Bodies: At the Crossroads of Post-Transcriptional Pathways." [In eng]. *Nat Rev Mol Cell Biol* 8, no. 1 (Jan 2007): 9-22.

Fan, A. C., and A. K. Leung. "Rna Granules and Diseases: A Case Study of Stress Granules in Als and Ftld." [In eng]. *Adv Exp Med Biol* 907 (2016): 263-96.

Fang, M. Y., S. Markmiller, A. Q. Vu, A. Javaherian, W. E. Dowdle, P. Jolivet, P. J. Bushway*, et al.* "Small-Molecule Modulation of Tdp-43 Recruitment to Stress Granules Prevents Persistent Tdp-43 Accumulation in Als/Ftd." [In eng]. *Neuron* 103, no. 5 (Sep 4 2019): 802-19 e11.

Franich, N. R., M. Basso, E. A. Andre, J. Ochaba, A. Kumar, S. Thein, G. Fote*, et al.* "Striatal Mutant Huntingtin Protein Levels Decline with Age in Homozygous Huntington's Disease Knock-in Mouse Models." [In eng]. *J Huntingtons Dis* 7, no. 2 (2018): 137-50.

Frank, F., N. Sonenberg, and B. Nagar. "Structural Basis for 5'-Nucleotide Base-Specific Recognition of Guide Rna by Human Ago2." [In eng]. *Nature* 465, no. 7299 (Jun 10 2010): 818-22.

Friedman, R. C., K. K. Farh, C. B. Burge, and D. P. Bartel. "Most Mammalian Mrnas Are Conserved Targets of Microrna." [In eng]. *Genome Res* 19, no. 1 (Jan 2009): 92-105.

Friend, L. R., S. P. Han, J. A. Rothnagel, and R. Smith. "Differential Subnuclear Localisation of Hnrnps a/B Is Dependent on Transcription and Cell Cycle Stage." [In eng]. *Biochim Biophys Acta* 1783, no. 10 (Oct 2008): 1972-80.

Friend, L. R., M. J. Landsberg, A. S. Nouwens, Y. Wei, J. A. Rothnagel, and R. Smith. "Arginine Methylation of Hnrnp A2 Does Not Directly Govern Its Subcellular Localization." [In eng]. *PLoS One* 8, no. 9 (2013): e75669.

Fukuda, I., A. Ito, G. Hirai, S. Nishimura, H. Kawasaki, H. Saitoh, K. Kimura, M. Sodeoka, and M. Yoshida. "Ginkgolic Acid Inhibits Protein Sumoylation by Blocking Formation of the E1-Sumo Intermediate." [In eng]. *Chem Biol* 16, no. 2 (Feb 27 2009): 133-40.

Fulda, S., A. M. Gorman, O. Hori, and A. Samali. "Cellular Stress Responses: Cell Survival and Cell Death." [In eng]. *Int J Cell Biol* 2010 (2010): 214074.

Furukawa, Y., K. Kaneko, G. Matsumoto, M. Kurosawa, and N. Nukina. "Cross-Seeding Fibrillation of Q/N-Rich Proteins Offers New Pathomechanism of Polyglutamine Diseases." [In eng]. *J Neurosci* 29, no. 16 (Apr 22 2009): 5153-62.

Ganz, J., T. Shacham, M. Kramer, M. Shenkman, H. Eiger, N. Weinberg, O. Iancovici*, et al.* "A Novel Specific Perk Activator Reduces Toxicity and Extends Survival in Huntington's Disease Models." [In eng]. *Sci Rep* 10, no. 1 (Apr 23 2020): 6875.

Ge, Q., Y. Zhou, J. Lu, Y. Bai, X. Xie, and Z. Lu. "Mirna in Plasma Exosome Is Stable under Different Storage Conditions." [In eng]. *Molecules* 19, no. 2 (Jan 27 2014): 1568-75.

Geiss-Friedlander, R., and F. Melchior. "Concepts in Sumoylation: A Decade On." [In eng]. *Nat Rev Mol Cell Biol* 8, no. 12 (Dec 2007): 947-56.

Genetic Modifiers of Huntington's Disease, Consortium. "Identification of Genetic Factors That Modify Clinical Onset of Huntington's Disease." [In eng]. *Cell* 162, no. 3 (Jul 30 2015): 516-26.

Genetic Modifiers of Huntington's Disease Consortium. Electronic address, gusella helix mgh harvard edu, and Consortium Genetic Modifiers of Huntington's Disease. "Cag Repeat Not Polyglutamine Length Determines Timing of Huntington's Disease Onset." [In eng]. *Cell* 178, no. 4 (Aug 8 2019): 887-900 e14.

Geuens, T., D. Bouhy, and V. Timmerman. "The Hnrnp Family: Insights into Their Role in Health and Disease." [In eng]. *Hum Genet* 135, no. 8 (Aug 2016): 851-67.

Ghildiyal, M., and P. D. Zamore. "Small Silencing Rnas: An Expanding Universe." [In eng]. *Nat Rev Genet* 10, no. 2 (Feb 2009): 94-108.

Gil, J. M., and A. C. Rego. "The R6 Lines of Transgenic Mice: A Model for Screening New Therapies for Huntington's Disease." [In eng]. *Brain Res Rev* 59, no. 2 (Mar 2009): 410-31.

Gilks, N., N. Kedersha, M. Ayodele, L. Shen, G. Stoecklin, L. M. Dember, and P. Anderson. "Stress Granule Assembly Is Mediated by Prion-Like Aggregation of Tia-1." [In eng]. *Mol Biol Cell* 15, no. 12 (Dec 2004): 5383-98.

Goncalves, A. C., E. R. Towers, N. Haq, J. A. Porco, Jr., J. Pelletier, S. J. Dawson, and J. E. Gale. "Drug-Induced Stress Granule Formation Protects Sensory Hair Cells in Mouse Cochlear Explants During Ototoxicity." [In eng]. *Sci Rep* 9, no. 1 (Aug 29 2019): 12501.

Gorlach, M., M. Wittekind, R. A. Beckman, L. Mueller, and G. Dreyfuss. "Interaction of the Rna-Binding Domain of the Hnrnp C Proteins with Rna." [In eng]. *EMBO J* 11, no. 9 (Sep 1992): 3289-95.

Gould, S. J., and G. Raposo. "As We Wait: Coping with an Imperfect Nomenclature for Extracellular Vesicles." [In eng]. *J Extracell Vesicles* 2 (2013).

Grapp, M., I. A. Just, T. Linnankivi, P. Wolf, T. Lucke, M. Hausler, J. Gartner, and R. Steinfeld. "Molecular Characterization of Folate Receptor 1 Mutations Delineates Cerebral Folate Transport Deficiency." [In eng]. *Brain* 135, no. Pt 7 (Jul 2012): 2022-31.

Grapp, M., A. Wrede, M. Schweizer, S. Huwel, H. J. Galla, N. Snaidero, M. Simons*, et al.* "Choroid Plexus Transcytosis and Exosome Shuttling Deliver Folate into Brain Parenchyma." [In eng]. *Nat Commun* 4 (2013): 2123.

Griffiths-Jones, S., H. K. Saini, S. van Dongen, and A. J. Enright. "Mirbase: Tools for Microrna Genomics." [In eng]. *Nucleic Acids Res* 36, no. Database issue (Jan 2008): D154-8.

Group, The Huntington's Disease Collaborative Research. "A Novel Gene Containing a Trinucleotide Repeat That Is Expanded and Unstable on Huntington's Disease Chromosomes. The Huntington's Disease Collaborative Research Group." [In eng]. *Cell* 72, no. 6 (Mar 26 1993): 971-83.

Gui, Y., H. Liu, L. Zhang, W. Lv, and X. Hu. "Altered Microrna Profiles in Cerebrospinal Fluid Exosome in Parkinson Disease and Alzheimer Disease." [In eng]. *Oncotarget* 6, no. 35 (Nov 10 2015): 37043-53.

Gutekunst, C. A., S. H. Li, H. Yi, J. S. Mulroy, S. Kuemmerle, R. Jones, D. Rye*, et al.* "Nuclear and Neuropil Aggregates in Huntington's Disease: Relationship to Neuropathology." [In eng]. *J Neurosci* 19, no. 7 (Apr 1 1999): 2522-34.

Ha, M., and V. N. Kim. "Regulation of Microrna Biogenesis." [In eng]. *Nat Rev Mol Cell Biol* 15, no. 8 (Aug 2014): 509-24.

Hammond, S. M. "An Overview of Microrna." [In eng]. *Adv Drug Deliv Rev* 87 (Jun 29 2015): 3-14.

Han, N., W. Li, and M. Zhang. "The Function of the Rna-Binding Protein Hnrnp in Cancer Metastasis." [In eng]. *J Cancer Res Ther* 9 Suppl (Nov 2013): S129-34.

Han, S. P., L. R. Friend, J. H. Carson, G. Korza, E. Barbarese, M. Maggipinto, J. T. Hatfield, J. A. Rothnagel, and R. Smith. "Differential Subcellular Distributions and Trafficking Functions of Hnrnp A2/B1 Spliceoforms." [In eng]. *Traffic* 11, no. 7 (Jul 1 2010): 886-98.

Han, S. P., Y. H. Tang, and R. Smith. "Functional Diversity of the Hnrnps: Past, Present and Perspectives." [In eng]. *Biochem J* 430, no. 3 (Sep 15 2010): 379-92.

Harding, C., J. Heuser, and P. Stahl. "Endocytosis and Intracellular Processing of Transferrin and Colloidal Gold-Transferrin in Rat Reticulocytes: Demonstration of a Pathway for Receptor Shedding." [In eng]. *Eur J Cell Biol* 35, no. 2 (Nov 1984): 256-63.

Harding, C. V., J. E. Heuser, and P. D. Stahl. "Exosomes: Looking Back Three Decades and into the Future." [In eng]. *J Cell Biol* 200, no. 4 (Feb 18 2013): 367-71.

Harrington, M. G., A. N. Fonteh, E. Oborina, P. Liao, R. P. Cowan, G. McComb, J. N. Chavez*, et al.* "The Morphology and Biochemistry of Nanostructures Provide Evidence for Synthesis and Signaling Functions in Human Cerebrospinal Fluid." [In eng]. *Cerebrospinal Fluid Res* 6 (Sep 7 2009): 10.

Hart, S. N., T. M. Therneau, Y. Zhang, G. A. Poland, and J. P. Kocher. "Calculating Sample Size Estimates for Rna Sequencing Data." [In eng]. *J Comput Biol* 20, no. 12 (Dec 2013): 970-8.

Herbert, J., J. N. Wilcox, K. T. Pham, R. T. Fremeau, Jr., M. Zeviani, A. Dwork, D. R. Soprano*, et al.* "Transthyretin: A Choroid Plexus-Specific Transport Protein in Human Brain. The 1986 S. Weir Mitchell Award." [In eng]. *Neurology* 36, no. 7 (Jul 1986): 900-11.

Hertel, J., M. Lindemeyer, K. Missal, C. Fried, A. Tanzer, C. Flamm, I. L. Hofacker, and P. F. Stadler. "The Expansion of the Metazoan Microrna Repertoire." [In eng]. *BMC Genomics* 7 (Feb 15 2006): 25.

Hessvik, N. P., and A. Llorente. "Current Knowledge on Exosome Biogenesis and Release." [In eng]. *Cell Mol Life Sci* 75, no. 2 (Jan 2018): 193-208.

Hickey, M. A., K. Gallant, G. G. Gross, M. S. Levine, and M. F. Chesselet. "Early Behavioral Deficits in R6/2 Mice Suitable for Use in Preclinical Drug Testing." [In eng]. *Neurobiol Dis* 20, no. 1 (Oct 2005): 1-11.

Hodges, A., A. D. Strand, A. K. Aragaki, A. Kuhn, T. Sengstag, G. Hughes, L. A. Elliston*, et al.* "Regional and Cellular Gene Expression Changes in Human Huntington's Disease Brain." [In eng]. *Hum Mol Genet* 15, no. 6 (Mar 15 2006): 965-77.

Hoffner, G., and P. Djian. "Monomeric, Oligomeric and Polymeric Proteins in Huntington Disease and Other Diseases of Polyglutamine Expansion." [In eng]. *Brain Sci* 4, no. 1 (Mar 3 2014): 91-122.

———. "Polyglutamine Aggregation in Huntington Disease: Does Structure Determine Toxicity?" [In eng]. *Mol Neurobiol* 52, no. 3 (Dec 2015): 1297-314.

Hosp, F., S. Gutierrez-Angel, M. H. Schaefer, J. Cox, F. Meissner, M. S. Hipp, F. U. Hartl*, et al.* "Spatiotemporal Proteomic Profiling of Huntington's Disease Inclusions Reveals Widespread Loss of Protein Function." [In eng]. *Cell Rep* 21, no. 8 (Nov 21 2017): 2291-303.

Hoss, A. G., V. K. Kartha, X. Dong, J. C. Latourelle, A. Dumitriu, T. C. Hadzi, M. E. Macdonald*, et al.* "Micrornas Located in the Hox Gene Clusters Are Implicated in Huntington's Disease Pathogenesis." [In eng]. *PLoS Genet* 10, no. 2 (Feb 2014): e1004188.

Hoss, A. G., A. Labadorf, J. C. Latourelle, V. K. Kartha, T. C. Hadzi, J. F. Gusella, M. E. MacDonald*, et al.* "Mir-10b-5p Expression in Huntington's Disease Brain Relates to Age of Onset and the Extent of Striatal Involvement." [In eng]. *BMC Med Genomics* 8 (Mar 1 2015): 10.

Hughes, D., and G. R. Mallucci. "The Unfolded Protein Response in Neurodegenerative Disorders - Therapeutic Modulation of the Perk Pathway." [In eng]. *FEBS J* 286, no. 2 (Jan 2019): 342-55.

Hunter, M. P., N. Ismail, X. Zhang, B. D. Aguda, E. J. Lee, L. Yu, T. Xiao*, et al.* "Detection of Microrna Expression in Human Peripheral Blood Microvesicles." [In eng]. *PLoS One* 3, no. 11 (2008): e3694.

Huntzinger, E., and E. Izaurralde. "Gene Silencing by Micrornas: Contributions of Translational Repression and Mrna Decay." [In eng]. *Nat Rev Genet* 12, no. 2 (Feb 2011): 99-110.

Hutten, S., and D. Dormann. "Hnrnpa2/B1 Function in Neurodegeneration: It's a Gain, Not a Loss." [In eng]. *Neuron* 92, no. 4 (Nov 23 2016): 672-74.

"Induced Pluripotent Stem Cells from Patients with Huntington's Disease Show Cag-Repeat-Expansion-Associated Phenotypes." [In eng]. *Cell Stem Cell* 11, no. 2 (Aug 3 2012): 264-78.

Jain, S., J. R. Wheeler, R. W. Walters, A. Agrawal, A. Barsic, and R. Parker. "Atpase-Modulated Stress Granules Contain a Diverse Proteome and Substructure." [In eng]. *Cell* 164, no. 3 (Jan 28 2016): 487-98.

Janas, T., M. M. Janas, and K. Sapon. "Mechanisms of Rna Loading into Exosomes." [In eng]. *FEBS Lett* 589, no. 13 (Jun 4 2015): 1391-8.

Jeon, I., F. Cicchetti, G. Cisbani, S. Lee, E. Li, J. Bae, N. Lee*, et al.* "Human-to-Mouse Prion-Like Propagation of Mutant Huntingtin Protein." [In eng]. *Acta Neuropathol* 132, no. 4 (Oct 2016): 577-92.

Jeon, I., N. Lee, J. Y. Li, I. H. Park, K. S. Park, J. Moon, S. H. Shim*, et al.* "Neuronal Properties, in Vivo Effects, and Pathology of a Huntington's Disease Patient-Derived Induced Pluripotent Stem Cells." [In eng]. *Stem Cells* 30, no. 9 (Sep 2012): 2054-62.

Johnson, R., C. Zuccato, N. D. Belyaev, D. J. Guest, E. Cattaneo, and N. J. Buckley. "A Microrna-Based Gene Dysregulation Pathway in Huntington's Disease." [In eng]. *Neurobiol Dis* 29, no. 3 (Mar 2008): 438-45.

Josiassen, R. C., L. M. Curry, and E. L. Mancall. "Development of Neuropsychological Deficits in Huntington's Disease." [In eng]. *Arch Neurol* 40, no. 13 (Dec 1983): 791-6.

Kamma, H., H. Horiguchi, L. Wan, M. Matsui, M. Fujiwara, M. Fujimoto, T. Yazawa, and G. Dreyfuss. "Molecular Characterization of the Hnrnp A2/B1 Proteins: Tissue-Specific Expression and Novel Isoforms." [In eng]. *Exp Cell Res* 246, no. 2 (Feb 1 1999): 399-411.

Kanninen, K. M., N. Bister, J. Koistinaho, and T. Malm. "Exosomes as New Diagnostic Tools in Cns Diseases." [In eng]. *Biochim Biophys Acta* 1862, no. 3 (Mar 2016): 403-10.

Kedersha, N., and P. Anderson. "Mammalian Stress Granules and Processing Bodies." [In eng]. *Methods Enzymol* 431 (2007): 61-81.

Kedersha, N. L., M. Gupta, W. Li, I. Miller, and P. Anderson. "Rna-Binding Proteins Tia-1 and Tiar Link the Phosphorylation of Eif-2 Alpha to the Assembly of Mammalian Stress Granules." [In eng]. *J Cell Biol* 147, no. 7 (Dec 27 1999): 1431-42.

Kedersha, N., G. Stoecklin, M. Ayodele, P. Yacono, J. Lykke-Andersen, M. J. Fritzler, D. Scheuner*, et al.* "Stress Granules and Processing Bodies Are Dynamically Linked Sites of Mrnp Remodeling." [In eng]. *J Cell Biol* 169, no. 6 (Jun 20 2005): 871-84.

Keryer, G., J. R. Pineda, G. Liot, J. Kim, P. Dietrich, C. Benstaali, K. Smith*, et al.* "Ciliogenesis Is Regulated by a Huntingtin-Hap1-Pcm1 Pathway and Is Altered in Huntington Disease." [In eng]. *J Clin Invest* 121, no. 11 (Nov 2011): 4372-82.

Kim, H. J., N. C. Kim, Y. D. Wang, E. A. Scarborough, J. Moore, Z. Diaz, K. S. MacLea*, et al.* "Mutations in Prion-Like Domains in Hnrnpa2b1 and Hnrnpa1 Cause Multisystem Proteinopathy and Als." [In eng]. *Nature* 495, no. 7442 (Mar 28 2013): 467-73.

Kim, H. J., A. R. Raphael, E. S. LaDow, L. McGurk, R. A. Weber, J. Q. Trojanowski, V. M. Lee*, et al.* "Therapeutic Modulation of Eif2alpha Phosphorylation Rescues Tdp-43 Toxicity in Amyotrophic Lateral Sclerosis Disease Models." [In eng]. *Nat Genet* 46, no. 2 (Feb 2014): 152-60.

Kim, Y. M., W. H. Jang, M. M. Quezado, Y. Oh, K. C. Chung, E. Junn, and M. M. Mouradian. "Proteasome Inhibition Induces Alpha-Synuclein Sumoylation and Aggregate Formation." [In eng]. *J Neurol Sci* 307, no. 1-2 (Aug 15 2011): 157-61.

Kitamura, A., H. Kubota, C. G. Pack, G. Matsumoto, S. Hirayama, Y. Takahashi, H. Kimura*, et al.* "Cytosolic Chaperonin Prevents Polyglutamine Toxicity with Altering the Aggregation State." [In eng]. *Nat Cell Biol* 8, no. 10 (Oct 2006): 1163-70.

Klein, F. A., G. Zeder-Lutz, A. Cousido-Siah, A. Mitschler, A. Katz, P. Eberling, J. L. Mandel, A. Podjarny, and Y. Trottier. "Linear and Extended: A Common Polyglutamine Conformation Recognized by the Three Antibodies Mw1, 1c2 and 3b5h10." [In eng]. *Hum Mol Genet* 22, no. 20 (Oct 15 2013): 4215-23.

Klockgether, T., C. Mariotti, and H. L. Paulson. "Spinocerebellar Ataxia." [In eng]. *Nat Rev Dis Primers* 5, no. 1 (Apr 11 2019): 24.

Ko, J., S. Ou, and P. H. Patterson. "New Anti-Huntingtin Monoclonal Antibodies: Implications for Huntingtin Conformation and Its Binding Proteins." [In eng]. *Brain Res Bull* 56, no. 3-4 (Oct-Nov 1 2001): 319-29.

Kocerha, J., Y. Xu, M. S. Prucha, D. Zhao, and A. W. Chan. "Microrna-128a Dysregulation in Transgenic Huntington's Disease Monkeys." [In eng]. *Mol Brain* 7 (Jun 13 2014): 46.

Kodali, M., O. W. Castro, D. K. Kim, A. Thomas, B. Shuai, S. Attaluri, R. Upadhya*, et al.* "Intranasally Administered Human Msc-Derived Extracellular Vesicles Pervasively Incorporate into Neurons and Microglia in Both Intact and Status Epilepticus Injured Forebrain." [In eng]. *Int J Mol Sci* 21, no. 1 (Dec 26 2019).

Kopkova, A., J. Sana, P. Fadrus, and O. Slaby. "Cerebrospinal Fluid Micrornas as Diagnostic Biomarkers in Brain Tumors." [In eng]. *Clin Chem Lab Med* 56, no. 6 (May 24 2018): 869-79.

Koyuncu, S., A. Fatima, R. Gutierrez-Garcia, and D. Vilchez. "Proteostasis of Huntingtin in Health and Disease." [In eng]. *Int J Mol Sci* 18, no. 7 (Jul 19 2017).

Kozomara, A., M. Birgaoanu, and S. Griffiths-Jones. "Mirbase: From Microrna Sequences to Function." [In eng]. *Nucleic Acids Res* 47, no. D1 (Jan 8 2019): D155-D62.

Kozu, T., B. Henrich, and K. P. Schafer. "Structure and Expression of the Gene (Hnrpa2b1) Encoding the Human Hnrnp Protein A2/B1." [In eng]. *Genomics* 25, no. 2 (Jan 20 1995): 365-71.

Labadorf, A., A. G. Hoss, V. Lagomarsino, J. C. Latourelle, T. C. Hadzi, J. Bregu, M. E. MacDonald*, et al.* "Rna Sequence Analysis of Human Huntington Disease Brain Reveals an Extensive Increase in Inflammatory and Developmental Gene Expression." [In eng]. *PLoS One* 10, no. 12 (2015): e0143563.

Lajoie, P., and E. L. Snapp. "Formation and Toxicity of Soluble Polyglutamine Oligomers in Living Cells." [In eng]. *PLoS One* 5, no. 12 (Dec 28 2010): e15245.

Lakhal, S., and M. J. Wood. "Intranasal Exosomes for Treatment of Neuroinflammation? Prospects and Limitations." [In eng]. *Mol Ther* 19, no. 10 (Oct 2011): 1754-6.

Langmead, B., and S. L. Salzberg. "Fast Gapped-Read Alignment with Bowtie 2." [In eng]. *Nat Methods* 9, no. 4 (Mar 4 2012): 357-9.

Le Ber, I., I. Van Bortel, G. Nicolas, K. Bouya-Ahmed, A. Camuzat, D. Wallon, A. De Septenville*, et al.* "Hnrnpa2b1 and Hnrnpa1 Mutations Are Rare in Patients with "Multisystem Proteinopathy" and Frontotemporal Lobar Degeneration Phenotypes." [In eng]. *Neurobiol Aging* 35, no. 4 (Apr 2014): 934 e5-6.

Lee, R. C., R. L. Feinbaum, and V. Ambros. "The C. Elegans Heterochronic Gene Lin-4 Encodes Small Rnas with Antisense Complementarity to Lin-14." [In eng]. *Cell* 75, no. 5 (Dec 3 1993): 843-54.

Lee, S. T., K. Chu, W. S. Im, H. J. Yoon, J. Y. Im, J. E. Park, K. H. Park*, et al.* "Altered Microrna Regulation in Huntington's Disease Models." [In eng]. *Exp Neurol* 227, no. 1 (Jan 2011): 172-9.

Lee, Y., M. Kim, J. Han, K. H. Yeom, S. Lee, S. H. Baek, and V. N. Kim. "Microrna Genes Are Transcribed by Rna Polymerase Ii." [In eng]. *EMBO J* 23, no. 20 (Oct 13 2004): 4051-60.

Legleiter, J., G. P. Lotz, J. Miller, J. Ko, C. Ng, G. L. Williams, S. Finkbeiner, P. H. Patterson, and P. J. Muchowski. "Monoclonal Antibodies Recognize Distinct Conformational Epitopes Formed by Polyglutamine in a Mutant Huntingtin Fragment." [In eng]. *J Biol Chem* 284, no. 32 (Aug 7 2009): 21647-58.

Legleiter, J., E. Mitchell, G. P. Lotz, E. Sapp, C. Ng, M. DiFiglia, L. M. Thompson, and P. J. Muchowski. "Mutant Huntingtin Fragments Form Oligomers in a Polyglutamine Length-Dependent Manner in Vitro and in Vivo." [In eng]. *J Biol Chem* 285, no. 19 (May 7 2010): 14777-90.

Leitman, J., B. Barak, R. Benyair, M. Shenkman, U. Ashery, F. U. Hartl, and G. Z. Lederkremer. "Er Stress-Induced Eif2-Alpha Phosphorylation Underlies Sensitivity of Striatal Neurons to Pathogenic Huntingtin." [In eng]. *PLoS One* 9, no. 3 (2014): e90803.

Leitman, J., F. Ulrich Hartl, and G. Z. Lederkremer. "Soluble Forms of Polyq-Expanded Huntingtin Rather Than Large Aggregates Cause Endoplasmic Reticulum Stress." [In eng]. *Nat Commun* 4 (2013): 2753.

Leonardi, A., G. Abbruzzese, L. Arata, L. Cocito, and M. Vische. "Cerebrospinal Fluid (Csf) Findings in Amyotrophic Lateral Sclerosis." [In eng]. *J Neurol* 231, no. 2 (1984): 75-8.

Lepko, T., M. Pusch, T. Muller, D. Schulte, J. Ehses, M. Kiebler, J. Hasler*, et al.* "Choroid Plexus-Derived Mir-204 Regulates the Number of Quiescent Neural Stem Cells in the Adult Brain." [In eng]. *EMBO J* 38, no. 17 (Sep 2 2019): e100481.

Li, H., B. Handsaker, A. Wysoker, T. Fennell, J. Ruan, N. Homer, G. Marth, G. Abecasis, and R. Durbin. "The Sequence Alignment/Map Format and Samtools." [In eng]. *Bioinformatics* 25, no. 16 (Aug 15 2009): 2078-9.

Li, J. Y., N. Popovic, and P. Brundin. "The Use of the R6 Transgenic Mouse Models of Huntington's Disease in Attempts to Develop Novel Therapeutic Strategies." [In eng]. *NeuroRx* 2, no. 3 (Jul 2005): 447-64.

Li, P. A., Q. He, T. Cao, G. Yong, K. M. Szauter, K. S. Fong, J. Karlsson, M. F. Keep, and K. Csiszar. "Up-Regulation and Altered Distribution of Lysyl Oxidase in the Central Nervous System of Mutant Sod1 Transgenic Mouse Model of Amyotrophic Lateral Sclerosis." [In eng]. *Brain Res Mol Brain Res* 120, no. 2 (Jan 5 2004): 115-22.

Li, S. H., G. Schilling, W. S. Young, 3rd, X. J. Li, R. L. Margolis, O. C. Stine, M. V. Wagster*, et al.* "Huntington's Disease Gene (It15) Is Widely Expressed in Human and Rat Tissues." [In eng]. *Neuron* 11, no. 5 (Nov 1993): 985-93.

Li, T., E. Evdokimov, R. F. Shen, C. C. Chao, E. Tekle, T. Wang, E. R. Stadtman, D. C. Yang, and P. B. Chock. "Sumoylation of Heterogeneous Nuclear Ribonucleoproteins, Zinc Finger Proteins, and Nuclear Pore Complex Proteins: A Proteomic Analysis." [In eng]. *Proc Natl Acad Sci U S A* 101, no. 23 (Jun 8 2004): 8551-6.

Li, X., A. L. Corbett, E. Taatizadeh, N. Tasnim, J. P. Little, C. Garnis, M. Daugaard*, et al.* "Challenges and Opportunities in Exosome Research-Perspectives from Biology, Engineering, and Cancer Therapy." [In eng]. *APL Bioeng* 3, no. 1 (Mar 2019): 011503.

Li, Y. R., O. D. King, J. Shorter, and A. D. Gitler. "Stress Granules as Crucibles of Als Pathogenesis." [In eng]. *J Cell Biol* 201, no. 3 (Apr 29 2013): 361-72.

Liddelow, S. A. "Development of the Choroid Plexus and Blood-Csf Barrier." [In eng]. *Front Neurosci* 9 (2015): 32.

Liebelt, F., and A. C. Vertegaal. "Ubiquitin-Dependent and Independent Roles of Sumo in Proteostasis." [In eng]. *Am J Physiol Cell Physiol* 311, no. 2 (Aug 1 2016): C284-96.

Lim, R. G., C. Quan, A. M. Reyes-Ortiz, S. E. Lutz, A. J. Kedaigle, T. A. Gipson, J. Wu*, et al.* "Huntington's Disease Ipsc-Derived Brain Microvascular Endothelial Cells Reveal Wnt-Mediated Angiogenic and Blood-Brain Barrier Deficits." [In eng]. *Cell Rep* 19, no. 7 (May 16 2017): 1365-77.

Lione, L. A., R. J. Carter, M. J. Hunt, G. P. Bates, A. J. Morton, and S. B. Dunnett. "Selective Discrimination Learning Impairments in Mice Expressing the Human Huntington's Disease Mutation." [In eng]. *J Neurosci* 19, no. 23 (Dec 1 1999): 10428-37.

Liu-Yesucevitz, L., A. Bilgutay, Y. J. Zhang, T. Vanderweyde, A. Citro, T. Mehta, N. Zaarur*, et al.* "Tar DNA Binding Protein-43 (Tdp-43) Associates with Stress Granules: Analysis of Cultured Cells and Pathological Brain Tissue." [In eng]. *PLoS One* 5, no. 10 (Oct 11 2010): e13250.

Liu, B., and S. B. Qian. "Translational Reprogramming in Cellular Stress Response." [In eng]. *Wiley Interdiscip Rev RNA* 5, no. 3 (May-Jun 2014): 301-15.

Liu, J., M. A. Valencia-Sanchez, G. J. Hannon, and R. Parker. "Microrna-Dependent Localization of Targeted Mrnas to Mammalian P-Bodies." [In eng]. *Nat Cell Biol* 7, no. 7 (Jul 2005): 719-23.

Liu, Z., Y. Lv, N. Zhao, G. Guan, and J. Wang. "Protein Kinase R-Like Er Kinase and Its Role in Endoplasmic Reticulum Stress-Decided Cell Fate." [In eng]. *Cell Death Dis* 6 (Jul 30 2015): e1822.

Lotvall, J., A. F. Hill, F. Hochberg, E. I. Buzas, D. Di Vizio, C. Gardiner, Y. S. Gho*, et al.* "Minimal Experimental Requirements for Definition of Extracellular Vesicles and Their Functions: A Position Statement from the International Society for Extracellular Vesicles." [In eng]. *J Extracell Vesicles* 3 (2014): 26913.

Love, M. I., W. Huber, and S. Anders. "Moderated Estimation of Fold Change and Dispersion for Rna-Seq Data with Deseq2." [In eng]. *Genome Biol* 15, no. 12 (2014): 550.

Lugli, G., A. M. Cohen, D. A. Bennett, R. C. Shah, C. J. Fields, A. G. Hernandez, and N. R. Smalheiser. "Plasma Exosomal Mirnas in Persons with and without Alzheimer Disease: Altered Expression and Prospects for Biomarkers." [In eng]. *PLoS One* 10, no. 10 (2015): e0139233.

Lun, M. P., E. S. Monuki, and M. K. Lehtinen. "Development and Functions of the Choroid Plexus-Cerebrospinal Fluid System." [In eng]. *Nat Rev Neurosci* 16, no. 8 (Aug 2015): 445-57.

Lunkes, A., K. S. Lindenberg, L. Ben-Haiem, C. Weber, D. Devys, G. B. Landwehrmeyer, J. L. Mandel, and Y. Trottier. "Proteases Acting on Mutant Huntingtin Generate Cleaved Products That Differentially Build up Cytoplasmic and Nuclear Inclusions." [In eng]. *Mol Cell* 10, no. 2 (Aug 2002): 259-69.

Luthi-Carter, R., S. A. Hanson, A. D. Strand, D. A. Bergstrom, W. Chun, N. L. Peters, A. M. Woods*, et al.* "Dysregulation of Gene Expression in the R6/2 Model of Polyglutamine Disease: Parallel Changes in Muscle and Brain." [In eng]. *Hum Mol Genet* 11, no. 17 (Aug 15 2002): 1911-26.

Luthi-Carter, R., A. Strand, N. L. Peters, S. M. Solano, Z. R. Hollingsworth, A. S. Menon, A. S. Frey*, et al.* "Decreased Expression of Striatal Signaling Genes in a Mouse Model of Huntington's Disease." [In eng]. *Hum Mol Genet* 9, no. 9 (May 22 2000): 1259-71.

Mangiarini, L., K. Sathasivam, M. Seller, B. Cozens, A. Harper, C. Hetherington, M. Lawton*, et al.* "Exon 1 of the Hd Gene with an Expanded Cag Repeat Is Sufficient to Cause a Progressive Neurological Phenotype in Transgenic Mice." [In eng]. *Cell* 87, no. 3 (Nov 1 1996): 493-506.

Marcellin, D., D. Abramowski, D. Young, J. Richter, A. Weiss, A. Marcel, J. Maassen*, et al.* "Fragments of Hdhq150 Mutant Huntingtin Form a Soluble Oligomer Pool That Declines with Aggregate Deposition Upon Aging." [In eng]. *PLoS One* 7, no. 9 (2012): e44457.

Markmiller, S., S. Soltanieh, K. L. Server, R. Mak, W. Jin, M. Y. Fang, E. C. Luo*, et al.* "Context-Dependent and Disease-Specific Diversity in Protein Interactions within Stress Granules." [In eng]. *Cell* 172, no. 3 (Jan 25 2018): 590-604 e13.

Marmor-Kollet, H. "Spatio-Temporal Proteomic Analysis of Stress Granule Disassembly Using Apex Reveals Regulation by Sumoylation and Links to Als Pathogenesis." *Biorxiv* (2020).

Marti, E., L. Pantano, M. Banez-Coronel, F. Llorens, E. Minones-Moyano, S. Porta, L. Sumoy, I. Ferrer, and X. Estivill. "A Myriad of Mirna Variants in Control and Huntington's Disease Brain Regions Detected by Massively Parallel Sequencing." [In eng]. *Nucleic Acids Res* 38, no. 20 (Nov 2010): 7219-35.

Martin, K. C., and A. Ephrussi. "Mrna Localization: Gene Expression in the Spatial Dimension." [In eng]. *Cell* 136, no. 4 (Feb 20 2009): 719-30.

Martin, S., L. Zekri, A. Metz, T. Maurice, K. Chebli, M. Vignes, and J. Tazi. "Deficiency of G3bp1, the Stress Granules Assembly Factor, Results in Abnormal Synaptic Plasticity and Calcium Homeostasis in Neurons." [In eng]. *J Neurochem* 125, no. 2 (Apr 2013): 175-84.

Martinez, F. J., G. A. Pratt, E. L. Van Nostrand, R. Batra, S. C. Huelga, K. Kapeli, P. Freese*, et al.* "Protein-Rna Networks Regulated by Normal and Als-Associated Mutant Hnrnpa2b1 in the Nervous System." [In eng]. *Neuron* 92, no. 4 (Nov 23 2016): 780-95.

Mathieu, M., L. Martin-Jaular, G. Lavieu, and C. Thery. "Specificities of Secretion and Uptake of Exosomes and Other Extracellular Vesicles for Cell-to-Cell Communication." [In eng]. *Nat Cell Biol* 21, no. 1 (Jan 2019): 9-17.

Matsuki, H., M. Takahashi, M. Higuchi, G. N. Makokha, M. Oie, and M. Fujii. "Both G3bp1 and G3bp2 Contribute to Stress Granule Formation." [In eng]. *Genes Cells* 18, no. 2 (Feb 2013): 135-46.

Matsuzaki, S., L. Lee, E. Knock, T. Srikumar, M. Sakurai, L. N. Hazrati, T. Katayama*, et al.* "Sumo1 Affects Synaptic Function, Spine Density and Memory." [In eng]. *Sci Rep* 5 (May 29 2015): 10730.

Mattis, V. B., C. Tom, S. Akimov, J. Saeedian, M. E. Ostergaard, A. L. Southwell, C. N. Doty*, et al.* "Hd Ipsc-Derived Neural Progenitors Accumulate in Culture and Are Susceptible to Bdnf Withdrawal Due to Glutamate Toxicity." [In eng]. *Hum Mol Genet* 24, no. 11 (Jun 1 2015): 3257-71.

Matunis, E. L., R. Kelley, and G. Dreyfuss. "Essential Role for a Heterogeneous Nuclear Ribonucleoprotein (Hnrnp) in Oogenesis: Hrp40 Is Absent from the Germ Line in the

Dorsoventral Mutant Squid." [In eng]. *Proc Natl Acad Sci U S A* 91, no. 7 (Mar 29 1994): 2781-4.
Maxwell, D. S., and D. C. Pease. "The Electron Microscopy of the Choroid Plexus." [In eng]. *J Biophys Biochem Cytol* 2, no. 4 (Jul 25 1956): 467-74.
McDonald, K. K., A. Aulas, L. Destroismaisons, S. Pickles, E. Beleac, W. Camu, G. A. Rouleau, and C. Vande Velde. "Tar DNA-Binding Protein 43 (Tdp-43) Regulates Stress Granule Dynamics Via Differential Regulation of G3bp and Tia-1." [In eng]. *Hum Mol Genet* 20, no. 7 (Apr 1 2011): 1400-10.
Mehrabi, N. F., H. J. Waldvogel, L. J. Tippett, V. M. Hogg, B. J. Synek, and R. L. Faull. "Symptom Heterogeneity in Huntington's Disease Correlates with Neuronal Degeneration in the Cerebral Cortex." [In eng]. *Neurobiol Dis* 96 (Dec 2016): 67-74.
Meijer, H. A., E. M. Smith, and M. Bushell. "Regulation of Mirna Strand Selection: Follow the Leader?" [In eng]. *Biochem Soc Trans* 42, no. 4 (Aug 2014): 1135-40.
Menalled, L. B., and M. F. Chesselet. "Mouse Models of Huntington's Disease." [In eng]. *Trends Pharmacol Sci* 23, no. 1 (Jan 2002): 32-9.
Mi, H., and P. Thomas. "Panther Pathway: An Ontology-Based Pathway Database Coupled with Data Analysis Tools." [In eng]. *Methods Mol Biol* 563 (2009): 123-40.
Miller, J., M. Arrasate, E. Brooks, C. P. Libeu, J. Legleiter, D. Hatters, J. Curtis*, et al.* "Identifying Polyglutamine Protein Species in Situ That Best Predict Neurodegeneration." [In eng]. *Nat Chem Biol* 7, no. 12 (Oct 30 2011): 925-34.
Mizukami, K., M. Ishikawa, M. Iwakiri, M. D. Ikonomovic, S. T. Dekosky, H. Kamma, and T. Asada. "Immunohistochemical Study of the Hnrnp A2 and B1 in the Hippocampal Formations of Brains with Alzheimer's Disease." [In eng]. *Neurosci Lett* 386, no. 2 (Sep 30 2005): 111-5.
Mohagheghi, F., M. Prudencio, C. Stuani, C. Cook, K. Jansen-West, D. W. Dickson, L. Petrucelli, and E. Buratti. "Tdp-43 Functions within a Network of Hnrnp Proteins to Inhibit the Production of a Truncated Human Sort1 Receptor." [In eng]. *Hum Mol Genet* 25, no. 3 (Feb 1 2016): 534-45.
Molliex, A., J. Temirov, J. Lee, M. Coughlin, A. P. Kanagaraj, H. J. Kim, T. Mittag, and J. P. Taylor. "Phase Separation by Low Complexity Domains Promotes Stress Granule Assembly and Drives Pathological Fibrillization." [In eng]. *Cell* 163, no. 1 (Sep 24 2015): 123-33.
Montoya, A., M. Pelletier, M. Menear, E. Duplessis, F. Richer, and M. Lepage. "Episodic Memory Impairment in Huntington's Disease: A Meta-Analysis." [In eng]. *Neuropsychologia* 44, no. 10 (2006): 1984-94.
Moore, M. J., T. K. Scheel, J. M. Luna, C. Y. Park, J. J. Fak, E. Nishiuchi, C. M. Rice, and R. B. Darnell. "Mirna-Target Chimeras Reveal Mirna 3'-End Pairing as a Major Determinant of Argonaute Target Specificity." [In eng]. *Nat Commun* 6 (Nov 25 2015): 8864.
Moreno, J. A., H. Radford, D. Peretti, J. R. Steinert, N. Verity, M. G. Martin, M. Halliday*, et al.* "Sustained Translational Repression by Eif2alpha-P Mediates Prion Neurodegeneration." [In eng]. *Nature* 485, no. 7399 (May 6 2012): 507-11.
Myers, R. H. "Huntington's Disease Genetics." [In eng]. *NeuroRx* 1, no. 2 (Apr 2004): 255-62.
Nana, A. L., E. H. Kim, D. C. Thu, D. E. Oorschot, L. J. Tippett, V. M. Hogg, B. J. Synek*, et al.* "Widespread Heterogeneous Neuronal Loss across the Cerebral Cortex in Huntington's Disease." [In eng]. *J Huntingtons Dis* 3, no. 1 (2014): 45-64.

Narita, K., and S. Takeda. "Cilia in the Choroid Plexus: Their Roles in Hydrocephalus and Beyond." [In eng]. *Front Cell Neurosci* 9 (2015): 39.

Neueder, A., C. Landles, R. Ghosh, D. Howland, R. H. Myers, R. L. M. Faull, S. J. Tabrizi, and G. P. Bates. "The Pathogenic Exon 1 Htt Protein Is Produced by Incomplete Splicing in Huntington's Disease Patients." [In eng]. *Sci Rep* 7, no. 1 (May 2 2017): 1307.

Nichols, R. C., X. W. Wang, J. Tang, B. J. Hamilton, F. A. High, H. R. Herschman, and W. F. Rigby. "The Rgg Domain in Hnrnp A2 Affects Subcellular Localization." [In eng]. *Exp Cell Res* 256, no. 2 (May 1 2000): 522-32.

Niyazova, R., O. Berillo, S. Atambayeva, A. Pyrkova, A. Alybayeva, and A. Ivashchenko. "Mir-1322 Binding Sites in Paralogous and Orthologous Genes." [In eng]. *Biomed Res Int* 2015 (2015): 962637.

Nolte-'t Hoen, E. N., H. P. Buermans, M. Waasdorp, W. Stoorvogel, M. H. Wauben, and P. A. t Hoen. "Deep Sequencing of Rna from Immune Cell-Derived Vesicles Uncovers the Selective Incorporation of Small Non-Coding Rna Biotypes with Potential Regulatory Functions." [In eng]. *Nucleic Acids Res* 40, no. 18 (Oct 2012): 9272-85.

Nunes, C., I. Mestre, A. Marcelo, R. Koppenol, C. A. Matos, and C. Nobrega. "Msgp: The First Database of the Protein Components of the Mammalian Stress Granules." [In eng]. *Database (Oxford)* 2019 (Jan 1 2019).

Nuro-Gyina, P. K., and J. D. Parvin. "Roles for Sumo in Pre-Mrna Processing." [In eng]. *Wiley Interdiscip Rev RNA* 7, no. 1 (Jan-Feb 2016): 105-12.

Nuzziello, N., F. Craig, M. Simone, A. Consiglio, F. Licciulli, L. Margari, G. Grillo, S. Liuni, and M. Liguori. "Integrated Analysis of Microrna and Mrna Expression Profiles: An Attempt to Disentangle the Complex Interaction Network in Attention Deficit Hyperactivity Disorder." [In eng]. *Brain Sci* 9, no. 10 (Oct 22 2019).

O'Rourke, J. G., J. R. Gareau, J. Ochaba, W. Song, T. Rasko, D. Reverter, J. Lee*, et al.* "Sumo-2 and Pias1 Modulate Insoluble Mutant Huntingtin Protein Accumulation." [In eng]. *Cell Rep* 4, no. 2 (Jul 25 2013): 362-75.

Ochaba, J., T. Lukacsovich, G. Csikos, S. Zheng, J. Margulis, L. Salazar, K. Mao*, et al.* "Potential Function for the Huntingtin Protein as a Scaffold for Selective Autophagy." [In eng]. *Proc Natl Acad Sci U S A* 111, no. 47 (Nov 25 2014): 16889-94.

Ochaba, J., A. M. Monteys, J. G. O'Rourke, J. C. Reidling, J. S. Steffan, B. L. Davidson, and L. M. Thompson. "Pias1 Regulates Mutant Huntingtin Accumulation and Huntington's Disease-Associated Phenotypes in Vivo." [In eng]. *Neuron* 90, no. 3 (May 4 2016): 507-20.

Ochaba, J., E. L. Morozko, J. G. O'Rourke, and L. M. Thompson. "Fractionation for Resolution of Soluble and Insoluble Huntingtin Species." [In eng]. *J Vis Exp*, no. 132 (Feb 27 2018).

Ogawa, Y., Y. Miura, A. Harazono, M. Kanai-Azuma, Y. Akimoto, H. Kawakami, T. Yamaguchi*, et al.* "Proteomic Analysis of Two Types of Exosomes in Human Whole Saliva." [In eng]. *Biol Pharm Bull* 34, no. 1 (2011): 13-23.

Pan, B. T., and R. M. Johnstone. "Fate of the Transferrin Receptor During Maturation of Sheep Reticulocytes in Vitro: Selective Externalization of the Receptor." [In eng]. *Cell* 33, no. 3 (Jul 1983): 967-78.

Pan, B. T., K. Teng, C. Wu, M. Adam, and R. M. Johnstone. "Electron Microscopic Evidence for Externalization of the Transferrin Receptor in Vesicular Form in Sheep Reticulocytes." [In eng]. *J Cell Biol* 101, no. 3 (Sep 1985): 942-8.

Park, S. M. "Hopping from One Cell to Another: Huntington's Disease Propagates." [In eng]. *Exp Neurobiol* 26, no. 6 (Dec 2017): 319-20.

Paul, K. R., A. Molliex, S. Cascarina, A. E. Boncella, J. P. Taylor, and E. D. Ross. "Effects of Mutations on the Aggregation Propensity of the Human Prion-Like Protein Hnrnpa2b1." [In eng]. *Mol Cell Biol* 37, no. 8 (Apr 15 2017).

Paulson, H. L. "The Spinocerebellar Ataxias." [In eng]. *J Neuroophthalmol* 29, no. 3 (Sep 2009): 227-37.

Pecho-Vrieseling, E., C. Rieker, S. Fuchs, D. Bleckmann, M. S. Esposito, P. Botta, C. Goldstein*, et al.* "Transneuronal Propagation of Mutant Huntingtin Contributes to Non-Cell Autonomous Pathology in Neurons." [In eng]. *Nat Neurosci* 17, no. 8 (Aug 2014): 1064-72.

Pellegrini, L., C. Bonfio, J. Chadwick, F. Begum, M. Skehel, and M. A. Lancaster. "Human Cns Barrier-Forming Organoids with Cerebrospinal Fluid Production." [In eng]. *Science* (Jun 11 2020).

Perrier, A., and M. Peschanski. "How Can Human Pluripotent Stem Cells Help Decipher and Cure Huntington's Disease?" [In eng]. *Cell Stem Cell* 11, no. 2 (Aug 3 2012): 153-61.

Petersen, A., J. Gil, M. L. Maat-Schieman, M. Bjorkqvist, H. Tanila, I. M. Araujo, R. Smith*, et al.* "Orexin Loss in Huntington's Disease." [In eng]. *Hum Mol Genet* 14, no. 1 (Jan 1 2005): 39-47.

Pinol-Roma, S., Y. D. Choi, M. J. Matunis, and G. Dreyfuss. "Immunopurification of Heterogeneous Nuclear Ribonucleoprotein Particles Reveals an Assortment of Rna-Binding Proteins." [In eng]. *Genes Dev* 2, no. 2 (Feb 1988): 215-27.

Pisitkun, T., R. F. Shen, and M. A. Knepper. "Identification and Proteomic Profiling of Exosomes in Human Urine." [In eng]. *Proc Natl Acad Sci U S A* 101, no. 36 (Sep 7 2004): 13368-73.

Poirier, M. A., H. Li, J. Macosko, S. Cai, M. Amzel, and C. A. Ross. "Huntingtin Spheroids and Protofibrils as Precursors in Polyglutamine Fibrilization." [In eng]. *J Biol Chem* 277, no. 43 (Oct 25 2002): 41032-7.

Pollard, V. W., W. M. Michael, S. Nakielny, M. C. Siomi, F. Wang, and G. Dreyfuss. "A Novel Receptor-Mediated Nuclear Protein Import Pathway." [In eng]. *Cell* 86, no. 6 (Sep 20 1996): 985-94.

Pritchard, C. C., H. H. Cheng, and M. Tewari. "Microrna Profiling: Approaches and Considerations." [In eng]. *Nat Rev Genet* 13, no. 5 (Apr 18 2012): 358-69.

R: A Language and Environment for Statistical Computing. R Foundation for Statistical Computing.

Rabinowits, G., C. Gercel-Taylor, J. M. Day, D. D. Taylor, and G. H. Kloecker. "Exosomal Microrna: A Diagnostic Marker for Lung Cancer." [In eng]. *Clin Lung Cancer* 10, no. 1 (Jan 2009): 42-6.

Radford, H., J. A. Moreno, N. Verity, M. Halliday, and G. R. Mallucci. "Perk Inhibition Prevents Tau-Mediated Neurodegeneration in a Mouse Model of Frontotemporal Dementia." [In eng]. *Acta Neuropathol* 130, no. 5 (Nov 2015): 633-42.

Ramaswami, M., J. P. Taylor, and R. Parker. "Altered Ribostasis: Rna-Protein Granules in Degenerative Disorders." [In eng]. *Cell* 154, no. 4 (Aug 15 2013): 727-36.

Ramdzan, Y. M., M. M. Trubetskov, A. R. Ormsby, E. A. Newcombe, X. Sui, M. J. Tobin, M. N. Bongiovanni*, et al.* "Huntingtin Inclusions Trigger Cellular Quiescence, Deactivate

Apoptosis, and Lead to Delayed Necrosis." [In eng]. *Cell Rep* 19, no. 5 (May 2 2017): 919-27.

Raposo, G., and W. Stoorvogel. "Extracellular Vesicles: Exosomes, Microvesicles, and Friends." [In eng]. *J Cell Biol* 200, no. 4 (Feb 18 2013): 373-83.

Ratajczak, J., M. Wysoczynski, F. Hayek, A. Janowska-Wieczorek, and M. Z. Ratajczak. "Membrane-Derived Microvesicles: Important and Underappreciated Mediators of Cell-to-Cell Communication." [In eng]. *Leukemia* 20, no. 9 (Sep 2006): 1487-95.

Ratovitski, T., E. Chighladze, N. Arbez, T. Boronina, S. Herbrich, R. N. Cole, and C. A. Ross. "Huntingtin Protein Interactions Altered by Polyglutamine Expansion as Determined by Quantitative Proteomic Analysis." [In eng]. *Cell Cycle* 11, no. 10 (May 15 2012): 2006-21.

Rattray, I., E. Smith, R. Gale, K. Matsumoto, G. P. Bates, and M. Modo. "Correlations of Behavioral Deficits with Brain Pathology Assessed through Longitudinal Mri and Histopathology in the R6/2 Mouse Model of Hd." [In eng]. *PLoS One* 8, no. 4 (2013): e60012.

Reddy, P. S., and D. E. Housman. "The Complex Pathology of Trinucleotide Repeats." [In eng]. *Curr Opin Cell Biol* 9, no. 3 (Jun 1997): 364-72.

Redzic, Z. B., J. E. Preston, J. A. Duncan, A. Chodobski, and J. Szmydynger-Chodobska. "The Choroid Plexus-Cerebrospinal Fluid System: From Development to Aging." [In eng]. *Curr Top Dev Biol* 71 (2005): 1-52.

Reed, E. R., J. C. Latourelle, J. H. Bockholt, J. Bregu, J. Smock, J. S. Paulsen, and R. H. Myers. "Micrornas in Csf as Prodromal Biomarkers for Huntington Disease in the Predict-Hd Study." [In eng]. *Neurology* 90, no. 4 (Jan 23 2018): e264-e72.

Reineke, L. C., S. A. Cheema, J. Dubrulle, and J. R. Neilson. "Chronic Starvation Induces Noncanonical Pro-Death Stress Granules." [In eng]. *J Cell Sci* 131, no. 19 (Oct 5 2018).

Reineke, L. C., and J. R. Neilson. "Differences between Acute and Chronic Stress Granules, and How These Differences May Impact Function in Human Disease." [In eng]. *Biochem Pharmacol* 162 (Apr 2019): 123-31.

Rhee, H. W., P. Zou, N. D. Udeshi, J. D. Martell, V. K. Mootha, S. A. Carr, and A. Y. Ting. "Proteomic Mapping of Mitochondria in Living Cells Via Spatially Restricted Enzymatic Tagging." [In eng]. *Science* 339, no. 6125 (Mar 15 2013): 1328-31.

Riancho, J., J. L. Vazquez-Higuera, A. Pozueta, C. Lage, M. Kazimierczak, M. Bravo, M. Calero, *et al.* "Microrna Profile in Patients with Alzheimer's Disease: Analysis of Mir-9-5p and Mir-598 in Raw and Exosome Enriched Cerebrospinal Fluid Samples." [In eng]. *J Alzheimers Dis* 57, no. 2 (2017): 483-91.

Rieux, M., M. Alpaugh, G. Sciacca, M. Saint-Pierre, M. Masnata, H. L. Denis, S. A. Levesque*, et al.* "Shedding a New Light on Huntington's Disease: How Blood Can Both Propagate and Ameliorate Disease Pathology." [In eng]. *Mol Psychiatry* (Jun 8 2020).

Rosas, H. D., D. H. Salat, S. Y. Lee, A. K. Zaleta, V. Pappu, B. Fischl, D. Greve, N. Hevelone, and S. M. Hersch. "Cerebral Cortex and the Clinical Expression of Huntington's Disease: Complexity and Heterogeneity." [In eng]. *Brain* 131, no. Pt 4 (Apr 2008): 1057-68.

Ross, C. A., M. Kronenbuerger, W. Duan, and R. L. Margolis. "Mechanisms Underlying Neurodegeneration in Huntington Disease: Applications to Novel Disease-Modifying Therapies." [In eng]. *Handb Clin Neurol* 144 (2017): 15-28.

Rub, U., K. Seidel, H. Heinsen, J. P. Vonsattel, W. F. den Dunnen, and H. W. Korf. "Huntington's Disease (Hd): The Neuropathology of a Multisystem Neurodegenerative Disorder of the Human Brain." [In eng]. *Brain Pathol* 26, no. 6 (Nov 2016): 726-40.

Rubinsztein, D. C., J. Leggo, R. Coles, E. Almqvist, V. Biancalana, J. J. Cassiman, K. Chotai*, et al.* "Phenotypic Characterization of Individuals with 30-40 Cag Repeats in the Huntington Disease (Hd) Gene Reveals Hd Cases with 36 Repeats and Apparently Normal Elderly Individuals with 36-39 Repeats." [In eng]. *Am J Hum Genet* 59, no. 1 (Jul 1996): 16-22.

Ryberg, H., J. An, S. Darko, J. L. Lustgarten, M. Jaffa, V. Gopalakrishnan, D. Lacomis, M. Cudkowicz, and R. Bowser. "Discovery and Verification of Amyotrophic Lateral Sclerosis Biomarkers by Proteomics." [In eng]. *Muscle Nerve* 42, no. 1 (Jul 2010): 104-11.

Sanz-Rubio, D., I. Martin-Burriel, A. Gil, P. Cubero, M. Forner, A. Khalyfa, and J. M. Marin. "Stability of Circulating Exosomal Mirnas in Healthy Subjects." [In eng]. *Sci Rep* 8, no. 1 (Jul 9 2018): 10306.

Sathasivam, K., A. Neueder, T. A. Gipson, C. Landles, A. C. Benjamin, M. K. Bondulich, D. L. Smith*, et al.* "Aberrant Splicing of Htt Generates the Pathogenic Exon 1 Protein in Huntington Disease." [In eng]. *Proc Natl Acad Sci U S A* 110, no. 6 (Feb 5 2013): 2366-70.

Saudou, F., and S. Humbert. "The Biology of Huntingtin." [In eng]. *Neuron* 89, no. 5 (Mar 2 2016): 910-26.

Saul, J., E. Hutchins, R. Reiman, M. Saul, L. W. Ostrow, B. T. Harris, K. Van Keuren-Jensen, R. Bowser, and N. Bakkar. "Global Alterations to the Choroid Plexus Blood-Csf Barrier in Amyotrophic Lateral Sclerosis." [In eng]. *Acta Neuropathol Commun* 8, no. 1 (Jun 26 2020): 92.

Savas, J. N., B. Ma, K. Deinhardt, B. P. Culver, S. Restituito, L. Wu, J. G. Belasco, M. V. Chao, and N. Tanese. "A Role for Huntington Disease Protein in Dendritic Rna Granules." [In eng]. *J Biol Chem* 285, no. 17 (Apr 23 2010): 13142-53.

Savas, J. N., A. Makusky, S. Ottosen, D. Baillat, F. Then, D. Krainc, R. Shiekhattar, S. P. Markey, and N. Tanese. "Huntington's Disease Protein Contributes to Rna-Mediated Gene Silencing through Association with Argonaute and P Bodies." [In eng]. *Proc Natl Acad Sci U S A* 105, no. 31 (Aug 5 2008): 10820-5.

Scherzinger, E., R. Lurz, M. Turmaine, L. Mangiarini, B. Hollenbach, R. Hasenbank, G. P. Bates*, et al.* "Huntingtin-Encoded Polyglutamine Expansions Form Amyloid-Like Protein Aggregates in Vitro and in Vivo." [In eng]. *Cell* 90, no. 3 (Aug 8 1997): 549-58.

Schmieder, R., and R. Edwards. "Quality Control and Preprocessing of Metagenomic Datasets." [In eng]. *Bioinformatics* 27, no. 6 (Mar 15 2011): 863-4.

Schobel, S. A., G. Palermo, P. Auinger, J. D. Long, S. Ma, O. S. Khwaja, D. Trundell*, et al.* "Motor, Cognitive, and Functional Declines Contribute to a Single Progressive Factor in Early Hd." [In eng]. *Neurology* 89, no. 24 (Dec 12 2017): 2495-502.

Schulte, J., and J. T. Littleton. "The Biological Function of the Huntingtin Protein and Its Relevance to Huntington's Disease Pathology." [In eng]. *Curr Trends Neurol* 5 (Jan 1 2011): 65-78.

Schwab, C., T. Arai, M. Hasegawa, S. Yu, and P. L. McGeer. "Colocalization of Transactivation-Responsive DNA-Binding Protein 43 and Huntingtin in Inclusions of Huntington Disease." [In eng]. *J Neuropathol Exp Neurol* 67, no. 12 (Dec 2008): 1159-65.

Scott, H. "Extracellular Micrornas as Messengers in the Central and Peripheral Nervous System." *Neuronal Signal* 1, no. 4 (December 22, 2017 2017).

Sen, G. L., and H. M. Blau. "Argonaute 2/Risc Resides in Sites of Mammalian Mrna Decay Known as Cytoplasmic Bodies." [In eng]. *Nat Cell Biol* 7, no. 6 (Jun 2005): 633-6.

Seredenina, T., and R. Luthi-Carter. "What Have We Learned from Gene Expression Profiles in Huntington's Disease?" [In eng]. *Neurobiol Dis* 45, no. 1 (Jan 2012): 83-98.

Serot, J. M., M. C. Bene, and G. C. Faure. "Choroid Plexus, Aging of the Brain, and Alzheimer's Disease." [In eng]. *Front Biosci* 8 (May 1 2003): s515-21.

Serot, J. M., M. C. Bene, B. Foliguet, and G. C. Faure. "Morphological Alterations of the Choroid Plexus in Late-Onset Alzheimer's Disease." [In eng]. *Acta Neuropathol* 99, no. 2 (Feb 2000): 105-8.

Shacham, T., N. Sharma, and G. Z. Lederkremer. "Protein Misfolding and Er Stress in Huntington's Disease." [In eng]. *Front Mol Biosci* 6 (2019): 20.

Shahmoradian, S. H., J. G. Galaz-Montoya, M. F. Schmid, Y. Cong, B. Ma, C. Spiess, J. Frydman, S. J. Ludtke, and W. Chiu. "Tric's Tricks Inhibit Huntingtin Aggregation." [In eng]. *Elife* 2 (Jul 9 2013): e00710.

Shan, J., T. P. Munro, E. Barbarese, J. H. Carson, and R. Smith. "A Molecular Mechanism for Mrna Trafficking in Neuronal Dendrites." [In eng]. *J Neurosci* 23, no. 26 (Oct 1 2003): 8859-66.

Shelkovnikova, T. A., P. Dimasi, M. S. Kukharsky, H. An, A. Quintiero, C. Schirmer, L. Buee, M. C. Galas, and V. L. Buchman. "Chronically Stressed or Stress-Preconditioned Neurons Fail to Maintain Stress Granule Assembly." [In eng]. *Cell Death Dis* 8, no. 5 (May 11 2017): e2788.

Sheth, U., and R. Parker. "Decapping and Decay of Messenger Rna Occur in Cytoplasmic Processing Bodies." [In eng]. *Science* 300, no. 5620 (May 2 2003): 805-8.

Shurtleff, M. J., M. M. Temoche-Diaz, K. V. Karfilis, S. Ri, and R. Schekman. "Y-Box Protein 1 Is Required to Sort Micrornas into Exosomes in Cells and in a Cell-Free Reaction." [In eng]. *Elife* 5 (Aug 25 2016).

Sieradzan, K. A., and D. M. Mann. "The Selective Vulnerability of Nerve Cells in Huntington's Disease." [In eng]. *Neuropathol Appl Neurobiol* 27, no. 1 (Feb 2001): 1-21.

Simons, M., and G. Raposo. "Exosomes--Vesicular Carriers for Intercellular Communication." [In eng]. *Curr Opin Cell Biol* 21, no. 4 (Aug 2009): 575-81.

Singh-Bains, M. K., L. J. Tippett, V. M. Hogg, B. J. Synek, R. H. Roxburgh, H. J. Waldvogel, and R. L. Faull. "Globus Pallidus Degeneration and Clinicopathological Features of Huntington Disease." [In eng]. *Ann Neurol* 80, no. 2 (Aug 2016): 185-201.

Sipione, S., D. Rigamonti, M. Valenza, C. Zuccato, L. Conti, J. Pritchard, C. Kooperberg, J. M. Olson, and E. Cattaneo. "Early Transcriptional Profiles in Huntingtin-Inducible Striatal Cells by Microarray Analyses." [In eng]. *Hum Mol Genet* 11, no. 17 (Aug 15 2002): 1953-65.

Smith, R., K. Myers, J. Ravits, and R. Bowser. "Amyotrophic Lateral Sclerosis: Is the Spinal Fluid Pathway Involved in Seeding and Spread?" [In eng]. *Med Hypotheses* 85, no. 5 (Nov 2015): 576-83.

Smith, T., A. Heger, and I. Sudbery. "Umi-Tools: Modeling Sequencing Errors in Unique Molecular Identifiers to Improve Quantification Accuracy." [In eng]. *Genome Res* 27, no. 3 (Mar 2017): 491-99.

Soares Martins, T., J. Catita, I. Martins Rosa, A. B. da Cruz E Silva O, and A. G. Henriques. "Exosome Isolation from Distinct Biofluids Using Precipitation and Column-Based Approaches." [In eng]. *PLoS One* 13, no. 6 (2018): e0198820.

Somasekharan, S. P., F. Zhang, N. Saxena, J. N. Huang, I. C. Kuo, C. Low, R. Bell*, et al.* "G3bp1-Linked Mrna Partitioning Supports Selective Protein Synthesis in Response to Oxidative Stress." [In eng]. *Nucleic Acids Res* (May 14 2020).

Sontag, E. M., L. A. Joachimiak, Z. Tan, A. Tomlinson, D. E. Housman, C. G. Glabe, S. G. Potkin, J. Frydman, and L. M. Thompson. "Exogenous Delivery of Chaperonin Subunit Fragment Apicct1 Modulates Mutant Huntingtin Cellular Phenotypes." [In eng]. *Proc Natl Acad Sci U S A* 110, no. 8 (Feb 19 2013): 3077-82.

Sontag, E. M., G. P. Lotz, N. Agrawal, A. Tran, R. Aron, G. Yang, M. Necula*, et al.* "Methylene Blue Modulates Huntingtin Aggregation Intermediates and Is Protective in Huntington's Disease Models." [In eng]. *J Neurosci* 32, no. 32 (Aug 8 2012): 11109-19.

Sontag, E. M., G. P. Lotz, G. Yang, C. J. Sontag, B. J. Cummings, C. G. Glabe, P. J. Muchowski, and L. M. Thompson. "Detection of Mutant Huntingtin Aggregation Conformers and Modulation of Sds-Soluble Fibrillar Oligomers by Small Molecules." [In eng]. *J Huntingtons Dis* 1, no. 1 (2012): 119-32.

Spargo, E., I. P. Everall, and P. L. Lantos. "Neuronal Loss in the Hippocampus in Huntington's Disease: A Comparison with Hiv Infection." [In eng]. *J Neurol Neurosurg Psychiatry* 56, no. 5 (May 1993): 487-91.

Steffan, J. S., N. Agrawal, J. Pallos, E. Rockabrand, L. C. Trotman, N. Slepko, K. Illes*, et al.* "Sumo Modification of Huntingtin and Huntington's Disease Pathology." [In eng]. *Science* 304, no. 5667 (Apr 2 2004): 100-4.

Steffan, J. S., L. Bodai, J. Pallos, M. Poelman, A. McCampbell, B. L. Apostol, A. Kazantsev*, et al.* "Histone Deacetylase Inhibitors Arrest Polyglutamine-Dependent Neurodegeneration in Drosophila." [In eng]. *Nature* 413, no. 6857 (Oct 18 2001): 739-43.

Steinfeld, R., M. Grapp, R. Kraetzner, S. Dreha-Kulaczewski, G. Helms, P. Dechent, R. Wevers, S. Grosso, and J. Gartner. "Folate Receptor Alpha Defect Causes Cerebral Folate Transport Deficiency: A Treatable Neurodegenerative Disorder Associated with Disturbed Myelin Metabolism." [In eng]. *Am J Hum Genet* 85, no. 3 (Sep 2009): 354-63.

Street, J. M., P. E. Barran, C. L. Mackay, S. Weidt, C. Balmforth, T. S. Walsh, R. T. Chalmers, D. J. Webb, and J. W. Dear. "Identification and Proteomic Profiling of Exosomes in Human Cerebrospinal Fluid." [In eng]. *J Transl Med* 10 (Jan 5 2012): 5.

Strong, T. V., D. A. Tagle, J. M. Valdes, L. W. Elmer, K. Boehm, M. Swaroop, K. W. Kaatz, F. S. Collins, and R. L. Albin. "Widespread Expression of the Human and Rat Huntington's Disease Gene in Brain and Nonneural Tissues." [In eng]. *Nat Genet* 5, no. 3 (Nov 1993): 259-65.

Sutton, M. A., and E. M. Schuman. "Dendritic Protein Synthesis, Synaptic Plasticity, and Memory." [In eng]. *Cell* 127, no. 1 (Oct 6 2006): 49-58.

Swanson, M. S., and G. Dreyfuss. "Classification and Purification of Proteins of Heterogeneous Nuclear Ribonucleoprotein Particles by Rna-Binding Specificities." [In eng]. *Mol Cell Biol* 8, no. 5 (May 1988): 2237-41.

Szlachcic, W. J., P. M. Switonski, W. J. Krzyzosiak, M. Figlerowicz, and M. Figiel. "Huntington Disease Ipscs Show Early Molecular Changes in Intracellular Signaling, the Expression of Oxidative Stress Proteins and the P53 Pathway." [In eng]. *Dis Model Mech* 8, no. 9 (Sep 2015): 1047-57.

Tabrizi, S. J., R. Ghosh, and B. R. Leavitt. "Huntingtin Lowering Strategies for Disease Modification in Huntington's Disease." [In eng]. *Neuron* 101, no. 5 (Mar 6 2019): 801-19.

Tabrizi, S. J., B. R. Leavitt, G. B. Landwehrmeyer, E. J. Wild, C. Saft, R. A. Barker, N. F. Blair*, et al.* "Targeting Huntingtin Expression in Patients with Huntington's Disease." [In eng]. *N Engl J Med* 380, no. 24 (Jun 13 2019): 2307-16.

Takahashi, K., and S. Yamanaka. "Induction of Pluripotent Stem Cells from Mouse Embryonic and Adult Fibroblast Cultures by Defined Factors." [In eng]. *Cell* 126, no. 4 (Aug 25 2006): 663-76.

Takahashi, T., S. Kikuchi, S. Katada, Y. Nagai, M. Nishizawa, and O. Onodera. "Soluble Polyglutamine Oligomers Formed Prior to Inclusion Body Formation Are Cytotoxic." [In eng]. *Hum Mol Genet* 17, no. 3 (Feb 1 2008): 345-56.

Tam, S., R. Geller, C. Spiess, and J. Frydman. "The Chaperonin Tric Controls Polyglutamine Aggregation and Toxicity through Subunit-Specific Interactions." [In eng]. *Nat Cell Biol* 8, no. 10 (Oct 2006): 1155-62.

Tam, S., M. S. Tsao, and J. D. McPherson. "Optimization of Mirna-Seq Data Preprocessing." [In eng]. *Brief Bioinform* 16, no. 6 (Nov 2015): 950-63.

Tarassishin, L., H. S. Suh, and S. C. Lee. "Lps and Il-1 Differentially Activate Mouse and Human Astrocytes: Role of Cd14." [In eng]. *Glia* 62, no. 6 (Jun 2014): 999-1013.

Tatham, M. H., I. Matic, M. Mann, and R. T. Hay. "Comparative Proteomic Analysis Identifies a Role for Sumo in Protein Quality Control." [In eng]. *Sci Signal* 4, no. 178 (Jun 21 2011): rs4.

Thery, C., M. Ostrowski, and E. Segura. "Membrane Vesicles as Conveyors of Immune Responses." [In eng]. *Nat Rev Immunol* 9, no. 8 (Aug 2009): 581-93.

Thery, C., K. W. Witwer, E. Aikawa, M. J. Alcaraz, J. D. Anderson, R. Andriantsitohaina, A. Antoniou*, et al.* "Minimal Information for Studies of Extracellular Vesicles 2018 (Misev2018): A Position Statement of the International Society for Extracellular Vesicles and Update of the Misev2014 Guidelines." [In eng]. *J Extracell Vesicles* 7, no. 1 (2018): 1535750.

Thind, A., and C. Wilson. "Exosomal Mirnas as Cancer Biomarkers and Therapeutic Targets." [In eng]. *J Extracell Vesicles* 5 (2016): 31292.

Thomas, M. G., M. Loschi, M. A. Desbats, and G. L. Boccaccio. "Rna Granules: The Good, the Bad and the Ugly." [In eng]. *Cell Signal* 23, no. 2 (Feb 2011): 324-34.

Thomou, T., M. A. Mori, J. M. Dreyfuss, M. Konishi, M. Sakaguchi, C. Wolfrum, T. N. Rao*, et al.* "Adipose-Derived Circulating Mirnas Regulate Gene Expression in Other Tissues." [In eng]. *Nature* 542, no. 7642 (Feb 23 2017): 450-55.

Thouvenot, E., M. Lafon-Cazal, E. Demettre, P. Jouin, J. Bockaert, and P. Marin. "The Proteomic Analysis of Mouse Choroid Plexus Secretome Reveals a High Protein

Secretion Capacity of Choroidal Epithelial Cells." [In eng]. *Proteomics* 6, no. 22 (Nov 2006): 5941-52.

Tietje, A., K. N. Maron, Y. Wei, and D. M. Feliciano. "Cerebrospinal Fluid Extracellular Vesicles Undergo Age Dependent Declines and Contain Known and Novel Non-Coding Rnas." [In eng]. *PLoS One* 9, no. 11 (2014): e113116.

Tourriere, H., K. Chebli, L. Zekri, B. Courselaud, J. M. Blanchard, E. Bertrand, and J. Tazi. "The Rasgap-Associated Endoribonuclease G3bp Assembles Stress Granules." [In eng]. *J Cell Biol* 160, no. 6 (Mar 17 2003): 823-31.

Trams, E. G., C. J. Lauter, N. Salem, Jr., and U. Heine. "Exfoliation of Membrane Ecto-Enzymes in the Form of Micro-Vesicles." [In eng]. *Biochim Biophys Acta* 645, no. 1 (Jul 6 1981): 63-70.

Trottier, Y., V. Biancalana, and J. L. Mandel. "Instability of Cag Repeats in Huntington's Disease: Relation to Parental Transmission and Age of Onset." [In eng]. *J Med Genet* 31, no. 5 (May 1994): 377-82.

Trottier, Y., D. Devys, G. Imbert, F. Saudou, I. An, Y. Lutz, C. Weber*, et al.* "Cellular Localization of the Huntington's Disease Protein and Discrimination of the Normal and Mutated Form." [In eng]. *Nat Genet* 10, no. 1 (May 1995): 104-10.

Truant, R., R. S. Atwal, and A. Burtnik. "Nucleocytoplasmic Trafficking and Transcription Effects of Huntingtin in Huntington's Disease." [In eng]. *Prog Neurobiol* 83, no. 4 (Nov 2007): 211-27.

Uchino, M., Y. Ando, Y. Tanaka, T. Nakamura, E. Uyama, S. Mita, T. Murakami, and M. Ando. "Decrease in Cu/Zn- and Mn-Superoxide Dismutase Activities in Brain and Spinal Cord of Patients with Amyotrophic Lateral Sclerosis." [In eng]. *J Neurol Sci* 127, no. 1 (Dec 1 1994): 61-7.

"Unified Huntington's Disease Rating Scale: Reliability and Consistency. Huntington Study Group." [In eng]. *Mov Disord* 11, no. 2 (Mar 1996): 136-42.

Valor, L. M. "Transcription, Epigenetics and Ameliorative Strategies in Huntington's Disease: A Genome-Wide Perspective." [In eng]. *Mol Neurobiol* 51, no. 1 (Feb 2015): 406-23.

van Iterson, M., S. Bervoets, E. J. de Meijer, H. P. Buermans, P. A. t Hoen, R. X. Menezes, and J. M. Boer. "Integrated Analysis of Microrna and Mrna Expression: Adding Biological Significance to Microrna Target Predictions." [In eng]. *Nucleic Acids Res* 41, no. 15 (Aug 2013): e146.

Vanderweyde, T., H. Yu, M. Varnum, L. Liu-Yesucevitz, A. Citro, T. Ikezu, K. Duff, and B. Wolozin. "Contrasting Pathology of the Stress Granule Proteins Tia-1 and G3bp in Tauopathies." [In eng]. *J Neurosci* 32, no. 24 (Jun 13 2012): 8270-83.

Vargas, T., C. Ugalde, C. Spuch, D. Antequera, M. J. Moran, M. A. Martin, I. Ferrer, F. Bermejo-Pareja, and E. Carro. "Abeta Accumulation in Choroid Plexus Is Associated with Mitochondrial-Induced Apoptosis." [In eng]. *Neurobiol Aging* 31, no. 9 (Sep 2010): 1569-81.

Vejnar, C. E., and E. M. Zdobnov. "Mirmap: Comprehensive Prediction of Microrna Target Repression Strength." [In eng]. *Nucleic Acids Res* 40, no. 22 (Dec 2012): 11673-83.

Vella, L. J., R. A. Sharples, V. A. Lawson, C. L. Masters, R. Cappai, and A. F. Hill. "Packaging of Prions into Exosomes Is Associated with a Novel Pathway of Prp Processing." [In eng]. *J Pathol* 211, no. 5 (Apr 2007): 582-90.

Villarroya-Beltri, C., C. Gutierrez-Vazquez, F. Sanchez-Cabo, D. Perez-Hernandez, J. Vazquez, N. Martin-Cofreces, D. J. Martinez-Herrera*, et al.* "Sumoylated Hnrnpa2b1 Controls the Sorting of Mirnas into Exosomes through Binding to Specific Motifs." [In eng]. *Nat Commun* 4 (2013): 2980.

Vonsattel, J. P., M. P. Del Amaya, and C. E. Keller. "Twenty-First Century Brain Banking. Processing Brains for Research: The Columbia University Methods." [In eng]. *Acta Neuropathol* 115, no. 5 (May 2008): 509-32.

Vonsattel, J. P., and M. DiFiglia. "Huntington Disease." [In eng]. *J Neuropathol Exp Neurol* 57, no. 5 (May 1998): 369-84.

Vonsattel, J. P., R. H. Myers, T. J. Stevens, R. J. Ferrante, E. D. Bird, and E. P. Richardson, Jr. "Neuropathological Classification of Huntington's Disease." [In eng]. *J Neuropathol Exp Neurol* 44, no. 6 (Nov 1985): 559-77.

Waelter, S., A. Boeddrich, R. Lurz, E. Scherzinger, G. Lueder, H. Lehrach, and E. E. Wanker. "Accumulation of Mutant Huntingtin Fragments in Aggresome-Like Inclusion Bodies as a Result of Insufficient Protein Degradation." [In eng]. *Mol Biol Cell* 12, no. 5 (May 2001): 1393-407.

Waldvogel, H. J., E. H. Kim, L. J. Tippett, J. P. Vonsattel, and R. L. Faull. "The Neuropathology of Huntington's Disease." [In eng]. *Curr Top Behav Neurosci* 22 (2015): 33-80.

Wang, L., and L. Zhang. "Circulating Exosomal Mirna as Diagnostic Biomarkers of Neurodegenerative Diseases." [In eng]. *Front Mol Neurosci* 13 (2020): 53.

Wang, Y., S. Juranek, H. Li, G. Sheng, T. Tuschl, and D. J. Patel. "Structure of an Argonaute Silencing Complex with a Seed-Containing Guide DNA and Target Rna Duplex." [In eng]. *Nature* 456, no. 7224 (Dec 18 2008): 921-6.

Wanker, E. E., E. Scherzinger, V. Heiser, A. Sittler, H. Eickhoff, and H. Lehrach. "Membrane Filter Assay for Detection of Amyloid-Like Polyglutamine-Containing Protein Aggregates." [In eng]. *Methods Enzymol* 309 (1999): 375-86.

Watanabe, M., Y. J. Kang, L. M. Davies, S. Meghpara, K. Lau, C. Y. Chung, J. Kathiriya, A. K. Hadjantonakis, and E. S. Monuki. "Bmp4 Sufficiency to Induce Choroid Plexus Epithelial Fate from Embryonic Stem Cell-Derived Neuroepithelial Progenitors." [In eng]. *J Neurosci* 32, no. 45 (Nov 7 2012): 15934-45.

Weber, S. C., and C. P. Brangwynne. "Getting Rna and Protein in Phase." [In eng]. *Cell* 149, no. 6 (Jun 8 2012): 1188-91.

Weiss, A., C. Klein, B. Woodman, K. Sathasivam, M. Bibel, E. Regulier, G. P. Bates, and P. Paganetti. "Sensitive Biochemical Aggregate Detection Reveals Aggregation Onset before Symptom Development in Cellular and Murine Models of Huntington's Disease." [In eng]. *J Neurochem* 104, no. 3 (Feb 2008): 846-58.

Wen, G. Y., H. M. Wisniewski, and R. J. Kascsak. "Biondi Ring Tangles in the Choroid Plexus of Alzheimer's Disease and Normal Aging Brains: A Quantitative Study." [In eng]. *Brain Res* 832, no. 1-2 (Jun 19 1999): 40-6.

Wexler, N. S., J. Lorimer, J. Porter, F. Gomez, C. Moskowitz, E. Shackell, K. Marder*, et al.* "Venezuelan Kindreds Reveal That Genetic and Environmental Factors Modulate Huntington's Disease Age of Onset." [In eng]. *Proc Natl Acad Sci U S A* 101, no. 10 (Mar 9 2004): 3498-503.

Willms, E., H. J. Johansson, I. Mager, Y. Lee, K. E. Blomberg, M. Sadik, A. Alaarg*, et al.* "Cells Release Subpopulations of Exosomes with Distinct Molecular and Biological Properties." [In eng]. *Sci Rep* 6 (Mar 2 2016): 22519.

Wolozin, B. "Regulated Protein Aggregation: Stress Granules and Neurodegeneration." [In eng]. *Mol Neurodegener* 7 (Nov 20 2012): 56.
Wolozin, B., and P. Ivanov. "Stress Granules and Neurodegeneration." [In eng]. *Nat Rev Neurosci* 20, no. 11 (Nov 2019): 649-66.
Yagi, Y., T. Ohkubo, H. Kawaji, A. Machida, H. Miyata, S. Goda, S. Roy*, et al.* "Next-Generation Sequencing-Based Small Rna Profiling of Cerebrospinal Fluid Exosomes." [In eng]. *Neurosci Lett* 636 (Jan 1 2017): 48-57.
Yang, J. S., and E. C. Lai. "Alternative Mirna Biogenesis Pathways and the Interpretation of Core Mirna Pathway Mutants." [In eng]. *Mol Cell* 43, no. 6 (Sep 16 2011): 892-903.
Yang, P., C. Mathieu, R. M. Kolaitis, P. Zhang, J. Messing, U. Yurtsever, Z. Yang*, et al.* "G3bp1 Is a Tunable Switch That Triggers Phase Separation to Assemble Stress Granules." [In eng]. *Cell* 181, no. 2 (Apr 16 2020): 325-45 e28.
Yang, Y., Y. He, X. Wang, Z. Liang, G. He, P. Zhang, H. Zhu, N. Xu, and S. Liang. "Protein Sumoylation Modification and Its Associations with Disease." [In eng]. *Open Biol* 7, no. 10 (Oct 2017).
Yi, Y. W., J. H. Lee, S. Y. Kim, C. G. Pack, D. H. Ha, S. R. Park, J. Youn, and B. S. Cho. "Advances in Analysis of Biodistribution of Exosomes by Molecular Imaging." [In eng]. *Int J Mol Sci* 21, no. 2 (Jan 19 2020).
Zhang, J., S. Li, L. Li, M. Li, C. Guo, J. Yao, and S. Mi. "Exosome and Exosomal Microrna: Trafficking, Sorting, and Function." [In eng]. *Genomics Proteomics Bioinformatics* 13, no. 1 (Feb 2015): 17-24.
Zhang, K., J. G. Daigle, K. M. Cunningham, A. N. Coyne, K. Ruan, J. C. Grima, K. E. Bowen*, et al.* "Stress Granule Assembly Disrupts Nucleocytoplasmic Transport." [In eng]. *Cell* 173, no. 4 (May 3 2018): 958-71 e17.
Zhang, Q. C., T. L. Yeh, A. Leyva, L. G. Frank, J. Miller, Y. E. Kim, R. Langen*, et al.* "A Compact Beta Model of Huntingtin Toxicity." [In eng]. *J Biol Chem* 286, no. 10 (Mar 11 2011): 8188-96.
Zhang, X., E. R. Abels, J. S. Redzic, J. Margulis, S. Finkbeiner, and X. O. Breakefield. "Potential Transfer of Polyglutamine and Cag-Repeat Rna in Extracellular Vesicles in Huntington's Disease: Background and Evaluation in Cell Culture." [In eng]. *Cell Mol Neurobiol* 36, no. 3 (Apr 2016): 459-70.
Zhang, Y. J., T. F. Gendron, M. T. W. Ebbert, A. D. O'Raw, M. Yue, K. Jansen-West, X. Zhang*, et al.* "Poly(Gr) Impairs Protein Translation and Stress Granule Dynamics in C9orf72-Associated Frontotemporal Dementia and Amyotrophic Lateral Sclerosis." [In eng]. *Nat Med* 24, no. 8 (Aug 2018): 1136-42.
Zhao, X. "Sumo-Mediated Regulation of Nuclear Functions and Signaling Processes." [In eng]. *Mol Cell* 71, no. 3 (Aug 2 2018): 409-18.
Zheng, W., and Q. Zhao. "Establishment and Characterization of an Immortalized Z310 Choroidal Epithelial Cell Line from Murine Choroid Plexus." [In eng]. *Brain Res* 958, no. 2 (Dec 27 2002): 371-80.
Zhu, X., M. Badawi, S. Pomeroy, D. S. Sutaria, Z. Xie, A. Baek, J. Jiang*, et al.* "Comprehensive Toxicity and Immunogenicity Studies Reveal Minimal Effects in Mice Following Sustained Dosing of Extracellular Vesicles Derived from Hek293t Cells." [In eng]. *J Extracell Vesicles* 6, no. 1 (2017): 1324730.

Zuccato, C., M. Tartari, A. Crotti, D. Goffredo, M. Valenza, L. Conti, T. Cataudella*, et al.* "Huntingtin Interacts with Rest/Nrsf to Modulate the Transcription of Nrse-Controlled Neuronal Genes." [In eng]. *Nat Genet* 35, no. 1 (Sep 2003): 76-83.